SUSTAINABLE CHEMISTRY SOLUTIONS FOR INDUSTRIAL CHALLENGES: MECHANISMS OF PVC DEGRADATION AND STABILIZATION; REVERSIBLE IONIC LIQUIDS FOR CO_2 CAPTURE; EFFICIENT SUZUKI COUPLING OF BASIC, NITROGEN CONTAINING SUBSTRATES

A Dissertation
Presented to
The Academic Faculty

by

Amber Rumple

In Partial Fulfillment
of the Requirements for the Degree
Doctor of Philosophy in the
School of Chemistry

Georgia Institute of Technology
December 2014

SUSTAINABLE CHEMISTRY SOLUTIONS FOR INDUSTRIAL CHALLENGES: MECHANISMS OF PVC DEGRADATION AND STABILIZATION; REVERSIBLE IONIC LIQUIDS FOR CO_2 CAPTURE; EFFICIENT SUZUKI COUPLING OF BASIC, NITROGEN CONTAINING SUBSTRATES

Approved by:

Dr. Charles Liotta, Co-Advisor
School of Chemistry and Biochemistry
Georgia Institute of Technology

Dr. Adegboyega Oyelere
School of Chemistry and Biochemistry
Georgia Institute of Technology

Dr. Charles Eckert, Co-Advisor
School of Chemical and Biomolecular Engineering
Georgia Institute of Technology

Dr. Christopher Jones
School of Chemical and Biomolecular Engineering
Georgia Institute of Technology

Dr. Stefan France
School of Chemistry and Biochemistry
Georgia Institute of Technology

Date Approved: August 06, 2014

To my family and friends, especially my parents, JoAnne and Paul, and my brother, Bryan, without whom I would not be the person I am today.

ACKNOWLEDGEMENTS

I would like to begin by thanking my advisors Dr. Charles Liotta and Dr. Charles Eckert. The opportunity to work with such skilled scientists and kind mentors is a rare one, and I am extremely glad I had the opportunity to learn from them. I have always been in awe of their brilliance (I'm pretty sure they have each forgotten more than I'll ever learn, and they still know so much), but their kindness and encouragement has helped prepare me for my future career and my future in general. The emphasis they displayed on interdisciplinary collaboration and communication will serve me well in both my professional and personal lives. I would also like to thank my committee members for their support through each obstacle I have faced in my graduate career. Your questions and insight have proven invaluable in my continuing research.

I would next like to thank all of my colleagues, former and current. Our collaborative efforts towards the advancement of our projects have provided invaluable life lessons. Dr. Pamela Pollet, in particular, has been a steady source of encouragement, advice and mentorship. Her advice and vision have proven instrumental in my development as a chemist, and she has really gone above and beyond in her efforts to help and guide us. To all my colleagues, it's been a pleasure working with you and joking with you. We've all become good friends over the years, inside and outside of work, and I look forward to maintaining that friendship as we go our separate ways. To Chris Butch, especially, we started at the same time and are finishing at the same time. We've shared an office for four years and your company and friendship have been my saving grace.

Rebeca Vindas, thank you for being such a great friend and a source of relief from the testosterone-fueled environment we sometimes felt overwhelmed by.

To my family and friends here in Atlanta, GA, home in Dayton, OH, and all over the globe, you are the main reason I've made it this far. Thank you for keeping me grounded and focused and for providing an escape from life when it got too serious. I understand the phrase "work-life balance" all because of you.

TABLE OF CONTENTS

LIST OF TABLES

Page

LIST OF FIGURES

Page

LIST OF SYMBOLS AND ABBREVIATIONS

ΔH_{rxn}	enthalpy of reaction
ACN	acetonitrile
ATR-FTIR	attenuated total reflectance Fourier-transform infrared (spectroscopy)
BTU	British thermal unit
CHO	1,2-cyclohexene oxide
CO_2	carbon dioxide
DEHP	bis(2-ethylhexyl) phthalate
DIDP	diisodecyl phthalate
DINP	diiosononyl phthalate
DIPEA	diisopropyl ethylamine
DMESA	3-(aminopropyl)dimethylethylsilane
DMF	dimethyl formamide
DMSO	dimethyl sulfoxide
DOE	Department of Energy
DSC	differential scanning calorimetry
EH	1,2-epoxyhexane
GC-FID	gas chromatography – flame ionization detector
GC-MS	gas chromatography – mass spectrometry
HPLC	high-performance liquid chromatography

LC-MS	liquid chromatography – mass spectrometry
MEA	monoethanolamine
MW	megawatt
NMR	nuclear magnetic resonance (spectroscopy)
NSF	National Science Foundation
phr	parts per hundred resin
ppm	parts per million
PTC	phase transfer catalyst
PVC	polyvinyl chloride
RevIL	reversible ionic liquid
RT	room temperature
SDMESA	N-methyl-3-(aminopropyl)dimethylethylsilane
STEtSA	N-methyl-3-(triethylsilyl)propan-1-amine
TESA	triethoxysilylpropylamine
TEtSA	3-(aminopropyl) triethylsilane
TEtSBA	4-(aminobutyl) triethylsilane
TEtSEtA	2-(aminoethyl) triethylsilane
TEtSMA	1-(aminomethyl) triethylsilane
THF	tetrahydrofuran
THSA	3-(aminopropyl) trihexylsilane
TMSA	trimethoxysilylpropylamine

TPSA	3-(aminopropyl) tripropylsilane
trans-TEtSA	(trans)-3-(triethylsilyl)prop-2-en-1-amine
trans-α,αDMe-TEtSA	2-methyl-4-(triethylsilyl)-butyl-2-amine
trans-α,αDMe-TPSA	2-methyl-4-(tripropylsilyl)-butyl-2-amine
TSIL	task-specific ionic liquid
UV-visible	ultraviolet-visible (spectrospcoy)
α,αDMe-TEtSA	2-methyl-4-(triethylsilyl)-butyl-2-amine
αMe-TEtSA	4-(triethylsilyl)-butyl-2-amine
βMe-TEtSA	2-methyl-3-(triethylsilyl)propylamine

SUMMARY

Three projects were investigated which utilized green chemistry as a guideline towards the development of sustainable chemistries for industry. In the first project, a study was performed on the thermal degradation and stabilization of PVC in the presence of both plasticizers and thermal stabilizers. The study combined both model compound experiments as well as work with bulk PVC blends to gain a holistic understanding of the processes that take place during the degradation and stabilization of PVC. A comprehensive mechanism was proposed for the degradation and stabilization of PVC with metal stearates.

The second project investigated silylamines and their application as reversible ionic liquids for CO_2 capture from post-combustion flue gas streams. The effect of silylamine structure was thoroughly researched to develop a comprehensive library of silylamines and an accompanying set of structure-property relationships. The proposed solvent systems have the potential to present significant energy savings, as design has focused on their use in a non-aqueous, solvent-free environment.

Finally, the design of an efficient and simple system for the Suzuki coupling of 4-amino-2-halopyridines in quantitative yields by utilizing increased water content and CO_2 pressure with readily available triphenylphosphine-based ligands is presented. The discovery of a susbtrate dependent optimum pH for efficient coupling of amines and the use of Hammet Plots to investigate electronic effects and their influence on the reaction mechanism are discussed.

CHAPTER 1

Introduction

1.1 Green Chemistry Principles

A "new" field is making a breakthrough in the world of chemistry: green chemistry. Green chemistry is the conscious design of chemical processes which use the maximum amount of the raw materials incorporated, in an energy efficient and safe manner, with the least waste generated as possible.[1] While the idea is not actually new – the concept was proposed by Paul Anastas in 1991 – interest in the field has increased in recent years, in part due to increased consumer demand for products that are green or sustainable. Though similar movements promoting green chemistry were witnessed in the 1970's and 1980's, they focused on the role of the individual in sustainability. The current movement focuses on the role of industry in sustainability and, to that end, the 12 principles of green chemistry were defined by Paul Anastas and John Warner in their book *Green Chemistry: Theory and Practice* (Table 1).[2] The current form of green chemistry is considered an innovative, non-regulatory, and economocially driven approach towards sustainability.[3]

Table 1 – Twelve principles of green chemistry.

Twelve Principles of Green Chemistry	
1.	It's better to prevent waste than to treat or clean up waste after it is formed.
2.	Synthetic methods should be designed to maximize the incorporation of all materials used in the process into the final product.
3.	Wherever practicable, synthetic methodologies should be designed to use and generate substances that possess little or no toxicity to human health and the environment.
4.	Chemical products should be designed to preserve efficacy of function while reducing toxicity.
5.	The use of auxiliary substances (e.g. solvents, separation agents, etc.) should be made unnecessary wherever possible and, innocuous when used.
6.	Energy requirements should be recognized for their environmental and economic impacts and should be minimized. Synthetic methods should be conducted at ambient temperature and pressure.
7.	A raw material of feedstock should be renewable rather than depleting wherever technically and economically practicable.
8.	Unnecessary derivization (blocking group, protection/deprotection, and temporary modification of physical/chemical processes) should be avoided whenever possible.
9.	Catalytic reagents (as selective as possible) are superior to stochiometric reagents.
10.	Chemical products should be designed so that at the end of their function they do not persist in the environment and break down into innocuous degradation products.
11.	Analytical methodologies need to be further developed to allow for real time, in-process monitoring and control prior to the formation of hazardous substances.
12.	Substances and the form of a substance used in a chemical process should be chosen so as to minimize the potential for chemical accidents, including releases, explosions, and fires.

In order for the application of green chemistry to be viable in industry, however, the economics of the process also need to be taken into account. Industry will not adopt the methods of green chemistry unless it is affordable and profits can be maintained or increased. The combination of green chemistry and viable economics is what defines a sustainable process. The projects presented here are aimed at the development of sustainable solutions for industrially relevant problems. Certain aspects of green chemistry are used as a guideline for the goals of the projects, with an emphasis on industrial viability (green and economic solutions).

The first project - degradation and stabilization of polyvinylchloride: integrating model and bulk polymer studies (and the corresponding appendix) - involved an investigation into the effectiveness of traditional and novel thermal stabilizers in plasticized PVC formulations. Plasticizers derived from renewable resources (i.e. soybean oil) were investigated to replace petroleum-derived plasticizers (Principle 7). The second project – the design, synthesis and evaluation of nonaqueous silylamines for efficient CO_2 capture – details the development of novel solvents for CO_2 capture from coal-fired power plants. The novel solvents were developed to eliminate the need for added water (Principle 5) and to minimize the energy needed for reversal and recycle (Principle 6). Finally, the third project – the effect of CO_2 pressure and pH on the Suzuki coupling of basic, nitrogen containing substrates – seeks to eliminate the use of protection/deprotection strategies (Principle 8) and additional, expensive ligands to reduce waste (Principle 1). Instead, we employ CO_2 as a renewable resource (Principle 7) to promote the efficient coupling of basic, nitrogen containing substrates.

The work conducted in the Eckert-Liotta group is done in multidisciplinary research groups of chemists and chemical engineers. As such, the work outlined within this thesis contains elements of both organic chemistry and chemical engineering. This approach has allowed for both fundamental design and application of fundamental studies. The remainder of this chapter provides a brief background for each of the three aforementioned projects and highlights the motivation for the work presented in later chapters.

1.2 Degradation and Stabilization of Polyvinylchloride: Integrating Model and Bulk Polymer Studies

Polyvinylchloride (PVC) is a plastic that is used in a variety of applications. For electrical wire coatings, the application of concern for this thesis, the PVC formulations typically include numerous additives. At a minimum the formulations include a

plasticizer and thermal stabilizers. Plasticizers are utilized to increase the flexibility of the polymer. Thermal stabilizers are utilized to prevent degradation of the polymer backbone by either substitution of the stabilizer for labile chlorides or scavenging the HCl released from the degradation process.[4] HCl released as part of the degradation process can catalyze further degradation by coordinating to labile chlorides and promoting their elimination from the backbone.

Phthalates such as diisodecyl phthalate (DIDP), bis(2-ethylhexyl) phthalate (DEHP), and diisononyl phthalate (DINP) are the most commonly utilized plasticizers for PVC formulations. In fact, they represent 85% of the global plasticizer consumption (6 Mton/year).[5] However, phthalate plasticizers are derived entirely from crude oil, which is a nonrenewable fossil fuel whose costs are constantly increasing (Figure 1).[6] Additionally, the leaching of low weight phthalate plasticizers such as DEHP from the polymer is facing increased scrutiny due to health concerns.[7]

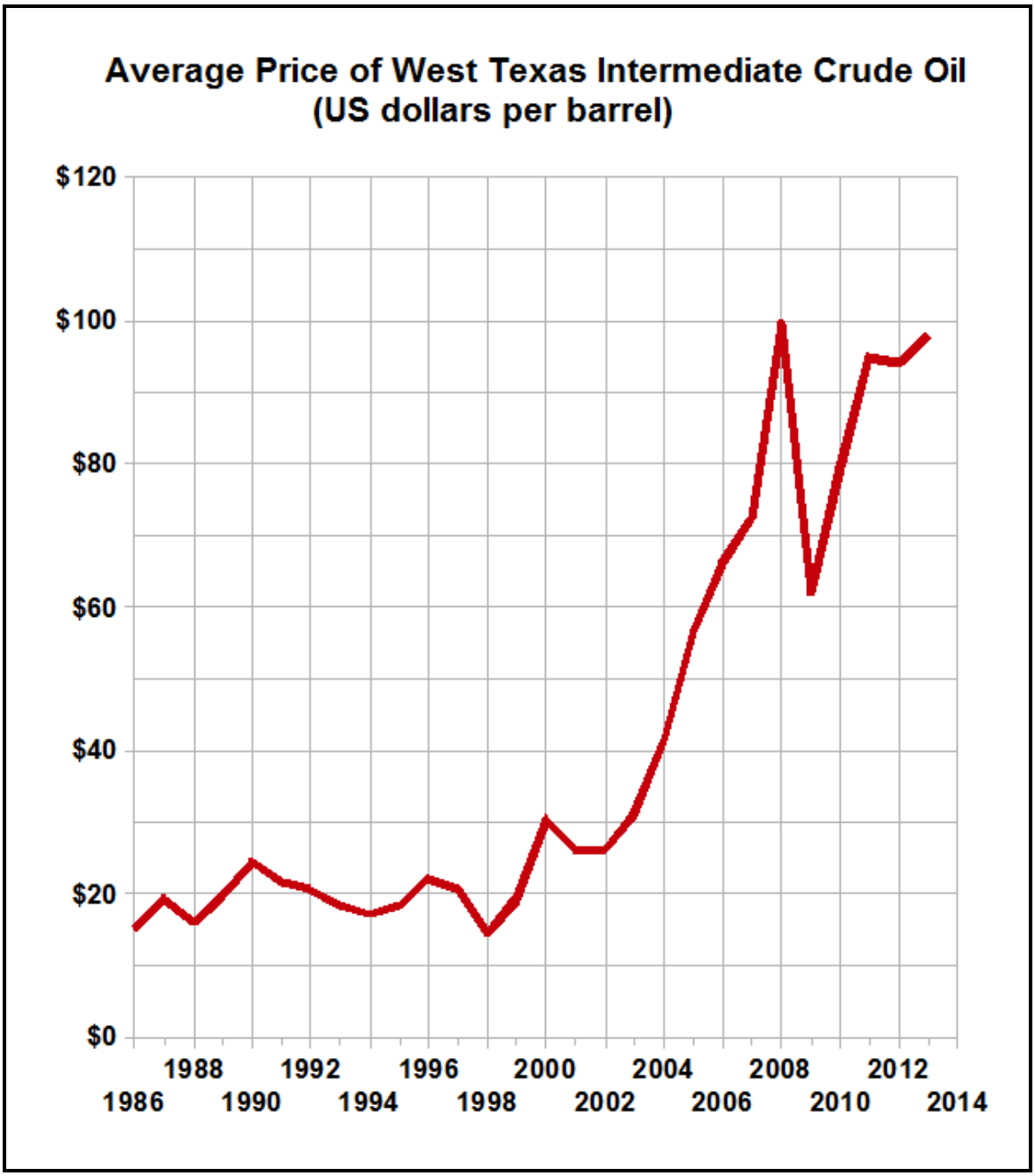

Figure 1 - Average price of West Texas Intermediate Crude Oil in USD per barrel.

Bio-based plasticizers derived from the oils of plants or from starch - such as castor, soybean, palm, grapeseed, sunflower and linseed – are being investigated as replacements for phthalate plasticizers. Plasticizers derived from plant oils contain double bonds which are often epoxidized to increase solubility in the PVC polymer.[8-10] The use

of bio-based stabilizers is hoped to introduce long-term sustainability to the PVC market due to the renewability of the feed-stock used for plasticizer production.

In order to maintain polymer performance after processing, thermal stabilizers such as metal soaps of stearates (ex. zinc stearate, calcium stearate) are also added to the PVC formulation.[4-5] While the thermal degradation and stabilization of PVC in the presence of phthalate plasticizers has been studied, the research is largely segmented and focused on model studies in reaction solvents. Chapter 2 details the integration of model studies and bulk PVC studies on the thermal degradation and stabilization of the polymer in the presence of stearate stabilizers and phthalate plasticizers. A comprehensive mechanism of the stabilization and degradation via zinc and calcium stearates is described. Furthermore, the development and investigation of new, novel stabilizers derived from natural products and their use in conjunction with phthalate and bio-based plasticizers is presented in Appendix A.

1.3 Design, Synthesis and Evaluation of Nonaqueous Silylamines for Efficient CO_2 Capture

Energy is a commodity that is in high demand in the United States, with 95 quadrillion BTUs of energy consumed in 2012 over all energy sectors (Figure 2). Electricity power generation is responsible for a major portion of the energy usage in the US (40%).[11] There is also rising concern over the emissions of greenhouse gasses such as carbon dioxide (CO_2) in the U.S. and their impact on the environment, and electric power generation is responsible for 34% of the total emissions of CO_2 in the nation.[12]

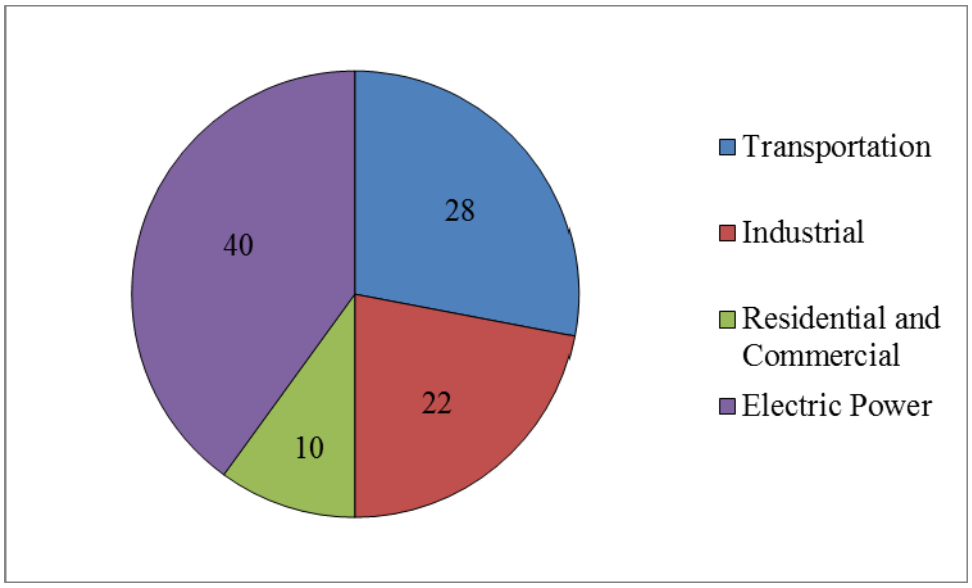

Figure 2 - 2012 US energy use by sector.

The majority of the electric power in the US is generated (41%) by coal-fired power plants (Figure 3). Alternative sources are available but individually account for only small percentages of electricity generation: renewable energy (12%), natural gas (24%), petroleum (1%), and nuclear (21%).[11] Coal remains the preferred method for energy generation due to the fact that it is an established industry, it is cheap, and coal is abundant. In fact, coal is projected to remain the predominant source of electricity generation through 2035 by the independent US Energy and Information Administration.[13] The administration predicts that coal will be accountable for 43% of the electricity generation in 2035, a number similar to now. However, energy use across the nation is predicted to increase annually at a rate of 0.7% through 2035, so the actual amount of coal used will increase significantly.[13]

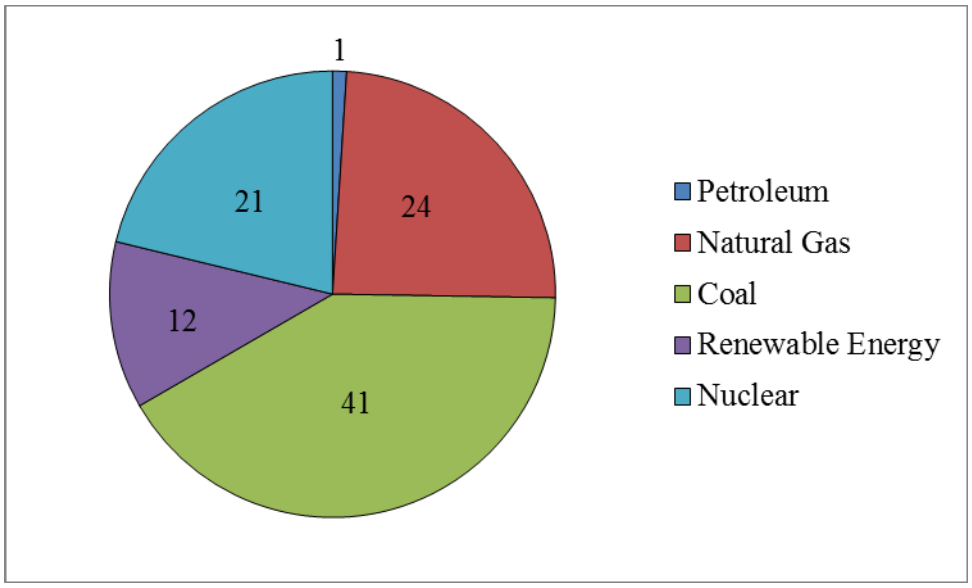

Figure 3 - 2012 US electric power generation by source.

Coal-fired power plants are the primary contributor to CO_2 emissions in terms of electricity generation. The electricity generated from coal emits more CO_2 per unit energy than natural gas and petroleum sources. An outline of the historical CO_2 emissions from electricity generation (coal, petroleum and natural gas) is displayed in Figure 4. In fact, approximately 79% of total CO_2 emissions from the electricity generation sector are attributed to coal.[13] Additionally, the Department of Energy predicts 94.5% of the CO_2 emissions from coal-fired power plants through 2020 will result from the coal-fired power plants already in operation.[14] As such, coal-fired power plants are and will remain a significant source of CO_2 emissions in terms of electricity generation. In order to mitigate CO_2 emissions from the electricity sector, effective CO_2 capture technologies which can be adapted to coal-fired power plants already in operation must be developed.

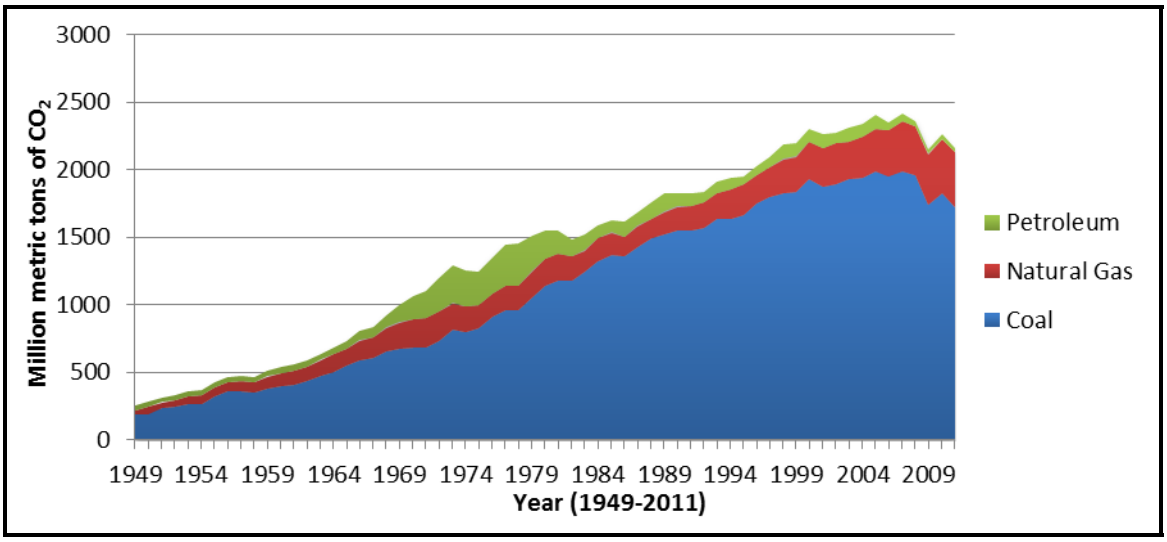

Figure 4 - US CO_2 emissions from electricity generation (1949-2011).

Numerous methods of CO_2 capture are being researched, and include the use of membranes, solid absorbents, and liquid solvents.[15-17] Membranes rely on size exclusion to achieve separation.[18-21] Solid adsorbents and liquid adsorbents both utilize either chemical reaction or physical absorption to capture CO_2.[15, 22-25] Liquid absorbents are considered the most developed of the two and current technologies that are able to capture CO_2 by chemical reaction have demonstrated 75-90% recoveries, producing a high purity CO_2 product stream.[26]

Chapter 3 presents the design, synthesis and evaluation of a novel class of liquid absorbents: reversible ionic liquids from silylamines for the capture and release of CO_2 in non-aqueous processes. Iterative structural modifications and the resulting effects on relevant CO_2 capture properties were utilized to establish structure-property relationships which could be used to develop solvents for particular applications and energy minimization goals.

1.4 Effect of CO_2 Pressure and pH on the Suzuki Coupling of Basic, Nitrogen Containing Substrates

Many pharmaceutical and biologically active molecules contain heterocyclic biaryl moieties, particularly nitrogen containing heterocycles such as pyridines.[27-31] Many synthetic methods have been utilized to couple aromatic reaction partners to form biaryl products. The Suzuki coupling reaction, a palladium catalyzed coupling of organohalides and organoborons, has emerged as the most versatile of the synthetic protocols.[31-34] The mild reaction conditions of the Suzuki reaction, along with a demonstrated tolerance towards a variety of functional groups and wide availability of substrates have promoted the rising popularity of the reaction. However, it has been reported that basic, nitrogen containing substrates are generally poor substrates for Suzuki couplings, reacting slowly and/or producing low yields of the desired products.[35-39] This is believed to be due to coordination of the amine to palladium decreasing reactivity of the catalyst.[35, 40-41] As a result, additional protection/deprotection strategies or expensive designer ligands are utilized to achieve reasonable rates and high yields.[35, 40, 42-43]

Entire textbooks exist detailing the use of, as well as the many different kinds of, protection/deprotection strategies.[44-45] However, the use of protection/deprotection strategies requires a minimum of two additional steps. The addition of these steps can drastically lower the efficiency of the synthesis process as well as lead to unwanted side reactions.[46] This strategy also results in an increased waste stream and decreased atom economy. The solvents and reagents utilized to protect and then deprotect the product, as well as the protecting group itself, are generally discarded. In general, Trost et al. have shown that for every kilogram of fine chemical and pharmecutical product produced, between 5-100 times that in chemical waste is generated.[47-49]

The addition of specially designed ligands also increases waste. The recycle of catalyst and ligands would be an ideal method to prevent added waste, however that is

one of the challenges of the Suzuki reaction that is still involved in ongoing investigations.[50] Some designer ligands are available commercially, but the additional cost can be prohibitive for certain processes. And if the designer ligand required is not commercially available, then added time, cost and manpower is required to produce them.

Industrially, it would be desirable to avoid both of these approaches. As an alternative to the typical strategies, Chapter 4 introduces the design of an efficient and simple system for the Suzuki coupling of 4-amino-2-halopyridines in quantitative yields by utilizing increased water content and CO_2 pressure with readily available triphenylphosphine-based ligands. CO_2 is regarded as a green solvent, as it is natural, renewable, non-flammable, nontoxic, and readily evaporating. It can be rapidly separated from products and catalysts by simple depressurization and can be recaptured for reuse. Further its ability to be recycled eliminates waste generation and no additional steps are required. The effect of CO_2 on the system is complex and the determination of the dominant factors involved is discussed.

1.5 References

1. Anastas, P. T.; Williamson, T. C., *Green Chemistry: Designing Chemistry for the Environment* 1 EPA: U. Washington, D.C., 1996.

2. Anastas, P. T.; Warner, J. C., Eds., *Green chemistry: theory and practice*. Oxford University Press: Oxford, England, 1998.

3. Manley, J. B.; Anastas, P. T.; Cue Jr., B. W., *Journal of Cleaner Production* **2008,** *16*, 743.

4. Minkser, K. S.; Zaikov, G. E., *Chemistry of Chlorine-Containing Polymers: Syntheses, Degradation, Stabilization*. NOVA Science Publishers: Huntington, 2000.

5. Wilkes, C. E.; Summers, J. W.; Daniels, C. A., *PVC Handbook*. Carl Hanser Verlag: 2005.

6. BBC. "What is driving oil prices so high?" 2007.

7. Europa 2005. europa.eu.

8. Bouchareb, B.; Benaniba, M. T., *Journal of Applied Polymer Science* **2007,** *107*, 3442.

9. Matthysen, L.; Martinz, D. O., *Solvay* **2011,** *2013*.

10. Sun, B.; Chaudhary, B. I.; Shen, C.-Y.; Mao, D.; Yuan, D.-M.; Dai, G.-C.; Li, B.; Cogen, J. M., *Polymer Engineering and Science* **2012**.

11. DOE U.S. Energy Information Administration, Primary Energy Consumption by Source and Sector, 2012. http://www.eia.gov/totalenergy/data/monthly/pdf/flow/primary_energy.pdf.

12. *U.S. Environmental Protection Agency* **2008**.

13. "Annual Energy Outlook 2011 with Projections to 2035," U.S. Energy Information Administration. 2011.

14. Ciferno, J. P.; Litynski, J. L.; Plasynski, S. I. "DOE/NETL Carbon Dioxide Capture and Storage RD&D Roadmap," *National Energy Technology Laboratory* [Online], 2010.

15. Aaron, D.; Tsouris, C., *Separation Science and Technology* **2005,** *401*, 321.

16. Han, S.; Huang, Y.; Watanabe, T.; Dai, Y.; Walton, K. S.; Nair, S.; Sholl, D. S.; Meredith, J. C., *ACS Combinatorial Science* **2012,** *14*, 263.

17. Jones, C. W., Annual Review of Chemical and Biomolecular Engineering. **2011,** *2*, 31.

18. Brunetti, A.; Scura, F.; Barbieri, G.; Drioli, E., *Journal of Membrane Science* **2010,** *359*, 115.

19. Lively, R. P.; Chance, R. R.; Kelley, B. T.; Deckman, H. W.; Drese, J. H.; Jones, C. W.; Koros, W. J., *Industrial & Engineering Chemistry Research* **2009,** *48*, 7314.

20. Powell, C. E.; Qiao, G. G., *Journal of Membrane Science* **2006,** *279*, 1.

21. Zhang, X.; He, X.; Gundersen, T., *Energy & Fuels* **2013,** *Articles ASAP*, Articles ASAP.

22. Burtch, N. C.; Jasuja, H.; Dubbeldam, D.; Walton, K. S., *Journal of the American Chemical Society* **2013,** *135*, 7172.

23. Choi, S.; Drese, J. H.; Eisenberger, P. M.; Jones, C. W., *Environmental Science and Technology* **2011,** *45*, 2420.

24. Didas, S. A.; Kulkarni, A. R.; Sholl, D. S.; Jones, C. W., *ChemSusChem* **2012,** *5*, 2058.

25. Switzer, J. R.; Ethier, A. L.; Flack, K. M.; Biddinger, E. J.; Gelbaum, L.; Pollet, P.; Eckert, C., A; Liotta, C. L., Enhanced CO_2 Cpature with Silylamines by Carbamic Acid Stabilization. *Industrial & Engineering Chemistry Research* **2013,** *52* (13), 13159-13160.

26. Kohl, A. L.; Nielsen, R., *Gas purification*. 5th ed.; Gulf Publishing Company: Houston, 1997.

27. Bansal, Y.; Silakari, O., The therapeutic journey of benzimidazoles: A review. *Bioorgan Med Chem* **2012,** *20* (21), 6208-6236.

28. Boren, J.; Cascante, M.; Marin, S.; Comin-Anduix, B.; Centelles, J. J.; Lim, S.; Bassilian, S.; Ahmed, S.; Lee, W. N. P.; Boros, L. G., Gleevec (ST1571) influences metabolic enzyme activities and glucose carbon flow toward nucleic acid and fatty acid synthesis in myeloid tumor cells. *J Biol Chem* **2001,** *276* (41), 37747-37753.

29. Cerecetto, H.; Gerpe, A.; Gonzalez, M.; Aran, V. J.; de Ocariz, C. O., Pharmacological properties of indazole derivatives: Recent developments. *Mini-Rev Med Chem* **2005,** *5* (10), 869-878.

30. Criscione, L.; Degasparo, M.; Buhlmayer, P.; Whitebread, S.; Ramjoue, H. P. R.; Wood, J., Pharmacological Profile of Valsartan - a Potent, Orally-Active, Nonpeptide Antagonist of the Angiotensin-Ii At1-Receptor Subtype. *Brit J Pharmacol* **1993,** *110* (2), 761-771.

31. Roughley, S. D.; Jordan, A. M., The Medicinal Chemist's Toolbox: An Analysis of Reactions Used in the Pursuit of Drug Candidates. *J Med Chem* **2011,** *54* (10), 3451-3479.

32. Bellina, F.; Carpita, A.; Rossi, R., Palladium catalysts for the Suzuki cross-coupling reaction: An overview of recent advances. *Synthesis-Stuttgart* **2004,** (15), 2419-2440.

33. Miyaura, N.; Suzuki, A., Palladium-Catalyzed Cross-Coupling Reactions of Organoboron Compounds. *Chem Rev* **1995,** *95*, 2457-2483.

34. Suzuki, A., Cross-coupling reactions of organoboranes: an easy way to construct C-C bonds (Nobel Lecture). *Angew Chem Int Ed Engl* **2011,** *50* (30), 6722-37.

35. Itoh, T.; Mase, T., Direct synthesis of hetero-biaryl compounds containing an unprotected NH2 group via Suzuki–Miyaura reaction. *Tetrahedron Lett* **2005,** *46* (20), 3573-3577.

36. Norcross, R. D. Thiazolopyridine. March 24, 2005, 2005.

37. Thompson, A. E.; Hughes, G.; Batsanov, A. S.; Bryce, M. R.; Parry, P. R.; Tarbit, B., Palladium-catalyzed cross-coupling reactions of pyridylboronic acids with heteroaryl halides bearing a primary amine group: Synthesis of highly substituted bipyridines and pyrazinopyridines. *Journal of Organic Chemistry* **2005,** *70* (1), 388-390.

38. Vagnini, M. T.; Smeigh, A. L.; Blakemore, J. D.; Eaton, S. W.; Schley, N. D.; D'Souza, F.; Crabtree, R. H.; Brudvig, G. W.; Co, D. T.; Wasielewski, M. R., Ultrafast photodriven intramolecular electron transfer from an iridium-based water-oxidation catalyst to perylene diimide derivatives. *P Natl Acad Sci USA* **2012,** *109* (39), 15651-15656.

39. Wang, K.; Fu, Q.; Zhou, R.; Zheng, X.; Fu, H. Y.; Chen, H.; Li, R. X., Tetraphosphine/palladium-catalyzed Suzuki–Miyaura coupling of heteroaryl halides with 3-pyridine-and 3-thiopheneboronic acid: an efficient catalyst for the formation of biheteroaryls. *Applied Organicmetallic Chemistry* **2013,** *27* (4), 232-238.

40. Lee, D. H.; Choi, M.; Yu, B. W.; Ryoo, R.; Taher, A.; Hossain, S.; Jin, M. J., Expanded Heterogeneous Suzuki-Miyaura Coupling Reactions of Aryl and Heteroaryl Chlorides under Mild Conditions. *Advanced Synthesis & Catalysis* **2009,** *351* (17), 2912-2920.

41. Wagaw, S.; Buchwald, S. L., The Synthesis of Aminopyridines: A Method Employing Palladium-Catalyzed Carbon-Nitrogen Bond Formation. *J Org Chem* **1996,** *61*, 7240-7241.

42. Caron, S.; Massett, S.; Bogle, D.; Castaldi, M.; Braish, T., An Efficient and Cost-Effective Synthesis of 2-Phenyl-3-aminopyridine. *Org Proc R&D* **2001,** *5*, 254-256.

43. MARTIN, R.; BUCHWALD, S. L., Palladium-Catalyzed Suzuki-Miyaura Cross-Coupling Reactions Employing Dialkylbiaryl Phosphine Ligands. *Accounts Chem Res* **2008,** *41* (11), 1461-1473.

44. Kocienski, P. J., *Protecting Group*. 3 ed.; Thieme: New York, 2005.

45. Wuts, P. G. M., *Greene's protective groups in organic synthesis;*. 4 ed.; Wiley-Interscience: Hoboken, N.J, 2007.

46. Sierra, M. A.; de la Torre, M. C., *Dead Ends and Detours, Direct Ways to Successful Total Synthesis*. Wiley-VCH: Weinheim, 2004.

47. Sheldon, R. A., *Green Chemistry* **2007,** *9*, 1273.

48. Trost, B. M., *Science* **1991,** *254*, 1471.

49. Trost, B. M., *PNAS* **2008,** *105*, 13197.

50. Phan, N. T. S.; Van Der Sluys, M.; Jones, C. W., On the Nature of the Active Species in Palladium Catalyzed Mizoroki–Heck and Suzuki–Miyaura Couplings – Homogeneous or Heterogeneous Catalysis, A Critical Review. *Advanced Synthesis & Catalysis* **2006,** *348* (6), 609-679.

CHAPTER 2

Degradation and Stabilization of Polyvinyl Chloride: Integrating Model and Bulk Polymer Studies

2.1 Introduction

Maintaining the structure of polyvinyl chloride (PVC) is vital for maintaining the polymer's performance after processing. Exposure to high temperatures, like what is seen during processing and extrusion, can initiate a thermal degradation of PVC which continues even after cooling, though at a slower rate. This degradation process, dehydrochlorination, results in the formation of conjugated double bonds along the backbone of the polymer which results in decreased polymer performance.[1] As such, typical polymer formulations include additives to enhance the desired polymer properties, such as plasticizers (diisodecyl phthalate, expoxidized soybean oil, etc.) and thermal stabilizers (Zn, Ca, Sn or Be stearate salts, etc.). Thermal stabilizers are generally utilized to great effect; however, a fundamental understanding of the mechanisms of degradation and stabilization for these formulations remains somewhat fragmented.

Dehydrochlorination occurs through the loss of HCl from a labile chlorine, for example an allylic chlorine, to form a double bond (Figure 5). The degradation process is autocatalytic because the HCl released then catalyzes further degradation - by coordinating to a labile chlorine and assisting the chlorine's removal - to release more HCl and increase conjugation. The increased conjugation produces undesirable color in the polymer system, changes the polymer's properties, and also destabilizes the system towards further degradation (multiple double bonds in conjugation with a chlorine weaken the C-Cl bond by resonance). Stabilizers such as zinc and calcium stearates

($ZnSt_2$, $CaSt_2$) are thought to stabilize the system by both absorbing HCl released during dehydrochlorination and substituting the stearate for the labile chlorine to form a more stable ester and prevent further degradation.[2-4] Reaction of HCl with metal stearates forms stearic acid, a weaker acid than HCl, and $ZnCl_2$. The steric bulk of stearic acid would likely prevent coordination to labile chlorines so it is less likely to catalyze degradation than HCl. $ZnCl_2$, however, is a strong Lewis acid which can further degradation by coordinating to labile chlorines and promoting dehydrochlorination. The most effective PVC formulations include $CaSt_2$. $CaSt_2$ reacts with $ZnCl_2$ to produce $ZnSt_2$ and $CaCl_2$, preventing the strong Lewis acid from furthering the degradation of PVC.[5-7]

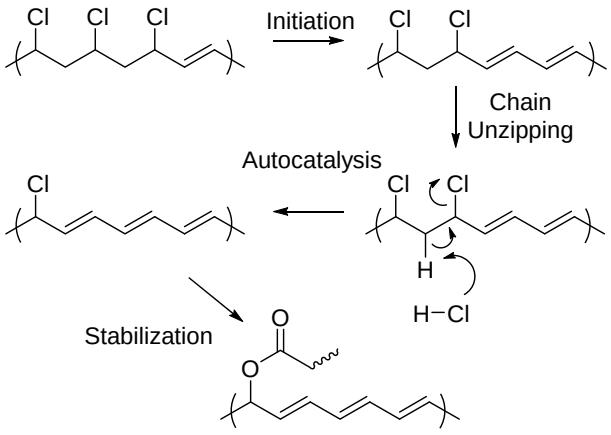

Figure 5 - Degradation, chain unzipping, autocatalysis, and stabilization of PVC.

The localized structural changes that arise due to degradation within the polymer matrix, however, are difficult to observe, analyze, quantify and interpret. Analysis of the bulk PVC formulations through standard analytical techniques is therefore complex and fundamental investigations are often approached *via* model studies instead. PVC models are chosen to represent micro-structures found in the polymer due to differing stereochemical orientations (tacticity) and/or defects which form during synthesis of the

polymer. In general, PVC consists of alternating -CH_2- and -CHCl- units which display different areas of tacticity: isotactic, syndiotactic and atactic (Figure 6). However, there are additional structural features which form during polymerization and are considered defects. Common defects found in PVC include allylic, tertiary and vicinal defects. Some of these defects are generally considered to be "weak points" and the initiation points for thermal degradation.[2, 5, 8-9]

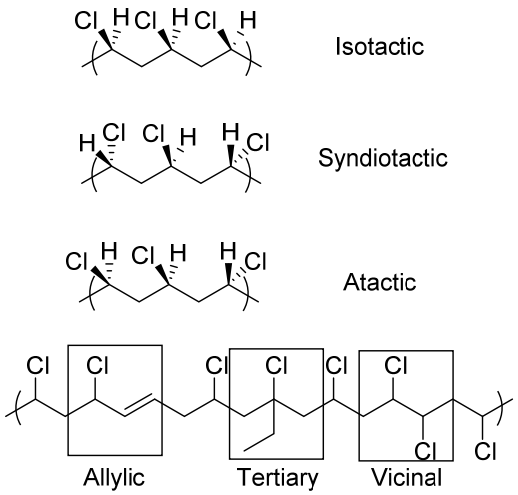

Figure 6 - Microstructures commonly observed in PVC.

Model studies are in fact the major approach utilized to understand the mechanisms of degradation and stabilization of PVC.[10-18] Though a great deal of useful information has been provided by these studies, some used dilute solutions of model compounds which is not an accurate portrayal of the PVC system; still others do not investigate the commercial $ZnSt_2$/$CaSt_2$ stabilizer systems currently in use.[19-20] We have investigated the kinetics of neat model systems with model acetates and with $ZnSt_2$ and

$CaSt_2$ combinations. Specifically, we utilized "naked" acetates - formed by the reaction of sodium acetate (NaOAc) with a phase transfer catalyst (PTC) to yield the acetate anion in the presence of a non-coordinating cation - in reactions with neat PVC models to isolate the effect of the carboxylate. Kinetics and product formation were analyzed for each PVC model. Also, the color stability and model conversion of the reaction of 2,4-dichloropentane and combinations of $ZnSt_2$ and $CaSt_2$ were observed. This information was combined with thermal stability through thermogravimetric analysis (TGA) and color stability studies on bulk polymer formulations (with diisodecyl phthalate (DIDP) plasticizer and combinations of $ZnSt_2$ and $CaSt_2$) to propose a comprehensive mechanism for the degradation and stabilization of PVC with zinc and calcium stearates.

2.2 Results and Discussion

A library of model compounds was designed to investigate the kinetics of critical micro-structures present in the PVC backbone (Table 2). The kinetics of primary versus secondary chlorines were investigated with 1,3-dichlorobutane (**1**). **1** was also utilized to determine the kinetics of calcium, zinc and sodium acetates and optimum reaction conditions for the subsequent model studies. 2,4-Dichloropentane (**2**) afforded the opportunity to survey the kinetics of defect-free, isotactic versus syndiotactic regions by observing the kinetics of the *meso*- and enantiomeric pair ((2*R*,4*R*)- and (2*S*,4*S*)-) stereoisomers, respectively. The kinetics of the most common defects were probed through reactions of models **3**-**6**. The kinetics of reaction at tertiary chlorines were determined with 3-chloro-3-ethylpentane (**3**). Vicinal chlorines, or chlorines on carbons directly adjacent, were modeled by a mixture of *meso*- and *d,l*-3,4-dichlorohexane (**4**). 3-Chloro-1-butene (**5**) and (E)-6-chlorononon-4-ene (**6**) were chosen to investigate the kinetics of allylic micro-structures.

These models were utilized in the studies of: (1) the kinetics and product identification for the reaction with "naked" acetate nucleophiles to understand the effect

of the carboxylate ion separate from a coordinating cation; and (2) the qualitative kinetics and color stability of 2,4-dichloropentane with combinations of $CaSt_2$ and $ZnSt_2$ to observe the effect of sterically hindered systems incorporating coordinating cations. Four of the model compounds were synthesized for use in the kinetic studies. General descriptions are provided in the next section. Detailed descriptions of the syntheses are located in the experimental section (**Section 2.5**).

Table 2 - Model compound library.

#	Structure	Model	Source
1	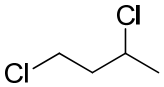	1° Cl 2° Cl	Commercial
2	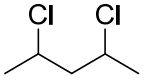	2° Cl Tacticity	Synthesized
3	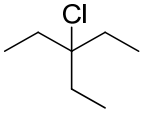	3° Cl	Synthesized
4	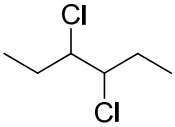	Vicinal	Synthesized
5	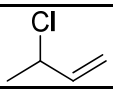	Allylic	Commercial
6	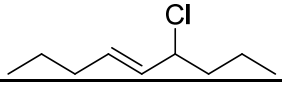	Allylic	Synthesized

2.2.1 Synthesis of Model Compounds

2.2.1.1 Synthesis of 2,4-Dichloropentane from Acetylacetone[21]

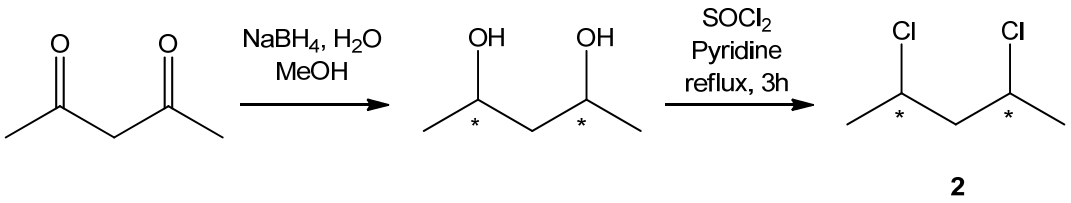

Figure 7 - Synthesis of 2,4-dichloropentane.

2,4-Dichloropentane was synthesized in two steps from acetylacetone (Figure 7). A solution of acetylacetone in methanol was added dropwise to a solution sodium borohydride ($NaBH_4$,) and (NaOH) in water (25 mL) at 20°C. The mixture was stirred for 15 minutes. The solvent was then removed *in vacuo*, yielding a white solid. The solid was then extracted into glycerol (50 mL). The extract was distilled at 60-70°C (0.45 mmHg) and, subsequently, fractionally distilled at 70-75°C (3.5 mmHg) in order to remove trace amounts of glycerol. of 2,4-pentanediol (1) as a colorless liquid was obtained in 60% yield.

Chlorination of 2,4-pentanediol was achieved by the dropwise addition of thionyl chloride ($SOCl_2$) to a solution of 2,4-pentanediol in pyridine at 0°C under an argon atmosphere. The mixture was refluxed for 3 hours. After the reaction was cooled to room temperature, ice was added to quench any unreacted $SOCl_2$. The mixture was extracted twice with diethyl ether and the combined organic layers were dried over magnesium sulfate ($MgSO_4$) and the solvent removed *in vacuo* (75 mmHg). Distillation (140-150°C, atm. pressure) yielded 41% yield of 2,4-dichloropentane (2) as a colorless liquid. ^{1}H and ^{13}C NMR were utilized to confirm product formation and purity. 2,4-Dichloropentane

incorporates two stereoisomers: *meso* **2a** and enantiomeric pair (*d,l*-) **2b** in a diastereomeric ratio of 1:6, respectively.

2.2.1.2 Synthesis of 3-chloro-3-ethylpentane (3) from 3-ethyl-3-pentanol [22]

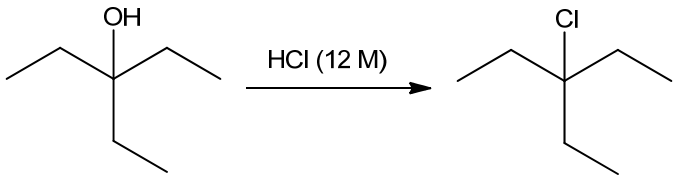

3

Figure 8 - Synthesis of 3-chloro-3-ethylpentane.

S_N1 substitution of the hydroxyl group of 3-ethyl-3-pentanol was achieved by simply stirring hydrochloric acid (HCl) with 3-ethyl-3-pentanol (Figure 8). The biphasic mixture was stirred at room temperature for 2 hours. The organic layer was then separated, dried over magnesium sulfate and purified over a silica plug with hexanes as the eluent. The solvent was removed under vacuum at 75 mmHg, 25°C to yield 90% of 3-chloro-3-ethylpentane (3) as a clear liquid. Product formation and purity were confirmed by ^{1}H and ^{13}C NMR.

2.2.1.3 Synthesis of 3,4-dichlorohexane (4) from 3-hexene [23]

4

Figure 9 - Synthesis of 3,4-dichlorohexane.

Phosphorus pentachloride (PCl_5) suspended in carbon tetrachloride (CCl_4) was utilized to add chlorine across the double bond of 3-hexene (Figure 9). The suspension was heated to 50°C and 3-hexene was slowly added to the suspension and stirred overnight at 50ºC. The byproduct, PCl_5, and solvent were removed by distillation. The product was purified by distillation at 12-14 mmHg and 40°C to 20% yield of 3,4-dichlorohexane as a clear liquid. Product formation and purity were confirmed by ^{1}H and ^{13}C NMR. 3,4-Dichlorohexane also incorporates two stereoisomers: *meso* **2a** and enantiomeric pair (*d,l*-) **2b** in a diastereomeric ratio of 1:4, respectively.

2.2.1.4 Synthesis of (*E*)-6-Chloronon-4-ene (5) from *trans*-2-hexen-1-al[24]

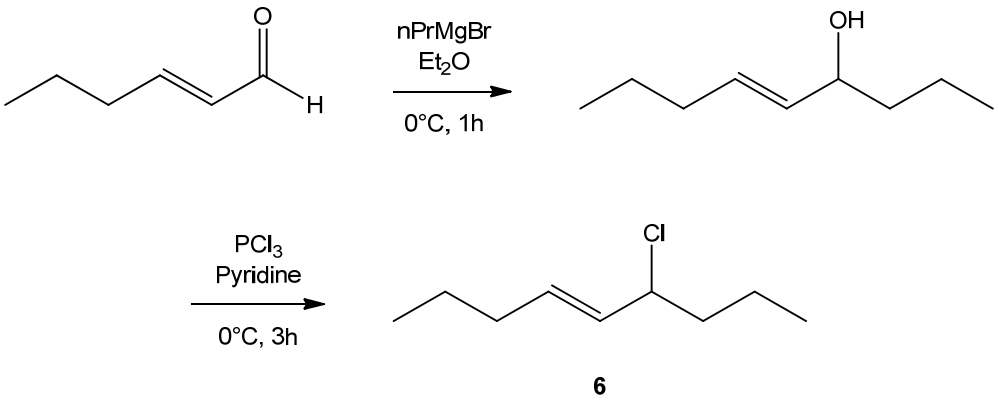

Figure 10 - Synthesis of (*E*)-6-chloronon-4-ene.

(*E*)-6-Chloronon-4-ene was prepared in two steps from *trans*-2-hexen-1-al (Figure 10). Grignard addition of n-propylmagnesium (nPrMgBr) bromide to *trans*-2-hexen-1-al in anhydrous diethyl ether (Et_2O) was achieved over the course of 30 min at 0°C. The resulting pale yellow mixture was stirred for 1 hour at room temperature. After 1 hour, the reaction mixture was quenched with a saturated aqueous ammonium chloride solution (NH_4Cl). The organic layer was separated and the aqueous layer was extracted with Et_2O. The combined organic layers were dried over $MgSO_4$ and the solvent was removed to yield 88% yield of (*E*)-non-4-ene-6-ol (5) as a pale yellow oil.

Substitution of the chlorine was then achieved by the drop wise addition of phosphorous trichloride (PCl_3) to (*E*)-non-4-ene-6-ol and anhydrous pyridine at 0°C. The resulting pale yellow mixture was stirred for 3 hours at 0 °C. After 3 hours, the upper layer was separated and distilled at reduced pressure (31 °C, 0.3 mmHg) to yield 70% of (E)-6-chloronon-4-ene as a pale yellow oil. Product formation and purity were confirmed by ^{1}H and ^{13}C NMR.

2.2.2 Kinetic Studies of Model Compounds and "Naked" Acetate

Previous model studies have involved various solvents such as THF or o-dichlorobenzene.[14, 18, 20] We chose instead to utilize neat models as both solvent and reactant to avoid solvent effects and more closely approximate bulk PVC formulations. To simplify analysis metal acetates were initially employed as models for metal stearates. We conjecture that the relative rates of reaction for the acetates will be similar to the metal stearates in PVC, as the size of the ligand does not drastically affect substitution rate relative to each other.[12]

Various metal stabilizers such as dibutyltin diacetate, dibutyltin dilaurate, or salts of cadmium, zinc, lead and barium have been investigated previously.[12-13, 17] However, these stabilizers involve a coordinating cation. It is important to note at this point that the model acetates were not soluble in the PVC models. We chose to utilize a PTC, tetra-n-butylammonium chloride, to improve the solubility of the acetate ion and to determine the effect of the "naked" acetate. The tetra-n-butylammonium cation is non-coordinating and would not be involved the reaction, it merely acts as a shuttle for the otherwise insoluble acetate ion into the model compound. The goal of this study was to determine the relative kinetics and to identify the products formed from the substitution (stabilization) or degradation (elimination) of the various micro-structures represented by the model compounds (Figure 11).

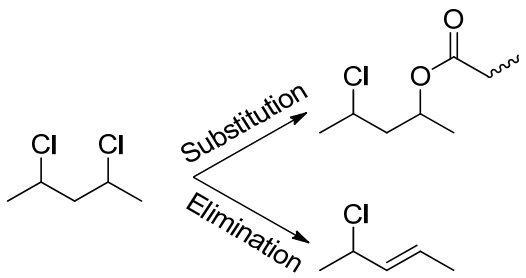

Figure 11 – Reaction pathways of model compounds and metal carboxylates: stabilization (substitution) and elimination (degradation).

1,3-Dichlorobutane was reacted with zinc, calcium and sodium acetates in the presence of PTC at 100°C for 20 hours. Tetradecane was added as an internal standard and THF was utilized to dilute the sample for GC/MS analysis after reaction. Each reaction was repeated at least twice for reproducibility. A representative GC chromatogram of the reaction mixtures is shown below (Figure 12). The peaks were identified using mass spectroscopy as: 'a' – THF; 'b' – 1,3-dichlorobutane; 'c' 4-chlorobutan-2-yl acetate; 'd' – 3-chlorobutyl acetate; 'e' – butane-1,3-diyl diacetate; 'f' - PTC. For the reaction with sodium acetate, substitution mainly occurred at the primary position, producing a majority of 3-chlorobutyl acetate (d). Smaller amounts of mono-substitution occurred at the secondary position producing 4-chlorobutan-2-yl acetate (c). The di-substituted product, butane-1,3-diyl diacetate (e), was also formed in a similar ratio to the secondary mono-substitution product (c). No elimination products were observed. The same product distributions were observed for calcium and zinc acetates.

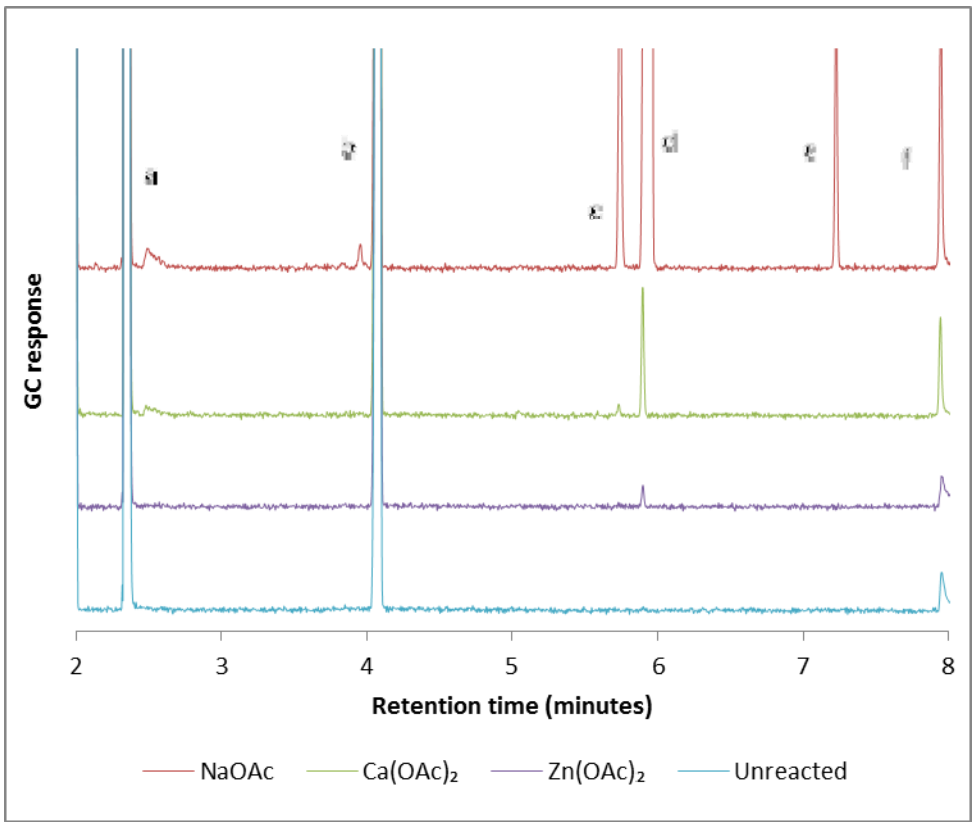

Figure 12 - GC chromatograph of the reaction of 1,3-dichlorobenzene (0.04 mol) with NaOAc, $Ca(OAc)_2$, and $Zn(OAc)_2$ (0.02 mol $^-$OAc) in the presence of PTC (0.001 mol) at 100 °C with added tetradecane (0.001 mol) as internal standard. Reaction proceeded for 20 hours. Peaks were identified using mass spectroscopy as: 'a' – THF; 'b' – 1,3-dichlorobutane; 'c' 4-chlorobutan-2-yl acetate; 'd' – 3-chlorobutyl acetate; 'e' – butane-1,3-diyl diacetate; 'f' - PTC.

As no sign of elimination was seen, both primary and secondary chlorines appear to be primarily susceptible to substitution by the "naked" acetate. The primary chlorine underwent substitution first, followed by the secondary chlorine, as expected. The mechanism for acetate substitution of 1,3-dichlorobutane is outline in Figure 13.

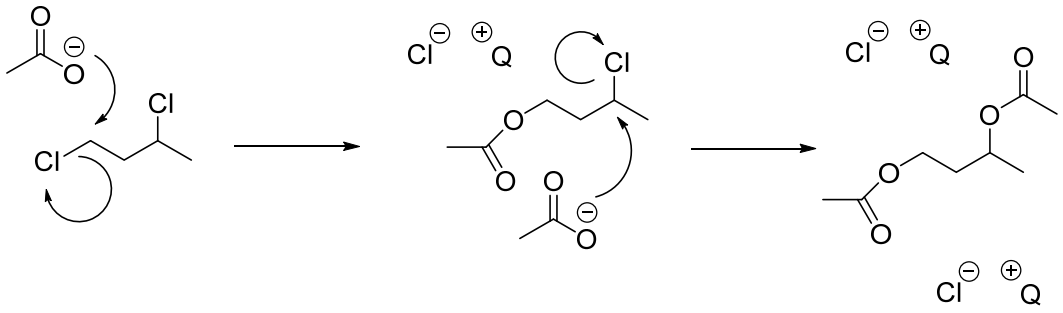

Figure 13 - Mechanism of acetate substitution on 1,3-dichlorobutane.

The kinetics of each reaction were determined from the starting material conversion, based on the integration of GC areas. The ratio of the starting material area to the combined product and starting material areas was used to determine conversion. Representative examples of conversion versus time for *meso*- and enantiomeric (*d,l*)-2,4-dichloropentane and (*E*)-6-chloronon-4-ene are shown in Figure 14. The conversion of enantiomeric 2,4-dichloropentane (13% after 26 hours) proceeds at a slower rate than the conversion of the *meso* isomer (38% after 26 hours). The allylic model, (*E*)-6-chloronon-4-ene demonstrated the fastest conversion of the three with a conversion of 92% after 24 hours.

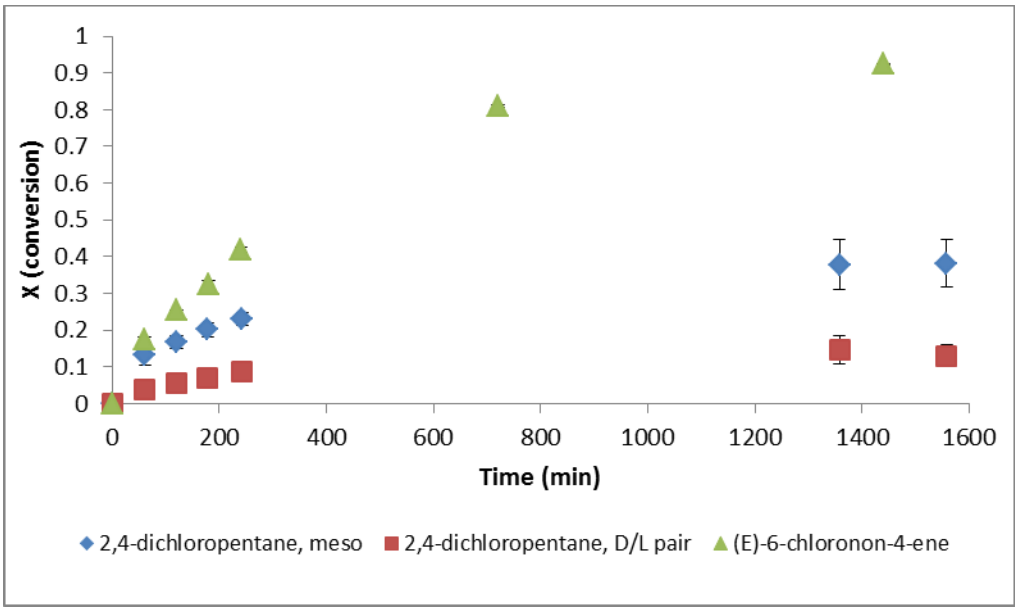

Figure 14 - Conversion versus time for the reactions of 2,4-dichloropentane with NaOAc (*meso*- and *d,l*- isomers) and of (*E*)-6-chlorononon-4-ene with NaOAc, at 100 °C in the presence of PTC.

Pseudo-first order reaction rate constants (k_{pseudo}) were determined for the reaction of 1,3-dichlorobutane (Table 3) with each metal acetate/PTC system, and for the reaction of each model compound with sodium acetate/PTC system (Table 4). The pseudo-first order reaction rate constants were determined given

$$-\frac{dC_1}{dt} = kC_1 C_{MOAc} = k_{pseudo} C_1$$

where k is the reaction rate constant, C_1 is the concentration of the model compound and C_{MOAc} is the concentration of the acetate anion (assumed to be constant due to the presence of a PTC[25]). The solution of the differential equation gives

$$(1 - X) = e^{-kt}$$

where X is conversion of the model compound. Plotting ln(1-X) vs time gives a slope equal to -*k*. Examples of these plots for *meso*- and *d,l*-2,4-dichloropentante and (*E*)-6-chloronon-4-ene are shown in Figure 15.

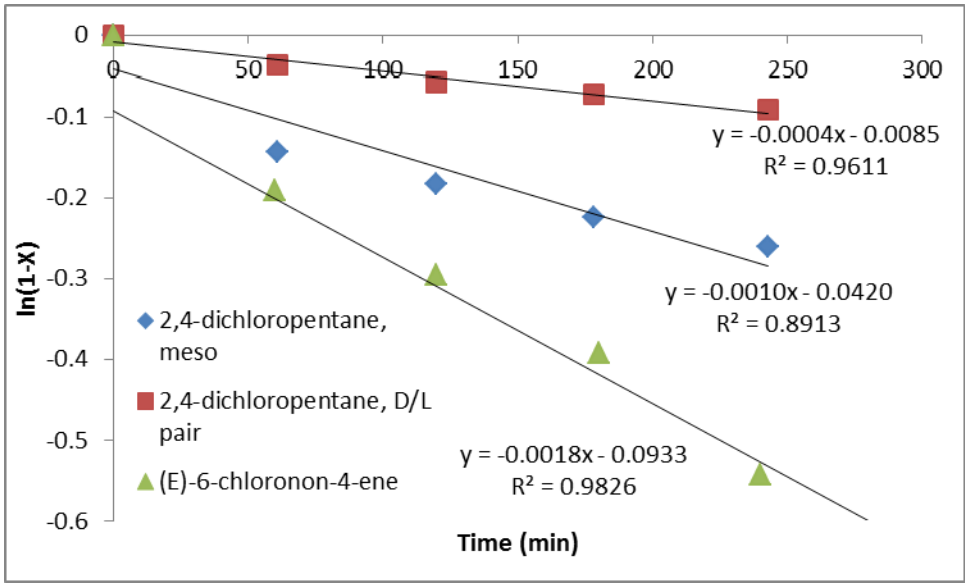

Figure 15 - Kinetic plot for the reactions of *meso*-, *d,l*-2,4-dichloropentane and (*E*)-6-chloronon-4-ene with NaOAc at 100 °C in the presence of PTC.

The rate of conversion of **1** (Table 3) increases from zinc ($4.5 \cdot 10^{-4}$ min^{-1}) to calcium ($1.4 \cdot 10^{-4}$ min^{-1}) to sodium acetate ($0.5 \cdot 10^{-4}$ min^{-1}). However, the product distributions, as discussed above, were unchanged between the three acetates. Thus, the size of the cation in solution with the acetate ion is not changing, or we would see a different distribution between both mono and di-substituted products. Instead, the amount of acetate ion in solution is different, which suggests the PTC is more effective at solubilizing NaOAc. The increased reaction rate of the sodium acetate/PTC system led us to utilize this system in the kinetic studies of each model compound.

Table 3 - Pseudo-first order reaction rate constants for 1,3-dichlorobutane with metal acetate/PTC. 1,3-Dichlorobutane with various metal acetates (1 eq $^-$OAc) and tetra-n-butylammonium chloride (0.010 eq) at 100°C.

Metal Acetate	k_{pseudo} k_{app} ($\cdot 10^{-4}$ min^{-1})
NaOAc	4.45 ± 0.13
$Ca(OAc)_2$	1.35 ± 0.22
$Zn(OAc)_2$	0.510 ± 0.102

Table 4 - Pseudo-first order reaction rate constants and major products for the reaction of model compounds with sodium acetate (0.1 eq NaOAc) at 100°C.

#	Structure	k_{pseudo} ($\cdot 10^{-4}$ min^{-1})	Major Products
1	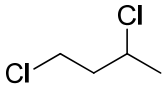	4.45 ± 0.13	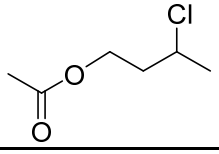
2a	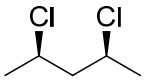	9.99 ± 0.64	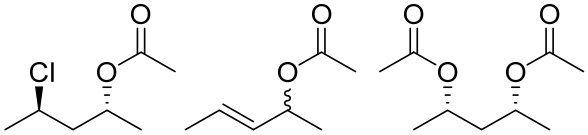
2b	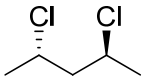	3.56 ± 0.27	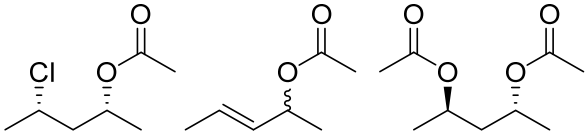
3[1]	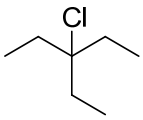	3.91 ± 1.28[2]	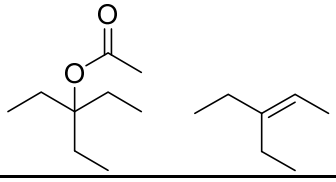
4a	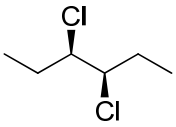	2.25 ± 0.13	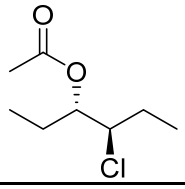
4b	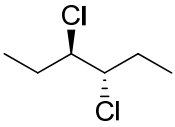	0.40 ± 0.25	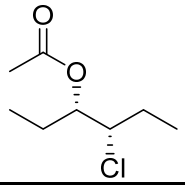
5[3]	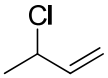	27.8 ± 2.1	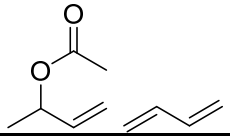
6[4]	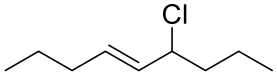	18.1 ± 0.13	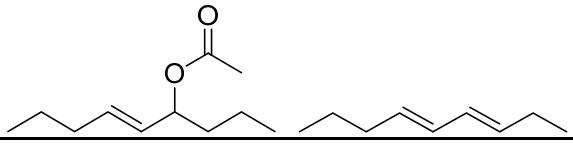

[1]Substitution product seen during first hour; disappeared by end of reaction

[2]Proceeds via a zero-order reaction (k_{app} units of 10^{-4} mol $min^{-1}L^{-1}$)

[3]Butadiene is not actually observed due to its volatility; it is a hypothesized product of this reaction

[4]Substitution product observed through 4 hours; disappeared by end of reaction

The reaction rates and major products for the different model compounds with 0.1 eq sodium acetate and PTC at 100°C are outlined in Table 4. The defect-free model 2,4-dichloropentane incorporates two stereoisomers: *meso* **2a** and enantiomeric pair (*d,l*-) **2b** in a diastereomeric ratio of 1:6 respectively. Each stereoisomer corresponds to a different region of tacticity in the PVC polymer: isotactic (*meso*) and syndiotactic (enantiomeric pair). Also, the stereoisomers are each clearly discernable by GC-MS and NMR and the conversions were followed separately. In the reaction of 2,4-dichloropentane with NaOAc/PTC at 100°C, the *meso*-isomer **2a** ($9.99 \cdot 10^{-4}$ min^{-1}) reacts more than twice as fast as **2b**, ($3.56 \cdot 10^{-4}$ min^{-1}) while both isomers form primarily 4-chloropentan-2-yl acetate and eventually pentan-2,4-diyl acetate. This supports literature reports which state that isotactic PVC is more readily stabilized toward S_N2 substitution, with sodium thiopentate in cyclohexanone, than syndiotactic.[26-27] In contrast to 1,3-dichlorobutane, some partial elimination of 2,4-dichloropentane was observed. The partial elimination product pent-3-en-2-yl acetate was observed in a ratio of 4:1 monosubstitution products to elimination products. However, no sign of complete elimination of 2,4-dichloropentane (pentadiene) was observed.

The "naked" acetate anion has higher basicity and nucleophilicity than coordinated acetate and is expected to follow a bimolecular S_N2 mechanism for substitution and a bimolecular mechanism for elimination (Figure 16). The faster reaction rate of the *meso*-isomer over the enantiomeric pair supports this mechanism. Substitution is expected to occur before elimination as 4-chloro-2-pentene was not detected.

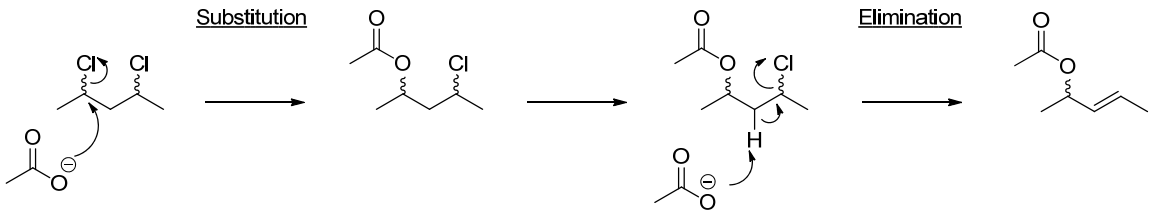

Figure 16 - Substitution and elimination mechanisms of 2,4-dichloropentane with "naked" acetate.

In the reaction with NaOAc/PTC at 100°C, tertiary chlorine 3-chloro-3-ethylpentane (**3**) exhibited a small amount of the substitution product 3-ethylpentan-3-yl after 1 hour but the only product observed after 1 day was the eliminated product 3-ethylpent-2-ene. Dissociation of the tertiary chlorine, even in non-polar conditions, is rapid enough to occur significantly. It is also unlikely that substitution would occur through an S_N2 mechanism, due to the steric bulk of the ethyl groups. Therefore, substitution likely occurs through an S_N1 mechanism. Conversion of **3** displays zero-order kinetics (k_{pseudo}: $3.91 \cdot 10^{-4}$ min^{-1}) which corresponds with an S_N1 mechanism, as the rate is dependent on the maximum possible amount of dissociated chloride ions in solution.

The vicinal defect model 3,4-dichlorohexane is a mixture of *meso*- (**4a**) and enantiomeric pair (**4b**) isomers. The vicinal models react slowly (k_{pseudo} of **4a**: $2.25 \cdot 10^{-4}$ min^{-1}; k_{pseudo} of **4b**: $0.40 \cdot 10^{-4}$ min^{-1}) compared to the defect-free PVC models **2a** and **2b**, though they react in a similar manner with the *meso*-isomer reacting almost six times faster than the enantiomeric pair. This can again be explained by sterics of the adjacent chlorines which block attack by the “naked” acetate, which is even greater when the chlorines are on adjacent carbons. Product distributions between mono and di-substituted products are similar to **2a** and **2b**. It is unlikely, however, that the vicinal defect plays a significant role in degradation or stabilization of PVC.

Allylic model 3-chloro-1-butene (**5**) was obtained commercially. The reaction of NaOAc/PTC with allylic models **5** and (E)-6-chloro-4-nonene (**6**) yielded substitution

products. No elimination products were observed for **5**. However, 1,3-butadiene is a volatile product (-4.4°C boiling point) which would not likely remain in the reaction mixture. The internal allylic model **6**, whose longer side chains more closely resemble PVC as compared to **5**, shows mainly substitution in the first 4 hours which then rapidly converts to the elimination product nona-3,5-diene. After 24 hours nearly all of **6** was converted to the elimination product and there was no sign of the substitution product. Rate of reaction for both was fast: **5**, k_{pseudo}: $27.8 \cdot 10^{-4}$ min^{-1}; **6**, k_{pseudo}: $18.1 \cdot 10^{-4}$ min^{-1}.

Allylic and tertiary chlorines are labile chlorines in the PVC system. However, of the three models for these "labile" defects, the tertiary model **3** shows the slowest reaction even with "naked" acetate in solution, which is highly nucleophilic. The bulky ethyl groups (Figure 17) slow substitution and sterically hinder S_N2 attack, so the reaction proceeds via an S_N1 mechanism, which is supported by the zero order kinetics it displays. Sterics therefore play a large role in stabilization of the PVC system. This hypothesis is further supported by the difference between the two allylic models. **5** is a smaller, less hindered molecule and undergoes apparently mostly substitution. However, when the chain length on both sides is increased, as in **6**, elimination is the major product. This suggests that as the model system more closely resembles PVC, specifically as to sterics, elimination becomes the dominant pathway over substitution.

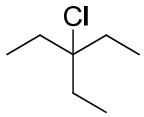

3-chloro-3-ethylpentane

Figure 17 - Structure of 3-chloro-3-ethylpentane.

This is a significant difference from literature reports. For example, the reaction of dibutyltin dilaurate stabilizers (tin versions of the metal carboxylate salts) with model

compounds including 4-chloro-2-pentene was reported to yield only substitution products. In comparing their results with the bulk system, the authors suggest it is the coordination of the metal of the stabilizer to the chlorine on the model compound which assists substitution (Figure 18).[17] Our system incorporates a PTC, of which the tetrabutylammonium cation is non-coordinating. Thus, no coordinating cations are present in solution we are able to observe the kinetics of the "naked" acetate anion.

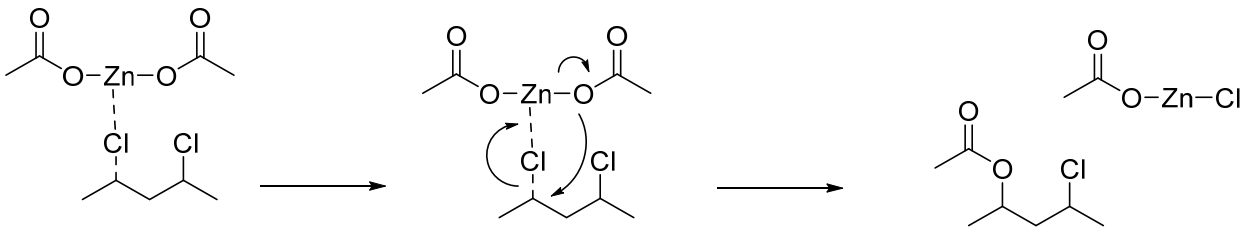

Figure 18 - Metal coordination assisted substituion of acetate on 2,4-dichloropentane.

The kinetic results and product distributions line up well with literature, though our system does not involve the use of additional solvent. Also, the kinetics observed are for the "naked" acetate anion, as the use of a PTC results in the presence of a non-coordinating cation which is not involved in the reaction of acetate and model compound. The relative rates of reaction increase from vicinal (**4a**, *meso*-, $2.25 \cdot 10^{-4}$ min^{-1}; **4b**, enantiomeric pair, $0.40 \cdot 10^{-4}$ min^{-1}) to *meso*-2,4-dichloropentane (**2a**, $9.99 \cdot 10^{-4}$ min^{-1}), suggesting the vicinal moieties are unlikely to play a part in the stabilization or degradation of PVC. Tertiary chlorine **3** ($3.91 \cdot 10^{-4}$ min^{-1}) converts at a similar rate to *d,l*-2,4-dichloropentane (**2b**, $3.56 \cdot 10^{-4}$ min^{-1}) but undergoes elimination through zero-order kinetics, such that the acetate is not involved which is likely due to sterics. Allylic models **5** ($27.8 \cdot 10^{-4}$ min^{-1}) and **6** ($18.1 \cdot 10^{-4}$ min^{-1}) display the fastest kinetics, though the more sterically hindered **6** is slower to convert than the smaller allylic model **5**.

Though the data agrees with the propensity of "labile" chlorines such as allylic and tertiary chlorines to be weak links in the PVC system and locations for initiation of degradation, there is evidence that substitution may not be the dominant mechanism. Increasing steric hindrance appears to promote elimination, and in PVC the mass transfer limitations are expected to further reduce the likelihood of substitution in favor of elimination mechanisms with carboxylates. Results from the reaction of 2,4-dichloropentane with $ZnSt_2$ and $CaSt_2$, outlined in the following section, support the hypothesis that though substitution is seen in systems where both "stabilizer" and model compound are small and unhindered, as the size and/or sterics of either is increased elimination becomes the dominant pathway.

2.2.3 Color Stability Studies of 2,4-Dichloropentane with Metal Stearates

Switching to $ZnSt_2$ and $CaSt_2$ we observed the effect of stabilization of the defect free model 2,4-dichloropentane in a model system more similar to bulk PVC formulations. The metal stearates, while insoluble in 2,4-dichloropentane at room temperature, are soluble at elevated temperatures and do not require a PTC. We observed both the rate of color change as a function of heat and time - one factor associated with degradation in PVC formulations[8, 28-29] - and conversion of the model over time.

The reactions were carried out in sealed glass vessels and color change was monitored by qualitatively observation over time. Neat 2,4-dichloropentane remained a colorless liquid when heated at 140°C for over three days. However, when combined with stabilizers (5 phr total) the reaction mixture typically progressed from colorless to yellow to brown to black (Figure 20). The rates of color progression for different combinations of stabilizers are summarized in Table 5. $ZnSt_2$ (5 phr, 0.063 mmol) produced the most dramatic color change compared to combinations of $CaSt_2$ and $ZnSt_2$ and neat 2,4-dichloropentane. It changed color from colorless to brown in 8 minutes and to black in 11 minutes. The swift degradation is likely due to the formation of $ZnCl_2$. The

coordination of $ZnSt_2$, a Lewis acid, to a chlorine of 2,4-dichloropentane and subsequent abstraction forms ZnStCl. A second abstraction then forms $ZnCl_2$ which is a stronger Lewis acid than $ZnSt_2$ and can increase the degradation of the model. When $ZnCl_2$ (equimolar in Zn to $ZnSt_2$) is reacted with 2,4-dichloropentane the color changes to brown in as little as 5 minutes, and after 8 minutes the system has turned black, despite the low solubility of $ZnCl_2$ in the model. However, $ZnSt_2$ is rarely used as the sole stabilizer, it is often used in combination with other metal stearates such as $CaSt_2$.[30] Indeed, combinations of $ZnSt_2$ and $CaSt_2$ at 1:1 (0.0315 mmol and 0.0328 mmol, respectively) and 2:1 (0.063 mmol and 0.0328 mmol, respectively) yielded significantly slower rates of color change. $CaSt_2$ can react with $ZnCl_2$ to restore $ZnSt_2$ and produce the much less Lewis acidic $CaCl_2$ as a byproduct (Figure 19).

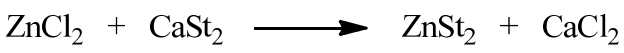

Figure 19 - Reaction of $ZnCl_2$ with $CaSt_2$ to form $ZnSt_2$ and $CaCl_2$.

The reaction of 1:1 $ZnSt_2$:$CaSt_2$ with 2,4-dichloropentane showed no sign of color for over 100 minutes while 2:1 $ZnSt_2$:$CaSt_2$ remained colorless for less time 85 minutes. This makes sense, since an excess of $ZnSt_2$ in the second reaction would mean that not all the $ZnCl_2$ would be reacted with $CaSt_2$ so degradation would occur more quickly. The addition of $CaSt_2$ to $ZnCl_2$ also displays a delayed color formation compared to $ZnCl_2$ alone further supporting the role of $CaSt_2$ in preventing buildup of $ZnCl_2$. No color formation was observed until around 21 minutes for the combination of $ZnCl_2$ and $CaSt_2$, in contrast to $ZnCl_2$ and $ZnSt_2$ on their own, both of which progressed directly to brown in 5 and 8 minutes respectively.

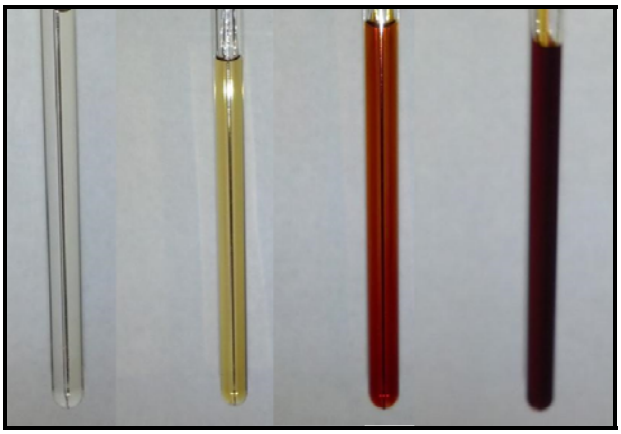

Figure 20 - Typical color change of 2,4-dichloropentane with ZnSt2 and CaSt2 during the degradation process.

Table 5 - Qualitative color change study for the reaction of 2,4-dichloropentane with various additives at 140°C. NR - No reaction in 180 minutes. NA - Color change not seen.

Additive 1	Additive 2	Time to Color Change (minutes)		
		Yellow	Brown	Black
None	None	NR	NR	NR
$ZnSt_2$ (5 phr)	None	NA	8±2	11±1
$ZnSt_2$ (2.5 phr)	$CaSt_2$ (2.5 phr)	102±10	131±6	159±20
$ZnSt_2$ (5 phr)	$CaSt_2$ (2.5 phr)	85±5	100±0	119±12
$ZnCl_2$[1]	None	NA	5±2	8±2
$ZnCl_2$[1]	$CaSt_2$ (2.5 phr)	21±0	27±2	43±2

[1]**Equimolar in Zn to $ZnSt_2$.**

The reactions of 2,4-dichloropentane and metal stearates at 140°C after 3 hours were also analyzed by NMR to follow the conversion of the model compound as a function of time and determine what products were formed. The NMR spectra were obtained at 100°C to ensure sample homogeneity. As mentioned, the stearates are soluble in 2,4-dichloropentane at room temperature. Figure 21 displays the neat NMR spectra of 2,4-dichloropentane (top) and $ZnSt_2$ (bottom). The protons ipso to the chlorines of the *meso*- (**2a**, labeled b′) and *d,l*- (**2b**, labeled b) stereoisomers are clearly distinguishable in the NMR. The aliphatic protons of the metal stearates (labeled f) remain constant

throughout reaction and were used as an internal standard for peak area integration. Figure 22 represents a typical NMR time course for the reaction of 2,4-dichloropentane with metal stearates ($ZnSt_2$ in this case) at 140°C for 0 h (top), 1.5 hours (middle) and 3 hours (bottom).

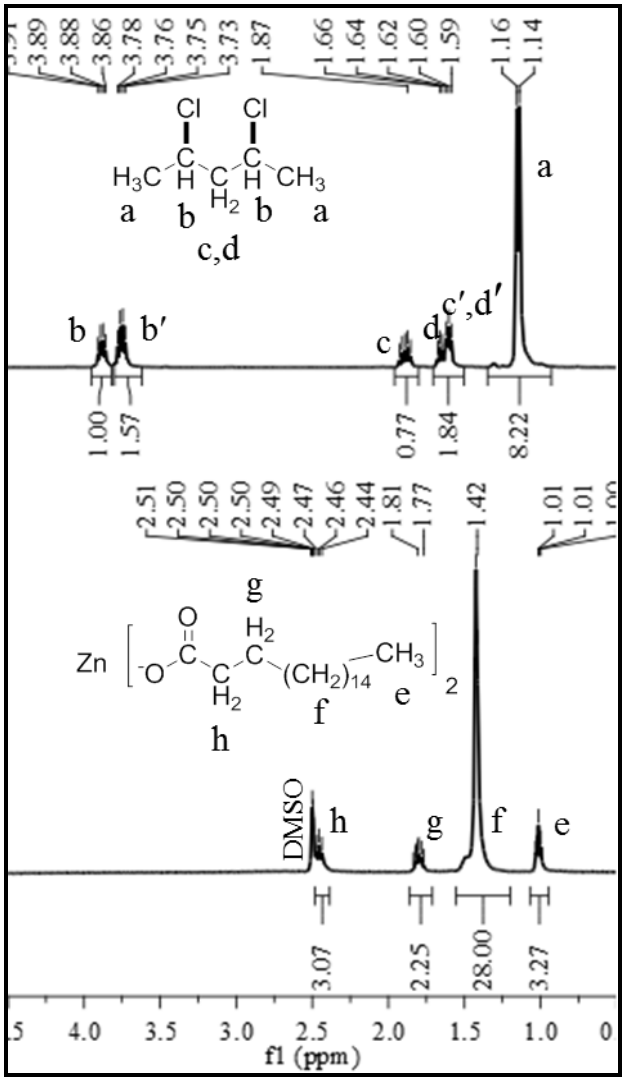

Figure 21 - NMR spectra of starting materials at 100°C. TOP - ^{1}H NMR of neat meso-2,4-dichloropentane (denoted with ′) and (2S*,4S*)-dichloropentane with DMSO capillary. BOTTOM – ^{1}H NMR of zinc stearate in o-dichlorobenzene (a nonreactive solvent) with a DMSO capillary.

The ratio of the areas of the *meso*:enantiomeric pair isomers and the conversion of 2,4-dichloropentane were calculated as a function of additives (Table 6). Similarly to the model studies with NaOAc/PTC the *meso* stereoisomer reacts more readily than the enantiomeric pair, however no significant product peaks were observed in the NMR spectra. The total areas of both isomers of 2,4-dichloropentane did decrease, as referenced to the internal standard (aliphatic protons of the stearate) which confirmed the model was reacting. However, since the NMR spectra were obtained at an elevated temperature of 100°C any volatile products could be located in the head space of the reactor, and therefore not observable by NMR. The head space was analyzed by GC-MS, which will be discussed momentarily.

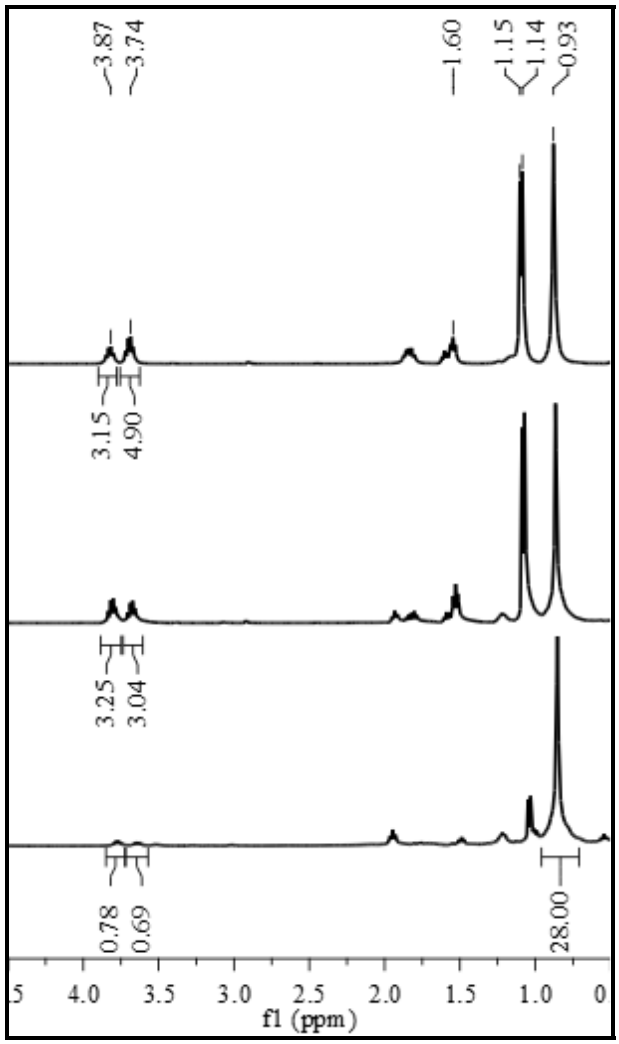

Figure 22 - ^{1}H NMR spectra from the reaction of 2,4-dichloropentane with $ZnSt_2$ at 140°C. TOP – Prior to reaction. MIDDLE – 1.5 hours of reaction time. BOTTOM – 3 hours of reaction time. Each spectrum is normalized to the aliphatic protons of the stearate (CH_2's labeled f in Figure 21).

Similar results were seen in the conversion of the model as with the effect of stabilizers on color stability. Though no reaction is seen without additive, the addition of $ZnSt_2$ (0.05 eq) resulted in 75% conversion of the model after 3 hours. Addition of $CaSt_2$ to $ZnSt_2$ in a ratio of 1:2 slows conversion to 56%. Increasing the ratio of $CaSt_2$ to $ZnSt_2$ to 1:1 slows conversion further to 42% after 3 hours. When the reaction was extended until no more 2,4-dichloropentane was observed in solution, the only remaining material

was stearic acid (confirmed by ^{13}C NMR). No sign of solid was observed, suggesting the zinc was still in solution in some form. In the solution no substitution products were evident. Unlike in the case of the "naked" acetate, $ZnSt_2$ was likely promoting elimination of the model, supporting the hypothesis that increasing sterics results in elimination as the dominant pathway. Literature reports also suggest minimal substitution in reactions of model compounds with metal stearates.[2-4]

Table 6 - Summary of reactions of 2,4-dichloropentane with various additives at 140°C for 3 hours.

Additive 1	Additive 2	*Meso*:Enantiomeric Pair	2,4-Dichloropentane Conversion (%)
PRIOR TO REACTION		1.57	--
NONE	NONE	1.57	0
$ZnSt_2$ (0.1 eq)	NONE	0.71	75
$ZnSt_2$ (0.05 eq)	$CaSt_2$ (0.05 eq)	0.99	42
$ZnSt_2$ (0.1 eq)	$CaSt_2$ (0.05 eq)	0.74	56

To confirm that elimination is the dominant pathway, GC-MS was utilized to analyze the head space of the reaction for volatile products. The gas chromatograph (Figure 23) showed numerous new peaks after reaction (top) as compared to before reaction (bottom). Through mass spectroscopy we identified the peaks as possible carbocation intermediates of elimination products, examples of which are outlined in Figure 24. This supports elimination as the dominant pathway for the reaction of 2,4-dichloropentane and metal stearates.

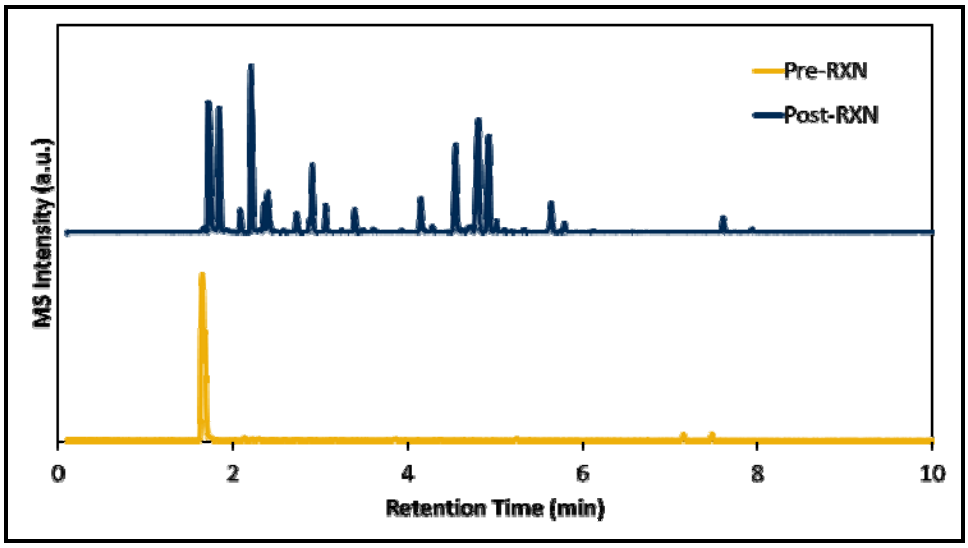

Figure 23 - Gas chromatograph of the vapor phase from the reaction of 2,4-dichloropentane with $ZnSt_2$ at 140°C.

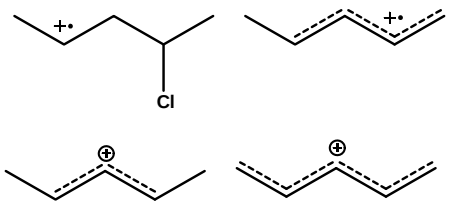

Figure 24 - Carbocation intermediate species from the reaction of 2,4-dichloropentane with $ZnSt_2$ at 140 °C.

As in the case of the model compounds and "naked" acetates, sterics play a large role in determining the dominant pathway for reaction with the metal stearates. When a non-coordinating cation is utilized, the "naked" acetate anion is small and nucleophilic enough to susbtitute for a chlorine on the model compounds. As the models' size increases to more closely resemble PVC, sterics begin to interfere and even the "naked" acetate facilitates elimination of the chlorines. Similarly, as the carboxylate is increased in size and mass transfer becomes more difficult elimination becomes the primary mechanism, even with a coordinating cation.

2.2.4 Bulk PVC Formulations: Thermal Weight Loss and Color Stability

In parallel to the model studies, PVC bulk formulations were prepared with different stabilizers and analyzed *via* thermogravimetric analysis to qualitatively determine weight loss (thermal stability) and color change (color stability) over time. Diisodecyl phthalate (DIDP) plasticized PVC was blended with combinations of $ZnSt_2$ and $CaSt_2$ at typical industrial ratios (3 g PVC, 30 parts per hundres resin (phr) DIDP, and 5 phr total metal stearates) and analyzed by thermogravimetric analysis (TGA) at 170°C. As mentioned before, though PVC is only momentarily exposed to higher temperatures like 170°C during processing, this can initiate the degradation which then continues even after cooling, just at a slower rate. In order to simulate the amount of degradation observed over months and years in an experimentally viable time period 170°C was utilized for TGA analysis. Each blend was prepared at least twice for reproducibility and representative thermograms are displayed in Figure 25 and examples of color stability after heating in Figure 26.

The thermogram of neat PVC displays the least mass loss over time, 0.81% lost after 2 hours at 170°C (Figure 25). However, the powder itself displays a drastic color change from a white powder before heating to a brown powder (A, Figure 26). Neat PVC is too brittle and rigid for most applications so plasticizers such as DIDP are typically incorporated to increase processibility. DIDP was utilized in our system as a plasticizer that would not be involved in a secondary manner. The epoxide functionalities of epoxidized soybean oil (ESO), another common plasticizer for example, react with HCl to form chlorohydrins. Thus, ESO acts as both stabilizer and plasticizer by acting as an HCl sink. DIDP-plasticized PVC loses more mass than neat PVC, 5.5% over 2 hours, possibly due to less mass transfer constraints resulting in the release of more HCl from the blend. It also displays poor color stability by resulting in a brown powder after

heating for 2 hours (B). This information was utilized as a baseline for the blends incorporating stabilizers.

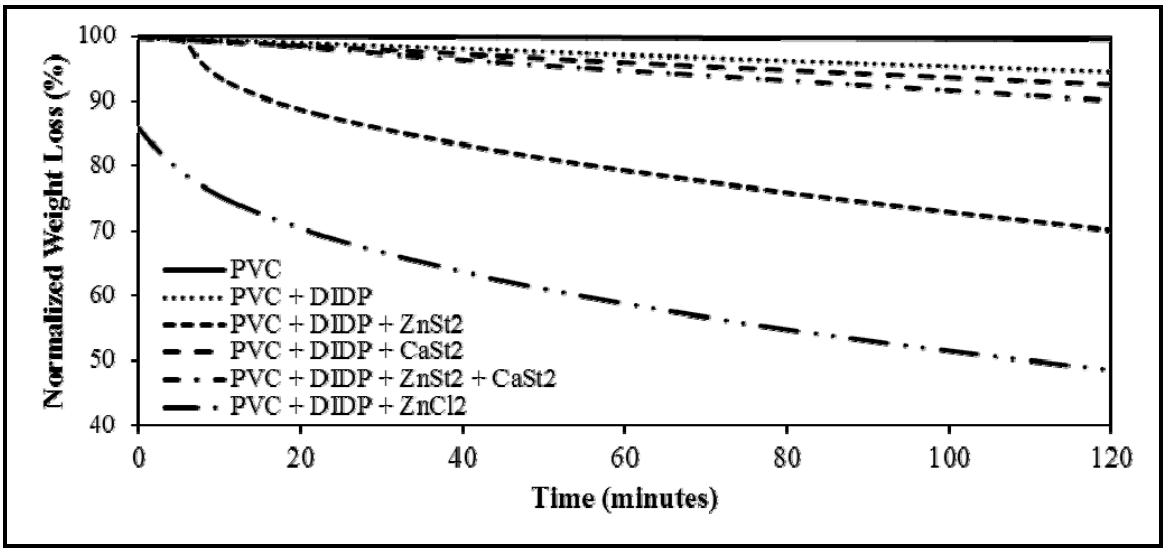

Figure 25 - Weight loss of PVC blends during the heat treatment and degradation process at 170 °C. Weight normalized against the mass of PVC in each blend.

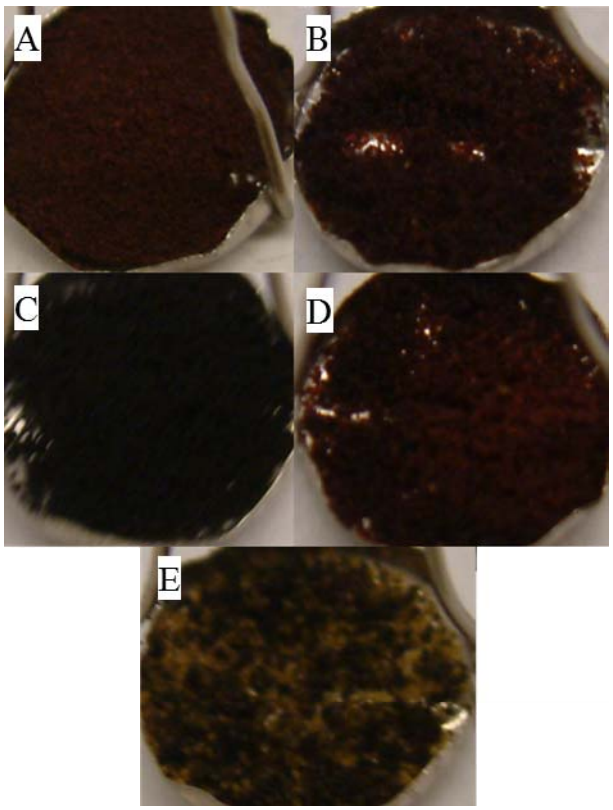

Figure 26 - Images of blends of PVC after heat treatment. A) PVC, B) PVC + DIDP, C) PVC + DIDP + $ZnSt_2$, D) PVC + DIDP + $CaSt_2$, and E) PVC + DIDP + $ZnSt_2$ + $CaSt_2$.

A blend of $ZnSt_2$ and DIDP-impregnated PVC resulted in an initial stability with less than 1% weight loss over the first 10 minutes of thermal treatment (Figure 25). However, weight loss increased drastically from that point resulting in 30% loss of mass after 2 hours. This blend also displayed the worst color stability, resulting in a black powder (C, Figure 26). A blend of $CaSt_2$ with plasticized PVC resulted in 7.5% weight loss and similar color stability (D) to neat PVC and DIDP- PVC. PVC blended with a 1:1 mixture of $CaSt_2$ and $ZnSt_2$ showed stability (E) changing from a white powder to a mixture of yellow and black powder, though it lost 9.9% of its original mass over 2 hours. The heterogeneity of color is possibly due to non-uniform blending of the sample. This supports our conclusions before, that $CaSt_2$ is necessary to prevent formation of $ZnCl_2$. A blend of $ZnCl_2$ (equimolar in zinc to the $ZnSt_2$ blend) and DIDP-plasticized

PVC was analyzed in comparison and showed the most dramatic weight loss, losing 51.5% of the original mass, and with a similar slope to $ZnSt_2$ after the initiation period.

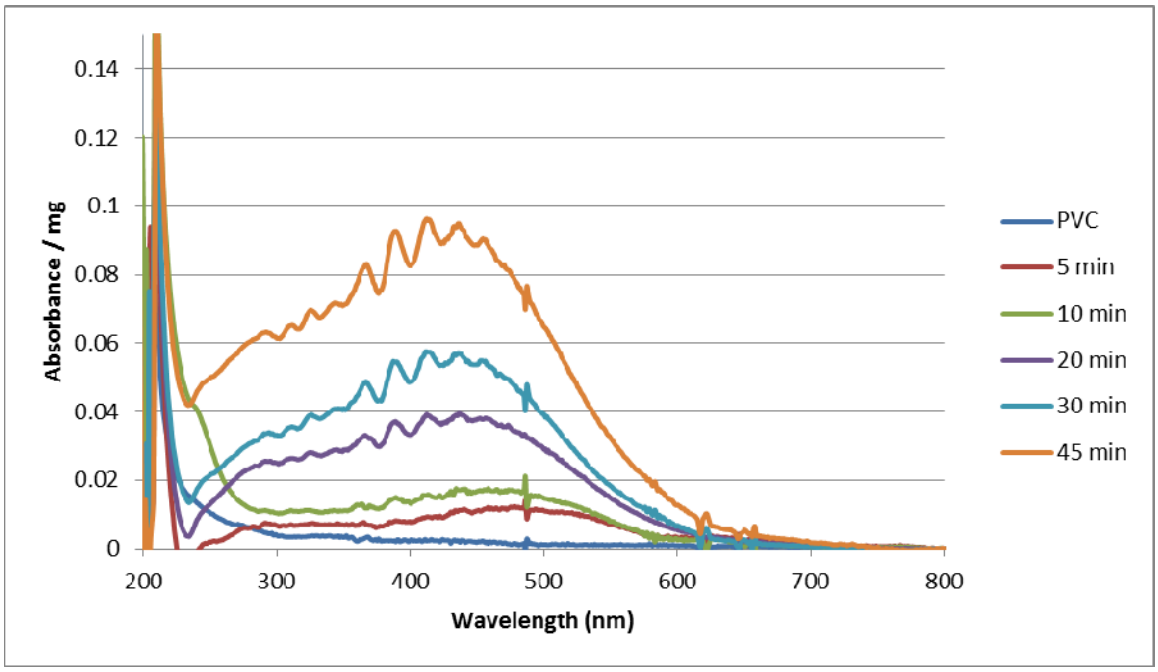

Figure 27 - UV-VIS of neat PVC heated at 170°C.

The color change of PVC over time is due to the formation of conjugated double bonds on the PVC backbone, as evidenced by the UV-VIS spectra of PVC heatd at 170°C over time which shows increased absorption in the area of 300-600 nm which corresponds to the formation of conjugated double bonds (Figure 27). It is therefore an important metric for analyzing these polymer blends. Though neither $CaSt_2$ nor $ZnSt_2$ on their own (C and D, Figure 26) show color stability, the synergistic blend of $CaSt_2$ and $ZnSt_2$ (E, Figure 26) maintains areas of ligher color which indicates that less degradation has occurred. Thus, the blend of both $CaSt_2$ and $ZnSt_2$ was effective in reducing the chain-unzipping that leads to areas of conjugated double bonds. This supports the conclusion of the previous section – $CaSt_2$ is utilized to prevent buildup of $ZnCl_2$ which

is formed from the reaction of $ZnSt_2$ with labile chlorines on the PVC backbone. $ZnSt_2$ contributes to the degradation of the bulk PVC polymer similarly to 2,4-dichloropentane. This is probably due to formation of $ZnCl_2$ which we've shown causes dramatic degradation of both PVC and the model compound. This is supported by the initial thermal stability witnessed in the thermograms for $ZnSt_2$ which then drastically declines, after $ZnCl_2$ has had sufficient time to build up in the system. Note that although the blend of $CaSt_2$ and $ZnSt_2$ has slightly less thermal stability than unstabilized PVC, the color stability is better.

2.2.5 Proposed Mechanism of Degradation and Stabilization

Based on the evidence presented above, the steric bulk of PVC and the steric bulk of the metal stearates would promote elimination of labile chlorines. Absorption of the released HCl by $ZnSt_2$ forms steric acid and $CaCl_2$ (from the reaction of $ZnCl_2$ with $CaSt_2$). A proposed mechanism is displayed in Figure 28 for the system with $ZnSt_2$ and $CaSt_2$. Zinc coordinates with a chlorine to assist removal (1), followed by proton abstraction by stearate to form stearic acid and ZnClSt (2). This reaction repeats resulting in $ZnCl_2$ formation, which is an even better Lewis acid and can begin to degrade the PVC. $CaSt_2$ then reacts to prevent build up of $ZnCl_2$, forming the enthalpically favored $CaCl_2$ and restoring $ZnSt_2$ to prevent further degradation (3).

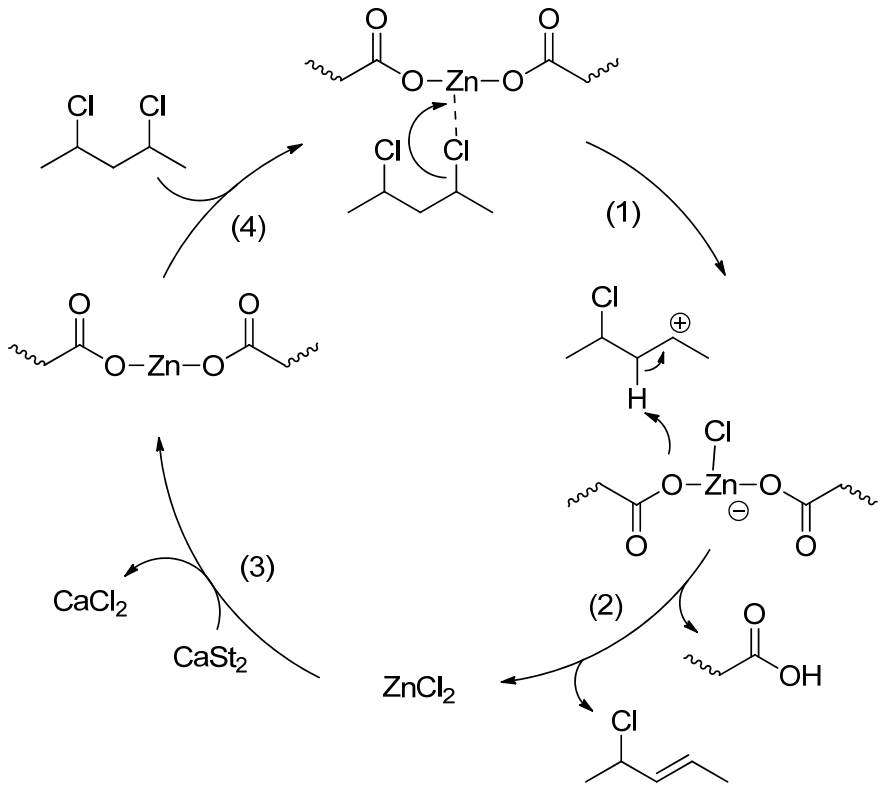

Figure 28 - Proposed mechanism of the degradation and stabilization of PVC with $ZnSt_2$ and $CaSt_2$.

2.3 Conclusions

We have developed a library of model compounds which incorporate various regio- and stereochemical chlorine arrangements to represent micro-structures present in bulk PVC polymer. The models were utilized neat, as both solvent and reactant to mimic the industrial conditions. The kinetics of each model was determined for the reaction with sodium acetate and PTC to analyze the effects of the "naked" acetate ion on our system. With the small, strongly nucleophilic "naked" acetate ion substitution of the chlorine was the dominant pathway observed with the model compounds.

The isotactic model meso-2,4-dichloropentane (**2a**) reacted quicker than syndiotactic *d,l*-2,4-dichloropentane (**2b**). This corresponds well to literature reports which report that isotactic PVC is more reactive than syndiotactic PVC. Vicinal models

meso-3,4-dichlorohexane (**4a)** and *d,l*-3,4-dichlorohexane (**4b)** react slowly, which suggests vicinal chlorines would have minimal participation in the stabilization or degradation of PVC. Allylic models 3-chloro-1-butene (**5)** and (*E*)-6-Chloronon-4-ene **(6)** react quickly and would be considered "labile" chlorines. Product distribution suggests a sterics strongly effect which pathway dominates: substitution versus elimination. The "defect-free" model, 2,4-dichloropentane displayed substitution products, as did the models for vicinal and allylic defects. However, the longer, sterically hindered allylic model **6** converted completely to the elimination product after reaction. Highly sterically hindered tertiary model 3-chloro-3-ethylpentane (**3)** also produced only elimination products after reaction completion. As the models approach the steric hindrance seen in PVC due to length (the allylic model) or due to branching (tertiary model) we observe that sterics begin to promote the elimination of chlorines over substitution.

Increased steric hindrance of the carboxylate in $ZnSt_2$ and $CaSt_2$ similarly leads to elimination in reaction with 2,4-dichloropentane. Though substitution is seen for this model with the "naked" acetate, no sign of substitution was observed for the metal stearate systems. This suggests $ZnSt_2$ acts in the method of an HCl sink to prevent autocatalyzed degradation. However, $ZnCl_2$ is formed as a result, which can promote degradation itself. The addition of $CaSt_2$ prevents build-up of $ZnCl_2$ through the enthalpically favored formation of $ZnSt_2$ and $CaCl_2$. This is supported by the observed degradation of both 2,4-dichloropentane with $ZnSt_2$ and DIDP-plasticized PVC blended with $ZnSt_2$. The thermograph of $ZnSt_2$ and plasticized PVC demonstrates a period of good stabilization of about 10 minutes, after which a catastrophic weight loss occurs which is similar to the thermograph resultant from the blend of $ZnCl_2$ and plasticized PVC. Similar color stability was witnessed for $ZnSt_2$ and $ZnCl_2$ in 2,4-dichloropentane. However, both color stability and thermal stability are increased in blends which include both $CaSt_2$ and $ZnSt_2$.

The information obtained from model kinetic and color change studies combined with that obtained from color change and weight-loss studies with the bulk PVC polymer led to the proposed mechanism discussed. We suggest that $ZnSt_2$ acts as an HCl sink to prevent auto-catalyzed degradation of PVC and $CaSt_2$ is necessary to prevent build-up of $ZnCl_2$, a much stronger Lewis acid which promotes degradation of PVC. The dominance of the elimination pathway in the more sterically hindered systems supports this hypothesis.

2.4 Experimental

2.4.1 Materials

Calcium acetate ($Ca(OAc)_2$), *o*-dichlorobenzene (anhydrous), 1,3-dichlorobutane, diisodecyl phthalate (DIDP), deuterated dimethylsulfoxide (d_6-DMSO), sodium acetate (NaOAc, anhydrous), tetradecane, tetrahydrofuran (THF, anhydrous, inhibitor-free), tetra-*n*-butylammonium chloride (TBAC), zinc acetate ($Zn(OAc)_2$), and zinc stearate ($ZnSt_2$, purum, 10-12% zinc metal basis), acetylacetone, sodium borohydride ($NaBH_4$), methanol (MeOH), thionyl chloride ($SOCl_2$), pyridine, hydrochloric acid (HCl), phosphorous pentachloride (PCl_5), carbon tetrachloride (CCl_4), propylmagnesium bromide (nPrMgBr), ethyl ether (Et_2O), phosphorous trichloride (PCl_3), and 3-chloro-1-butene were obtained from Sigma-Aldrich. Calcium stearate ($CaSt_2$) was obtained from Alfa Aesar. PVC powder (Oxyvinyls 240F) was provided by Dow Chemical Company. Helium and nitrogen were obtained from Airgas. All materials were >97% purity or ultra-high purity unless otherwise stated and used as received from the manufacturers.

2.4.2 Synthesis of Model Compounds

2,4-Dichloropentane from Acetylacetone[21]

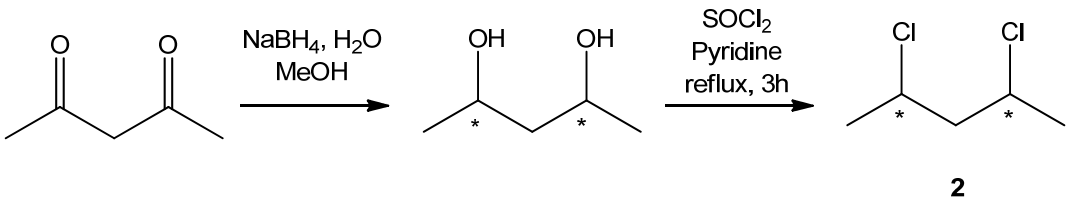

Figure 29 - Synthesis of 2,4-dichloropentane.

2,4-Pentanediol (1)

A solution of sodium borohydride ($NaBH_4$, 2.5 g, 0.066 mol) and sodium hydroxide (NaOH, 0.050 g, 0.0013 moles) in water (25 mL) was prepared and kept at approximately 20°C. A solution of acetylacetone (10 g, 0.099 moles) in methanol (MeOH, 30 mL) was added dropwise and stirred for 15 minutes. The solvent was removed *in vacuo*, yielding a white solid. The solid was then extracted into glycerol (50 mL). The extract was distilled at 60-70°C (0.45 mmHg) and, subsequently, fractionally distilled at 70-75°C (3.5 mmHg) in order to remove trace amounts of glycerol. 6.024 g (60% yield) of 2,4-pentanediol (colorless liquid) was obtained.

^{1}H NMR (400 MHz, acetone-d_6) δ 1.12 (t, J = 6.3 Hz, 6H), 1.47 (m, 2H), 3.97 (m, 2H), 4.06 (d, J = 4.68 Hz, 1H), 4.40 (d, J = 3.32 Hz, 1 H);

^{13}C NMR (100 MHz, acetone-d_6) δ 23.5 (2C), 47.1, 47.3, 64.1, 67.1.

2,4-Dichloropentane (2)

Thionyl chloride ($SOCl_2$, 27.9 mL, 0.384 moles) was added drop wise to a solution of 2,4-pentanediol (10. g, 0.096 moles) in pyridine (1.17 mL, 0.0146 moles) at

0°C under argon atmosphere. The mixture was refluxed for 3 hours. After being cooled to room temperature, ice was added to quench any unreacted $SOCl_2$. The mixture was extracted twice with diethyl ether (50 mL). The combined organic layers were dried over magnesium sulfate ($MgSO_4$) and the solvent removed *in vacuo* (75 mmHg). Distillation (140-150°C, atm. pressure) yielded 5.558 g (41% yield) of 2,4-dichloropentane as a colorless liquid.

^{1}H NMR (400 MHz, $CDCl_3$) δ 1.52 (2d, J = 10.8, 7.5 Hz, 6H), 1.98 (m, 1.3H), 2.28 (dt, J = 14.2, 7.7 Hz, 0.6H), 4.13 (m, 1.2H), 4.30 (m, 0.7H);

^{13}C NMR (100 MHz, $CDCl_3$) δ 24.5, 25.5, 50.1, 50.4, 54.7, 55.8.

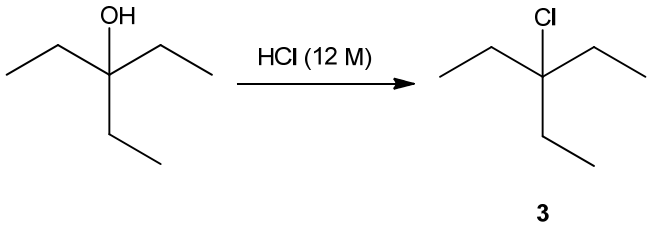

3

Figure 30 - Synthesis of 3-chloro-3-ethylpentane.

3-Chloro-3-ethylpentane (3) [22]

Hydrochloric acid (HCl, 12 M, 40 mL) was added to 3-ethyl-3-pentanol (40 mL, 0.289 mol). The biphasic mixture was stirred at room temperature for 2 hours. The organic layer was then separated, dried over magnesium sulfate and purified over a silica plug with hexanes as the eluent. The solvent was removed under vacuum at 75 mmHg, 25°C to yield 40 mL (90% yield) of 3-chloro-3-ethylpentane as a clear liquid.

^{1}H NMR (400 MHz, $CDCl_3$) δ 0.95 (t, J = 7.4 Hz, 9H), 1.77 (q, J = 7.4 Hz, 6H);

^{13}C NMR (100 MHz, $CDCl_3$) δ 8.6, 22.6, 79.8.

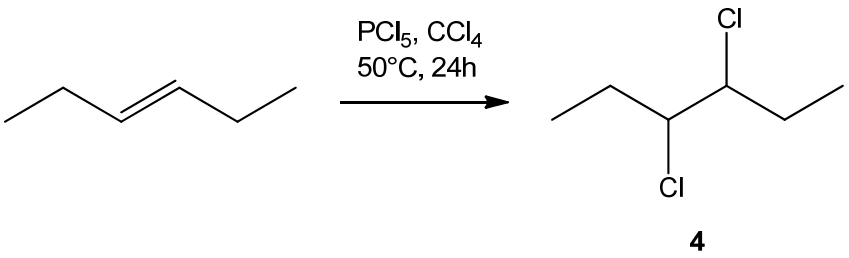

Figure 31 - Synthesis of 3,4-dichlorohexane.

3,4-Dichlorohexane (4)[23]

Phosphorus pentachloride (PCl_5, 12.37 g, 60 mmol) was suspended in carbon tetrachloride (CCl_4, 23 mL) and heated to 50°C. 3-Hexene (5 g, 60 mmol) was slowly added to the suspension and stirred overnight at 50ºC. The PCl_5 and CCl_4 were removed by distillation. The 3,4-dichlorohexane was purified by distillation at 12-14 mmHg and 40°C to yield 1.72 g (20% yield) of 3,4-dichlorohexane as a clear liquid.

^{1}H NMR (400 MHz, $CDCl_3$) δ 1.05 (m, 6H), 1.58-1.81 (m, 2 H), 1.96-2.07 (m, 2H), 3.91-3.96 (m, 2H);

^{13}C NMR (100 MHz, $CDCl_3$) δ 10.4, 11.4, 27.9, 28.0, 66.9, 67.1.

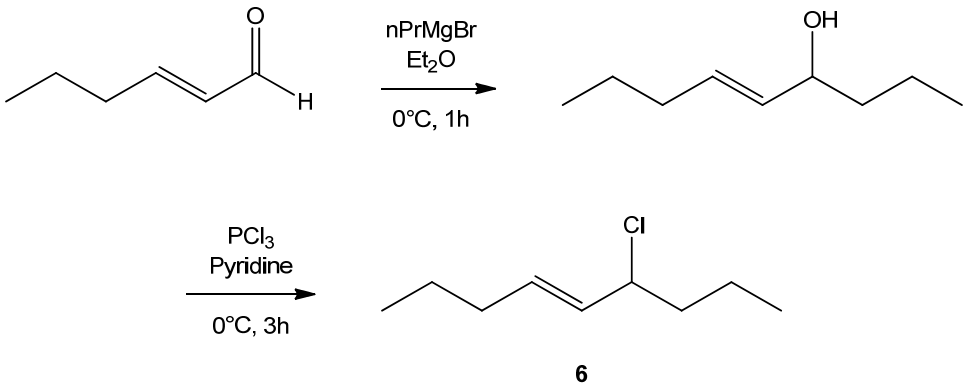

Figure 32 - Synthesis of (*E*)-6-chlorononon-4-ene.

Synthesis of (*E*)-6-Chlorononon-4-ene from *trans*-2-Hexen-1-al[24]

(E)-Non-4-ene-6-ol (5)

To a solution of *trans*-2-hexen-1-al (11.8 mL, 10.0 g, 0.102 mol) in anhydrous diethyl ether (Et_2O, 148 mL) was added, drop wise, a solution of n-propylmagnesium bromide (nPrMgBr, 51 mL, 0.102 mol) in anhydrous diethyl ether (25 mL) over the course of 30 min at 0°C. The resulting pale yellow mixture was stirred for 1 hour at room temperature. After 1 hour, the reaction mixture was quenched with a saturated aqueous ammonium chloride solution (NH_4Cl, 100 mL). The organic layer was separated and the aqueous layer was extracted twice with Et_2O (50 mL). The combined organic layer was dried over $MgSO_4$ and the solvent was removed to yield 12.8 g (88% yield) of (*E*)-non-4-ene-6-ol as a pale yellow oil.

^{1}H NMR (400 MHz, $CDCl_3$) δ 0.80 (m, 6H), 1.18-1.50 (m, 4H), 1.79 (q, 2H), 1.90 (q, 2H), 2.40 (s, 1H), 3.64 (m, 1H), 5.32 (m, 1H), 5.55 (m, 1H);

^{13}C NMR (100 MHz, $CDCl_3$) δ 13.48, 13.85, 18.58, 22.25, 34.18, 39.44, 67.73, 131.23, 133.36.

(E)-6-chlorononon-4-ene (6)

(*E*)-Non-4-ene-6-ol (12.8 g, 0.091 mol) and anhydrous pyridine (1.43 mL, 1.4 g, 0.018 mol) were combined and cooled to 0°C. Phosphorous trichloride (PCl_3, 2.9 mL, 7.2 g, 0.034 mol) was added drop wise over the course of 20 min at 0 °C. The resulting pale yellow mixture was stirred for 3 hours at 0 °C. After 3 hours, the upper layer was separated and distilled at reduced pressure (31 °C, 0.3 mmHg) to yield 10.1 g (70% yield) of (E)-6-chlorononon-4-ene as a pale yellow oil.

^{1}H NMR (400 MHz, $CDCl_3$) δ 0.9 (t, 6H), 1.4 (m, 4H), 1.79 (m, 2H), 2.0 (m, 2H), 4.37 (m, 1H), 5.5 (m, 1H), 5.59 (m, 1H);

^{13}C NMR (100 MHz, $CDCl_3$) δ 13.45, 13.57, 19.84, 22.18, 33.98, 40.93, 63.43, 131.22, 133.25.

2.4.3 Model Compound Kinetic Studies

Kinetics studies were performed on all of the model compounds with various metal acetates (NaOAc, $Ca(OAc)_2$, or $Zn(OAc)_2$). A solution of the phase transfer catalyst (PTC) tetra-*n*-butylammonium chloride in THF (3.0 mL of a 0.33 M solution, 0.001 mol, 0.05 eq) was added to the acetate salt (0.020 mol $^{-}$OAc, 1 eq) under an argon atmosphere with a condenser, heated to 60°C, and stirred overnight to allow the PTC to condition the acetate salt. The THF was then evaporated and tetradecane (0.001 mol) was added as an internal standard and heated to 100°C. The model compound (0.0400 mol, 2 eq) was then added and the resulting slurry was stirred throughout the reaction. Aliquots were taken periodically, filtered to remove any solids, and quantitatively diluted in THF for analysis.

2.4.4 Qualitative Studies of 2,4-Dichloropentane with Metal Stearates

Mechanistic studies using 2,4-dichloropentane with various stearates (e.g., $ZnSt_2$ and $CaSt_2$) at the parts per hundred resin scale (phr, grams of additive per 100 grams of polymer or model) were performed in sealed glass reaction vessels. For example, 2,4-

dichloropentane (5.655 mmol) was added to zinc stearate (0.0315 mmol, 2.5 phr) and calcium stearate (0.0328 mmol, 2.5 phr). The resulting slurry was transferred to the reaction vessel (thick walled NMR tube or Ace Glass pressure tube #8648-03) which was subsequently purged with argon and sealed (i.e., the NMR tube was flame sealed or the glass pressure tube capped). The reaction vessel was then heated *via* an oil bath for the desired reaction time then cooled. Higher concentration studies were also performed with 0.10 equivalents of additive (to 1 eq of 2,4-dichloropentane).

2.4.5 Bulk PVC Thermographic Studies

PVC and additive blends were prepared for thermal weight loss studies. Blends consisted of 3 g of PVC powder, 30 phr (0.9 g) plasticizer (diisodecyl pthalate, DIDP), and 5 phr (0.15 g) additional additives ($ZnSt_2$ and/or $CaSt_2$). The PVC powder and one-half of the plasticizer (0.45 g) were physically combined, heated to 95°C, and thoroughly mixed. Separately, the remaining plasticizer and all other additives were combined and heated to 95°C. The two mixtures were then combined and heated to 95°C and thoroughly mixed. Blending the plasticizer with the PVC in two separate steps allowed the complete uptake and uniform distribution of the additives which do not blend well with PVC on their own.

2.4.6 Analysis

Model compounds reactions were monitored via gas chromatography-mass spectroscopy (GC-MS) using a Shimadzu GCMS-QP2010P fitted with a Supelco PTA-5 (30m x 0.32 mm x 1.00 μm, length x inside diameter x film thickness) capillary column and/or nuclear magnetic resonance (NMR) using a Bruker DSX 300MHz NMR spectrometer fitted with a 5mm probe. Reaction samples were quantitatively diluted in THF and injected into the GC at 250°C with a mobile phase of helium (70.1 kPa, 40 cm/sec). The oven temperature was ramped from 50°C to 250°C at a rate of 15°C/min.

The MS was operated in electron impact mode with an ion source and interface temperature of 225°C. For NMR, a 1 mm d_6-DMSO capillary was used as the lock solvent. NMR spectra were gathered at 100°C to ensure homogeneity of the reaction mixture.

Thermal analysis measurements (thermal gravimetric analysis, TGA) of the bulk PVC blends were performed on a TA Instruments TGA Q50 under a flow of nitrogen. After the sample was loaded the weight loss was monitored while the temperature was brought quickly to 170°C and held isothermally for 2 hours. Images of the blends post reaction were obtained from TGA samples after heating.

2.5 References

1. Wypych, J., PVC thermal degradation. III. On the mechanism of action of metal carboxylates. *Journal of Polymer Science: Polymer Letters Edition* **1984,** *22* (8), 425-431.

2. Frye, A. H.; Horst, R. W., The Mechanism of Poly(Vinyl Chloride) Stabilization by Barium, Cadmium, and Zinc Carboxylates .1. Infrared Studies. *J Polym Sci* **1959,** *40* (137), 419-431.

3. Frye, A. H.; Horst, R. W., The mechanism of polyvinyl chloride stabilization by barium, cadmium, and zinc carboxylates. II. Radioactive tracer studies. *J Polym Sci* **1960,** *45* (145), 1-12.

4. Frye, A. H.; Horst, R. W.; Paliobagis, M. A., The chemistry of poly(vinyl chloride) stabilization. III. Organotin stabilizers having radioactively tagged alkyl groups. *Journal of Polymer Science Part A: General Papers* **1964,** *2* (4), 1765-1784.

5. Atakul, S.; Balköse, D.; Ülkü, S., Synergistic effect of metal soaps and natural zeolite on poly(vinyl chloride) thermal stability. *Journal of Vinyl and Additive Technology* **2005,** *11* (2), 47-56.

6. Bensemra, N.; Tran Van, H.; Guyot, A.; Gay, M.; Carette, L., Thermal dehydrochlorination and stabilization of poly(vinylchloride) in solution: Part IV—Synergistic effects of β-diketone compounds and metal soap stabilizers. *Polymer Degradation and Stability* **1989,** *24* (2), 89-111.

7. Ureta, E.; Cantú, M. E., Zinc maleate and zinc anthranilate as thermal stabilizers for PVC. *Journal of Applied Polymer Science* **2000,** *77* (12), 2603-2605.

8. Bacaloglu, R.; Fisch, M., Degradation and Stabilization of Poly(Vinyl Chloride) .1. Kinetics of the Thermal-Degradation of Poly(Vinyl Chloride). *Polymer Degradation and Stability* **1994,** *45* (3), 301-313.

9. Bengough, W. I.; Onozuka, M., Abnormal structures in polyvinylchloride I—A method of estimating labile chloride groups in polyvinylchloride. *Polymer* **1965,** *6* (12), 625-634.

10. Asahina, M.; Onozuka, M., Thermal decomposition of model compounds of polyvinyl chloride. I. Gaseous thermal decomposition of model compounds having secondary and tertiary chlorine. *Journal of Polymer Science Part A: General Papers* **1964,** *2* (8), 3505-3513.

11. Asahina, M.; Onozuka, M., Thermal decomposition of model compounds of polyvinyl chloride. II. Gaseous thermal decomposition of unsaturated chain end model compounds. *Journal of Polymer Science Part A: General Papers* **1964,** *2* (8), 3515-3522.

12. Ayrey, G.; Poller, R. C.; Siddiqui, I. H., Mechanism of stabilization of poly(vinyl chloride). *Journal of Polymer Science Part B: Polymer Letters* **1970,** *8* (1), 1-6.

13. Ayrey, G.; Siddiqui, I. H.; Poller, R. C., Use of Organotin Compounds in Thermal Stabilization of Polyvinyl-Chloride) .3. Reactions of Dialkyltin Mercaptides, Thioglycollates, and Carboxylates with Chlorohydrocarbons. *J Polym Sci A1* **1972,** *10* (3), 725-&.

14. Bacaloglu, R.; Fisch, M., Degradation and stabilization of poly(vinyl chloride). III. Correlation of activation enthalpies and entropies for dehydrochlorination of chloroalkanes, chloralkenes and poly(vinyl chloride). *Polymer Degradation and Stability* **1994,** *45* (3), 325-338.

15. Bacaloglu, R.; Fisch, M., Degradation and stabilization of poly (vinyl chloride). V. Reaction mechanism of poly(vinyl chloride) degradation. *Polymer Degradation and Stability* **1995,** *47* (1), 33-57.

16. Bacaloglu, R.; Fisch, M., Degradation and stabilization of poly (vinyl chloride). IV. Molecular orbital calculations of activation enthalpies for dehydrochlorination of chloroalkanes and chloroalkenes. *Polymer Degradation and Stability* **1995,** *47* (1), 9-32.

17. Klemchuk Peter, P., Poly(vinyl chloride) Stabilization Mechanisms. In *Stabilization of Polymers and Stabilizer Processes*, AMERICAN CHEMICAL SOCIETY: 1968; Vol. 85, pp 1-17.

18. Varma, I. K.; Grover, S. S., Thermal degradation of some model compounds of PVC. *Die Makromolekulare Chemie* **1974,** *175* (9), 2515-2524.

19. Blazso, M.; Jakab, E., Effect of metals, metal oxides, and carboxylates on the thermal decomposition processes of poly (vinyl chloride). *Journal of Analytical and Applied Pyrolysis* **1999,** *49* (1), 125-143.

20. Boughdady, N.; Chynoweth, K.; Hewitt, D., Thermal Dehydrochlorination of Poly (vinyl chloride) Model Compounds. I. *Australian Journal of Chemistry* **1991,** *44* (4), 567-579.

21. Pritchard, J. G.; Vollmar, R. L., The meso and Racemic Forms of 2,4-Pentanediol and Certain of Their Derivatives. *J. Org. Chem.* **1983,** *28*, 1545-1549.

22. Peters, R. H.; Crowe, D. F.; Tanabe, M.; Avery, M. A.; Chong, W. K. M., Steroidal Silicon Side-Chain Analogues as Potential Antifertility Agents. *Journal of Medicinal Chemistry* **1987,** *30* (4), 646-652.

23. Spiegler, L.; Tinker, J. M., Reactions of 3-hexene. I. Reactions with sulfuric acid, halogens and halogen acids. *Journal of the American Chemical Society* **1939,** *61*, 940-2.

24. Strotman, N. A.; Sommer, S.; Fu, G. C., *Angewandte Chemie, International Edition* **2007,** *46* (19), 3556-3558.

25. Starks, C. M.; Liotta, C. L.; Halpern, M., *Phase-transfer catalysis : fundamentals, applications, and industrial perspectives*. Chapman & Hall: New York, 1994; p xiv, 668 p.

26. Martínez, G.; Mijangos, C.; Millán, J., Selective Substitution Reactions on PVC. Lability of Some "Normal" Structures. *Journal of Macromolecular Science: Part A - Chemistry* **1982,** *17* (7), 1129-1148.

27. Mijangos, C.; Martínez, G.; Millán, J. L., New approaches to the study of labile structures in poly(vinyl chloride) by phenolysis. *European Polymer Journal* **1982,** *18* (8), 731-734.

28. Fisch, M. H.; Bacaloglu, R., Kinetics and mechanism of the thermal degradation of poly(vinyl chloride). *Journal of Vinyl Technology* **1995,** *1* (4), 233-240.

29. Fisch, M. H.; Bacaloglu, R., Mechanism of poly(vinyl chloride) stabilisation. *Plast Rubber Compos* **1999,** *28* (3), 119-124.

30. Kaseler, T. G., Nonlead Stabilizer Systems for Pvc Wire and Cable Extrusion - (an Update). *Soc Plast E* **1993,** *39*, 717-727.

CHAPTER 3

Design, Synthesis and Evaluation of Nonaqueous Silylamines for Efficient CO_2 Capture

3.1 Introduction

Coal-fired power plants are one of the major sources of electricity in the US[1] and are projected to remain the predominant fuel for electricity generation through 2035.[2] They also produce nearly one-third of all CO_2 emissions in the US.[3] A single coal-fired power plant producing around 1000 MW emits between 6 and 8 megatons of CO_2 per year,[3] for example. As the environmental impact of CO_2 grows, increasing efforts have been made to develop post-combustion CO_2 capture technologies which can be retrofitted to existing plants.[4-5]

We face a number of technical challenges in the capture of CO_2 from flue gas, however. Flue gas is composed mainly of nitrogen, with small amounts of carbon dioxide, water, and ppm levels of highly reactive SO_x and NO_x compounds. A small percentage of flue gas is composed of CO_2, 16% according to D'Alessandro (Figure 33), though this number varies depending on the source of the fuel.[6] Additionally, CO_2 capture would be required to operate around 40°C, the temperature of the flue gas where capture would likely be implemented.[7] As such post-combustion capture systems must meet certain requirements: (1) the system will have to be selective for CO_2, which makes up only a small percentage of the total stream; (2) the volume of CO_2 emitted is too large for any single use solvent, so the system must be recyclable;[6] and (3), in order to implement the system industrially, it must be cost effective. In order to be cost effective

the energy used to capture CO_2 must be at a minimum and the solvent used must be relatively cheap and be recyclable. The US Department of Energy (DOE) has outlined a goal for 90% CO_2 capture from coal-fired power plants without increasing energy costs more than 35%.[2, 8-9]

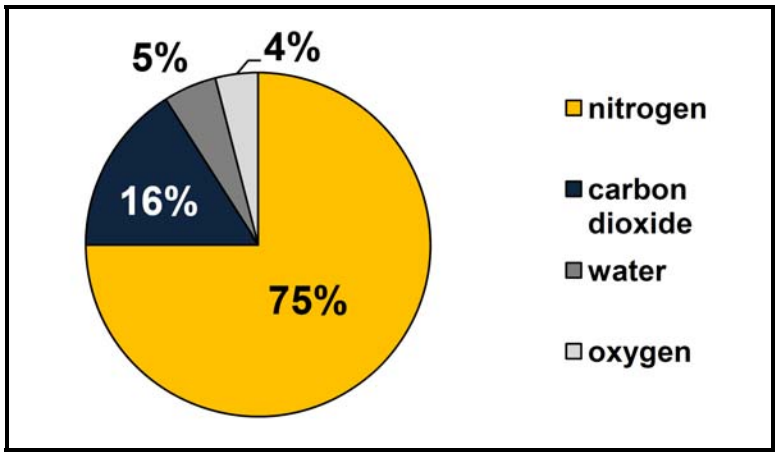

Figure 33 – Major components of flue gas by volume. Also present are ppm levels of NO_x and SO_x.

There are three main classifications of CO_2 scrubbers: membranes, solid adsorbents, and liquid absorbents.[10] Liquid absorbents are the most mature technology of the three and could be implemented in scrubber units which would be relatively simple to retrofit to existing power plants.[6] One of the most developed liquid adsorbents for CO_2 capture is a 20-30% aqueous solution of monoethanolamine (MEA) which is currently being used to scrub CO_2 from CO_2 contaminated natural gas reserves.[11]

MEA is composed of two parts: a hydroxyl group to lower the vapor pressure of the compound;[12] and an amine to chemically react with CO_2. Amines such as MEA react reversibly with CO_2 to form ammonium-carbamate ion pairs (top, Figure 34).[13] In the presence of water, however, the formation of ammonium carbonates will supersede the formation of the ammonium-carbamate (bottom). The ammonium-carbamate salt is liquid

at room temperature and is referred to as an ionic liquid. Stoichiometrically, MEA reacts in a 2:1 ratio with CO_2 and this reaction can be reversed by heating to reform the solvent. Thus, MEA is recyclable, and along with its low cost ($1.25/kg in 2004)[14] and chemoselectivity MEA is a promising liquid sorbent.

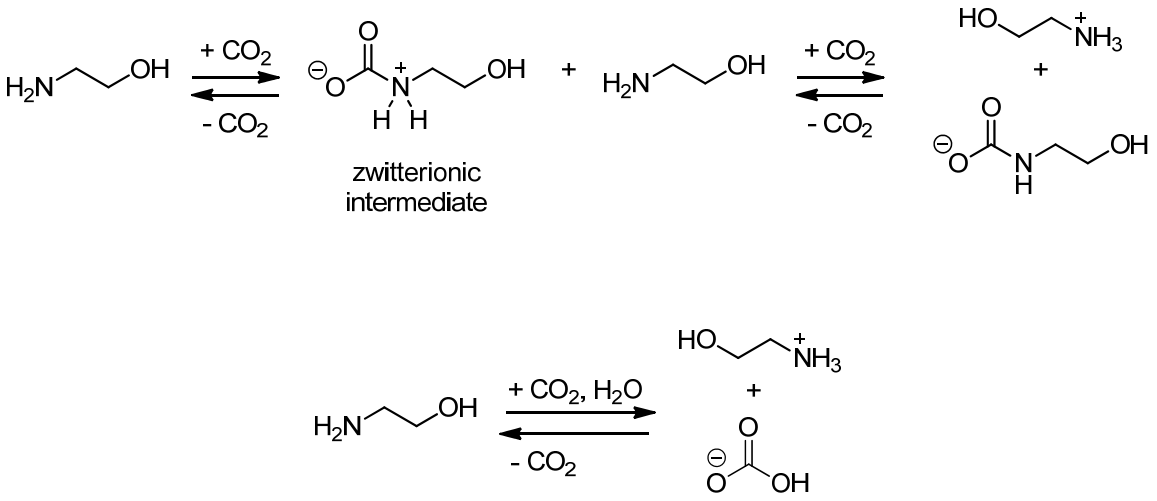

Figure 34 –Formation of MEA carbamate-ammonium ion pair from reaction with CO_2 via a zwitterionic intermediate (Top) and MEA ammonium carbonate pair from the reaction with CO_2 and H_2O (Bottom).

A simplified schematic of the CO_2 capture process involving a liquid sorbent such as MEA is illustrated in Figure 34. Flue gas enters an absorber column, which contains the liquid absorbent solution. The absorbent reacts selectively (ideally) with CO_2 to separate it from the flue gas. The resultant solution is then transferred to a stripper where it is steam heated to reverse the reaction, releasing CO_2 and reforming the original aqueous MEA solution. The MEA solution is then recycled to the absorber and the CO_2 can be removed for sequestration.[15]

The majority of the cost of the CO_2 capture process with aqueous MEA comes from the reversal step due to a high heat of regeneration.[16] Both the heat required for reaction reversal, and the heat required to heat the large excess of water utilized to the

reversal temperature of 120°C, contribute to the heat of regeneration. The ΔH of reversal at this temperature has been reported to be on the order of 96 kJ/mol CO_2 for loadings of 0.5 mol CO_2 per mole MEA.[17]

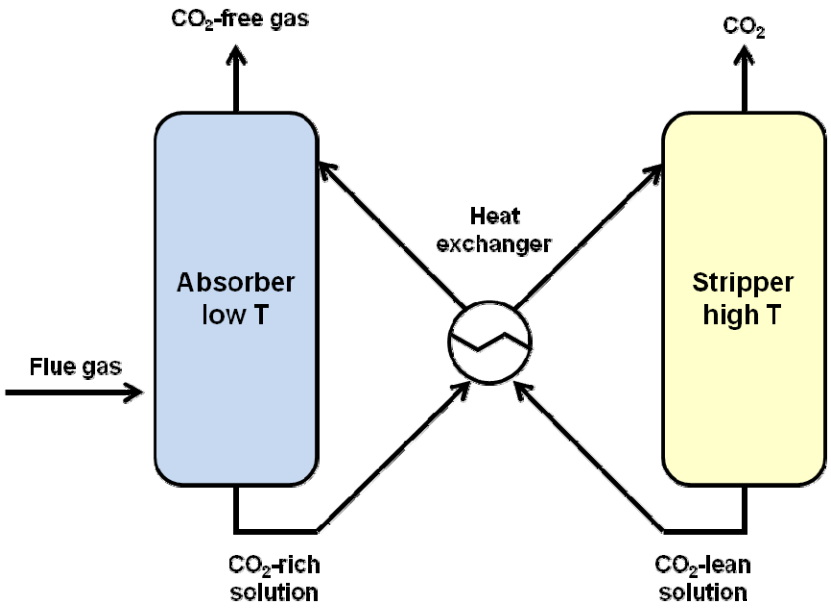

Figure 35 - Schematic of CO_2 capture and release by a recyclable solution of MEA. Diagram adapted from Puxty *et al.*[15]

10-20% Aqueous solutions of MEA are typically employed for a few reasons: (1) the water decreases the viscosity of the ionic liquid formed upon reaction with CO_2 and increases the capture capacity; and (2) MEA is one of the most highly corrosive alkanolamines being explored as CO_2 capture agents. Water is employed to reduce the corrosivity of the system.[18-19] However, the high heat capacity of water results in increased energy requirements for the regeneration step. The regeneration step alone can account for 70-80% of the energy required to run a typical power plant.[10] Additionally, the hydroxyl moiety of MEA contributes to various oxidative degradation pathways which produce small molecules such as ammonia and formaldehyde (Figure 36).[12] This results in a loss of up to 2.2 kilograms of MEA per metric ton of CO_2 captured.[18] Besides

needing to replace the lost MEA, removal of these byproducts requires the incorporation of a reclaimer into the process, which further increases operating costs.[20]

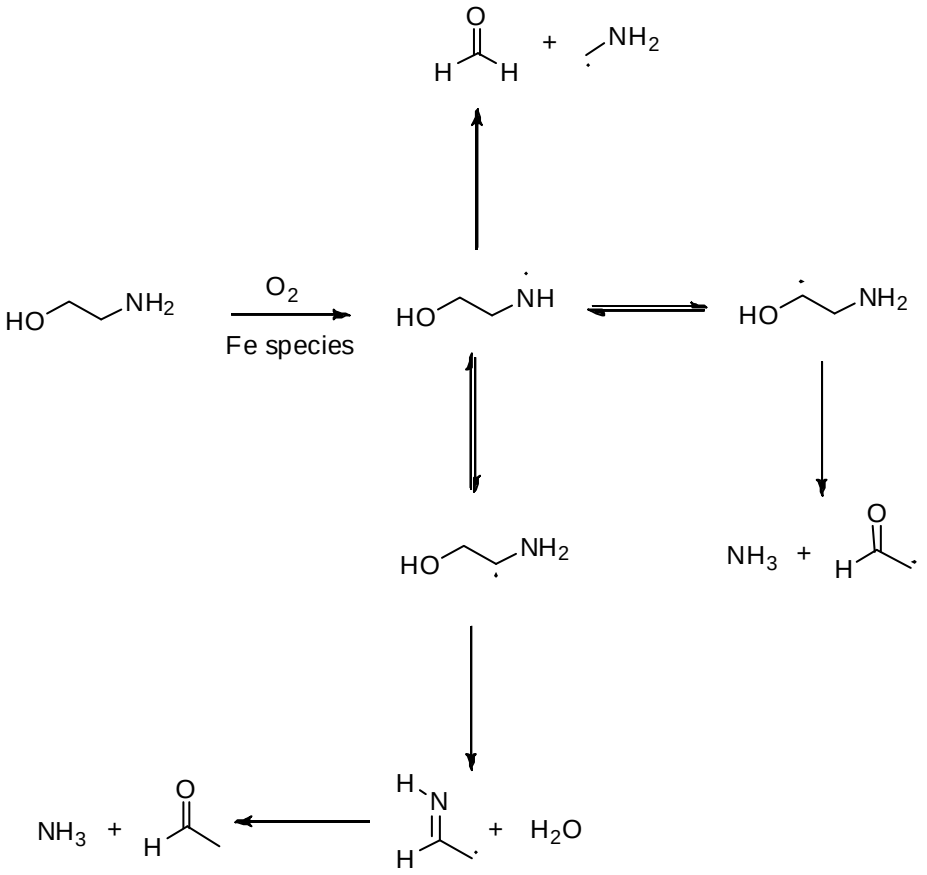

Figure 36 – Oxidative degradation pathways of aqueous MEA.

Though MEA is the only solvent-based process implemented at industrial scale as a CO_2 capture solvent, new regulations have prompted research towards other alternatives. Traditional ionic liquids (IL) have been proposed as alternatives to MEA. ILs capture CO_2 by physical absorption (physisorption), as opposed to MEA which chemically reacts with CO_2 (chemisorption). The reaction of amines to form ammonium-carbamates occurs in a 2:1 stoichiometric ratio of amine to CO_2 (Figure 37). Theoretically, the maximum absorption possible for non-aqueous amines would be 0.5

moles CO_2 per mole of amine. In practice, aqueous solutions of MEA capture CO_2 at loadings near 0.2-0.3 moles of CO_2 per mole of amine with a maximum loading near the theoretical maximum.[21] Physisorption allows for greater absorption at higher pressures, where ILs have the advantage.[7] Another advantage of ILs, the reversal of physically absorbed CO_2 typically requires less energy to reverse than chemisorption.[22-25]

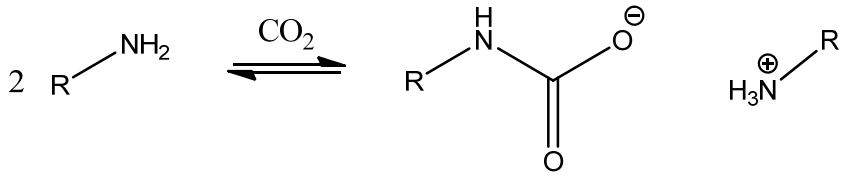

Figure 37 - Stoichiometry of the reaction of amines with CO_2 to form ammonium carbamates.

One class of ILs utilized for CO_2 capture are imidazoliom-based ILs (A, Figure 38). These ILs have demonstrated a preference for CO_2 over N_2 and O_2 and present capacities of 0.755 moles CO_2 per mole IL at 40°C and 93 bar of CO_2.[26] As mentioned, these ILs capture CO_2 by physisorption. However, to increase capture potentials, some ILs have been modified to include a reactive site, such as a primary amine, to form task specific ionic liquids (TSIL) which can both physically and chemically absorb CO_2. By tethering an amine functionality to a traditional imidazolium-based IL, Bates *et al*. developed a sorbent which demonstrated a CO_2 uptake approaching the chemisorption theoretical maximum of 0.5 moles CO_2 per mole IL at 1 atm CO_2 and room temperature (B).[27] Tethering the amine to the anion rather than the cation, as demonstrated by Brennecke *et al*., resulted in even higher capacities of nearly 1 mole CO_2 per mole of amine at 1 bar and 22°C (C).[28] Though high capacities were observed for these ILs and TSILs, the viscosities of ILs are typically very high. The upper operating limit for viscosity in industrial processes is usually 100 cP, but ILs including the ones mentioned here often exhibit viscosities several orders of magnitude higher. In fact, the TSILs'

already high viscosities of 360 – 460 cP increase drastically upon reaction with CO_2 up to 240 times the original viscosity.[26, 29] An example of a 16 v/v% solution of MEA in an IL was proposed to make use of both chemisorption and physisorption without increasing the viscosity of the IL (D). The intention was for MEA to react with CO_2 to form the ammonium-carbamate solubilized by the IL. The MEA ammonium-carbamate salt, however, were not soluble in the ILs and precipitated to form a biphasic mixture, which is not a feasible system for industrial application.[30]

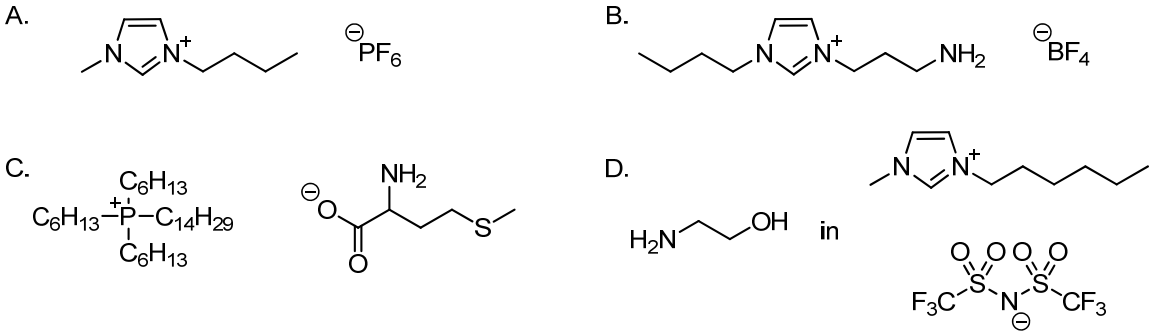

Figure 38 – Examples of IL based technologies explored for CO_2 capture.

3.2 Background

The Eckert-Liotta research group has sought to combine the idea of ionic liquids with the nature of conventional alkanol amine solvents in a switchable solvent system we refer to as reversible ionic liquids (RevILs). Switchable solvents are solvents which undergo step changes in response to an external stimulus, such as the step change observed in the reaction of CO_2 with neutral MEA to form ammonium-carbamate ionic liquids.

To this end, we have developed reversible ionic liquids (RevILs) from silylamines as a novel class of switchable solvents and have recently shown the utility of these solvents as chemical absorption based CO_2 capture solvents.[31-32] The reversible ionic

liquid systems we have developed are based on trialkyl- or trialkoxysilylamines (Figure 39) which react with CO_2 in the absence of water to form an ammonium-carbamate salt that is liquid at or near room temperature. The ability of the ionic salt to remain liquid after reaction with CO_2 is contributed to the presence of the silicon atom.[33-34] The silicon atom introduces weak Lewis acid functionality into the system and has been reported to decrease viscosity when incorporated in conventional ionic liquids.[35-37] Additionally, the acidity of the silicon may encourage coordination with the amine functionality similar to the coordination observed by Kost et al. for the hexavalent silicon dichelates shown in Figure 40 (orientation and coordination supported by x-ray crystallography analysis of the dichelates).[37] An alternative explanation for the lower viscosity of ILs incorporating silicons has also been attributed to the increased length of the silicon-carbon bond compared to a carbon-carbon bond, giving the molecule more flexibility.[38]

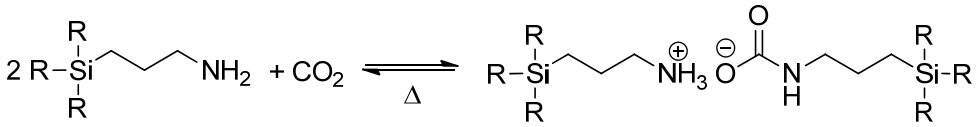

Figure 39 - Formation of RevIL through the reaction of 2 moles of silylamine with 1 mole of CO_2.

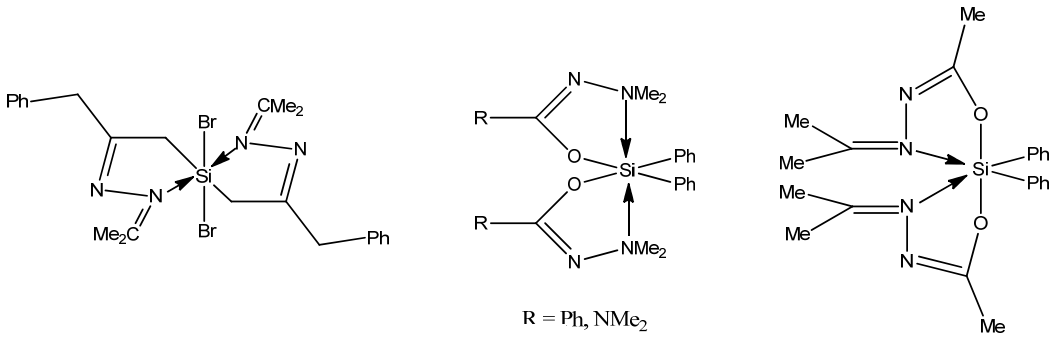

R = Ph, NMe_2

Fig 0 - Hexavalent dich s synthesized by Kost et

The Eckert-Liotta group has demonstrated the formation of RevILs from the reaction of trialkoxysilylamines with CO_2 (R = OMe, OEt, OPr, Figure 39). The ionic liquids formed reversed thermally, releasing CO_2 to reform the silylamine (also noted as the molecular liquid or ML). Theoretically, based on the stoichiometry of the reaction shown in Figure 39, these amines can reach CO_2 uptakes of up to 0.5 moles CO_2 per mole of amine. However, the formation of an ionic liquid can provide an additional capture mechanism *via* physisorption to produce a CO_2 swollen RevIL (Figure 41). Our RevILs therefore exhibit a dual CO_2 capture mechanism of both chemisorption and physisorption. Unfortunately, trialkoxysilanes were found to be susceptible to hydrolysis. The solvents degrade in the presence of water by the hydrolytic cleavage of the silicon-oxygen bond. We therefore transitioned to the more robust trialkylsilanes, for which the silicon-carbon bond is stable in water and not subject to hydrolytic cleavage.

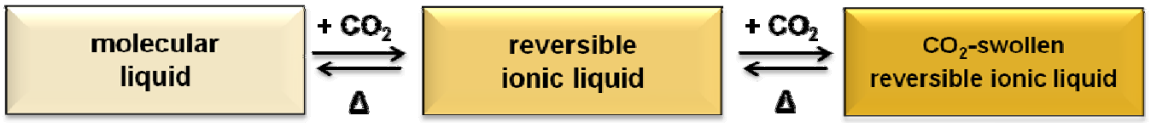

Figure 41- Reaction of molecular liquid with CO_2 to form RevIL (middle) followed by physisorption of additional CO_2 to form a CO_2 swollen RevIL (right).

The trialkylsilylamines have been demonstrated to react selectively with CO_2 over N_2, which comprises most of the bulk of the flue gas. SO_2, however, is present in ppm levels in flue gas even after scrubbing methods have removed 90% of SO_2 using wet or dry flue gas desulfurization systems.[39] My coworker, Farhana Momin, investigated the silylamine selectivity for reaction with CO_2 vs. SO_2.[40] She utilized a gas proportioner (model B from Aalborg) to sparge (200 mL/min, 20°C, 1 bar for 75 minutes) tripropylsilylamine with mixed gas streams of: (1) pure SO_2, (2) pure CO_2, (3) 4 vol%

SO_2 in CO_2, and (4) 50 vol% SO_2. Two products were formed (Figure 42): TPSA-RevIL from the reaction with CO_2 and TPSA-SO_2 product. It was expected that the reaction of SO_2 with TPSA would proceed similarly to TPSA and CO_2 and thus that the product formed would have a maximum theoretical CO_2 uptake of 0.5 moles SO_2 per mole of TPSA.

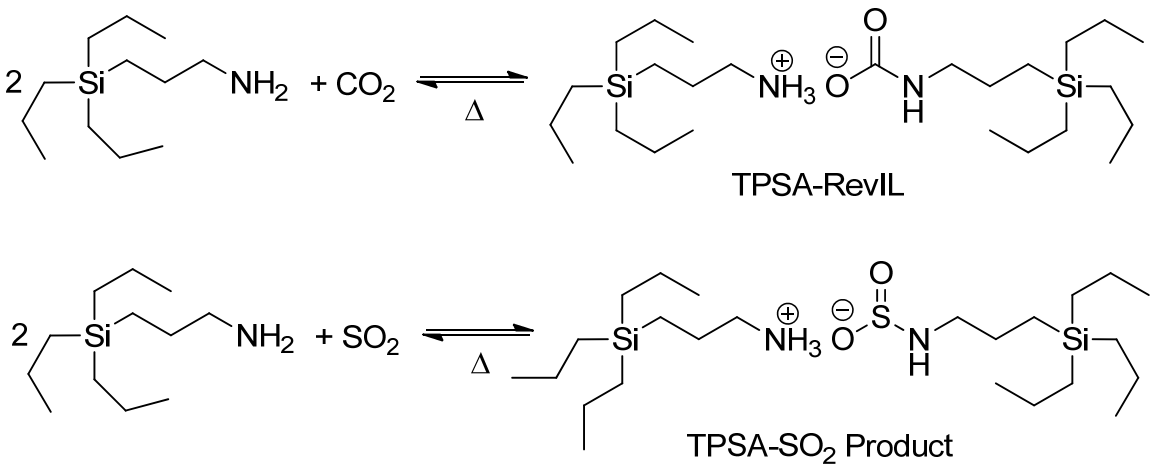

Figure 42 - Reaction of TPSA with SO_2 or CO_2 to form products.

The TPSA-SO_2 product was formed as the sole product from the pure SO_2 stream with a capture capacity of 1.378 mole SO_2 per mole ML (Figure 43). This enhanced uptake is likely due to physisorption of SO_2 into the ionic liquid and/or the formation of possible side products which would double the theoretical SO_2 uptake (Figure 44). The CO_2 uptake of TPSA for a 200 mL/min stream of pure CO_2 was 0.64 mole CO_2/mole ML forming solely the TPSA-RevIL. Both mixtures demonstrate higher capacities than TPSA-RevIL; 4 vol% SO_2 in CO_2 demonstrated 0.212 kg SO_2 per kg TPSA and 50 vol% demonstrated 0.327 kg SO_2 per kg TPSA.

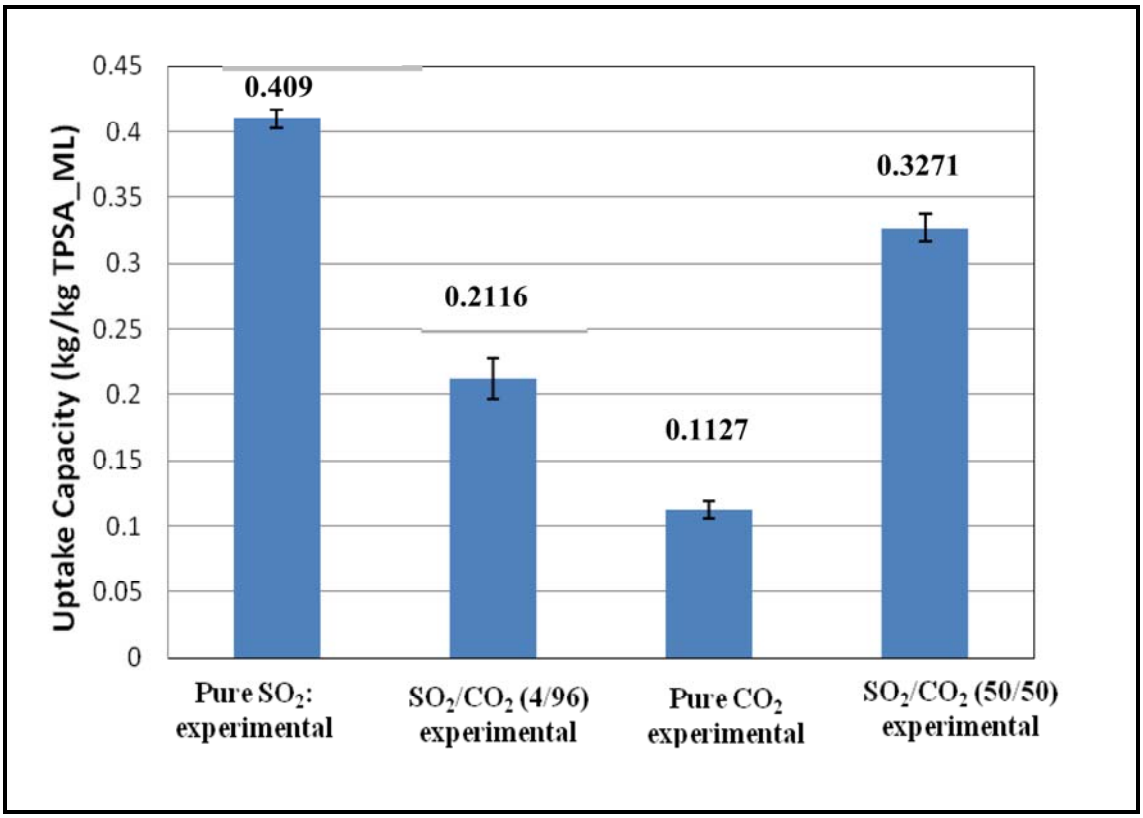

Figure 43 - Uptake capacities for the reaction of SO_2 and CO_2 mixed streams with TPSA.

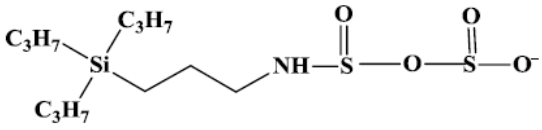

1.0 mol SO_2/mol TPSA_ML

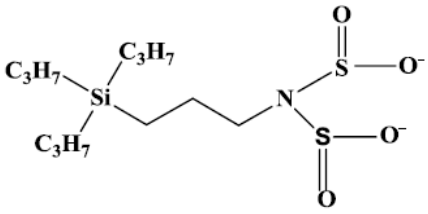

1.0 mol SO_2/mol TPSA_ML

Figure 44 - Possible side products formed from the reaction of SO_2 with TPSA which could demonstrate capacities of up to 1 mole SO_2 per mole of TPSA in conjunction with the ammonium partner.

FTIR was utilized to determine the major products of each reaction. The reaction of a 50 vol% SO_2 in CO_2 stream with TPSA resulted in the formation of a majority of the SO_2 product with TPSA (Figure 45). In contrast, the reaction of the mixed gas stream of 4 vol% SO_2 in CO_2 with TPSA resulted in the formation of mostly TPSA-RevIL. Additionally, she was unable to reverse the process and reform the molecular liquid from the TPSA-SO_2 product, even when heated to temperatures as high as 500°C in the TGA (thermal gravimetric analysis). Based on this work, at low concentrations (ppm) of SO_2 the majority of the product would be the TPSA-RevIL. However, some TPSA may still be lost over time to the formation of irreversible SO_2-TPSA products. This would require the addition of a slip stream to add more of the CO_2 capture solvent for the process to function as a continuous system.

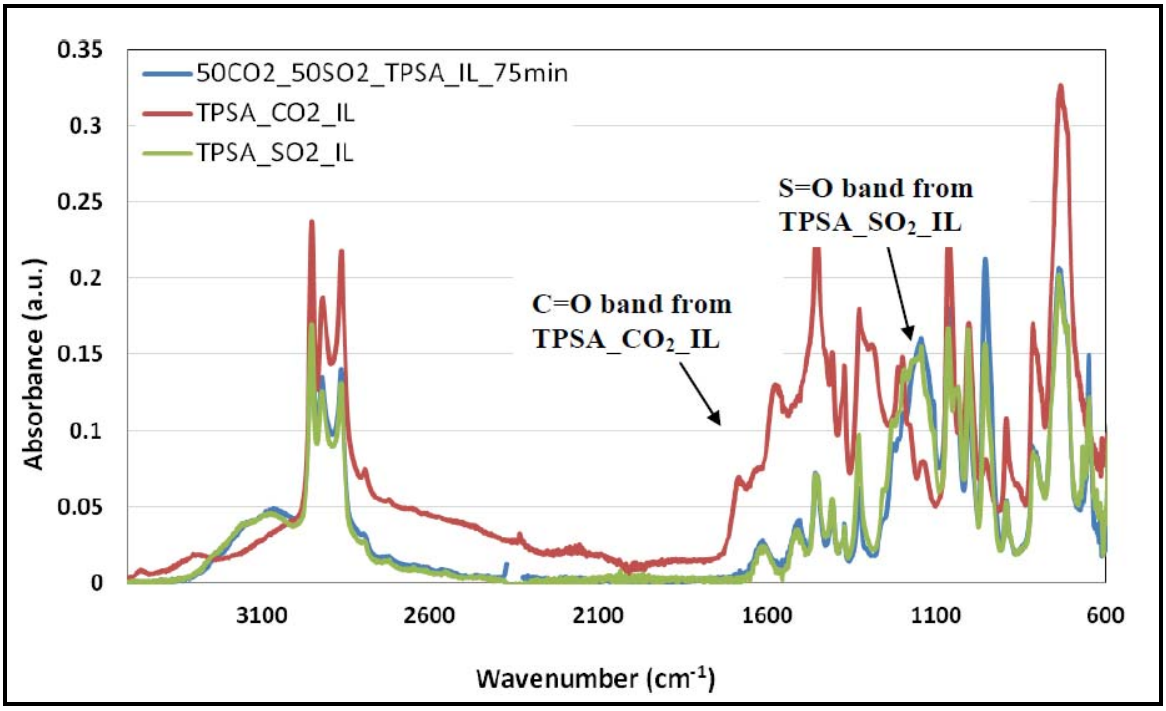

Figure 45 - FTIR spectrum of the reaction of 50/50 vol% SO_2/CO_2 with TPSA, 200 mL/min, 75 minutes, room temperature (blue). TPSA_RevIL (red) and TPSA-SO_2 product (green).

A number of trialkylsilylamine based reversible ionic liquids have been developed and previously reported by our group.[31] The solvents are versatile in that small changes in the structure of the starting amine can affect large changes in the physical and thermodynamic properties of the amine and the corresponding industrial parameters. The effect of increased size of the alkyl-groups around the silicon on industrially relevant parameters was investigated previously by my coworkers.[31] CO_2 capacity, viscosity, reversal temperature and enthalpy of regeneration were monitored as the alkyl groups on the silicon were modified from ethyl (TEtSA) to propyl (TPSA), hexyl (THSA), and then diisopropyl perfluoropentyl chains (FSA, Figure 46). The results of this study have been discussed previously and the initial development of a structure-property relationship was based upon this work.

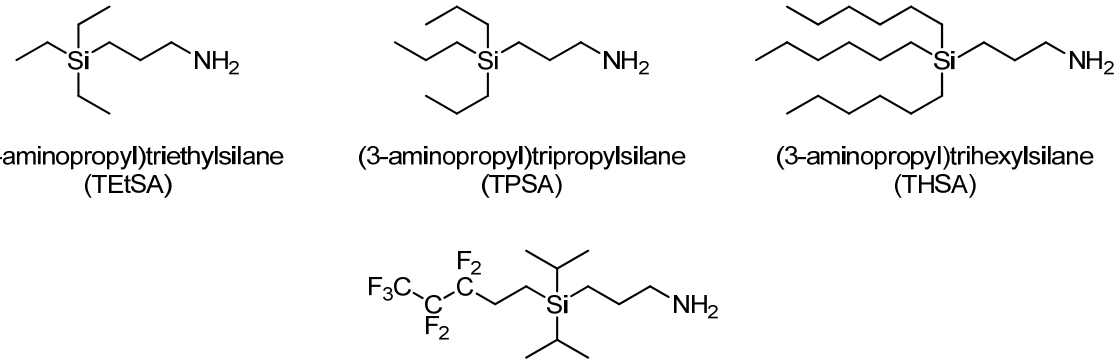

Figure 46 – Structures investigated to determine the effect of the silyl alkyl groups on industrially relevant properties.

The RevIL of each amine was formed by sparging the molecular liquid with CO_2 through a fritted, porous tube at 1 atm CO_2, 25°C, 200 mL/min for 75 minutes. Equilibrium conversions were determined gravimetrically over multiple trials to ensure

full conversion. CO_2 capacities as a function of moles of CO_2 per kg of molecular liquid (ML) were observed to increase as the molecular weight decreased (Figure 47). TEtSA, displayed the highest CO_2 uptake (3.66 mol CO_2/kg ML) while the fluorinated amine, FSA, demonstrated the lowest CO_2 uptake (1.67 mol CO_2/kg ML). However, all amines demonstrated capacities higher than the theoretically predicted capacity, based on the stoichiometry of the equation (0.5 moles CO_2/mole ML) and the molecular weight of the amine.

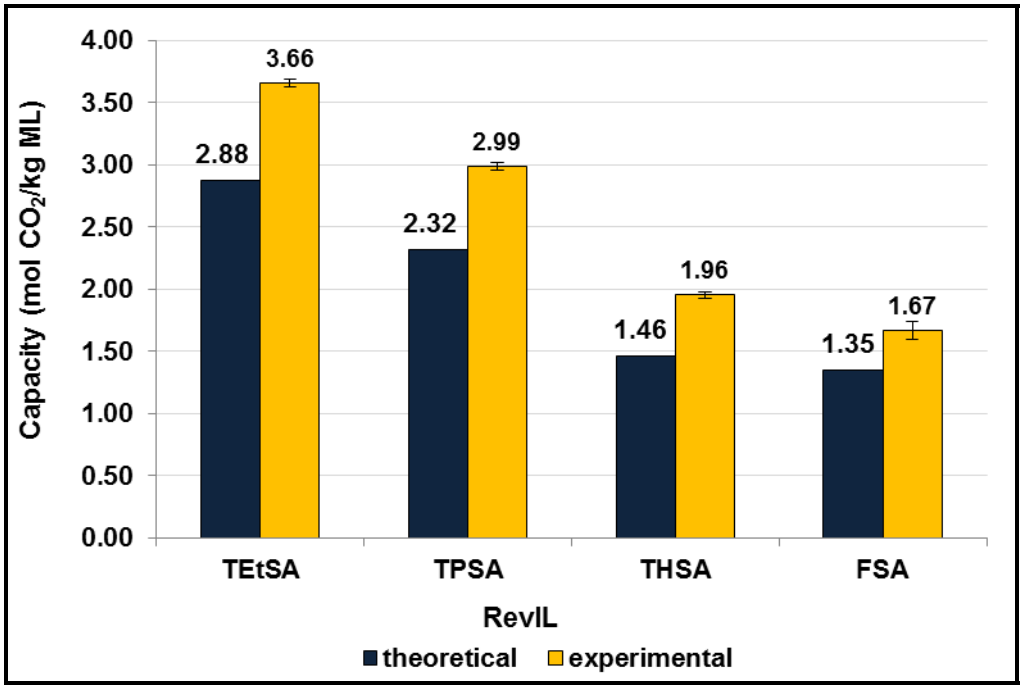

Figure 47 - Theoretical and experimental capacities for trialkylsilanes with varying alkyl groups about the silicon.

Though CO_2 uptake on a mole CO_2 per kg of amine basis is industrially preferred, analyzing uptake on a mole CO_2 /mole amine basis can provide insight into the stoichiometry of the reaction. Comparing the amines on a mole CO_2 /mole amine basis, it was noted that the amines demonstrated similar capture capacities (~0.64 mol CO_2 /mol

ML) (Figure 48), Only THSA demonstrated a slightly increased capacity (0.67 mol CO_2 /mol ML). In general the effect of altering chain length is more pertinent to the molecular weight of the amine and the capacity in terms of mole CO_2/kg amine. Again, the experimental values achieved were greater than the theoretical yields, and the cause of this enhanced capacity was investigated. The results are discussed in the Results and Discussion section of this chapter.

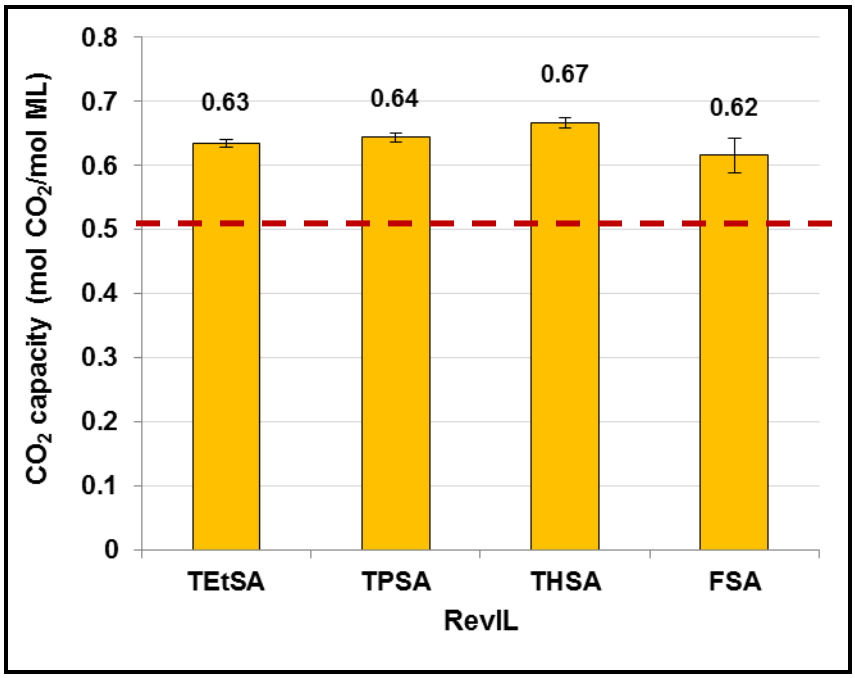

Figure 48 - Experimental CO_2 uptake capacities for trialkylsilanes on a mole CO_2/mole amine basis.

The reversal and evaporation temperatures were well separated; in most cases ~100°C or more separated the reversal and evaporation temperatures for each RevIL (Figure 49). This reduces the likelihood of solvent loss during reversal. Additonally, the reversal temperatures decreased with increasing size of the alkyl substitution about the silicon. TEtSA-RevIL demonstrated a reversal temperature of 71°C while FSA-RevIL demonstrated a reversal temperature 20°C lower.

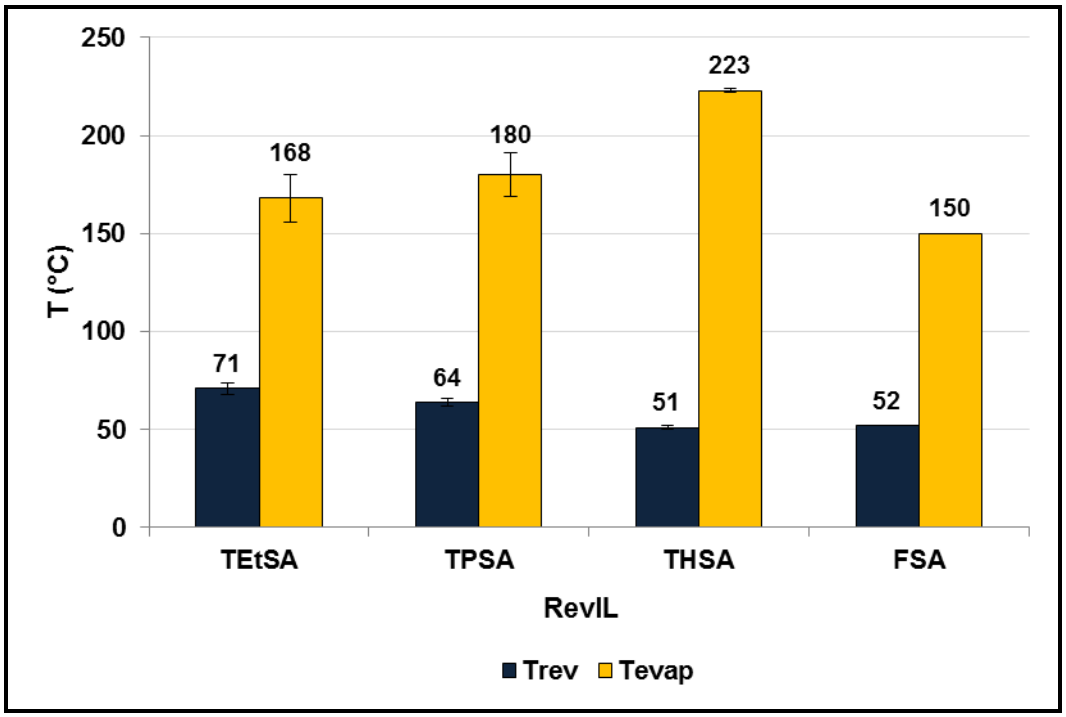

Figure 49 - Reversal and evaporation temperatures as a function of silicon substitution.

The viscosities of the ethyl, propyl and hexyl substituted RevILs at 25°C and 40°C decreased as chain length of the alkyl groups around the silane increased, though FSA demonstrated significantly higher viscosities than the other three RevILs (Figure 50). TEtSA-RevIL demonstrated a viscosity of 6,088 cP at 25°C and 1,303 cP at 40°C. The bulkier THSA-RevIL demonstrated viscosities of 2,359 cP at 25°C and 711 cP at 40°C. FSA demonstrated viscosities over twice as high as TEtSA.

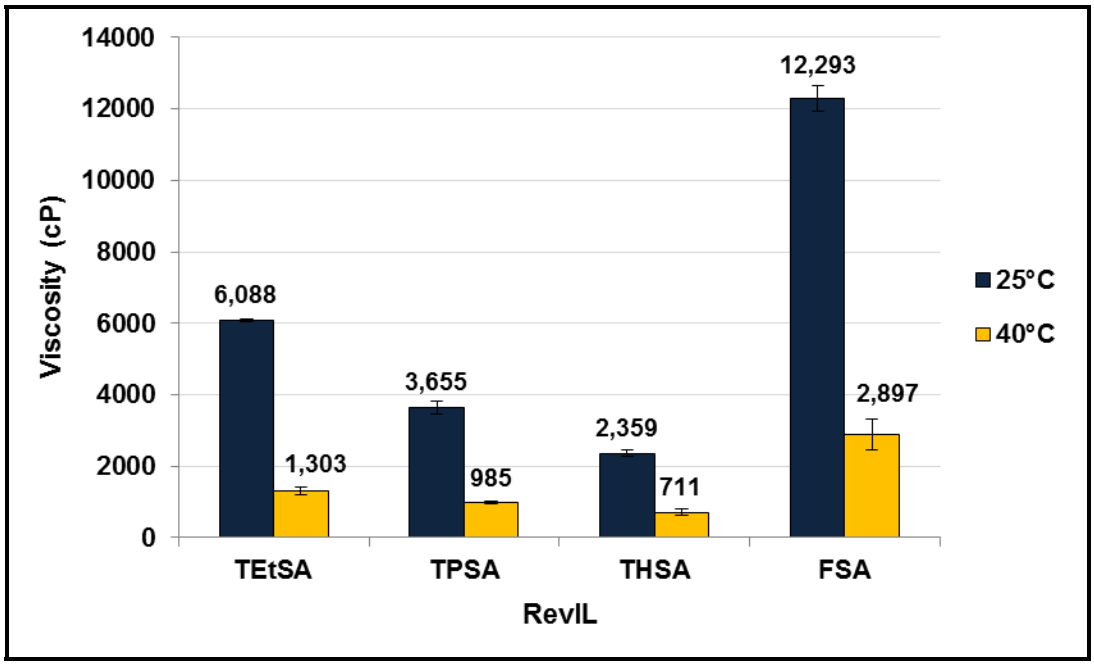

Figure 50 - RevIL viscosity as a function of silicon substition at 25°C and 40°C.

Though the viscosities observed at complete, equilibrium conversions are high - well above 100 cP, which is the upper limit for application of this technology in current industrial systems - it was found that viscosity could be controlled by limiting conversion of the amine to the RevIL. For example, TPSA demonstrates a hockey-stick like correlation between viscosity and conversion (Figure 51). A relatively composition-independent region of viscosity is observed below 50% conversion, where the viscosity remains at approximately 100 cP. This is likely due to solvation of the RevIL by unreacted silylamine (<<100 cP). At conversions greater than 50% a sharp increase in viscosity to 4000 cP at full conversion is observed. This non-linear increase in viscosity is a unique advantage for our systems – traditional ILs and amine-functionalized ILs remain highly viscous regardless of the extent of CO_2 capture.[7] 4EN

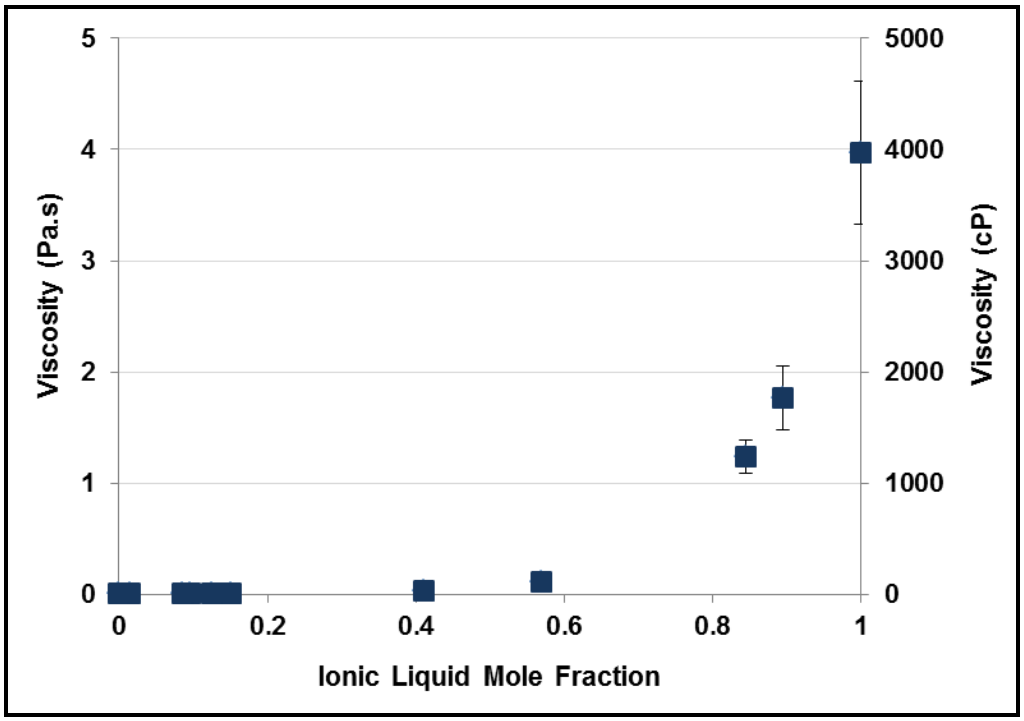

Figure 51- Viscosity of TPSA-RevIL as a function of conversion. Note the relatively composition-independent region below 60% conversion.

In order to complete the structure-property relationship, which can be utilized to design RevILs for desired CO_2 capture applications, we have investigated further structural modifications of the RevIL system. We sought to increase CO_2 capture efficiency while targeting a usable ionic liquid viscosity (< 100 cP) and minimizing the energy required for regeneration. We chose to modify the TEtSA structure to observe the effect of these modifications upon the industrially relevant parameters. The modifications investigated can be grouped into four main categories:

1. The effect of varying tether length between silicon atom and amine
2. Investigating the effect of alkyl branching along the propyl chain backbone of the silylamine
3. Investigating the effect of unsaturation in the propyl chain tether between the silicon and amine

4. Varying the order of the amine from primary to secondary my addition of a methyl group to the amine

Studies have provided evidence of the Lewis acidic character of silicon resulting in the chelation of amine functionalities, as discussed previously.[41] It has been documented that silicon can accept electron density into its low lying unfilled orbitals. 2KF By analogy, the silicon and amine of the silylamines may undergo similar chelation, through either intra- or intermolecular interactions (Figure 52). Donation of electron density from the amine to the silicon could reduce the amount of electron density available for reaction with CO_2, resulting in decreased CO_2 uptake. Reaction of the amine with CO_2 to form a RevIL would reduce interactions with the silicon. However, at this point the effect of the length of the RevIL could affect packing. Increased freedom of rotation from increased length could increase the packing of the molecules, resulting in increased viscosity. An balance between optimum parameters and less optimum parameters is often a difficult task which must be considered. We therefore varied the length of the alkyl tether between silicon and amine and observed the effect on the relevant industrial parameters.

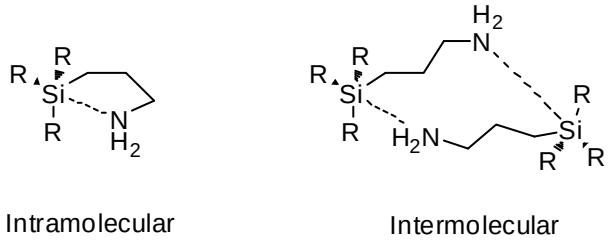

Figure 52 – Proposed intramolecular and intermolecular interactions between silicon and amine.

The effect of branching along the backbone of aqueous alkanolamines on rates of CO_2 has been studied by Sartori and Savage, who reported the reaction of CO_2 with

aqueous branched amines including AMP (2,2-dimethylethanolamine, Figure 53).[42] The bulky dimethyl group alpha to the amine increased the basicity of the amine by sterically destababilizing the carbamate and pushing the equilibrium towards the ammonium and carbonate ions rather than the ammonium-carbamate ion pair. The application of this effect in a non-aqueous system, we hypothesize, would destabilize the carbamate and reduce reversal temperatures. Reversal temperature is one of the key components in the cost of the reversal process. The more heat that is required to increase the temperature of the system to the reversal temperature, the more costly the process is likely to be.

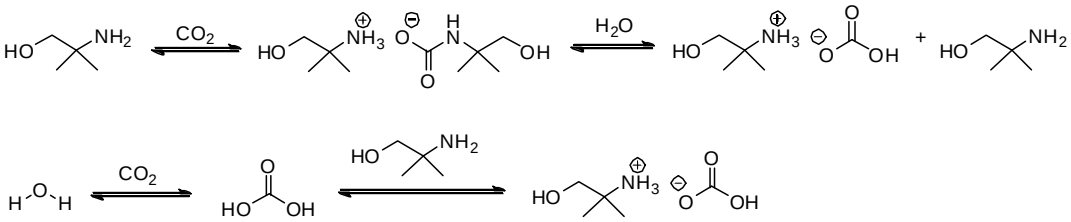

Figure 53 – Equilibrium reaction of aqueous AMP with CO_2.

Unsaturation, we hypothesized, would limit the degree of rotational freedom of the amine resulting in decreased packing and correspondingly decreased viscosity. Also, a slight increase in CO_2 capture, on a mole of CO_2 per kilogram of amine basis, would be likely due to the slight decrease in molecular weight. We synthesized unsaturated versions of the amines to test this theory. A mixture of *cis* and *trans* amines was originally pursued, as this would further decrease packing of the RevIL. Hydrosilylation of the propargylamines in the presence of Karstedt's catalyst and a phosphatrane ligand () exclusively yielded the *trans* isomer and the mixture was not pursued further at this time.

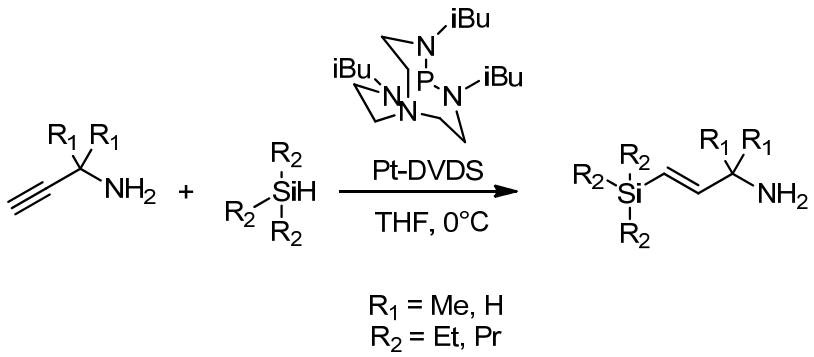

Figure 54 - General scheme for the coupling of propargylamines in the presence of phosphatrane ligand and Karstedt's catalyst, yielding only the *trans* product.

Amines used for CO_2 capture typically involve primary or secondary amines, such as MEA, diethanolamine (DEA), or a mixture of both.[43] Primary amines are known to react instantaneously with CO_2 while secondary amines tend to be slower to react; tertiary amines are unreactive towards CO_2.[42] However, secondary amines can display increased capacities compared to the primary amines due to increased basicity which promotes the formation of the ammonium ion over reaction with CO_2. A methyl group on the amine could also limit the interactions between the ammonium and carbamate ions of the ionic liquid. This could hypothetically lower the enthalpy of regeneration and decrease viscosity. As such, we investigated the effect of amine order by varying the order of the amine from primary to secondary.

Ultimately our motivation was to utilize the iterative structural modifications discussed to develop a complete structure-property relationship for our RevIL systems. This relationship could then be utilized to develop optimum CO_2 capture systems for implementation in coal-fired power plants. The results of this study are discussed herein.

3.3 Synthesis of Molecular Liquids and Reversible Ionic Liquids

The structure of TEtSA was modified as discussed above to develop a structure-property relationship that would allow us to tune the structure of our RevILs for the

desired, application specific, industrially relevant properties (CO_2 capacity, viscosity, reversal temperature, and enthalpy of regeneration). The structural modifications I will discuss herein are: (1) proximity of silicon and amine; (2) branching; (3) unsaturation; and (4) amine order. Silylamines (molecular liquids) were prepared from commercially available starting materials without further purification. The synthetic pathways and purification will be discussed in this section. Detailed experimental and characterization (^{1}H NMR, ^{13}C NMR, EA) of each compound is discussed in the Experimental section. Optimization of the syntheses was not pursued at this juncture as our primary goal was to evaluate the candidates for the physical properties and pursue optimization of the best candidates. When possible, silylamines like TEtSA were prepared via hydrosilylation as described below. However, when necessary we developed new synthetic routes to achieve the desired structural modification.

3.3.1 Proximity: Variation of Alkyl Tether Length Between Silicon and Amine

Four amines were selected to investigate the effect of proximity between silicon and amine (Table 7). The length of the alkyl tether was varied stepwise from methyl to ethyl, propyl, and then butyl.

Table 7 - Amines designed to investigate the effect of silane/amine proximity.

TESMA	TESEA	TEtSA	TESBA
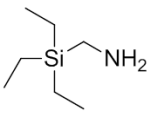	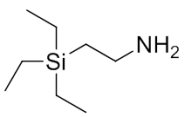	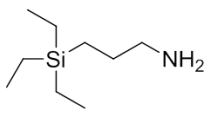	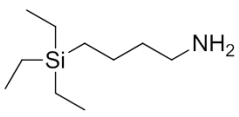

3.3.1.1 Synthesis of 3-Aminopropyltriethylsilane (TEtSA)

TEtSA was synthesized in one step from the hydrosilylation of allyl amine and triethylsilane (Figure 55) with Karstedt's catalyst (Pt-DVDS, Figure 56) in toluene at 110°C. The product was isolated from the reaction mixture *via* vacuum distillation to yield 3-aminopropyltriethylsilane as a colorless liquid in 89% isolated yield.

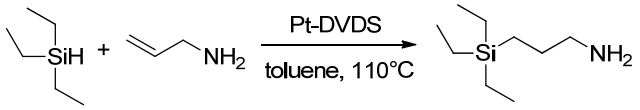

Figure 55 – Hydrosilylation of triethylsilane and allylamine to yield TEtSA.

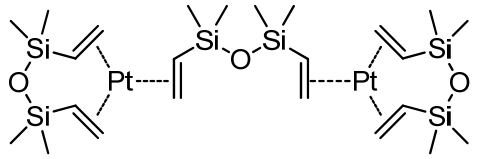

Figure 56 - Structure of Karstedt's catalyst.

3.3.1.2 Synthesis of 1-(aminomethyl)triethylsilane (TEtSMA)

TEtSMA was synthesized in three steps from trichloro(chloromethyl)silane (Figure 57). Grignard displacement of three chlorine atoms by EtMgCl yielded triethyl(chloromethyl)silane (85%).[44] The Gabriel synthesis, a common method for the synthesis of primary amines, was utilized to afford the amine moiety by substitution of the chloride with potassium phthalamide under basic conditions at 100°C (80%).Subsequent deprotection of triethylsilylphthalimidomethane was achieved through the Ing-Manske protocol with hydrazine in methanol.[45] Distilliation of the product was originally attempted with heat, however a yellow sludge formed in the distillation flask as the temperature approached 170°C. Instead, the crude product was distilled under vacuum at room temperature to yield 1-(aminomethyl)triethylsilane (27%) as a colorless

liquid. The low yield may be due to incomplete recovery of the product due to the necessity to avoid heat during distillation and/or decomposition of the product during isolation.

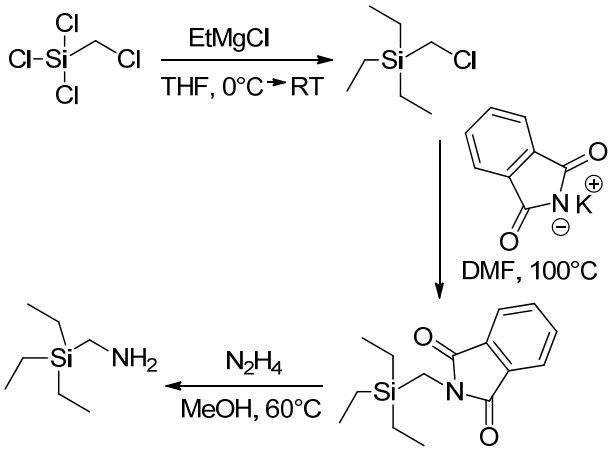

Figure 57 – Synthetic route to TEtSMA *via* Grignard displacement, Gabriel synthesis and Ing-Manske deprotection.

3.3.1.3 Synthesis of 2-(aminoethyl)triethylsilane (TEtSEtA)

Ethylene linker, TEtSEtA, was synthesized in two steps from triethylsilane and N-vinylphthalimide (Figure 58). Hydrosilylation of the two starting materials in the presence of Pt-DVDS in toluene at 110°C yielded the phthalimide protected 2-(aminoethyl)triethylsilane. The product was not purified but subjected directly to deprotection with hydrazine in methanol at 60°C yielded the crude product. Distillation yielded the pure 2-(aminomethyl)triethylsilane as a colorless liquid in a 25% isolated yield over two steps. A viscous mixture of solids and liquid is formed from the reaction of hydrazine with the phthalamide in which some of the product may be trapped, despite multiple extractions with organic solvent, resulting in a decreased overall yield.

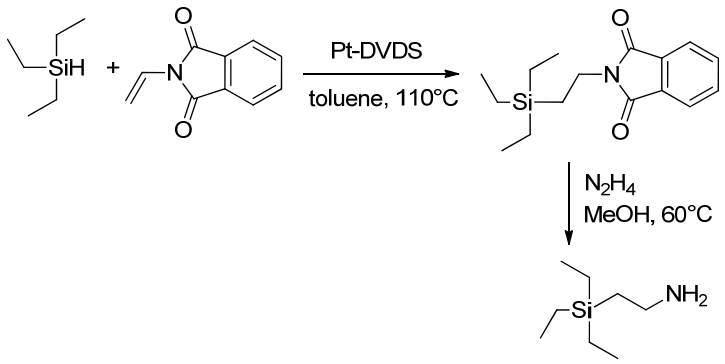

Figure 58 – Synthetic route to TEtSEtA *via* hydrosilylation and Ing-Manske deprotection.

3.3.1.4 Synthesis of 4-(aminobutyl)triethylsilane (TEtSBA)

4-(Aminobutyl)triethylsilane was synthesized *via* the hydrosilylation of triethylsilane and 4-amino-1-butene with Pt-DVDS in toluene at 80°C (Figure 59). Distillation yielded the pure TEtSBA as a colorless liquid in 66% isolated yield. Though typically a minor product, substitution at the alpha positon of the alkene has been observed for hydrosilylations with Pt-DVDS. Byproducts would not be carried through the distillation, and may account for the remainder of the yield. Analysis of the remainder of the mixture could confirm this possibility.

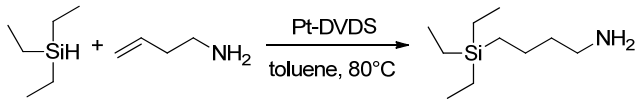

Figure 59 – Hydrosilylation of triethylsilane and 4-amino-1-butene to yield TEtSBA.

3.3.2 Branching

The effect of branching along the backbone upon the relevant industrial parameters was investigated by the addition of one or two methyl groups alpha and beta to the amine of TEtSA (Table 8).

Table 8 - Amines designed to probe the effect of branching.

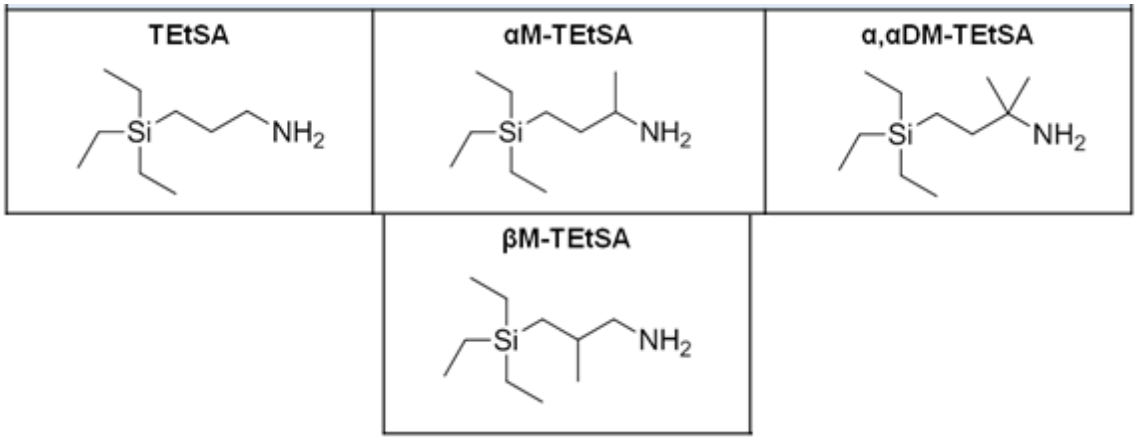

3.3.2.1 Synthesis of 4-(triethylsilyl)-butyl-2-amine (αMe-TEtSA)

Attempted Synthesis via Overman Rearrangement

Initially, we attempted to synthesize the branched silylamine αMe-TEtSA via the Overman rearrangement of crotyl alcohol, adapted from literature,[46] and subsequent deprotection of the resultant trichloroacetamide (Figure 60). The Overman rearrangement proceeded smoothly to yield N-(but-3-en-2-yl)-2,2,2-trichloroacetamide with no sign of the starting crotyl alcohol. Only 17% of the pure trichloroacetamide was isolated, however, due to losses resulting from column chromatography purification. Optimization of this step was not pursued, but it is possible interactions of the amine moiety with the column resulted in retention of the product on the column.

Hydrosililyation of the crude product could potentially surmount this issue and provide increased yields.

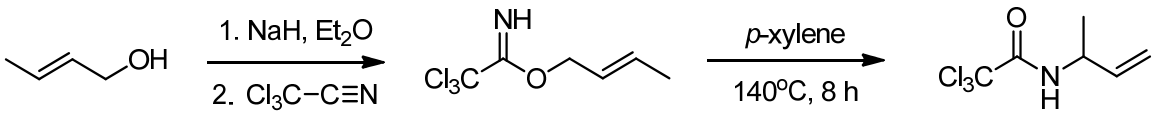

Figure 60 - Overman rearrangement of crotyl alcohol to form α-methyl trichloroacetamide precursor to αMe-TEtSA.

Hydrosilylation via the usual method (Figure 61), as described above for TEtSA and TEtSBA, also proceeded well. However, the trichloroacetamide protecting group proved difficult to remove. Several deprotection methods were attempted, including: prolonged heating with concentrated NaOH;[47] treatment with sodium borohydride;[48] and heating with cesium chloride in N,N-dimethylformamide.[49] Each deprotection was monitored by ^{1}H or ^{13}C NMR, but no sign of the free amine was observed. Ultimately, the Overman rearrangement method was abandoned in favor of an alternative route.

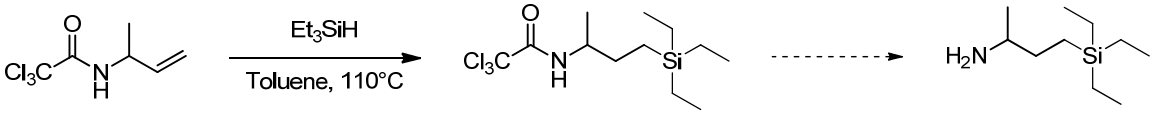

Figure 61. - Hydrosilylation of αMe-trichloroacetamide and attempted deprotection to form αMe-TEtSA.

Synthesis of αMe-TEtSA via Gabriel Addition and Ing-Manske Deprotection

The Gabriel synthesis of 3-phthalimido-1-butene was performed as reported by Semenow *et al.* (Figure 62) in 67% yield.[50] Subsequent hydrosilylation yielded the

protected αMe-TEtSA which was isolated *via* distillation under vacuum (75%). Ing-Manske deprotection afforded αMe-TEtSA, however vacuum distillation of the protected amine required high temperatures (160°C at the distillation head). Subsequent trials showed purification of the protected amine before deprotection was unnecessary. Deprotection of the crude protected amine and subsequent purification *via* vacuum distillation yielded αMe-TEtSA (67%) as a colorless liquid.

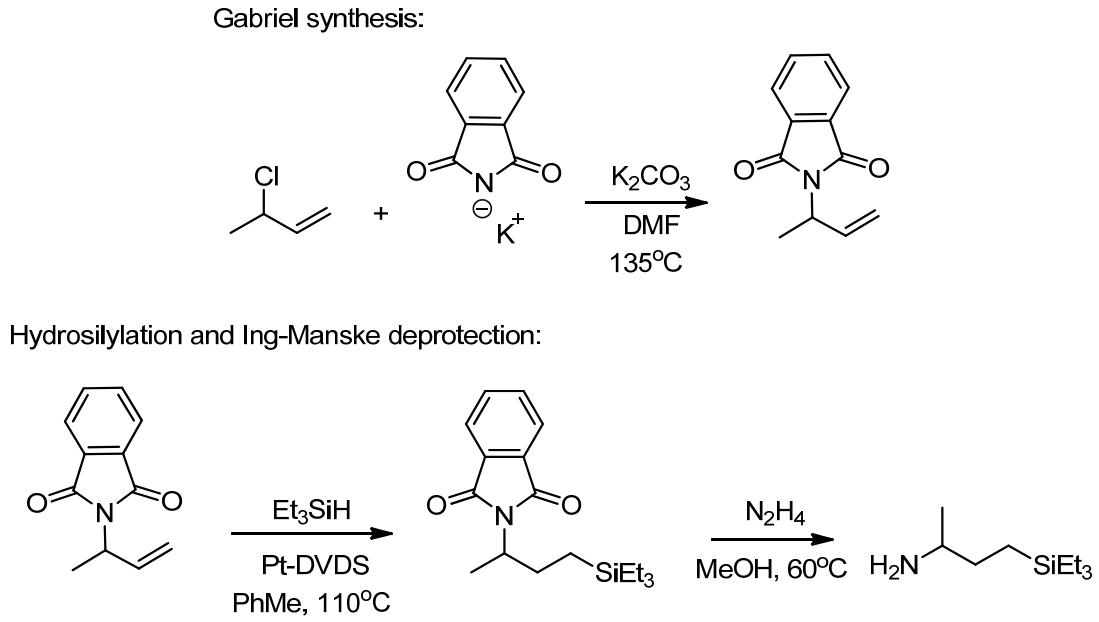

Figure 62 – Synthesis of αM-TETSA. Top, Gabriel synthesis using 3-chloro-1-butene to yield protected primary amine; bottom, hydrosilylation and Ing-Manske deprotection to yield 4-(triethylsilyl)-butyl-2-amine (αM-TEtSA).

3.3.2.2 Synthesis of 2-methyl-3-(triethylsilyl)propylamine (β-MeTEtSA)

Attempted Synthesis via Overman Rearrangement

The synthesis of β-MeTEtSA was also initially attempted *via* the Overman rearrangement of the addition product of 2-methyl-2-propenol and trichloroacetonitrile

(Figure 63). Synthesis of the trichloroacetamididate was successful and rearrangement was conducted without further purification. Though the trichloroacetamide was formed as evidenced by ^{13}C NMR, with no sign of the starting alcohol, attempted isolation by column chromatography resulted in degradation of the product. In the interest of expediency, this method was abandoned in favor of the simpler hydrosilylation reaction.

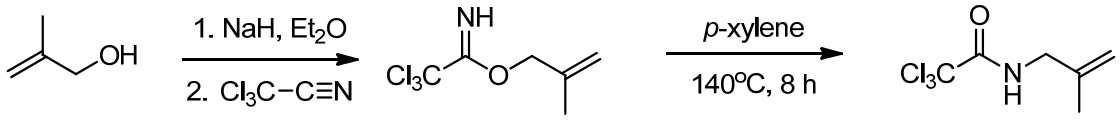

Figure 63 - Overman rearrangement of 2-methyl-2-propenol to form β-methyl trichloroacetamide precursor to βMe-TEtSA.

Synthesis via Hydrosilylation

β-MeTEtSA was synthesized by the hydrosilylation of triethylsilane and 2-methylallylamine in the presence of Karstedt's catalyst and refluxing toluene (Figure 64). Distillation under vacuum yielded pure 2-methyl-3-(triethylsilyl)propylamine (76%) as a colorless liquid.

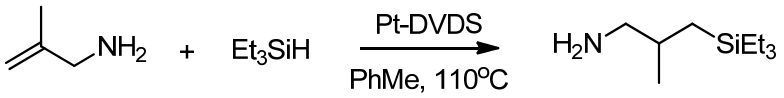

Figure 64 - Hydrosilylation of 2-methylallylamine to yield 2-methyl-3-(triethylsilyl)propylamine (βMe-TEtSA).

3.3.2.3 Synthesis of 2-methyl-4-(triethylsilyl)-butyl-2-amine (α,αDMe-TEtSA)

Attempted Synthesis via Overman Rearrangement

The synthesis of α,αDMe-TEtSA was attempted *via* an Overman rearrangement as well. The trichloroacetimidate product of prenyl alcohol and trichloroacetonitrile (Figure 65) was synthesized and rearranged *via* the Overman protocol following the work of Nagashima *et al*.[51] However, hydrosilylation of the trichloroacetamide was unsuccessful, possibly due to the steric bulk of the protected amine (Figure 65). Deprotection of the trichloroacetamide and isolation of the volatile α,α-dimethylallylamine *via* the literature methods mentioned previously were also unsuccessful (treatment with concentrated NaOH;[47] sodium borohydride;[48] and heating with cesium chloride in N,N-dimethylformamide[49]). Again, no sign of the deprotected amine was detected via ^{1}H NMR. An alternative method was developed and found to be successful.

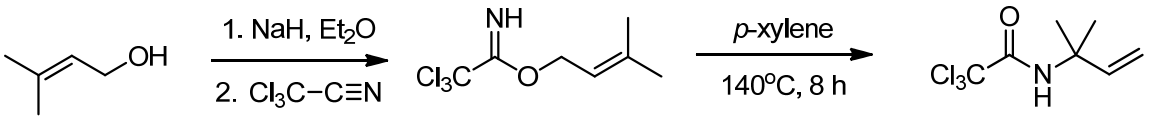

Figure 65 - Overman rearrangement of prenyl alcohol to form α-dimethyl trichloroacetamide precursor to α, αDMe-TEtSA.

Synthesis via Hydrosilylation and Subsequent Hydrogenation

Terminal alkynes can undergo hydrosilylation similar to alkenes, though Karstedt's catalyst has not been shown to be stereoselective in the hydrosilylation of alkynes and would likely produce a mixture of *cis* and *trans* isomers (Figure 66). Azaphosphatrane ligands 1b-1d (Figure 67), however, have been shown to facilitate regio- and stereoselective hydrosilylation of alkynes producing almost exclusively (98% yield) the trans-isomer for the hydrosilylation of propargyl alcohols with triphenylsilane.[52-53] Although use of the stereoselective ligand was not necessary to afford

α,αDMe-TEtSA, the *trans* intermediate, which is formed exclusively in the presence of the azaphosphatrane ligand, was hypothesized to potentially decrease viscosity, and was also synthesized and isolated for further study.

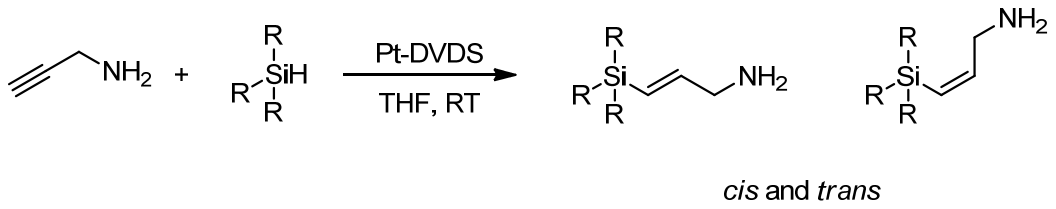

Figure 66 – Non-stereoselective hydrosilylation of alkynes to form both *cis* and *trans* isomers.

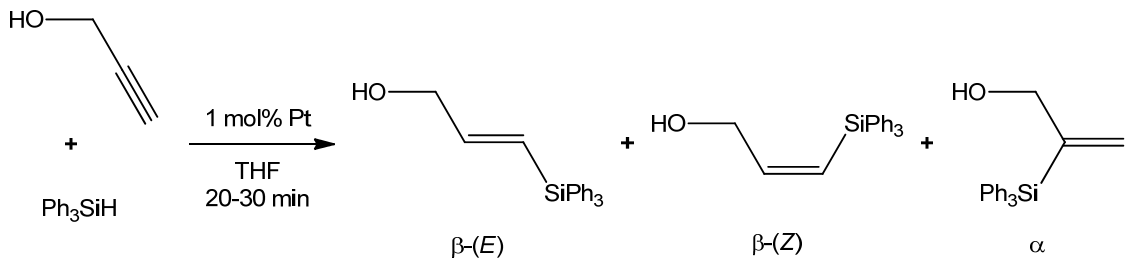

		Product Distribution		
Entry no.	Catalyst	β-(*E*)	β-(*Z*)	α
1	$[Pt_2(DVDS)_3]$	69	Trace	31
2	Pt(DVDS)/(**1a**)	76	Trace	24
3	Pt(DVDS)/(**1b**)	98		2
4	Pt(DVDS)/(**1c**)	98		2
5	Pt(DVDS)/(**1d**)	98		2

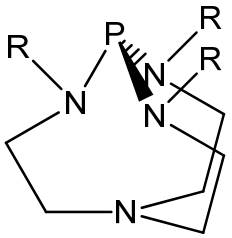

R	Me	iPr	iBu	Bn
L	**1a**	**1b**	**1c**	**1d**

Figure 67 - Stereoselective hydrosilylation to form *trans* isomers.

Synthesis of α,αDMe-TEtSA proceeded as outlined in Figure 68. Equimolar amounts of Pt-DVDS (1.268 mol% with respect to silane, 1.205 x 10^{-3} mol) and azaphosphatrane ligand (1.200 x 10^{-3} mol) were combined at 60°C for 10 minutes to form the azaphosphatrane-Pt(DVDS) complex. Tetrahydrofuran (THF) was added and the system was cooled to 0°C with an ice/brine bath before addition of triethylsilane. Subsequent addition of the alkyne causes a large exotherm, and the ice bath was carefully maintained until the exotherm had ceased. The system was then mixed at room temperature overnight. Hydrogenation of the *trans* intermediate with H_2 in the presence of palladium on carbon in hexanes at 50°C yielded α,αDMe-TEtSA (80%) as a colorless liquid after vacuum distillation.

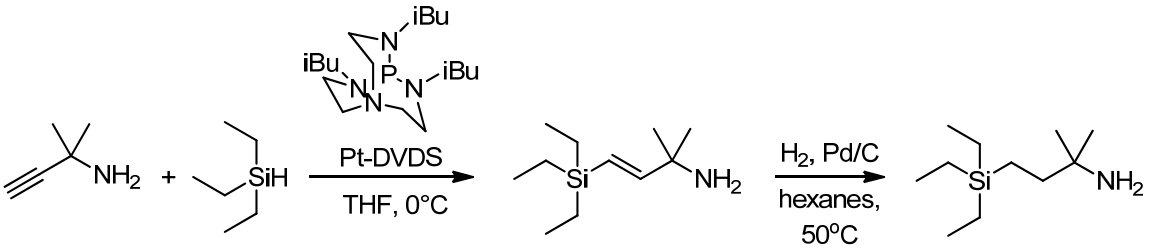

Figure 68 - Hydrosilylation of 2-methyl-3-butyn-2-amine with triethylsilane, followed by palladium-catalyzed hydrogenation.

3.3.3 Unsaturation

Three amines were prepared to investigate the effect of unsaturation upon the relevant industrial properties (Table 9).

Table 9 - Amines designed to probe the effect of unsaturation.

trans-TEtSA	*trans*-α,αDMe-TEtSA	*trans*-α,αDMe-TPSA
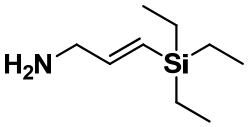	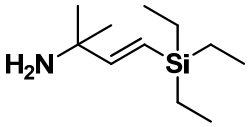	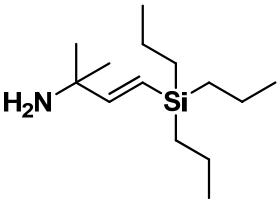

Synthesis of *trans*-3-(triethylsilyl)prop-2-ene-1-amine (*trans*-TEtSA), *trans*-2-methyl-4-(triethylsilyl)-butyl-2-amine (*trans*-α,αDMe-TEtSA) and *trans*-2-methyl-4-(tripropylsilyl)-butyl-2-amine (*trans*-α,αDMe-TPSA)

As discussed for the synthesis of α,αDMe-TEtSA, Aneetha *et al*. have demonstrated that the use of azaphosphatrane ligands for hydrosilylation of alkynes yield only the *trans* isomer.[52] Using the same procedure as described for the synthesis of α,αDMe-TEtSA without hydrogenation of the double bond, *trans*-TEtSA was synthesized from triethylsilane and propargylamine (Figure 69). α,α-Dimethylpropargylamine was utilized to synthesize *trans*-α,αDMe-TEtSA and *trans*-α,αDMe-TPSA from triethylsilane or tripropylsilane respectively. Distillation yielded each as a colorless liquid with the following isolated yields: *trans*-TEtSA, 46%; *trans*-α,αDMe-TEtSA, 80%; and *trans*-α,αDMe-TPSA, 68%. All reactions were monitored by following the disappearance of the alkyne peak at approximately 91 ppm by ^{1}H NMR. However, we did not monitor for the formation of α-substituted alkynes, which may have formed from the less sterically hindered propargylamine and may account for the decreased yield as compared to the other *trans*-silylamines.

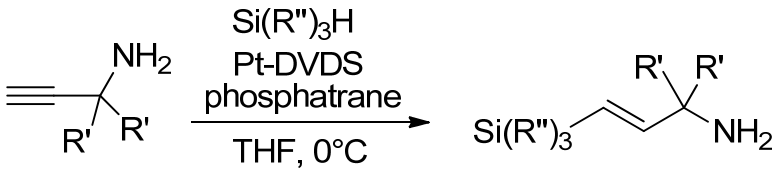

Figure 69 - Synthesis of *trans*-TEtSA (R'=H; R''=CH2CH3), *trans*-α,αDMe-TEtSA (R'=CH_3; R''=CH_2CH_3), *trans*-α,αDMe-TPSA (R'= CH_3; R''=$CH_2CH_2CH_3$) *via* hydrosilylation in the presence of Karstedt's catalyst and a phopsphatrane ligand.

3.3.4 Secondary and Primary Analogs of Trialkylsilylamines

Dimethylethylsilane (DMESA) was designed as an analog of TEtSA with smaller alkyl groups around the silicon (Table 10). Decrease in alkyl group size around the silicon has been shown to increase capacity on a mole of CO_2 per kg of amine basis, as discussed in the Background section. Secondary amines of both were also designed and synthesize to observe the effect of an N-methyl moiety upon the relevant industrial processes.

Table 10 - Secondary and primary analogs of TEtSA.

TEtSA	STEtSA	DMESA	SDMESA
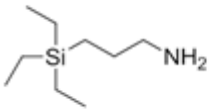	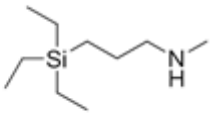	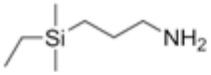	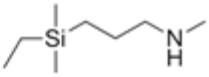

Synthesis of 3-(aminopropyl)dimethylethylsilane (DMESA)

DMESA was synthesized in an analogous fashion to TEtSA, *via* the hydrosilylation of dimethylethylsilane with allylamine (Figure 70). Distillation yielded the pure 3-(aminopropyl)dimethylethylsilane as a colorless liquid (58%).

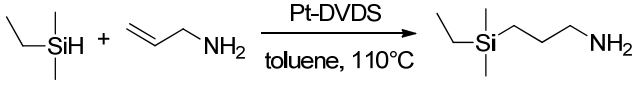

Figure 70 – Hydrosilylation of dimethylethylsilane and allylamine to yield DMESA.

Synthesis of N-methyl-3-(triethylsilyl)propan-1-amine (STEtSA) and N-methyl-3-(aminopropyl)dimethylethylsilane (SDMESA)

Secondary versions of both DMESA and TEtSA were formed in a similar manner (Figure 71). Preformed silylamine was stirred, neat, with ethylformate at 60°C under argon for 4 hours. Solvent and ethanol byproduct were removed *in vacuo* to yield 98% of the formamide. The formamide was then reduced with two equivalents lithium aluminum hydride ($LiAlH_4$) in THF at 60°C. After 18 hours excess $LiAlH_4$ was quenched with water and followed by a 10% NaOH aqueous solution. Isolation of the product by filtration through celite, concentration *in vacuo* and subsequent vacuum distillation of the crude product yielded colorless liquids. S-TEtSA was isolated in 73% isolated yield; DMESA in 49% isolated yield. Some product may have been trapped in the lithium salts formed from the reduction of the formamide resulting in reduced yields.

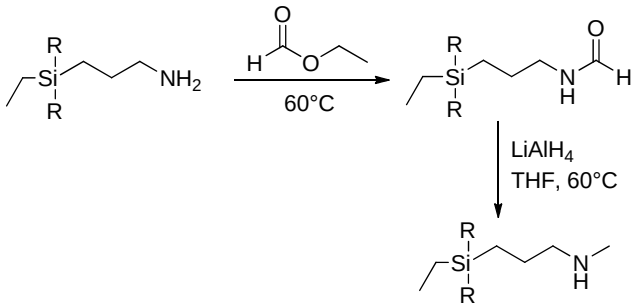

Figure 71 – Formylation and subsequent reduction *via* $LiAlH_4$ to yield S-TEtSA (R = CH_2CH_3) and S-DMESA (R = CH_3).

3.3.5 Formation of Reversible Ionic Liquid

Known amounts of silylamine (~1 g) were sparged with anhydrous CO_2 via a porous fritted tube (Ace Glass, 10 mm gas dispersion tube, porosity C) for 75 minutes at a flow rate of 200 mL/min at 25°C or 40°C and 1 bar. CO_2 uptake was determined gravimetrically. Multiple trials were conducted to ensure complete equilibrium conversions. The amines reacted to form ammonium-carbamate ion pairs which were liquid at room temperature. The ionic liquids are reversible upon heating, and thus dubbed Reversible Ionic Liquids, or RevILs (Figure 72).

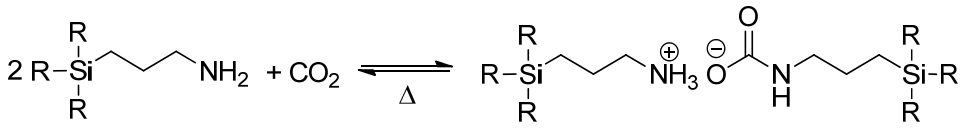

Figure 72 - Reaction of silylamine to form Reversible Ionic Liquid.

Analysis of the reaction mixtures showed distinct changes in ^{1}H NMR, ^{13}C NMR and FTIR upon formation of the RevIL. Sample ^{13}C NMR spectra of tripropylsilylamine (TPSA) and TPSA Rev-IL formed from reaction of ^{13}C labeled CO_2 with TPSA are displayed below. We observe splitting of the carbons alpha and beta to the amine around 28 and 46 ppm (carbons labeled a and b, Figure 73) to two sets of peaks (carbons labeled a, a', b and b' in Figure 74). Also, the formation of a carbon signal in the carbonyl region was observed, around 170 ppm, which corresponds to the carbonyl carbon of the carbamate (labeled g in Figure 74).

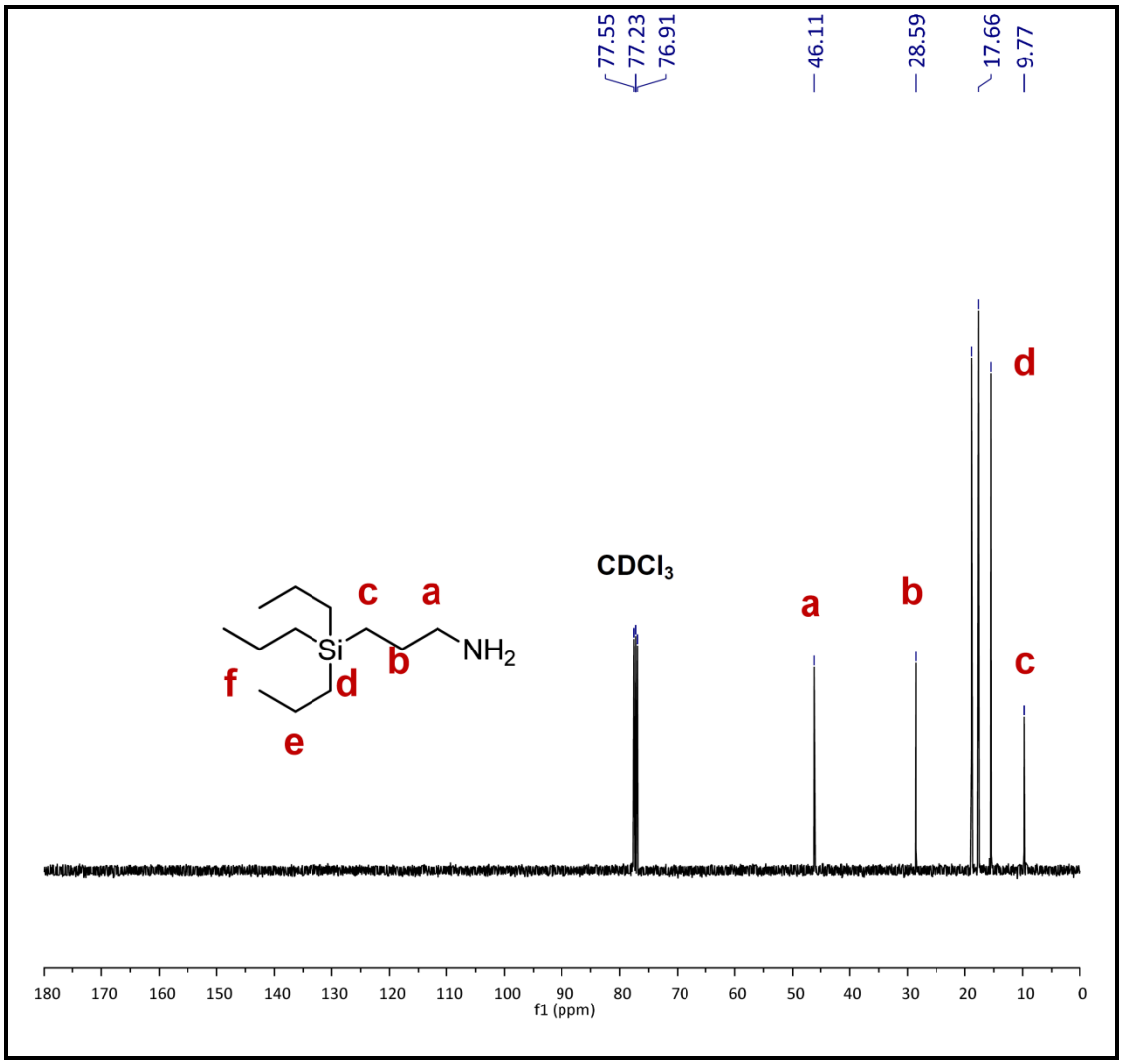

Figure 73 – ^{13}C NMR spectrum of TPSA molecular liquid.

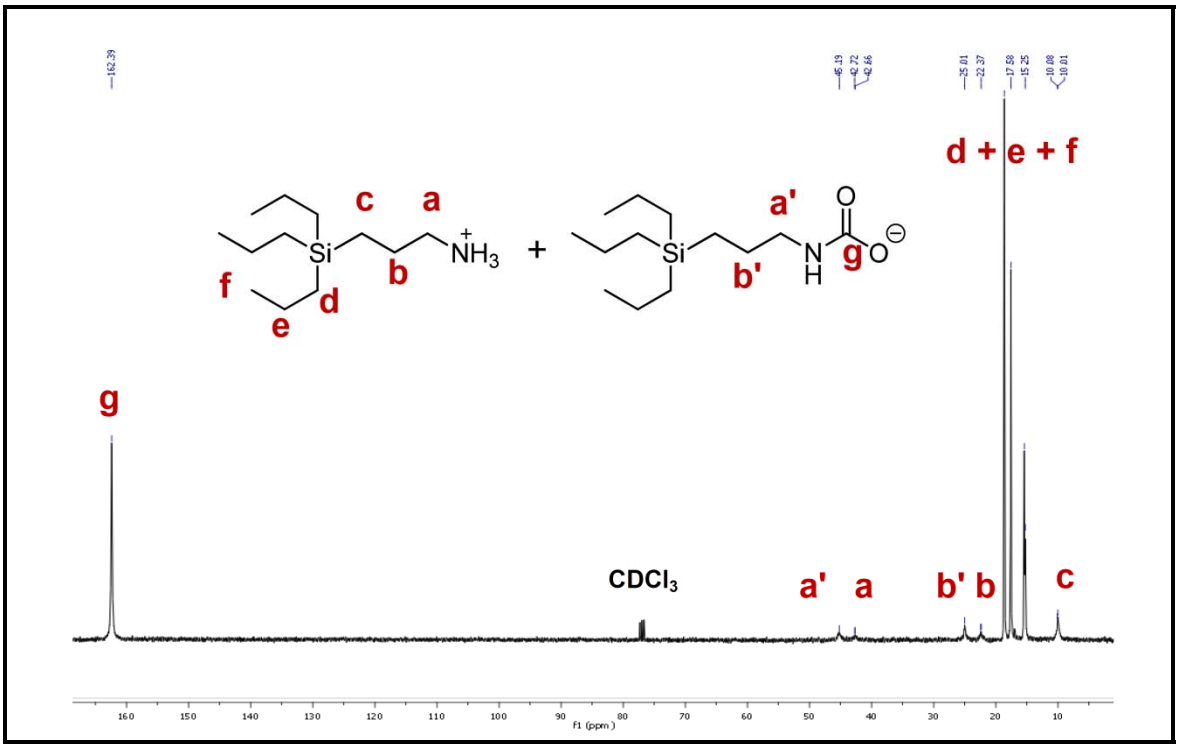

Figure 74 – ^{13}C NMR spectrum of TPSA RevIL.

3.4 Results and Discussion

3.4.1 CO_2 Capture Capacities

Known amounts of silylamine were reacted with 1 atm anhydrous CO_2 by sparging through a fritted bubbler at 25°C. Equilibrium conversions were measured gravimetrically over multiple samples, to ensure reproducibility. Gravimetric uptake is the result of both chemisorption from the ionic liquid and physisorption by the ionic liquid of additional CO_2. However, previous studies have shown the physical absorption at 1 atm CO_2 counts for only around 0.01 – 0.02 moles of CO_2 per mole of amine.[54] For reference a 30 wt% aqueous solution of MEA has been found to have a capacity (chemisorption) of 0.22 moles of CO_2 per mole of MEA.[4]

Carbon dioxide equilibrium uptake capacities are outlined in Table 11-Table 15 in two units: moles CO_2 per mole of silylamine to provide a stoichiometric view of the capacity; as well as moles CO_2 per kilogram of silylamine, which is an industrially relevant unit applicable when considering the viability of this system versus other systems. Increasing length of the alkyl tether from methyl (TEtSMA) to ethyl (TEtSEtA) to propyl (TEtSA) does not result in much change in the CO_2 capacity (Table 11). However, increased length of the alkyl tether from a propyl (TEtSA) to a butyl linker (TEtSBA) results in the formation of a solid (MP: 66 ± 4°C). Solid formation can impede mass transfer of CO_2 and resulted in a lower capacity of 0.35 mol CO_2/mol silylamine. TEtSEtA interestingly reaches a capacity similar to TEtSA despite also forming a solid (MP: 49 ± 1°C).

Table 11 - Effect of Proximity Upon Silylamine Capacity. Gravimetric CO_2 uptake capacities after reaction with 1 bar CO_2 at 25°C.

Abbreviation	Silylamine	CO_2 Uptake (mol CO_2/mol amine)	CO_2 Uptake (mol CO_2/kg amine)
TEtSMA	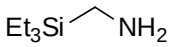	0.59 ± 0.01	4.09 ± 0.08
TEtSEtA	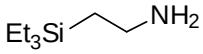	0.59 ± 0.01	3.67 ± 0.03
TEtSA	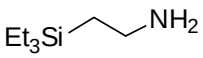	0.63 ± 0.01	3.66 ± 0.04
TEtSBA	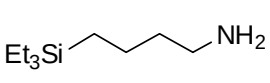	0.35 ± 0.03	1.9 ± 0.2

The placement of a single methyl group alpha to the amine (αMe-TEtSA) does not affect the capacity as compared to TEtSA (0.63 mol CO_2/mol amine, Table 11).

However, substitution of the carbon alpha to the amine with a two methyl groups (α,αDMe-TEtSA) results in a 27% lower capacity (0.48 mol CO_2/mol amine). Steric hindrance of the dimethyl group likely resulted in reduced reactivity with CO_2. Though a single methyl group alpha to the amine resulted in no change in capacity from TEtSA, a methyl group beta to the amine (βMe-TEtSA) interestingly resulted in a slight decrease from 0.63 moles CO_2 per mole for TEtSA of amine to 0.59 moles CO_2 per mole of amine.

Table 12 - Effect of Branching Upon Silylamine Capacity. Gravimetric CO_2 uptake capacities after reaction with 1 bar CO_2 at 25°C.

Abbreviation	Silylamine	CO_2 Uptake (mol CO_2/mol amine)	CO_2 Uptake (mol CO_2/kg amine)
αMe-TEtSA	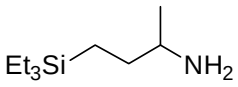	0.63 ± 0.03	3.36 ± 0.15
α,αDMe-TEtSA	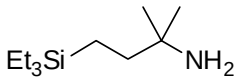	0.48 ± 0.03	2.4 ± 0.2
βMe-TEtSA	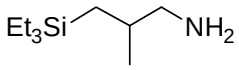	0.59 ± 0.01	3.15 ± 0.07

Unsaturation also has little effect on the CO_2 uptake in comparison to the saturated analogs (Table 13). Both *trans*-TEtSA (0.61 ± 0.03 mol CO_2/mol amine) and *trans*-α,αDMe-TEtSA (0.47 ± 0.03 mol CO_2/ mol amine) display capacities within experimental error of their saturated analogs. Synthesis of the tripropyl analog of *trans*-α,αDMe-TEtSA (*trans*-α,αDMe-TPSA) yielded a slightly decreased CO_2 uptake at 0.40 moles CO_2 per mole of amine.

Table 13 - Effect of Unsaturation Upon Silylamine Capacity. Gravimetric CO_2 uptake capacities after reaction with 1 bar CO_2 at 25°C.

Abbreviation	Silylamine	CO_2 Uptake (mol CO_2/mol amine)	CO_2 Uptake (mol CO_2/kg amine)
trans-TEtSA	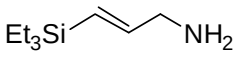	0.61 ± 0.03	3.56 ± 0.20
trans-α,αDMe-TEtSA	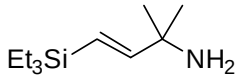	0.47 ± 0.03	2.35 ± 0.16
trans-α,αDMe-TPSA	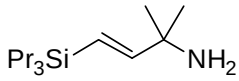	0.40 ± 0.000	1.65 ± 0.000

DMESA yielded a decreased CO_2 uptake (0.42 mol CO_2/mol amine) compared to TEtSA (Table 14). However, DMESA also formed a solid (MP: 66 ± 3°C) which could impede the uptake of CO_2 through mass transfer constraints. The secondary version (SDMESA) does not form a solid and exhibited a capacity of 0.62 moles CO_2 per mole of amine, which is a significant increase compared to DMESA and is comparable to TEtSA. STEtSA (0.65 mol CO_2/mol amine) also exhibits a capacity similar to TEtSA.

Table 14 - Effect of Primary and Secondary Analogs of TEtSA Upon Silylamine Capacity. Gravimetric CO_2 uptake capacities after reaction with 1 bar CO_2 at 25°C.

Abbreviation	Silylamine	CO_2 Uptake (mol CO_2/mol amine)	CO_2 Uptake (mol CO_2/kg amine)
TEtSA	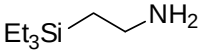	0.63 ± 0.01	3.66 ± 0.04
STEtSA	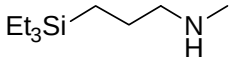	0.65 ± 0.01	3.49 ± 0.05
DMESA	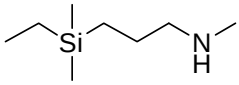	0.42 ± 0.04	2.85 ± 0.24
SDMESA	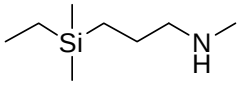	0.62 ± 0.02	3.87 ± 0.11

Though 25°C was utilized for the analyses of all silylamines to provide a stable comparison of CO_2 capacity - as some amines will be shown later on to have low reversal temperatures – a representative temperature of the flue gas for a post-combustion stream in a coal fired power plant would actually be around 40°C. The capacities for select amines, TEtSA, α,αDMe-TEtSA, and βMe-TEtSA were observed at 40°C (Table 15). Only TEtSA displayed any change, a modest drop of only 5% in capacity at the elevated temperature.

Table 15 - CO_2 uptake capacity at 40°C for a select group of silylamines.

Abbreviation	CO_2 Uptake at 40°C (mol CO_2/mol amine)	CO_2 Uptakk at 40°C (mol CO_2/kg amine)
TEtSA	0.603 ± 0.002	3.48 ± 0.01
α,αDMe-TEtSA	0.46 ± 0.02	2.29 ± 0.08
βMe-TEtSA	0.599 ± 0.003	3.19 ± 0.01

The average uptake of the silylamines discussed was 0.59 moles of CO_2 per mole of amine. Stoichiometrically, these amines demonstrate an enhanced capacity as compared to the predicted stoichiometric conversion of 0.5 moles CO_2 per mol amine based upon the reaction as shown in Figure 75.

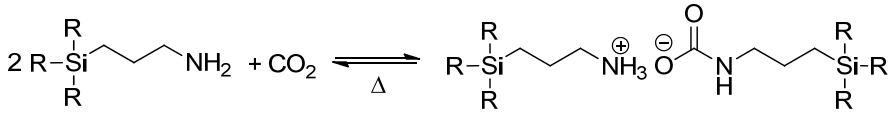

Figure 75 - Stoichiometry of the reaction of CO_2 with silylamines.

3.4.2 Enhanced CO_2 Capture Capacity

In an effort to understand the origin of the enhanced capacity we investigated various possible explanations. As mentioned previously, studies in our group have determined that though physisorption is a contributor to the overall capacity, it only accounts for 0.01-0.02 moles of CO_2 per mole of amine. Several possible other explanations were investigated. The presence of water is known to increase the CO_2 capacity of hindered amines by the formation of ammonium carbonates, which could theoretically result in CO_2 uptake of up to 1 mole of CO_2 per mole of amine. However, Karl Fischer titration concluded that an average of 0.12% water was present in TEtSA after distillation. Another possible explanation could have been entrainment of small bubbles of CO_2 within the viscous RevIL. Increased physisorption could be due to the high local partial pressures caused by the small radius of curvature of these bubbles. However, dynamic light scattering (DLS) analysis (a technique which is commonly used to size micelles or particles in solution) performed by my coworker, Amy Ethier, detected no evidence of entrained microbubbles. It did not completely rule out the possibility of entrapped CO_2,however it is unlikely that bubbles small enough to escape detection by

DLS would increase the uptake of CO_2 by 25%.[55] The final possibility we investigated was the formation of carbamic acid in the RevILs.

Though carbamic acid is an intermediate in the formation of the carbamate/ammonium ion pair (Figure 76) the equilibrium is traditionally, when in solution, considered to lie far to the right towards the ion pair. As mentioned previously, formation of the RevIL results in splitting of the ^{13}C NMR peaks alpha and beta to the amine (Figure 77). If the silylamines were indeed reacting in a fully 2:1 ratio with CO_2 to form only the RevIL and no carbamic acid, the peaks alpha and beta to the amine (α and β, Figure 77) would have equal integrations for each species. However, the quantitative ^{13}C NMR of 3-(aminopropyl)tripropylsilylamine (TPSA, R = $CH_2CH_2CH_3$) displayed an integration of 1.4:1 of those peaks. This suggests carbamic acid is still present in the system, we hypothesize stabilize by the carbamate-ammonium ion pair (Figure 78).[56] This established a new theoretical capacity of 0.67 moles of CO_2 per mole of amine. Several of the amines discussed approach this capacity.

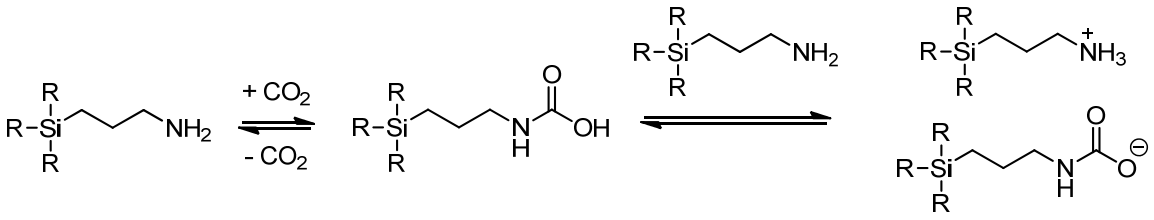

Figure 76 - Formation of carbamic acid as intermediate to fully converted RevIL form.

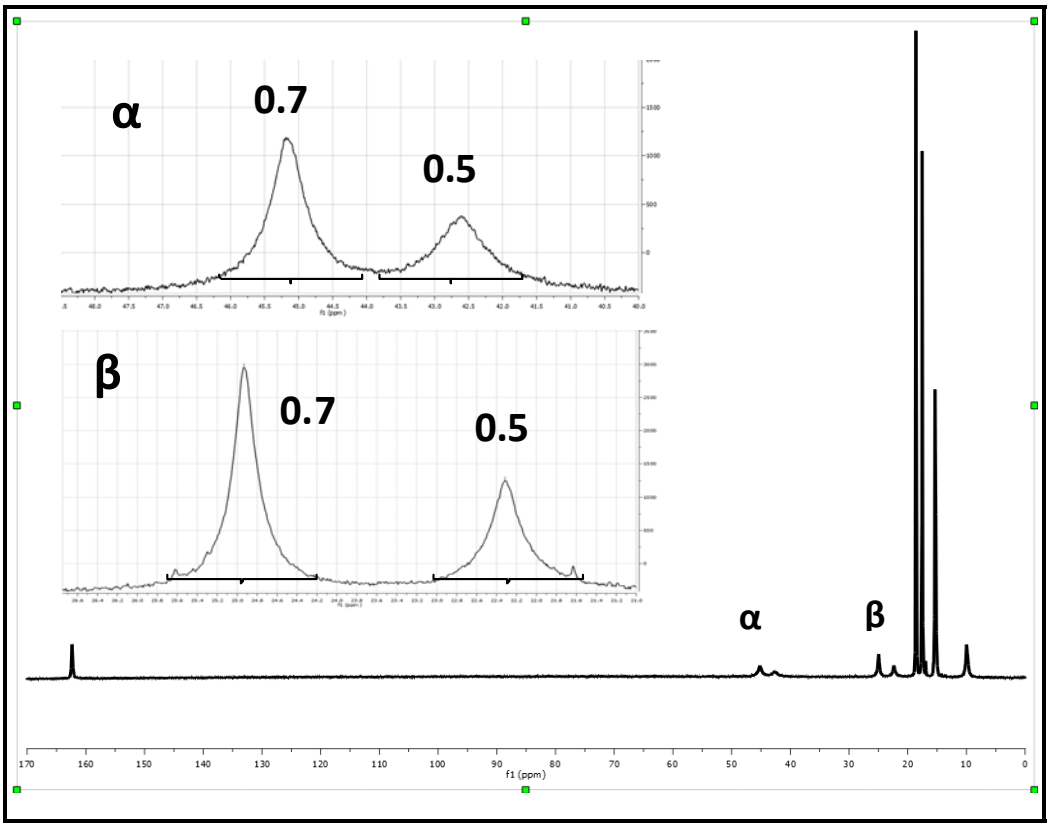

Figure 77 - Quantitative 13CNMR in the evaluation of carbamic acid formation for TPSA-IL.

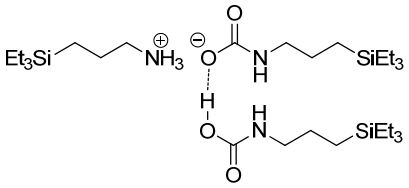

Figure 78 - Carbamic acid stabilized by the ammonium carbamate ion of the TEtSA reversible ionic liquid.

3.4.3 Viscosity

The viscosities at 25°C and 40°C for the 13 RevILs - at equilibrium conversions - formed from the reaction of silylamine with CO_2 are reported herein. The simple changes in silylamine structure result in a wide variation in viscosities, from <100 cP to 6,000 cP at 25°C. Though the viscosities at equilibrium conversions at 25°C are not industrially viable most industrial processes are conducted at higher temperatures, commonly 40°C,

where the viscosity is significantly reduced. The viscosities at 25°C do allow for direct comparison of all silylamines, however, since some reversible ionic liquids have reversal temperatures below 40°C.

The effects of varying the alkyl tether length on viscosity are outlined in Table 16. We anticipated that increasing the length of the alkyl tether between silicon and amine would result in increasing viscosity by increasing the degrees of rotational freedom in the molecule, thereby increasing packing. Changing the backbone length from a methylene linker (TEtSMA) to propylene linker (TEtSA) to a butylene linker (TEtSBA) followed the anticipated trend, with viscosities increasing from 2373 cP to 6088 cP to a solid. Surprisingly, the ethylene linker (TEtSEA) also formed a solid upon reaction with CO_2. The reason for this exception is currently unknown.

Table 16 - Effect of Proximity Upon RevILViscosity at 25°C and 40°C.

Abbreviation	Viscosity at 25°C (cP)	Viscosity at 40°C (cP)
TEtSMA	2373 ± 206	625 ± 58
TEtSEtA	Solid	Solid
TEtSA	6088 ± 36	1303 ± 100
TEtSBA	Solid	Solid

Compared to the viscosity of TEtSA (6088 cP, 25°C) branching along the backbone has a significant effect on viscosity (Table 17). The addition of a methyl group alpha to the amine (αMe-TEtSA) resulted in a slight increase in viscosity to 6915 cP. In the beta position (βMe-TEtSA), viscosity is decreased over 1000 cP. α,αDMe-TEtSA demonstrated a viscosity of 1257 cP at 25°C. Unreacted silylamine (<<100 cP) is likely still present, due to the reduced CO_2 uptake.

Table 17 - Effect of Branching Upon RevIL Viscosity.

Abbreviation	Viscosity at 25°C (cP)	Viscosity at 40°C (cP)
αMe-TEtSA	6915 ± 431	725 ± 164
α,αDMe-TEtSA	1257 ± 338	125 ± 22
βMe-TEtSA	5075 ± 141	1084 ± 62

The addition of unsaturation along the backbone (Table 18) resulted in a decrease of about 36% in the RevIL viscosity for *trans*-TEtSA (3889 cP) from the saturated analog TEtSA (6088 cP). We were able to determine the viscosities of *trans*-α,αDMe-TEtSA and *trans*-α,αDMe-TPSA are less than 100 cP, but an exact number was not possible as our apparatus does not currently measure viscosities under 100 cP. The viscosity for *trans*-α,αDMe-TEtSA was significantly decreased from the viscosity of the saturated model (α,αDMe-TEtSA, 1257 cP). However, both *trans*-α,αDMe-TEtSA and *trans*-α,αDMe-TPSA only reached equilibrium conversions of 0.47 and 0.40 moles CO_2 per mole amine respectively, as compared to the theoretical capacity of 0.67 mole CO_2 per mole of amine at 25°C. Again, presence of unreacted amine (<<100 cP) assists in lowering the viscosity.

Table 18 - Effect of Unsaturation Upon RevIL Viscosity.

Abbreviation	Viscosity at 25°C (cP)	Viscosity at 40°C (cP)
trans-TEtSA	3889 ± 252	362 ± 19
trans-α,αDMe-TEtSA	<100[a]	<100[a]
trans-α,αDMe-TPSA	<100[a]	<100[a]

[a]Measurements below 100 cP are below the reliable detection limits of the instrument used.

The RevIL of secondary model STEtSA (135 cP) displayed a significant drop in viscosity of over 98% (Table 19) as compared to TEtSA-RevIL (6088 cP) at 25°C, despite having similar CO_2 capture capacities. And while DMESA formed a solid upon reaction with CO_2 and reached a capacity of only 0.42 moles CO_2 per mole of amine, the secondary version (SDMESA) remained liquid upon reaction with CO_2, displaying a

higher capacity (0.62 mol CO_2/mol amine) and a viscosity of only 117 cP at 25°C. The viscosities at 40°C are not reliable for the secondary amines, however, due to reversion of the RevIL during measurement; the secondary amines displayed reversal temperatures <40°C.

Table 19 - Effect of Primary versus Secondary Analogs of TEtSA Upon RevIL Viscosity.

Abbreviation	Viscosity at 25°C (cP)	Viscosity at 40°C (cP)
TEtSA	6088 ± 36	1303 ± 100
STEtSA	135 ± 4	<100[a]
DMESA	Solid	Solid
SDMESA	117 ± 16	<100[a]

[a]**Measurements below 100 cP are below the reliable detection limits of the instrument used.**

In real world applications it would not be necessary to reach full conversion. Dissolution of the reversible ionic liquid in silylamine at lower conversions results in lower viscosities. TPSA, for example, exhibits a viscosity of 620 cP at 0.45 moles CO_2 per mole amine at 25°C (Figure 79). Above these conversions a sharp increase in viscosity is witnessed. A 50% increase in viscosity is observed between 0.45 and 0.50 moles CO_2 per mole amine for TPSA, which results in a hockey-stick like relationship. Conversion can therefore be controlled to maintain lower viscosities.

This relationship is even more valuable when uptake is measured at 40°C: higher capacities can be achieved at lower viscosities. A viscosity of 620 cP is not reached at 40°C until an uptake of nearly 0.52 moles of CO_2 per mole of amine is reached. In fact, an uptake of 0.39 moles CO_2 per mole amine for TPSA exhibits a viscosity of only 144 cP, which is nearing industrial viability while maintaining a capacity greater than the 30% aqueous MEA standard.

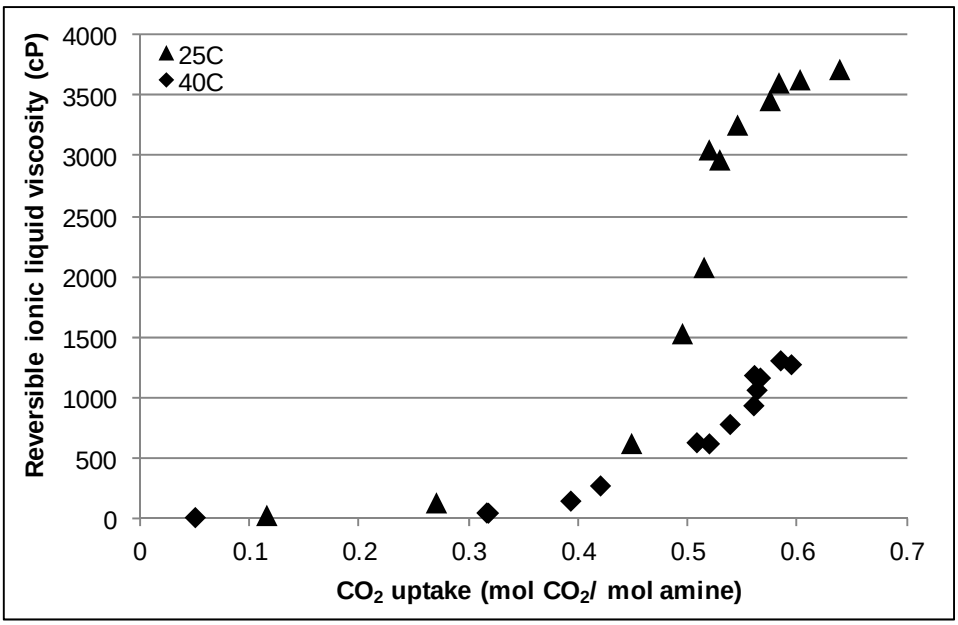

Figure 79 - 3-(Aminopropyl)tripropylsilane (TPSA) viscosity as a function of CO_2 uptake at 25°C and 40°C.

A similar curve is observed for other silylamines, though the endpoints and inflection points may be different. α,αDMe-TEtSA, for example, does not reach the same equilibrium conversion as TPSA at 25°C, but does display a similar curve of viscosity versus uptake (Figure 80). Though the increase in viscosity is sharper than for TPSA (1500 cP at 0.45 mol CO_2/mol amine for dimethyl versus 600 cP for TPSA at the same conversion), the viscosities below 0.35 moles CO_2 per mole amine were still within the industrially viable range. So controlling conversion allows us to maintain industrially viable viscosities for each silylamine.

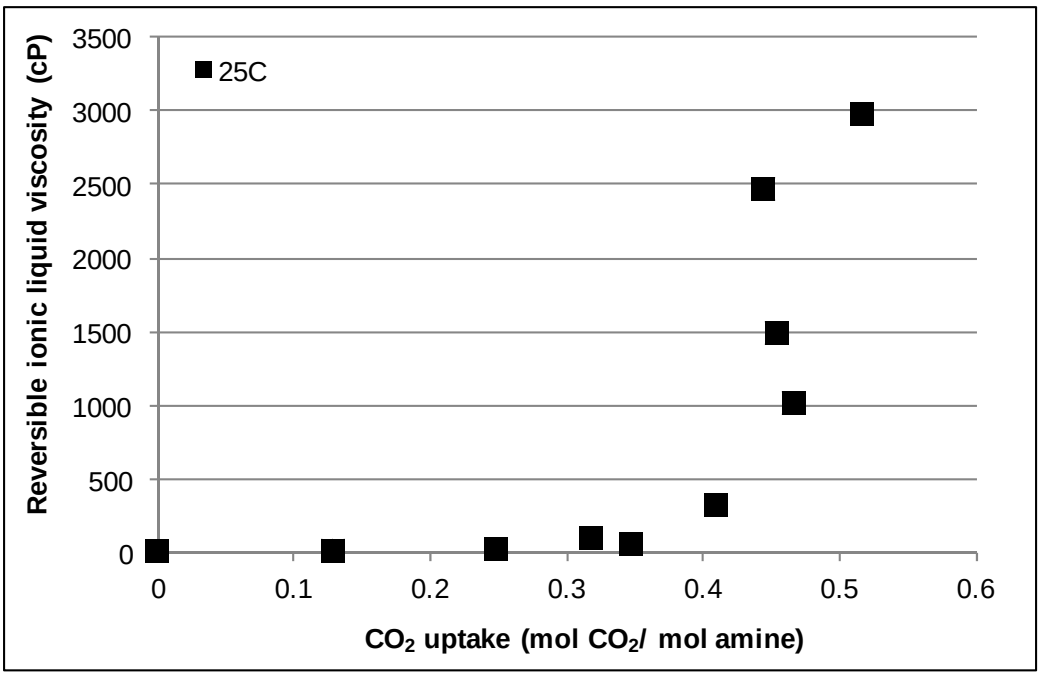

Figure 80 – Viscosity vs. CO_2 uptake for α,αDMe-TEtSA at 25°C.

3.4.4 Reversal Temperature

An advantage of our system is the ability to release CO_2 from the RevIL and reform the silylamine. Reversal occurs with heating, and the temperature at which reversal occurs is measured through differential scanning calorimetry (DSC). In DSC analysis the temperature of a sample is increased while the heat required to increase the temperature is monitored. Events such as melting and evaporation can be monitored via this method. Samples of RevIL (~2 mg) were sealed in aluminum pans and heated from -40°C to 400°C at a ramp rate of 5°C/min. Two events are typically observed for our RevILs: reversal of the RevIL and evaporation of the molecular liquid (Figure 81). The reversal and evaporation temperatures are then determined from the intercept of the baseline of the event with the line tangent to the peak. For those RevILs which were solid, an additional event was observed which corresponds to the melting of the solid RevIL (Figure 82).

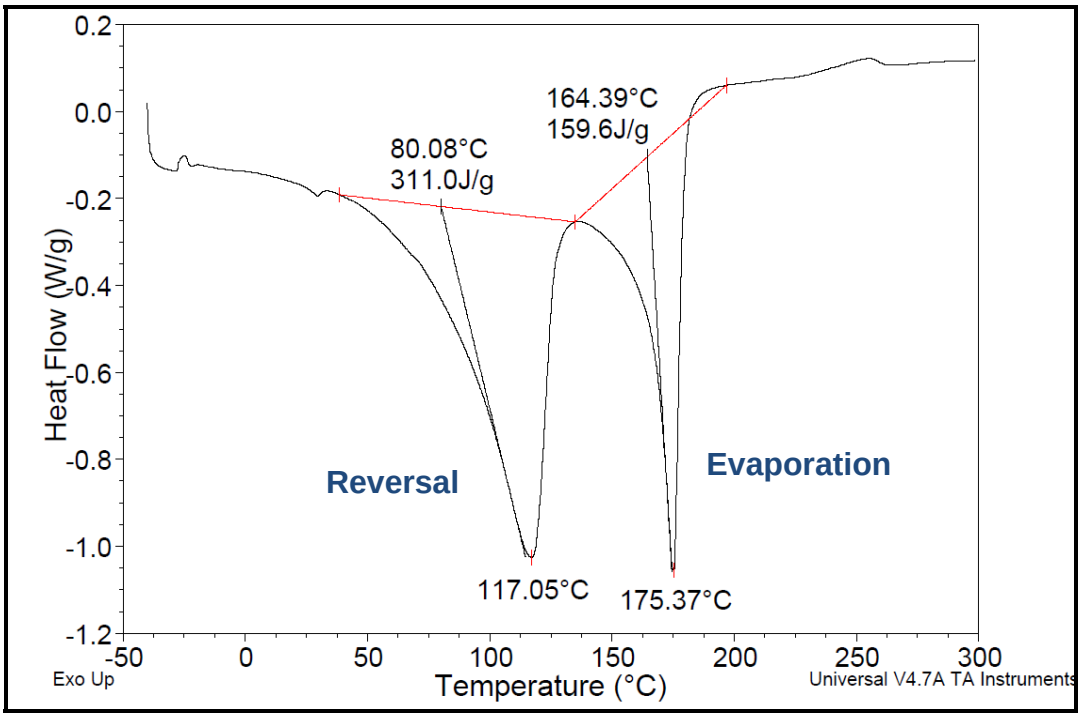

Figure 81 - DSC Thermogram of TESMA RevIL.

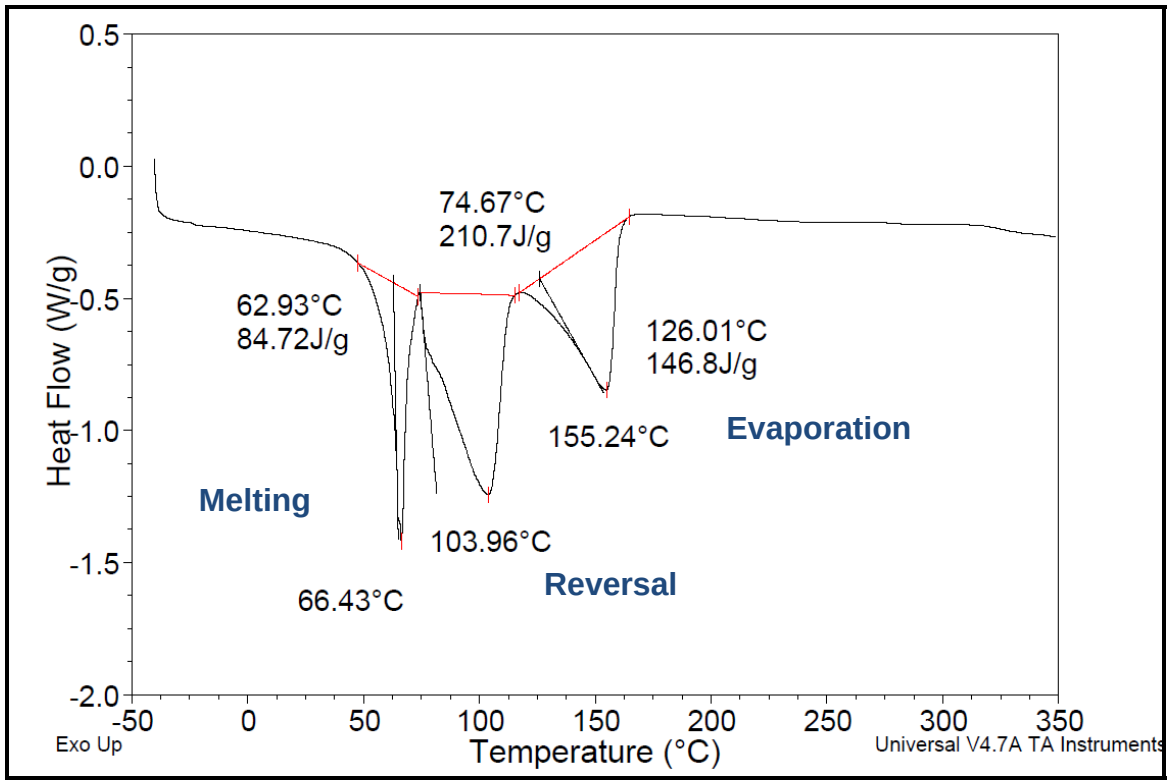

Figure 82 - DSC thermogram of solid forming DMESA-RevIL.

Lower reversal temperatures require less energy to heat the RevIL from the capture temperature to the point at which CO_2 is released. Branching, unsaturation and secondary amines all result in lower reversal temperatures as compared to TEtSA. However, some of the RevIL reversal temperatures are actually below the temperature at which CO_2 capture would most likely occur (~40°C), which would result in incomplete conversion to the RevIL. The ideal system would be a balance between lower reversal temperatures but not too close to the capture temperature. Also, ideally the system should display an evaporation temperature well above the reversal temperature to minimize solvent losses due to evaporation. Please note, that though it is not discussed explicitly herein, the evaporation temperatures for each molecular liquid were observed to be well separated (>30°C difference) from the reversal temperatures. Evaporation of the molecular amine is therefore not a concern for these amines.

Table 20 - Effect of Proximity Upon Reversal Temperature.

Abbreviation	Reversal Temperature (°C)
TEtSMA	78 ± 5
TEtSEtA	109 ± 3[a]
TEtSA	71 ± 3
TEtSBA	84 ± 4[b]

[a] Formed solid (MP 49 ± 1°C); [b] Formed solid (MP 66 ± 4°C).

Changing the length of the alkyl tether does not significantly affect the reversal temperature (Table 20), except for TEtSEtA which formed a solid with a higher reversal temperature (109°C) than TEtSA (71°C). Branching, however, resulted in a significant decrease in reversal temperatures as compared to TEtSA (Table 21). The addition of a methyl group alpha to the amine (αMe-TEtSA) or beta to the amine (βMe-TEtSA) resulted in the reduction of reversal temperature by 19°C and 14°C, respectively. The

addition of two methyl groups alpha to the amine reduced the reversal temperature even further. Though the reversal temperature of α,αDMe-TEtSA is too close to the 40°C capture conditions allow for complete conversion, this does demonstrate our ability to significantly affect the properties pertinent to industry.

Table 21 - Effect of Branching Upon Reversal Temperature.

Abbreviation	Reversal Temperature (°C)
αMe-TEtSA	52 ± 2
α,αDMe-TEtSA	41 ± 6
βMe-TEtSA	57 ± 7

Unsaturation results in reduced reversal temperatures as well (Table 22). The *trans* analog of TEtSA has a reversal temperature 23°C lower than the saturated analog. Interestingly, the combined effect of unsaturation and branching appears to have resulted in the lowest reversal temperatures of all effects. Though well below the 40°C capture condition, this serves to further illustrate the effect of structure upon the industrial properties. The entropic effect due to the inflexible, locked conformation of the unsaturated RevIL, we hypothesize, is the reason for the significantly reduced reversal temperature.

Table 22 - Effect of Unsaturation Upon Reversal Temperature.

Abbreviation	Reversal Temperature (°C)
trans-TEtSA	48 ± 2
trans-α,αDMe-TEtSA	11[a]
trans-α,αDMe-TPSA[b]	15 ± 2

[a]Reversal temperature difficult to measure due to broad events in the DSC thermogram. [b]Bottom of reversal curve at 48°C.

Though DMESA exhibits a reversal temperature similar to TEtSA (Table 23), SDMESA and STEtSA demonstrate reversal temperatures at least 40°C lower. Also, both secondary amines exhibit capacities equal to the primary amine at 25°C. The temperature at which CO_2 capture is likely to occur in the absorber is estimated to be 40°C. Both secondary RevILs demonstrate reversal temperatures below this point which would result in reduced capacity. Nonetheless, this does demonstrate the effect of the N-methyl moiety in destabilizing the carbamate, as hypothesized.

Table 23 - Effect of Primary and Secondary Analogs of TEtSA Upon Reversal Temperature.

Abbreviation	Reversal Temperature (°C)
TEtSA	71 ± 3
STEtSA	30 ± 3
DMESA	80 ± 8[a]
SDMESA	37 ± 2

[a]**Formed solid (MP 66 ± 3°C).**

Unsaturation, order of amine and branching can all be used to modify reversal temperatures for the desired applications.

3.4.5 Enthalpy of Regeneration

The enthalpy of regeneration is the heat required to strip the RevIL of CO_2 and reform the silylamine. A higher enthalpy of regeneration means more energy is required to recycle the solvent. As with reversal temperature, the heat of regeneration is calculated from the DSC thermogram. The amount of heat (J/g) was calculated by integration of the endotherm area from baseline to baseline. Since the sample mass and gravimetric uptake are known, the heat of regeneration in kJ/mole CO_2 was easily calculated. For solid RevILs please note that the heat of regeneration includes both the concurrent melting and CO_2 release DSC events.

The structural modifications produced both positive and negative deviations from the heat of regeneration for TEtSA. The effect of proximity is outlined in Table 24. Though increasing the length of the alkyl tether from methyl to ethyl to propyl does not induce significant change in the heat of regeneration, increasing the length to a butyl linker induces a significant increase. The heat of regeneration of TEtSBA (152 $kJ \cdot molCO_2^{-1}$) is nearly double the heat of regeneration of TEtSA (83 $kJ \cdot molCO_2^{-1}$). We believe this may be due to stabilization of the ammonium-carbamate and carbamic acid species through intramolecular interactions.[56]

Table 24 - Effect of Proximity on RevIL Enthalpy of Regeneration.

Abbreviation	Heat of Regeneration ($kJ \cdot molCO_2^{-1}$)
TEtSMA	76 ± 7
TEtSEtA	91 ± 16[a]
TEtSA	83 ± 6
TEtSBA	152 ± 19[b]

[a]Formed solid (MP 49 ± 1°C); [b]Formed solid (MP 66 ± 4°C).

The addition of branching to the TEtSA backbone yielded similar heats of regeneration for single methyl groups in either alpha or beta positions to the amine (Table 25). However, the addition of two methyl groups in the alpha position produced what appears to be an interesting result. α,αDMe-TEtSA does not reach full equilibrium conversion to the RevIL which is likely due to the steric hindrance of the dimethyl moiety destabilizing the carbamate ion.[57] This destabilizing effect should result in a lower heat of regeneration than TEtSA. In fact the heat of regeneration for α,αDMe-TEtSA (114 $kJ \cdot molCO_2^{-1}$) cannot be compared directly to TEtSA since the enthalpy is calculated based on the respective equilibrium conversions, and α,αDMe-TEtSA does not reach the same conversion to RevIL as TEtSA.

Table 25 - Effect of Branching Upon RevIL Enthalpy of Regeneration.

Abbreviation	Heat of Regeneration (kJ·molCO_2^{-1})
αMe-TEtSA	90 ± 5
α,αDMe-TEtSA	114 ± 16
βMe-TEtSA	89 ± 8

The *trans* analog of TEtSA displays a similar heat of regeneration to its saturated version (Table 26). However, both branched, unsaturated amines show significantly lower heats of regeneration: *trans*-α,αDMe-TEtSA, 7 kJ·molCO_2^{-1}; *trans*-α,αDMe-TPSA, 21 kJ·molCO_2^{-1}. The capacities for the branched and unsaturated systems did not reach as high a conversion as TEtSA, so the lower enthalpies are not unexpected, however they are still significant and suggest that branching and unsaturation together play an important role in lowering the enthalpy of regeneration for a system.

Table 26 - Effect of Unsaturation Upon RevIL Enthalpy of Regeneration.

Abbreviation	Heat of Regeneration (kJ·molCO_2^{-1})
trans-TEtSA	85 ± 7
trans-α,αDMe-TEtSA	7[a]
trans-α,αDMe-TPSA[b]	21 ± 6

[a]Enthalpy difficult to measure due to broad events in the DSC thermogram. [b]Bottom of reversal curve at 48°C.

DMESA (130 kJ·molCO_2^{-1}) displays a higher heat of regeneration than TEtSA (Table 27) probably due to the solid state of the RevIL formed upon reaction with CO_2. The heats of regeneration of the secondary versions, however, are both comparable to TEtSA. SDMESA (76 kJ·molCO_2^{-1}) is significantly lower than its primary analog, probably due to the liquid state of the RevIL.

Table 27 - Effect of Primary and Secondary Analogs of TEtSA Upon RevIL Enthalpy of Regeneration.

Abbreviation	Heat of Regeneration ($kJ \cdot mol CO_2^{-1}$)
TEtSA	83 ± 6
STEtSA	77 ± 6
DMESA	130 ± 14[a]
SDMESA	76 ± 2

[a]Formed solid (MP 66 ±3 °C).

3.5 Conclusions

Iterative structural modifications of 3-(aminopropyl)triethylsilane (TEtSA) were utilized to establish structure-property relationships through which CO_2 capture solvents can be designed to meet industrial specifications. The effects of Si-NH_2 proximity, branching, unsaturation, and amine order upon industrially relevant properties (CO_2 uptake capacity, viscosity, enthalpy of regeneration and reversal temperature) have been discussed. We have as a result demonstrated that we can design CO_2 capture solvents that achieve a competitive CO_2 uptake of, on average, 0.59 moles CO_2 per mole of amine while minimizing viscosity and energy of reversal.

The influence of tether length between silicon and amine on CO_2 uptake is evident. Methyl (TEtSMA) and propyl (TEtSA) linkers remain liquid in the RevIL state with capacities that approach the theoretical maximum of 0.67 moles CO_2 per mole amine. Increasing the tether to a butyl linker, however, results in the formation of a solid upon reaction with CO_2 which demonstrated reduced capacity. The increased degrees of rotational freedom of the butyl molecule likely lead to increased packing efficiency of the molecules. TEtSMA-RevIL and TEtSA-RevIL also demonstrate similar regeneration energies, but TEtSMA-RevIL has less than half the viscosity of TEtSA-RevIL.

The inclusion of methyl groups can result in the reduction of both reversal temperature and viscosity. A single methyl group alpha to the amine (αMe-TEtSA) reduced the reversal temperature by 20°C; two methyl groups alpha to the amine

(α,αDMe-TEtSA) reduced the viscosity by approximately 67%, though CO_2 uptake is also decreased. The first effect is probably due to destabilization of the carbamate due to sterics and formation of ammonium species in preference to ammoniuim carbamate. The second is possibly partly due to increased sterics around the amine and decreased packing, but the reduced CO_2 uptake also plays a major role.

The combination of branching and unsaturation results in even more significant effects. The viscosities of *trans*-α,αDMe-TEtSA and *trans*-α,αDMe-TPSA are less than 100 cP. This is in part due to low reversal temperatures (<30°C) and the presence of unreacted amine. However, due to incomplete conversion of the silylamine to the RevIL these values cannot be compared directly to TEtSA. *trans*-TEtSA, however, does demonstrate complete conversion to the RevIL and can be compared to TEtSA. The *trans* version of TEtSA exhibits a slightly higher viscosity but significantly reduced reversal temperature, over 20°C lower than the saturated version. Addition of a methyl group to the amine of TEtSA and DMESA also showed strong effects on viscosity and reversal temperature. The viscosity of SDMESA is reduced over 50-fold and the reversal temperature is reduced below 40°C as compared to TEtSA.

Viscosity can be controlled by both simple structural changes and by limiting conversion of the silylamine to the RevIL. Viscosities below 300 cP can be maintained at conversions of almost 70% at 40°C. This unique behavior provides an additional parameter of control in order to meet the criteria for industrial implementation.

This information can allow for the design of particular CO_2 capture solvents which meet the specifications of the end use application. Two amines have been identified from this study for further investigation: TEtSMA and *trans*-TEtSA. Both demonstrate high CO_2 uptake capacities, viable reversal temperatures, and reasonable enthalpies of regeneration (Table 28). Their viscosities are lower than the other amines studied and can be further reduced by controlling CO_2 uptake to meet industry-operating specifications.

Table 28 – Summary of the properties of TEtSMA and *trans*-TEtSA.

Property	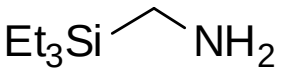 **TEtSMA**	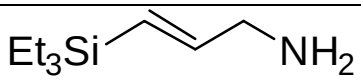 ***trans*-TEtSA**
CO_2 Uptake (mol CO_2/mol amine, 25°C)	0.59 ± 0.01	0.61 ± 0.03
CO_2 Uptake (mol CO_2/kg amine, 25°C)	4.09 ± 0.08	3.56 ± 0.20
Reversal Temperature (°C)	78 ± 5	48 ± 2
Enthalpy of Regeneration ($kJ \cdot molCO_2^{-1}$)	76 ± 7	85 ± 7
RevIL Viscosity at 25°C (cP)	2373 ± 206	3889 ± 252
RevIL Viscosity at 40°C (cP)	625 ± 58	362 ± 19

3.6 Experimental

3.6.1 Materials

All chemicals were purchased from Sigma-Aldrich and used as received unless otherwise noted. Chemicals used were: triethylsilane (99%); tripropylsilane (99%); allylamine (99+%); platinum(0)-1,3-divinyl-1,1,3,3-tetramethyldisiloxane complex solution in xylene (Karstedt's catalyst; 2 wt% Pt) (Pt-DVDS); toluene (anhydrous, 99.8%); 0.5 *M* 2,8,9-triisobutyl-2,5,8,9-tetraaza-1-phosphabicyclo[3.3.3]undecane in

diethyl ether; dimethylethylsilane (98%); 4-amino-1-butene (97%); tetrahydrofuran (THF; anhydrous, inhibitor-free, ≥99.9%); 3-chloro-1-butene (96%); potassium phthalimide (98%); hydrazine (anhydrous, 98%); 2-methyl-3-butyn-2-amine (95%); N-vinylphthalimide (99%); Pd on activated charcoal (5 wt% Pd basis); Celite 545; hexanes (anhydrous, mixture of isomers, ≥99%); and methanol (anhydrous, 99.8%). Propargylamine (95%) was acquired from TCI America, used as received and stored in the dark under inert atmosphere at 5°C. 2-methylallylamine (97%) was purchased from Acros Organics and used as received. All chemicals were stored under inert dry atmosphere. The CO_2 employed was SFC grade from Airgas, certified to contain less than < 250 ppb H_2O with a purity of 99.9999%.

3.6.2 Experimental Procedure

3.6.2.1 Synthesis of 1-(Aminomethyl)triethylsilane (TEtSMA)

Triethyl(chloromethyl)silane

A 217.5 mL (0.435 mol) portion of ethyl magnesium chloride (2M in THF) solution was added to a 1-L round bottomed flask under nitrogen atmosphere. The solution was cooled to 0°C with an ice bath. Separately, trichloro(chloromethyl)silane (25 g, 0.136 mol) was dissolved in anhydrous THF (200 mL) in an addition funnel under argon. The trichloro(chloromethyl)silane solution was added dropwise to the stirring Grignard over the course of about an hour. After complete addition, the solution was removed from the ice bath and allowed to reach room temperature. Precipitation of $MgCl_2$ was evident and the solution was allowed to stir vigorously overnight where the mixture became unable to be stirred. Saturated sodium bicarbonate solution was added slowly and the solids were then filtered under vacuum and washed with THF. The aqueous layer was separated and washed with more THF and DCM. These organics were

recombined with the original organic layer. It was washed with brine, dried over $MgSO_4$, and the solvents removed at 65 torr to yield 21.44 g of the desired triethyl(chloromethyl)silane in 85% yield.

^{1}H NMR (400 Hz, CDCl3) 2.84 (s, 2H), 0.97(t, 9H), 0.65(q, 6H)

^{13}C NMR (400 Hz, CDCl3) 27.55, 7.14, 2.20

Calculated % for $C_4H_{11}ClSi$ (MW: 122.67 g·mol^{-1}): Expected: C(51.03), H(10.40) found: C(50.98), H(10.32)

2-((Triethylsilyl)methyl)isoindoline-1,3-dione

Triethyl(chloromethyl)silane (20.15 g, 0.12 mol) was added to a stirring mixture of potassium phthalimide (27.83 g, 0.15 mol) and anhydrous K_2CO_3 (2.9 g, 0.02 mol) in anhydrous DMF (200 mL) under argon. The mixture was brought to 100°C and stirred for 20 hours. After cooling to room temperature, ice water (300 mL) was added, followed by 200 mL of diethyl ether. The ethereal layer was separated from the aqueous layer and washed with brine and dried over $MgSO_4$. The aqueous layer was brined with solid NaCl, washed twice more with 100 mL portions of ether, and the organic layer separated, washed with brine, dired over MgSO4 and combined with the original organic layer. The solution was rotovapped at 70°C under vacuum to yield 26.47 g of 2-((triethylsilyl)methyl)isoindoline-1,3-dione in 80% yield.

^{1}H NMR (400 Hz, CDCl3) 7.77 (m, 2H), 7.65 (m, 2H), 3.21 (s, 2H), 0.96 (t, 9H), 0.61 (q, 6H)

^{13}C NMR (400 Hz, $CDCl_3$) 168.47, 133.54, 132.28, 122.80, 25.15, 7.07, 3.04

Calculated % for $C_{13}H_{17}NO_2Si$ (MW: 247.37 g·mol^{-1}): Expected: C(65.41), (7.69), N(5.09) Found: C(65.13), H(7.71), N(5.04)

1-(Aminomethyl)triethylsilane (TEtSMA)

2-((Triethylsilyl)methyl)isoindoline-1,3-dione (25.92 g, 0.0945 mol) was dissolved in anhydrous MeOH (315 mL) under an inert atmosphere and stirred with mechanical stirring. Anhydrous hydrazine (8.9 mL, 0.284 mol) was added in one portion to the MeOH solution and the temperature of the solution was brought to 60°C. During the course of the reaction, phthalylhydrazide formation was evidenced by a cloudy-gel like precipitate. After 5 hours of reaction, the solution was cooled and 2M HCl was added until a solid white precipitate was formed in the single aqueous phase. The solid was filtered under vacuum and washed with more 2M HCl. The collected liquid layer was then basified with 1M NaOH until a pH of 14 was reached. Diethyl ether was added to extract the amine product. The ether was then washed with brine, dried over $MgSO_4$ and removed at 45°C by distillation. The crude (aminomethyl)triethylsilane was attempted to be distilled under argon but it was noticed that as the temperature increased to 170°C a yellow sludge formed in the distillation flask. The heat was removed and the crude distilled at 25°C at 0.6 mmHg to give 3.63 g of pure (aminomethyl)triethylsilane in a 27% isolated yield.

^{1}H NMR (400 Hz, $CDCl_3$) 2.24 (s, 2H), 1.74 (s, 2H), 0.95 (t, 9H), 0.57 (q, 6H)

^{13}C NMR (400 Hz, $CDCl_3$) 26.68, 7.36, 2.10

Calculated % for $C_7H19NSi$ (MW: 145.32 $g \cdot mol^{-1}$): Expected: C(57.86), H(13.18), N(9.64) found:C(56.56), H(13.28), N(9.13)

3.6.2.2 Synthesis of 2-(Aminoethyl)triethylsilane (TEtSEtA)

Triethylsilane (72.8 g, 0.626 mol) and Pt-DVDS (3.0 mL of 2 % Pt solution in xylene, 0.29 mmol) were added to a 3-neck round bottom flask fitted with a reflux condenser under inert atmosphere. To the mixture was transferred N-vinylphthalimide (25 g, 0.144 mol) dissolved in 250 mL anhydrous toluene using a double-tipped needle. The mixture was brought to 110 °C and stirred for 2 days. After cooling, the reaction

mixture was filtered through celite and toluene was removed using a rotary evaporator. To the crude product was added hydrazine solution (35 wt. % in H_2O, 200mL, 2.16mol) and methanol 200 mL. The solution was heated to 60 °C for 24 hours. After cooling, 150 mL of methanol was removed by distillation at atmospheric pressure, and the solution pH was adjusted to 1 using 6 N HCl aqueous solution at 0 °C. The solution was filtered through celite, and the mother liquor pH was adjusted to 12 using 30 % NaOH aqueous solution at 0 °C. It was extracted using Et_2O (300 mL, 6 times). The combined ether solution was dried over anhydrous $MgSO_4$, and ether was removed by evaporation. The residual crude was distilled under reduced pressure (bp: 30°C at 1mmHg) to give 2-(triethylsilyl)ethanamine (5.75g) in 25 % yield (2 steps).

^{1}H NMR (400 MHz, $CDCl_3$), δ (ppm): 2.73 (*t*,2H), 1.16 (broad, 2H), 0.92 (*t*,9H), 0.77 (*t*, 2H), 0.50 (*q*,

6H)

^{13}C NMR (100 MHz, $CDCl_3$), δ (ppm): 38.40, 17.83, 7.53, 3.56

Calculated % for $C_8H_{21}NSi$ (MW: 159.34 g·mol^{-1}): C(60.30), H(13.28), N(8.79), Si(17.63) found: C(59.89), H(13.24), N(8.65)

3.6.2.3 Synthesis of 3-(Aminopropyl)triethylsilane (TEtSA)

A typical synthesis was carried out as follows. To a 3-neck 250 mL round bottomed flask fitted with a condenser and magnetic stirbar under inert atmosphere was added anhydrous toluene (80 mL, 0.751 mol), triethylsilane (25.5 mL, 0.160 mol), and 2 wt% Pt-DVDS in xylenes (1.2 mL; 3.2 x 10^{-4} mol Pt; 0.20% catalyst loading wrt silane). This was allowed to stir at room temperature for approximately five minutes, at which point allylamine (24 mL, 0.320 mol) was added and the reaction was heated to 110°C overnight. Reaction progress was monitored via ^{1}H NMR for the disappearance of the silane proton (~3.7 ppm). Upon reaction completion, the reaction mixture was allowed to

cool to room temperature; the solvent and excess allylamine were then removed via rotary evaporator. The product (3-aminopropyl)triethylsilane (24.7916 g, 0.143 mol; 89.4% isolated yield) was distilled from the catalyst under reduced pressure (bp: 80°C at 2 mmHg).

^{1}H NMR (400.13 MHz, $CDCl_3$, 25°C) δ = 2.63 (t, 2H), 1.39 (p, 6H), 1.08 (s, 2H), 0.90 (t, 9H), 0.49 (q, 8H)

^{13}C NMR (100.57 MHz, $CDCl_3$, 25°C) δ = 45.47, 27.88, 18.63, 7.90, 6.95, 2.87

Calculated % for $C_9H_{23}NSi$ (MW: 173.37 $g \cdot mol^{-1}$): C(62.35), H(13.37), N(8.08), Si(16.20); found: C(62.41), H(13.42), N(7.94)

3.6.2.4 Synthesis of 4-(Aminobutyl)triethylsilane (TEtSBA)

To a 3-neck 250 mL round bottomed flask fitted with a condenser and magnetic stirbar under inert atmosphere was added 2 wt% Pt-DVDS in xylenes (0.6% catalyst loading wrt silane, 8.01 mL, 0.7 mmol) and triethylsilane (12.21 g, 105 mmol); the solution turned dark yellow. To this was added anhydrous toluene (40 mL) and 4-amino-1-butene (5.0 g, 70.3 mmol). The solution was heated to 80°C for 20 hours. Reaction progress was monitored via ^{1}H NMR for the disappearance of the silane proton (~3.7 ppm). When this peak was no longer present, the reaction mixture was allowed to cool to room temperature; the solvent and excess triethylsilane was then removed via rotary evaporator. The product 4-(aminobutyl)triethylsilane was distilled from the catalyst under reduced pressure (bp: 68°C at 1.95 mmHg) for an isolated yield of 66% (8.67 g; 46.3 mmol).

^{1}H NMR (400.13 MHz, $CDCl_3$, 25°C) δ = 2.62 (t, 2H), 1.40 (p, 2H), 1.27 (s, 2H), 1.17 (s, 2H), 0.86 (t, 9H), 0.44 (q, 8H)

^{13}C NMR (100.57 MHz, $CDCl_3$, 25°C) δ = 41.83, 37.95, 21.04, 11.09, 7.32, 3.16

Calculated % for $C_{10}H_{25}NSi$ (MW: 187.40 g·mol^{-1}): C(64.09), H(13.45), N(7.47), Si(14.99); found: C(62.34), H(13.33), N(7.47)

3.6.2.5 Attempted Synthesis of 4-(Triethylsilyl)-butyl-2-amine (αMe-TEtSA):

The Overman rearrangement was initially used in the synthesis of αMTEtSA. Although the protected branched amine was successfully used as a hydrosilylation substrate, removal of the protecting group in high yields was not attainable. An alternative method, wherein a Gabriel synthesis was used to form the protected branched amine, was used instead. This substrate was then successfully hydrosilylated and deprotected using the Ing-Manske protocol.

Overman Rearrangement

An example of a typical synthesis follows. A solution consisting of 8.5 mL crotonyl alcohol (99.96 mmol) in 15 mL anhydrous diethyl ether (0.1429 mol) was added to a 3-neck 250 mL round bottomed flask containing sodium hydride (60% dispersion in mineral oil; 0.492 g prior to washing with anhydrous heptane; 12.3 mmol) in 50 mL anhydrous Et_2O (0.476 mol) at -10°C. The reaction mixture was stirred at that temperature until evolution of hydrogen gas ceased. 10.1 mL trichloroacetonitrile (101 mmol) was then added dropwise over the course of 20 minutes. The reaction mixture became first yellow, then brown. It was allowed to warm to room temperature and the solvent was removed via rotavap. Upon addition of 100 mL of 99:1 hexanes:methanol to the resulting brown oil, a brown precipitate formed. This was removed via gravity filtration and 20.518 g of the crude product trichloroacetimidate was recovered. The trichloroacetimidate was not purified further and carried on “as-is” to the next step. The crude trichloroacetimidate was dissolved in 200 mL *p*-xylene and heated at reflux overnight. 20.518 g of the crude trichloroacetamide was recovered. Column

chromatography gave the pure trichloroacetamide in approximately 17% yield (mp: 30-32°C).

^{1}H NMR (400.13 MHz, $CDCl_3$, 25°C) 6.55 (s, 1H), 5.86 (ddd, *J* = 17.2, 10.5, 5.2 Hz, 1H), 5.25 (d, *J* = 17.2 Hz, 1H) 5.19 (d, *J* = 10.7 Hz, 1H), 4.53 (sextet, *J* = 6.8 Hz, 1H), 1.35 (d, *J* = 6.8 Hz, 3H)

^{13}C NMR (100.57 MHz, $CDCl_3$, 25°C) 160.98, 137.59, 115.56, 92.69, 49.04, 19.71

Hydrosilylation

In a round-bottomed flask fitted with a condenser, 2.8 g of the isolated α-methyl trichloroacetamide (13 mmol; 2.6 *M*) was combined with 2.5 mL triethylsilane (15.6 mmol; 3.12 *M*) and 7.5 x 10^{-2} mL 2 wt% Pt-DVDS in xylenes (6.57 x 10^{-6} mol Pt, 0.04% loading wrt silane) in 5 mL anhydrous toluene (46.9 mmol). The reaction mixture was then heated at 110°C for 48 hours; progress was monitored via ^{1}H NMR for the disappearance of the silane proton (~3.7 ppm). The reaction mixture was then allowed to cool to room temperature, and the solvent and excess silane was removed via rotavap to obtain 1.531 g of the desired silylated product (40% yield) as a yellow oil.

3.6.2.6 Synthesis of 4-(Triethylsilyl)-butyl-2-amine (αMe-TEtSA):

Gabriel Synthesis

A typical synthesis of αMe-TEtSA was achieved via the series of reactions detailed below. In a roundbottomed flask fitted with a condenser, 3-chloro-1-butene (9.05 g, 100 mmol), potassium phthalimide (24.17 g, 130 mmol), and potassium carbonate (4.14 g, 30 mmol) were added to DMF (90 mL, 0.969 mol) and heated at reflux overnight. The reaction mixture was then poured over ice, forming a brown precipitate, which was isolated via vacuum filtration. The solid was washed with 1 M NaOH (200

mL, 0.2 mol), distilled water (100 mL, 5.6 mol), 1 N HCl (100 mL, 0.1 mol), and distilled water (100 mL, 0.6 mol); it was then vacuum dried, resulting in a 67% yield of the desired 3-phthalimido-1-butene (mp: 76-79°C).

^{1}H NMR (400.13 MHz, $CDCl_3$, 25°C) δ = 7.82 (m, 2H), 7.70 (m, 2H), 6.19 (m, 1H), 5.23 (d, 1H), 5.15 (d, 1H), 4.93 (p, 1H), 1.58 (d, 3H)

^{13}CNMR (100.57 MHz, $CDCl_3$, 25°C) δ = 167.92, 136.80, 133.84, 133.02, 123.11, 116.33, 48.93, 18.21

Hydrosilylation

In a 250 mL 3-neck round-bottomed flask fitted with a condenser, the isolated 3-phthalimido-1-butene (20.1 g, 100 mmol) and 2 wt% Pt-DVDS in xylenes (1.54 mL, 1.35 x 10^{-4} mol Pt, 0.104% loading wrt silane) was added to anhydrous toluene (60 mL, 0.563 mol) under inert atmosphere. The reaction mixture was then heated to 50°C, at which point the protected amine became soluble. Triethylsilane (20.7 mL, 130 mmol) was then added to the reaction mixture, which was then heated to 110°C and kept at that temperature overnight. The reaction was allowed to cool; the solvent was removed via rotary evaporator and the crude 3-(phthalimidobutyl)triethylsilane was distilled under reduced pressure with a 75% yield of the desired product 3-phthalimidobutyl)triethylsilane (bp: 120°C at 0.7 mmHg).

^{1}H NMR (400.13 MHz, $CDCl_3$, 25°C) δ = 7.82 (m, 2H), 7.70 (m, 2H), 4.23 (s, 1H), 2.01 (m,1H), 1.72 (m,1H), 1.46 (d, 3H), 0.88 (trip, 9H), 0.48 (q,7H), 0.37 (t of d, 1H)

^{13}C NMR (100.57 MHz, $CDCl_3$, 25°C) δ = 168.61, 133.73, 132.01, 123.01, 50.58, 28.14, 18.30, 8.42, 7.37, 3.10

Ing-Manske Deprotection

3-(phthalimidobutyl)triethylsilane (16.9 g, 53 mmol) was dissolved in anhydrous methanol (250 mL, 6.172 mol). Anhydrous hydrazine (5 mL, 187 mmol) was slowly added and the reaction mixture was heated at 60°C for 4 hours. A cloudy white network formed, which was precipitated via addition of 2 *M* HCl. The resulting solid was removed from the desired liquid product mixture via vacuum filtration and washed with distilled water (100 mL, 5.6 mol). The solvent was removed via rotary evaporator and NaOH was added to the crude product until the pH was greater than 9. Extraction with ether, drying with $MgSO_4$, and distillation under reduced pressure yielded the pure product, 4-(triethylsilyl)-butan-2-amine in 62% yield (bp: 73°C at 2.7 mmHg).

^{1}H NMR (400.13 MHz, $CDCl_3$, 25°C) δ = 2.74 (s, 1H), 1.26 (m, 2H), 1.16 (s, 2H), 1.03 (d, 3H), 0.90 (t, 9H), 0.49 (q and m overlapping, 8H)

^{13}C NMR (100.57 MHz, $CDCl_3$, 25°C) δ = 49.71, 34.18, 23.25, 7.48, 7.37, 3.14

Calculated % for $C_{10}H_{25}NSi$ (MW: 187.40 g·mol^{-1}): C(64.09), H(13.45), N(7.47), Si(14.99); found: C(63.03), H(13.47), N(7.39)

3.6.2.7 Attempted Synthesis of 2-Methyl-3-(triethylsilyl)propylamine (βMe-TEtSA)

Several methods were attempted to synthesize βMTEtSA before a successful one was found. The initial synthesis attempts used the Overman rearrangement, but ultimately a simple hydrosilylation was successful.

Overman Rearrangement

A typical synthesis was carried out as follows. A solution consisting of 8.5 mL 2-methyl-2-propen-1-ol (0.101 mol) in 15 mL anhydrous diethyl ether (0.1429 mol)was added to a 3-neck 250 mL round bottomed flask containing sodium hydride (60% dispersion in mineral oil; 0.494 g prior to washing with anhydrous heptane; 1.24 x 10^{-2} mol) in 60 mL anhydrous Et_2O at -10°C. The reaction mixture was stirred at that

temperature until evolution of hydrogen gas ceased. 10 mL trichloroacetonitrile (0.100 mol) was then added dropwise over the course of 20 minutes. The reaction mixture became first yellow, then brown. It was allowed to warm to room temperature and the solvent was removed via rotavap. Upon addition of 100 mL of 99:1 hexanes:methanol to the resulting brown oil, a brown precipitate formed. This was removed via gravity filtration and 18.8450 of the crude product trichloroacetimidate was recovered. The trichloroacetimidate was not purified further and carried on "as-is" to the next step. The crude trichloroacetimidate was dissolved in 180 mL *p*-xylene and heated at reflux overnight. 19.8477 g of the crude trichloroacetamide was recovered.

3.6.2.8 Synthesis of 2-Methyl-3-(triethylsilyl)propylamine (βMe-TEtSA)

Hydrosilylation

Synthesis of βMTEtSA was carried out as follows. A 3-neck 250 mL round-bottomed flask was fitted with a condenser and stirbar and placed under argon. 40 mL anhydrous toluene (0.376 mol) was added to the flask, followed by 16.5 mL triethylsilane (103 mmol; 2.58 *M*) and 2.70 mL 2 wt% Pt-DVDS in xylenes (2.395×10^{-4} mol Pt; 0.23% loading wrt silane). The reaction mixture was allowed to stir at room temperature for several minutes; 5 g 2-methylallylamine (70.3 mmol; 1.75 *M*) was then added and the reaction mixture was heated at 110°C for 24 hours. Reaction progress was checked via ^{1}H NMR for disappearance of the vinyl peaks of the 2-methylallylamine. The solvent was removed via rotavap and the product distilled under reduced pressure to yield 10.0744 g product (53.7 mmol; 76.4% isolated yield).

^{1}H NMR (400.13 MHz, $CDCl_3$, 25°C) δ = 2.52 (dd, *J* = 12.5, 5.5 Hz, 1H), 2.42 (dd, *J* = 12.5, 5.5 Hz, 1H), 1.54 (m, 1H), 1.09 (s, 2H), 0.90 (m, 12H), 0.62 (dd, *J* = 14.7, 4.5 Hz, 1H), 0.50 (q, *J* = 7.9 Hz, 6H), 0.31 (dd, *J* = 14.7, 5.4 Hz, 1H)

^{13}C NMR (100.57 MHz, $CDCl_3$, 25°C) 51.75, 32.79, 20.39, 16.69, 7.46, 4.01

Calculated % for $C_{10}H_{25}NSi$ (MW: 187.40 g·mol^{-1}): C 64.09, H 13.45, N 7.47, Si 14.99; found: C 63.31 H 13.54, N 7.33

3.6.2.9 Attempted Synthesis of 2-Methyl-4-(triethylsilyl)-butyl-2-amine (α,αDMe-TEtSA)

Several methods were attempted to synthesize α,αDMe-TEtSA before a successful one was found. I was able to successfully use the Overman rearrangement to synthesize the trichloroacetamide-protected branched amine, but hydrosilylation using the protected branched amine was unsuccessful. An alternative method was used to synthesize multi-gram amounts of the desired αDMTEtSA: hydrosilylation using a branched alkyne substrate, followed by hydrogenation of the resulting internal double bond.

Overman Rearrangement

A solution consisting of 15.5 mL prenyl alcohol (0.1526 mol) in 25 mL anhydrous diethyl ether was added to a 3-neck 250 mL round bottomed flask containing sodium hydride (60% dispersion in mineral oil; 0.6998 g prior to washing with anhydrous heptane; 0.0175 mol) in 80 mL anhydrous Et_2O at -10°C. The reaction mixture was stirred until evolution of hydrogen gas ceased. 14.8 mL trichloroacetonitrile (0.1476 mol) was then added dropwise over the course of 20 minutes. The reaction mixture became first yellow, then brown. It was allowed to warm to room temperature and the solvent was removed via rotavap. Upon addition of 100 mL of 99:1 hexanes:methanol to the resulting brown oil, a brown precipitate formed. This was removed via gravity filtration and 31.833 of the crude product trichloroacetimidate was recovered. The trichloroacetimidate was not purified further and carried on “as-is” to the next step.

In a 1000 mL round bottomed flask, 31.833 g of the crude trichloroacetimidate was dissolved in 300 mL *p*-xylene (2.433 mol). The flask was then fitted with a condenser, purged with argon, and heated at 140°C overnight. The reaction was then allowed to cool to room temperature and the solvent was removed via rotavap to yield a yellow oil, which, upon standing and cooling, formed greasy yellow crystals (32.7269 g; 96.2 % crude yield). These were allowed to dry under vacuum for 2 days; the yield of the resulting dry trichloroacetamide was found to be 27.5893 g (0.120 mol; 81.08% yield). Although no impurities were detected via ^{1}H NMR, this product is described in literature as forming white needle-like crystals. Decolorization with activated charcoal (in ethanol) and filtration through Celite yielded pale yellow needle-like crystals.

^{1}H NMR (400.13 MHz, $CDCl_3$, 25°C) 6.60 (s, 1H), 6.00 (dd, J = 17.4, 10.7 Hz, 1H), 5.20 (d, J = 17.4 Hz, 1H), 5.15 (d, J = 9.0 Hz, 1H), 1.52 (s, 6H)

^{13}C NMR (100.57 MHz, $CDCl_3$, 25°C) 160.20, 141.86, 113.15, 93.14, 55.82, 26.34

Hydrosilylation

Hydrosilylation reactions using the α-dimethyl trichloroacetamide as the substrate with triethylsilane and 0.2 mol% Pt-DVDS were unsuccessful. No product was detected via ^{1}H NMR after a reaction time of 1 week in refluxing PhMe.

3.6.2.10 Synthesis of 2-Methyl-4-(triethylsilyl)-butyl-2-amine (α,αDMe-TEtSA)

Hydrosilylation and Hydrogenation

A 3-neck 250 mL round bottomed flask was fitted with a condenser and stirbar and placed under argon. To this was added 13.75 mL 2 wt% Pt-DVDS in xylenes (1.205 x 10^{-3} mol Pt; 1.268% catalyst loading wrt silane) and 2.4 mL 0.5 *M* 2,8,9-triisobutyl-

2,5,8,9-tetraaza-1-phosphabicyclo[3.3.3]undecane solution (1.200 x 10^{-3} mol) in diethyl ether. The reaction mixture was heated at 60°C for 10 minutes. After cooling to room temperature, 80 mL of anhydrous inhibitor-free THF (0.9865 mol) was added to the flask, which was then cooled to approximately -10°C in an ice-and-brine bath. 21.25 mL triethylsilane (0.133 mol) was then added dropwise to the flask and allowed to stir for approximately 5 minutes. 10 mL of 2-methyl-3-butyn-2-amine (9.503 x 10^{-2} mol) was then added dropwise to the reaction mixture, which was kept in the ice bath until the large exotherm had ceased. The reaction was then allowed to stir at room temperature overnight; reaction progress was monitored by the disappearance of the terminal alkyne carbon in the ^{13}C NMR (approximately δ91). The solvent and unreacted silane were removed via rotavap. Distillation under reduced pressure yielded 4.7772 g of the alkene product 2-methyl-4-(triethylsilyl)but-3-en-2-amine as a clear oil (bp 60°C at 5 mmHg; 79.8% yield).

^{1}H NMR (400.13 MHz, $CDCl_3$, 25°C) δ = 6.10 (dd, *J* = 19.0, 2.0 Hz, 1H), 5.55 (dd, *J* = 19.0, 2.0 Hz, 1H), 1.17 (s, 2H), 1.14 (s, 6H), 0.88 (t, *J* = 7.9 Hz, 9H), 0.52 (q, *J* = 7.9 Hz, 6H)

^{13}C NMR (100.57 MHz, $CDCl_3$, 25°C) 157.73, 118.81, 52.47, 30.43, 7.51, 3.70

Hydrogenation of the alkene was carried out in a Parr reactor. The reactor was first loaded with 0.1367 g 5 wt% Pd/C (6.42 x 10^{-5} mol Pd; 0.11% catalyst loading wrt alkene) and then purged several times with dry nitrogen. 30 mL anhydrous ethanol (0.513 mol) and 11.9032 mL of 2-methyl-4-(triethylsilyl)but-3-en-2-amine (59.69 mmol) were added to the reactor, which was then pressurized with hydrogen (80 psi) and heated at 50°C for 12 hours. Upon cooling the next morning, the excess H_2 was vented, and the catalyst was removed from the reaction mixture via filtration with Celite. ^{1}H NMR of the product mixture revealed the total absence of any alkene peaks, indicating that the reaction had gone to completion. Removal of the solvent via rotavap yielded 9.1850 g of

the desired saturated crude product, which was then distilled at reduced pressure (bp 65°C at 1.5 mmHg; 76.4% isolated yield).

^{1}H NMR (400.13 MHz, $CDCl_3$, 25°C) δ = 1.24 (m, 2H), 1.09 (s, 2H), 0.99 (s, 6H), 0.86 (t,
J = 8.0 Hz, 9H), 0.45 (m, 8H)

^{13}C NMR (100.57 MHz, $CDCl_3$, 25°C) 50.20, 38.76, 29.52, 7.42, 5.08, 3.15

Calculated % for $C_{11}H_{27}NSi$ (MW: 201.42 $g \cdot mol^{-1}$): C 65.59, H 13.51, N 6.95, Si 13.94; found: C 64.03, H 13.51, N 6.67

3.6.2.11 Synthesis of *trans*-3-(Triethylsilyl)prop-2-en-1-amine (*trans*-TEtSA)

A typical reaction was carried out as follows. In a 3-neck 250 mL round bottomed flask fitted with a condenser under inert atmosphere, 17.8 mL 2% Pt-DVDS in xylenes (1.560×10^{-3} mol Pt; 1.00% loading wrt silane) was combined with 3.1 mL 0.5 *M* 2,8,9-triisobutyl-2,5,8,9-tetraaza-1-phosphabicyclo[3.3.3]undecane solution (1.625×10^{-3} mol) in diethyl ether. The reaction mixture was heated at 60°C for 10 minutes and then allowed to cool to room temperature. 100 mL anhydrous inhibitor-free THF (1.233 mol) was added to the flask, which was then cooled to approximately -10°C in an ice-and-brine bath. 27.5 mL triethylsilane (0.172 mol) was then added dropwise to the flask and allowed to stir for approximately 5 minutes. 10 mL of propargylamine (0.156 mol) was then added dropwise to the reaction mixture, which was kept in the ice bath until the large exotherm had ceased. The reaction was then allowed to stir at room temperature overnight; reaction progress was monitored by the disappearance of the terminal alkyne carbon in the ^{13}C NMR (approximately δ91). The solvent and excess triethylsilane were then removed via rotary evaporator, and the product was distilled under reduced pressure (bp: 75°C at 6 mmHg) to yield 12.1926 g of the *trans*-isomer only (0.0711 mol; 45.57% yield).

^{1}H NMR (400.13 MHz, $CDCl_3$, 25°C) 6.13 (dt, *J* = 18.8, 4.8 Hz, 1H), 5.67 (dt, *J* = 18.9, 1.8 Hz, 1H), 3.33 (dd, *J* = 4.8, 1.8 Hz, 2H), 1.12 (s, 2H) 0.98 (t, *J* = 7.9 Hz, 9H) 0.57 (q, *J* = 7.9 Hz, 6H)

^{13}C NMR (100.57 MHz, $CDCl_3$, 25°C) 149.10, 124.22, 47.19, 7.55, 3.70

Calculated % for $C_9H_{21}NSi$ (MW: 171.36 g·mol^{-1}): C(63.08), H(12.35), N(8.17), Si(16.39); found: C(62.34), H(12.36), N(7.67)

3.6.2.12 Synthesis of 2-Methyl-4-(triethylsilyl)but-3-en-2-amine (*trans*-α,αDMe-TEtSA)

A 3-neck 250 mL round bottomed flask was fitted with a condenser and stirbar and placed under argon. To this was added 2 wt% Pt-DVDS in xylenes (13.75 mL, 1.205 x 10^{-3} mol Pt; 1.268% catalyst loading wrt silane) and 0.5 *M* 2,8,9-triisobutyl-2,5,8,9-tetraaza-1-phosphabicyclo[3.3.3]undecane solution in diethyl ether (2.4 mL, 1.200 x 10^{-3} mol). The reaction mixture was heated at 60°C for 10 minutes. After cooling to room temperature, anhydrous inhibitor-free THF (80 mL, 0.9865 mol) was added to the flask, which was then cooled to approximately -10°C in an ice-and-brine bath. Triethylsilane (21.25 mL, 0.133 mol) was then added dropwise to the flask and allowed to stir for approximately 5 minutes. 2-methyl-3-butyn-2-amine (10 mL, 9.503 x 10^{-2} mol) was then added dropwise to the reaction mixture, which was kept in the ice bath until the large exotherm had ceased. The reaction was then allowed to stir at room temperature overnight; reaction progress was monitored by the disappearance of the terminal alkyne carbon in the ^{13}C NMR (approximately δ91). The solvent and unreacted silane were removed via rotary evaporator. Distillation under reduced pressure yielded the alkene product 2-methyl-4-(triethylsilyl)but-3-en-2-amine as a clear oil (bp 60°C at 5 mmHg; 4.7772 g, 79.8% yield).

^{1}H NMR (400.13 MHz, $CDCl_3$, 25°C) δ = 6.10 (d, 1H), 5.55 (d, 1H), 1.17 (s, 2H), 1.14/1.13 (s, overlapping, (6H)), 0.88 (t of d, 9H), 0.52 (q of d, 6H)

^{13}C NMR (100.57 MHz, $CDCl_3$, 25°C) δ = 157.50, 118.58, 52.24, 30.20, 7.28, 3.47

Calculated % for $C_{11}H_{25}NSi$ (MW: 199.41 $g \cdot mol^{-1}$): C(66.25), H(12.64), N(7.02), Si(14.08); found: C(64.81), H(12.41), N(6.55)

3.6.2.13 Synthesis of 2-Methyl-4-(tripropylsilyl)-butyl-2-amine (*trans*-α,αDMe-TPSA)

Synthesized in the same manner as *trans*-α,αDMe-TEtSA. A 3-neck 250 mL round bottomed flask was fitted with a condenser and stirbar and placed under argon. To this was added 2 wt% Pt-DVDS in xylenes (13.75 mL, 1.205 x 10^{-3} mol Pt; 1.268% catalyst loading wrt silane) and 0.5 *M* 2,8,9-triisobutyl-2,5,8,9-tetraaza-1-phosphabicyclo[3.3.3]undecane solution in diethyl ether (2.4 mL, 1.200 x 10^{-3} mol). The reaction mixture was heated at 60°C for 10 minutes. After cooling to room temperature, anhydrous inhibitor-free THF (80 mL, 0.9865 mol) was added to the flask, which was then cooled to approximately -10°C in an ice-and-brine bath. Tripropylsilane (21.25 mL, 0.133 mol) was then added dropwise to the flask and allowed to stir for approximately 5 minutes. 2-methyl-3-butyn-2-amine (10 mL, 9.503 x 10^{-2} mol) was then added dropwise to the reaction mixture, which was kept in the ice bath until the large exotherm had ceased. The reaction was then allowed to stir at room temperature overnight; reaction progress was monitored by the disappearance of the terminal alkyne carbon in the ^{13}C NMR (approximately δ91). The solvent and unreacted silane were removed via rotary evaporator. Distillation under reduced pressure yielded the alkene product 2-methyl-4-(tripropylsilyl)-butyl-2-amine as a clear oil (68.1% yield).

^{1}H NMR (400.13 MHz, $CDCl_3$, 25°C) δ = 5.85 (d, 1H), 5.35 (d, 1H), 1.06 (s (br) overlapping sex, 8 H), 0.88 (s, 6H), 0.67 (t, 9H), 0.29 (d overlapping t, 6H)

^{13}C NMR (100.57 MHz, $CDCl_3$, 25°C) δ = 156.74, 119.31, 51.84, 29.79, 18.12, 17.01, 15.10

Calculated % for $C_{14}H_{31}NSi$ (MW: 241.49 g·mol^{-1}): C(69.63), H(12.94), N(5.80), Si(11.63); found: C(68.93), H(12.96), N(5.29)

3.6.2.14 Synthesis of N-Methyl-3-(triethylsilyl)propan-1-amine (STEtSA)

Formylation

To a round bottomed flask fitted with a condenser and magnetic stirbar under inert atmosphere was added 3-(aminopropyl)triethylsilane (8.69 g, 50 mmol). This was cooled to 10°C; ethylformate (5.25 mL, 65 mmol) was added then added dropwise over 15 minutes. The solution was then heated to 60°C and stirred for 3 hours. The byproduct EtOH and excess ethylformate were then removed under reduced pressure to yield 9.72 g (48.27 mmol) of the desired product *N*-(3-(triethylsilyl)propyl)formamide in 97% yield.

^{1}H NMR (400.13 MHz, $CDCl_3$, 25°C) δ = 8.13 (s)/8.01 (d)(1H), 5.96 (s, 1H), 3.23 (q)/3.15 (q) (2H), 1.47 (s, 2H), 0.89 (t, 9H), 0.48 (q, 8H)

^{13}C NMR (100.57 MHz, $CDCl_3$, 25°C) δ = 161.19, 41.43, 24.09, 8.51, 7.37, 3.13

Reduction

To a round bottomed flask fitted with a condenser and magnetic stirbar under inert atmosphere was added anhydrous THF (80 mL, 0.9865 mol) and *N*-(3-(triethylsilyl)propyl)formamide (8.49 g, 42 mmol). This solution was heated to 60°C, and $LiAlH_4$ in THF (50.7 mL, 50.7 mmol, 1 *M*) was added slowly over 45 minutes. An exotherm was observed. The reaction mixture was stirred for 18 hours at 60°C, at which point the resulting mixture was cooled to room temperature. DI H_2O (2.5 mL, 0.139 mol) and 10% NaOH (5 mL, 1.25 mmol) were added. An additional aliquot of H_2O (10.5 mL, 0.58 mol)) was then added; the mixture was filtered through Celite, then washed with hexane and MeOH. The organic layer was separated; the aqueous layer was washed with hexane, which was then combined with the previous organic layer. The solution was then

washed with brine and dried with $MgSO_4$. The solvents were removed via rotary evaporator. The resulting liquid was distilled under reduced pressure at 1 mmHg and 48°C to provide *N*-methyl-3-(triethylsilyl)propan-1-amine (5.68 g, 30.3 mmol), corresponding to a 73% isolated yield.

^{1}H NMR (400.13 MHz, $CDCl_3$, 25°C) δ = 2.54 (t, 2H), 2.42 (s, 3H), 1.46 (s, 2H), 1.37 (s, 1H), 0.91 (t, 9H), 0.50 (q, 8H)

^{13}C NMR (100.57 MHz, $CDCl_3$, 25°C) δ = 55.70, 36.37, 24.09, 8.73, 7.42, 3.23

Calculated % for $C_{10}H_{25}NSi$ (MW: 187.40 $g \cdot mol^{-1}$): C(64.09), H(13.45), N(7.47), Si(14.99); found: C(63.12), H(13.47), N(7.47)

3.6.2.15 Synthesis of N-Methyl-3-(aminopropyl)dimethylethylsilane (SDMESA)

Formylation

3-(Aminopropyl)dimethylethylsilane (DMEtSA) (7.3 g, 0.05 mol) was added to a RB flask under argon. Ethylformate (5.25 mL, 0.065 mol) was added dropwise over 15 minutes at 10°C. The temperature of the solution was increased to 60°C and stirred for 4 hours. The solution was then cooled and rotovapped to remove the by-product, EtOH, and excess ethylformate to provide 8.47 g of N-(3-(dimethylethylsilyl)propyl)formamide in 98% yield.

^{1}H NMR (400 Hz, $CDCl_3$) 8.14 (s)/ 8.00 (d) (1H), 5.79 (s, 1H), 3.25 (q)/3.16(q) (2H), 1.48 (s, 2H), 0.89 (t, 3H), 0.47 (q, 4H), -0.06 (s, 6H)

^{13}C NMR (400 Hz, $CDCl_3$) 161.11, 41.28, 24.12, 11.92, 7.25, 6.68, 4.07

Reduction

N-(3-(dimethylethylsilyl)propyl)formamide (7.83 g, 0.0452 mol) was added to 120 mL of anhydrous THF under an inert atmosphere in a RB flask. The solution temperature was brought to 60°C and solid $LiAlH_4$ (3.091 g, 0.081 mol) was added

slowly via solid addition arm over 30 minutes. After stirring for 18 hours at 60°C, the resulting mixture was cooled with a dry/ice acetone bath to keep the temperature at about 0°C. To it was added 3 mL H_2O followed by 6 mL of a 10% NaOH solution. 12 mL of H_2O were then added and the entire mixture was filtered through a pad of celite and washed with THF and H_2O. The collected solution was then introduced into a separatory funnel and heavily brined with NaCl. The organic layer was separated. The aqueous layer was washed with hexane and the organic layer was combined with the previous. They were both washed with brine and dried over $MgSO_4$. The solvents were removed via rotovap distillation. The resulting liquid was distilled under reduced pressure at 3.4 mmHg and 36°C to provide 3.54 g of the N-methyl-3-(dimethylethylsilyl)propan-1-amine corresponding to a 49% isolated yield.

^{1}H NMR (400 Hz, CDCl3) 2.47 (t, 2H), 2.35 (s, 3H), 1.40 (s, 2H), 1.00 (s, 1H), 0.84 (t, 3H), 0.40 (q, 2H), -0.12 (s, 6H)

^{13}C NMR (400 Hz, CDCl3) 55.47, 36.32, 24.10, 12.15, 7.21, 6.73, -4.10

Expected: C(60.30), H(13.28), N(8.79), Si(17.63) found: C(58.97), H(13.17), N(8.42)

3.6.2.16 Synthesis of 3-(Aminopropyl)dimethylethylsilane (DMESA):

To a 3-neck 250 mL round bottomed flask fitted with a condenser and magnetic stirbar under inert atmosphere was added anhydrous toluene (80 mL, 0.751 mol), dimethylethylsilane (10.56 mL, 80 mmol), and 2 wt% Pt-DVDS in xylenes (1.82 mL; 1.60 x 10^{-4} mol Pt; 0.20% catalyst loading wrt silane). This was allowed to stir at room temperature for approximately five minutes, at which point allylamine (12 mL, 0.160 mol) was added and the reaction was heated to 110°C overnight. Reaction progress was monitored via ^{1}H NMR for the disappearance of the silane proton (~3.7 ppm). When this peak was no longer present, the reaction mixture was allowed to cool to room temperature; the solvent and excess allylamine was then removed via rotary evaporator.

The product 3-(aminopropyl)dimethylethylsilane (58% isolated yield) was distilled from the catalyst under reduced pressure (bp: 38°C at 2.5 mmHg).

^{1}H NMR (400.13 MHz, $CDCl_3$, 25°C) δ = 2.61 (t, 2H), 1.37 (m, 2H), 1.15 (br, 2H), 0.44 (m, 4H), -0.09 (s, 6H)

^{13}C NMR (100.57 MHz, $CDCl_3$, 25°C) δ = 45.61, 28.22, 11.74, 7.24, 6.77, -4.04

Calculated % for $C_7H_{19}NSi$ (MW: 145.32 g·mol^{-1}): C(57.86), H(13.18), N(9.64), Si(19.33); found: C (57.50), H(13.01), N(8.94)

3.6.3 Reversible Ionic Liquid Formation

3.6.3.1 Measurements at 25°C

For all of the reversible ionic liquids discussed, synthesis was carried out as follows unless otherwise noted. A 2 dram vial was weighed; approximately one gram of the silylamine was added and the vial was weighed again. A porous fritted tube (Ace Glass, 10 mm gas dispersion tube, porosity C) was weighed and used to sparge dry carbon dioxide through the silylamine for 75 minutes at a flow rate of 200 mL·min^{-1} at 25°C and 1 bar. The resulting reversible ionic liquid, vial, and fritted tube were then weighed to determine CO_2 uptake capacity at 25°C.

3.6.3.2 Measurements at 40°C

A 2 dram vial was weighed; approximately one gram of the *silylamine* was added and the vial was weighed again. The vial and sample were placed in a 40°C sand bath in thermal equilibrium with a heated gas line. A porous fritted tube (Ace Glass, 10 mm gas dispersion tube, porosity C) was weighed and used to sparge dry carbon dioxide through the silylamine for 75 minutes at a flow rate of 200 mL·min^{-1} at 40°C and 1 bar. The resulting reversible ionic liquid, vial, and fritted tube were then weighed to determine CO_2 uptake capacity at 40°C.

3.6.4 Instrumentation

ATR FT-IR data was collected using a Shimadzu IRPrestige21 with a DLaTGS detector with 32 scans and a resolution of 1 cm^{-1}, used in combination with a Specac, Ltd. heated "Golden Gate" ATR accessory with a diamond crystal and zinc selenide lenses.[31, 58]

^{1}H and ^{13}C NMR spectra were collected on a Varian Mercury Vx 400, using $CDCl_3$ as the lock solvent. Due to the high viscosities of the ionic forms, the reversible ionic liquids were synthesized in the NMR tube under solvent-free conditions, and a capillary tube containing $CDCl_3$ was placed inside the sample.

Viscosities of all reversible ionic liquids were obtained using a Rheosys Merlin II viscometer with a temperature-controlled 2° cone and plate system. Densities of all silylamines and reversible ionic liquids (used in gravimetric calculation of CO_2 uptake) were obtained in triplicate using an Anton Paar DMA 38 Laboratory Density Meter. Elemental analysis (C, N, and H) of molecular liquids was performed by Atlantic Microlab in Norcross, GA. Samples were stored under inert gas and either delivered in person or sent via FedEx.

Differential scanning calorimetry (DSC) measurements were used to determine the reversal temperatures of the reversible ionic liquids and the evaporation temperatures of the silylamines. The instrument used was a Q20 TA Instruments DSC; hermetically sealed aluminum pans were used, into which approximately 2 mg of the compound under consideration was measured. The temperature was ramped from -40°C to 400°C with a ramp rate of $5°C \cdot min^{-1}$, and the temperatures of the reversal or boiling events were determined by the intersect of the baseline of the event and the line tangent to the peak of the event.

3.6.5 Quantitative ^{13}C Nuclear Magnetic Resonance (NMR) Spectroscopy

For the quantitative ^{13}C experiments, the starting amine (3-(aminopropyl) tripropylsilane) was added to an argon-purged tube sealed using a septa. One bar of CO_2 was then introduced by sparging using a long 18-gauge stainless steel needle (a 21 gauge needle was also used to vent the system). Weight measurements were made before and after CO_2 introduction, to calculate the gravimetric CO_2 uptake. The average CO_2 capacity measured gravimetrically in the quantitative NMR experiments was 0.62 ± 0.01 moles of CO_2 per mole of amine. It is assumed that the slightly lower CO_2 uptake observed in the NMR experiments compared to the gravimetric capacities reported is a result of mass transfer limitations in the NMR tube. To conduct quantitative ^{13}C NMR, three important experimental changes are needed over standard ^{13}C NMR. They include (1) a full 90° pulse, (2) extended delay time, and (3) proton decoupling only during the acquisition period. The first is to ensure complete excitation of the nucleus. The second is to allow full relaxation after the pulse is applied. To determine the appropriate delay time, an inversion recovery T_1 experiment was performed. For 3-(aminopropyl) tripropylsilane in its reversible ionic liquid form, the longest T_1 time comes from the carbonyl carbon (162.73 ppm) at 4.027 s. It is generally recommended that the delay time used be 5 times the longest T_1 time. As such, for all of the quantitative experiments performed, a delay time of 20 s was used. The last experimental change (3) is done to avoid a false and disproportional signal buildup during proton decoupling as a result of the Nuclear Overhauser Effect. The protocol is named inverse gated decoupling. To increase the signal-to-noise ratio, 2000 scans were performed for each experiment over a period of 12 h.

3.7 References

1. U.S. Energy Information Administration. Washington, 2011.

2. E. I. Administration. Washington, DC, 2000.

3. Olajire, A. A., CO_2 capture and separation technologies for end-of-pipe applications - A review. *Energy* **2010,** *35* (6), 2610-2628.

4. Rao, A. B.; Rubin, E. S., A Technical, Economic, and Environmental Assessment of Amine-Based CO2 Capture Technology for Power Plant Greenhouse Gas Control. *Environmental Science & Technology* **2002,** *36* (20), 4467-4475.

5. Rubin, E. S.; Mantripragada, H.; Marks, A.; Versteeg, P.; Kitchin, J., The outlook for improved carbon capture technology. *Progress in Energy and Combustion Science* **2012,** *38* (5), 630-671.

6. D'Alessandro, D. M.; Smit, B.; Long, J. R., Carbon Dioxide Capture: Prospects for New Materials. *Angewandte Chemie-International Edition* **2010,** *49* (35), 6058-6082.

7. Brennecke, J. E.; Gurkan, B. E., Ionic Liquids for CO_2 Capture and Emission Reduction. *Journal of Physical Chemistry Letters* **2010,** *1* (24), 3459-3464.

8. Ciferno, J. P.; Fout, T. E.; Jones, A. P.; Murphy, J. T., Capturing carbon from existing coal-fired power plants. *Chemical Engineering Progress* **2009,** *105* (4), 33-41.

9. Fisher, K. S.; Searcy, K.; Rochelle, G. T.; Ziaii, S.; Shubert, C. *Advanced Amine Solvent Formulations and Process Integration for Near-Term CO_2 Capture Success*; Pittsburgh, PA, 2007.

10. Aaron, D.; Tsouris, C., Separation of CO_2 from flue gas: A review. *Separation Science and Technology* **2005,** *40* (1-3), 321-348.

11. Shannon, M. S.; Bara, J. E., Reactive and Reversible Ionic Liquids for CO_2 Capture and Acid Gas Removal. *Separation Science and Technology* **2012,** *47* (2), 178-188.

12. Bello, A.; Idem, R. O., Pathways for the formation of products of the oxidative degradation of CO_2-loaded concentrated aqueous monoethanolamine solutions during CO_2 absorption from flue gases. *Industrial & Engineering Chemistry Research* **2005,** *44* (4), 945-969.

13. Danckwerts, P. V., The reaction of CO_2 with ethanolamines. *Chemical Engineering Science* **1979,** *34* (4), 443-446.

14. Abanades, J. C.; Rubin, E. S.; Anthony, E. J., Sorbent cost and performance in CO_2 capture systems. *Industrial & Engineering Chemistry Research* **2004,** *43* (13), 3462-3466.

15. Puxty, G.; Rowland, R.; Allport, A.; Yang, Q.; Bown, M.; Burns, R.; Maeder, M.; Attalla, M., Carbon Dioxide Postcombustion Capture: A Novel Screening Study of the Carbon Dioxide Absorption Performance of 76 Amines. *Environmental Science and Technology* **2009,** *43* (16), 6427-6433.

16. Rubin, E. S.; Chen, C.; Rao, A. B., Cost and performance of fossil fuel power plants with CO_2 capture and storage. *Energy Policy* **2007,** *35* (9), 4444-4454.

17. Kim, I.; Svendsen, H. F., Heat of absorption of carbon dioxide (CO2) in monoethanolamine (MEA) and 2-(Aminoethyl)ethanolamine (AEEA) solutions. *Industrial & Engineering Chemistry Research* **2007,** *46* (17), 5803-5809.

18. Strazisar, B. R.; Anderson, R. R.; White, C. M., Degradation pathways for monoethanolamine in a CO_2 capture facility. *Energy & Fuels* **2003,** *17* (4), 1034-1039.

19. Veawab, A.; Tontiwachwuthikul, P.; Bhole, S. D., Studies of corrosion and corrosion control in a CO_2-2-amino-2-methyl-1-propanol (AMP) environment. *Industrial & Engineering Chemistry Research* **1997,** *36* (1), 264-269.

20. Veawab, A.; Aroonwilas, A.; Chakma, A.; Tontiwachwuthikul, P., Solvent formulation for CO_2 separation from flue gas streams. In *First National Conference on Carbon Sequestration*, Washington, D.C., 2001.

21. Kohl, A.; Neilsen, R., *Gas Purification*. Gulf Publishing Company: Houston, TX, 1997; Vol. 5th edition.

22. Baltus, R. E.; Culbertson, B. H.; Dai, S.; Luo, H. M.; DePaoli, D. W., Low-pressure solubility of carbon dioxide in room-temperature ionic liquids measured with a quartz crystal microbalance. *Journal of Physical Chemistry B* **2004,** *108* (2), 721-727.

23. Bara, J. E.; Carlisle, T. K.; Gabriel, C. J.; Camper, D.; Finotello, A.; Gin, D. L.; Noble, R. D., Guide to CO_2 separations in imidazolium-based room-temperature ionic liquids. *Industrial & Engineering Chemistry Research* **2009,** *48* (6), 2739-2751.

24. Camper, D.; Scovazzo, P.; Koval, C.; Noble, R., Gas solubilities in room-temperature ionic liquids. *Industrial & Engineering Chemistry Research* **2004,** *43* (12), 3049-3054.

25. Condemarin, R.; Scovazzo, P., Gas permeabilities, solubilities, diffusivities, and diffusivity correlations for ammonium-based room temperature ionic liquids with comparison to imidazolium and phosphonium RTIL data. *Chemical Engineering Journal* **2009,** *147* (1), 51-57.

26. Gutowski, K. E.; Maginn, E. J., Amine-functionalized task-specific ionic liquids: A mechanistic explanation for the dramatic increase in viscosity upon complexation with CO_2 from molecular simulation. *Journal of the American Chemical Society* **2008,** *130* (44), 14690-14704.

27. Bates, E. D.; Mayton, R. D.; Ntai, I.; Davis, J. H., CO_2 capture by a task-specific ionic liquid. *Journal of the American Chemical Society* **2002,** *124* (6), 926-927.

28. Gurkan, B. E.; de la Fuente, J. C.; Mindrup, E. M.; Ficke, L. E.; Goodrich, B. F.; Price, E. A.; Schneider, W. F.; Brennecke, J. F., Equimolar CO_2 absorption by anion-functionalized ionic liquids. *Journal of the American Chemical Society* **2010,** *132* (7), 2116-2117.

29. Goodrich, B. F.; de la Fuente, J. C.; Gurkan, B. E.; Zadigian, D. J.; Price, E. A.; Huang, Y.; Brennecke, J. F., Experimental Measurements of Amine-Functionalized Anion-Tethered Ionic Liquids with Carbon Dioxide. *Industrial & Engineering Chemistry Research* **2011,** *50* (1), 111-118.

30. Camper, D.; Bara, J. E.; Gin, D. L.; Noble, R. D., Room-temperature ionic liquid-amine solutions: Tunable solvents for efficient and reversible capture of CO_2. *Industrial & Engineering Chemistry Research* **2008,** *47* (21), 8496-8498.

31. Rohan, A. L.; Switzer, J. R.; Flack, K. M.; Hart, R. J.; Sivaswamy, S.; Biddinger, E. J.; Talreja, M.; Verma, M.; Faltermeier, S.; Nielsen, P. T.; Pollet, P.; Schuette, G. F.; Eckert, C. A.; Liotta, C. L., The Synthesis and the Chemical and Physical Properties of Non-Aqueous Silylamine Solvents for Carbon Dioxide Capture. *ChemSusChem* **2012,** *5* (11), 2181-2187.

32. Gonzalez-Miquel, M.; Talreja, M.; Ethier, A. L.; Flack, K.; Switzer, J. R.; Biddinger, E. J.; Pollet, P.; Palomar, J.; Rodriguez, F.; Eckert, C. A.; Liotta, C. L., COSMO-RS Studies: Structure-Property Relationships for CO2 Capture by Reversible Ionic Liquids. *Industrial & Engineering Chemistry Research* **2012,** *51* (49), 16066-16073.

33. Blasucci, V.; Hart, R.; Mestre, V. L.; Hahne, D. J.; Burlager, M.; Huttenhower, H.; Thio, B. J. R.; Pollet, P.; Liotta, C. L.; Eckert, C. A., Single component, reversible ionic liquids for energy applications. *Fuel* **2010,** *89* (6), 1315-1319.

34. Hart, R.; Pollet, P.; Hahne, D. J.; John, E.; Llopis-Mestre, V.; Blasucci, V.; Huttenhower, H.; Leitner, W.; Eckert, C. A.; Liotta, C. L., Benign coupling of reactions and separations with reversible ionic liquids. *Tetrahedron* **2010,** *66* (5), 1082-1090.

35. Chuit, C.; Corriu, R. J. P.; Reye, C.; Young, J. C., Reactivity of penta- and hexacoordinate silicon compounds and their role as reaction intermediates. *Chemical Reviews* **1993,** *94*, 1371-1448.

36. Voronkov, M. G.; Frolov, Y. L.; D'Yakov, V. M.; Chipanina, N. N.; Gubanova, L. I.; Gavrilova, G. A.; Klyba, L. V.; Aksamentova, T. N., *Journal of Organometallic Chemistry* **1980,** *201*, 165.

37. Kost, D.; Gostevskii, B.; Kalikhman, I., *Pure and Applied Chemistry* **2007,** *79*, 1125.

38. EPA. Climate Change 2012. http://www.epa.gov/gateway/science/climatechange.html

39. Bench-Scale and Slipstream Development and Testing of Post-Combustion Carbon Dioxide Capture and Separation Technology for Application to Existing Coal-Fired Power Plants. U. S. Department of Energy, National Energy Technology Laboratory: 2011.

40. Momin, F. REACTION OF SULFUR DIOXIDE (SO2) WITH REVERSIBLE IONIC LIQUIDS (REVILS) FOR CARBON DIOXIDE (CO2) CAPTURE. Georgia Institute of Technology, 2012.

41. Sidorkin, V. E.; Belogolova, E. F.; Pestunovich, V. A., Molecular design of neutral intramolecular complexes bearing two silicon atoms anchored by a carbonyl oxygen atom: N,N '-bis(silylmethyl)propylene ureas. *Chemistry-a European Journal* **2006,** *12* (7), 2021-2031.

42. Sartori, G.; Savage, D. W., Sterically hindered amines for CO_2 removal from gases. *Industrial & Engineering Chemistry Fundamentals* **1983,** *22* (2), 239-249.

43. Bishnoi, S.; Rochelle, G. T., Absorption of carbon dioxide into aqueous piperazine: reaction kinetics, mass transfer and solubility. *Chemical Engineering Science* **2000,** *55* (22), 5531-5543.

44. Schirlin, D. G.; Collard, J.-N.; Danzin, C. Substituted Silyl Alkylene Amines. 1995.

45. Gibson, M. S.; Bradshaw, R. W., The Gabriel synthesis of primary amines. *Angewandte Chemie-International Edition* **1968,** *7* (12), 919-930.

46. Overman, L. E., General method for synthesis of amines by rearrangement of allylic trichloroacetamides. 1,3 transposition of alcohol and amine functions. *Journal of the American Chemical Society* **1976,** *98* (10), 2901-2910.

47. Fletcher, A. J.; Bax, M. N.; Willis, M. C., Palladium-catalysed N-annulation routes to indoles: the synthesis of indoles with sterically demanding N-substituents, including demethylasterriquinone A1. *Chemical Communications* **2007,** (45), 4764-4766.

48. Weygand, F.; Frauendorfer, E., Reduktive Entfernung des *N*-Trifluoracetyl- und *N*-Trichloracetylrestes durch Natriumborhydrid mit Anwendungen in der Peptidchemie. *Chemische Berichte-Recueil* **1970,** *103* (8), 2437-2449.

49. Urabe, D.; Sugino, K.; Nishikawa, T.; Isobe, M., A novel deprotection of trichloroacetamide. *Tetrahedron Letters* **2004,** *45* (51), 9405-9407.

50. Semenow, D.; Shih, C.-H.; Young, W. G., Allylic rearrangements. XL. The reaction of allylic diazonium ions in acetic acid. *Journal of the American Chemical Society* **1958,** *80* (20), 5472-5475.

51. Nagashima, H.; Wakamatsu, H.; Ozaki, N.; Ishii, T.; Watanabe, M.; Tajima, T.; Itoh, K., Transition metal catalyzed radical cyclization: new preparative route to γ-lactams from allylic alcohols via the [3.3]-sigmatropic rearrangement of allylic trichloroacetimidates and the subsequent ruthenium-catalyzed cyclization of *N*-allyltrichloroacetamides. *Journal of Organic Chemistry* **1992,** *57* (6), 1682-1689.

52. Aneetha, H.; Wu, W.; Verkade, J. G., Stereo- and regioselective Pt(DVDS)/P(^{i}BuNCH$_2$CH$_2$)$_3$N-catalyzed hydrosilylation of terminal alkynes. *Organometallics* **2005,** *24* (11), 2590-2596.

53. Marciniec, B., *Hydrosilylation: A comprehensive review on recent advances*. Springer: Dordrect, the Netherlands, 2009; Vol. 1.

54. Rohan, A. L.; Switzer, J. R.; Flack, K. M.; Hart, R. J.; Sivaswamy, S.; Biddinger, E. J.; Talreja, M.; Verma, M.; Faltermeier, S.; Nielsen, P. T.; Pollet, P.; Schuette, G. F.; Eckert, C. A.; Liotta, C. L., The synthesis and the chemical and physical properties of non-aqueous silylamine solvents for CO_2 capture. *Unpublished manuscript*.

55. Ethier, A. APPLICATIONS OF REVERSIBLE AND SUSTAINABLE AMINE-BASED CHEMISTRIES: CARBON DIOXIDE CAPTURE, *IN SITU* AMINE PROTECTION AND NANOPARTICLE SYNTHESIS. Georgia Institute of Technology, Atlanta, GA, 2013.

56. Switzer, J. R.; Ethier, A. L.; Flack, K. M.; Biddinger, E. J.; Gelbaum, L.; Pollet, P.; Eckert, C., A; Liotta, C. L., Enhanced CO_2 Cpature with Silylamines by Carbamic Acid Stabilization. *Industrial & Engineering Chemistry Research* **2013,** *52* (13), 13159-13160.

57. Mimura, T.; Simayoshi, H.; Suda, T.; Iijima, M.; Mituoka, S., Development of energy saving technology for flue gas carbon dioxide recovery in power plant by chemical absorption method and steam system. *Energy Conversion and Management* **1997,** *38*, S57-S62.

58. Kazarian, S. G.; Briscoe, B. J.; Welton, T., Combining ionic liquids and supercritical fluids: *in situ* ATR-IR study of CO2 dissolved in two ionic liquids at high pressures. *Chemical Communications* **2000,** (20), 2047-2048.

CHAPTER 4

The Effects of CO_2 Pressure and pH on the Suzuki Coupling of Basic Nitrogen Containing Substrates

4.1 Introduction

4.1.1 Overview of the Suzuki Reaction

Carbon-carbon bond forming reactions, such as the coupling reactions developed by Suzuki-Miyaura, Stille, and others, are critical processes for the synthesis of complex organic molecules. The Suzuki-Miyaura reaction, in particular, is a widely used method of forming C-C bonds between aryl moieties. Many pharmaceutical and biologically active molecules contain biaryl moieties.[1] Gleevac™ (Figure 83) is a pharmaceutical drug produced by Novartis, which is currently utilized in the treatment of certain forms of leukemia. One of the patented methods for producing Gleevac™ relies on a Suzuki-Miyaura coupling to form the bond highlighted in blue.[2] This pharmaceutical compound also highlights another important factor of many pharmaceuticals and natural products: many contain basic nitrogen centers. In fact pyridines, for example, are the most common heterocyclic compounds found in pharmaceutically active compounds.[3]

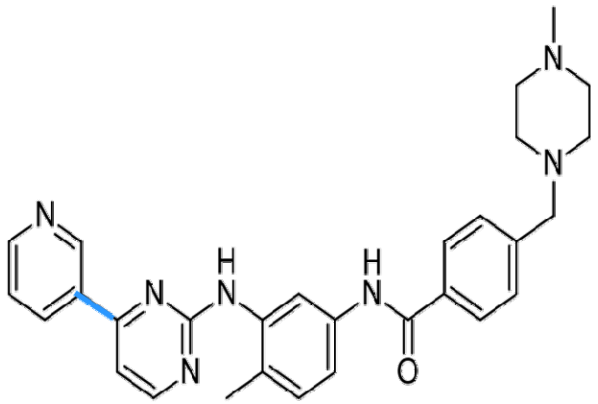

Figure 83 – Structure of Gleevac™, a cancer treatment drug.

Akira Suzuki, the chemist credited with discovering the Suzuki-Miyaura coupling reaction along with Norio Miyaura, was awarded the 2010 Nobel prize for his work on palladium-catalyzed cross-coupling reactions (in conjunction with Richard Heck and Ei-ichi Negishi). Since its discovery in 1979, investigations into the scope and development of the reaction have resulted in ~10,000 articles.[4] The Suzuki coupling reaction involves the coupling of a wide variety of organohalides (alkenyl, alkynyl, and aryl) with organoboronic acids and esters. The reactions proceed under relatively mild conditions in the presence of a catalyst (often palladium) and a base; a general scheme of the reaction is outlined in Figure 84.[5-6] Typically the solvent systems utilized are organic/aqueous; the organic can be either miscible with water (ACN, THF, etc.) or immiscible (toluene, benzene). Less commonly, there are examples of $scCO_2$, anhydrous organic solvents, and water alone being utilized as the solvent.[7-8] Other conditions include the use of inorganic or organic bases, and heterogenous or homogenous catalysts.

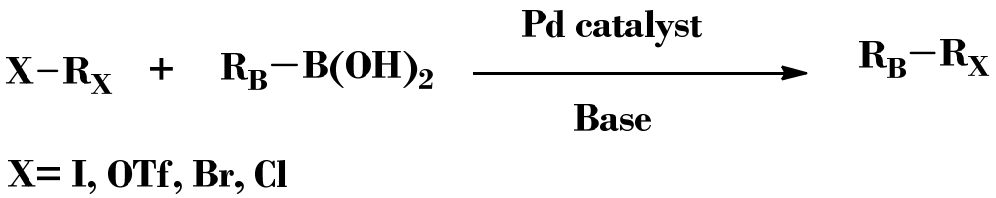

Figure 84 – Generalized Suzuki coupling reaction.

The Suzuki coupling is versatile reaction, applicable to a wide variety of alkenyl, aryl and alkynyl halides and triflates.[9-10] Further versatility of the reaction is demonstrated by its applicability to a variety of organoboranes. Boronic acids, esters, trialkylboranes, and other organoboranes can all be utilized in the reaction, though boronic acids are the most common due to their stability, availability, price and low toxicity. The reaction is also applicable to variously hybridized organoborons where the boron is bonded to sp-, sp^2-, and sp^3-carbons. The reaction is tolerant of a broad range of functional groups including esters, alcohols, amines and nitro groups; it also displays high stereo- and regio-selectivity. Alkenylhalides, for example, demonstrate retention of stereochemistry from reactant to product. Other advantages include: mild temperatures (<110°C); non-stoichiometric catalyst loadings - loadings as low as 0.0005% Pd have been successfully utilized; and a wide variety of commercially available organoboranes, organohalides and ligand/catalyst systems.[6, 11]

4.1.2 Mechanism of the Suzuki Reaction

The general mechanism of the Suzuki coupling, as outlined by Amatore, is displayed in Figure 85.[12] This has evolved from a simpler schematic proposed by Suzuki in 1995, based on the observation and isolation of intermediates.[13] The active form of the palladium catalyst in the catalytic cycle is speculated to be Pd(0), with anywhere from one to three ligands, depending on the ligand size and shape.[11, 14] The catalytic cycle begins by oxidative insertion of the Pd(0) into the carbon-halide bond of the arylhalide

(Oxidative Addition). Base such as hydroxide (when water is present in the system) then exchanges for the halide (Metathesis). Transmetallation then occurs through the transfer of the aryl species from the arylboronic acid to the palladium, followed by reductive elimination of the biaryl product and regeneration of the active catalyst. The initial and final steps (oxidative addition and reductive elimination) are relatively well supported and accepted as outlined below.[13, 15-17] The metathesis and transmetallation steps are the center of an ongoing debate, but for the purpose of this dissertation can be defined as outlined in the figure below.

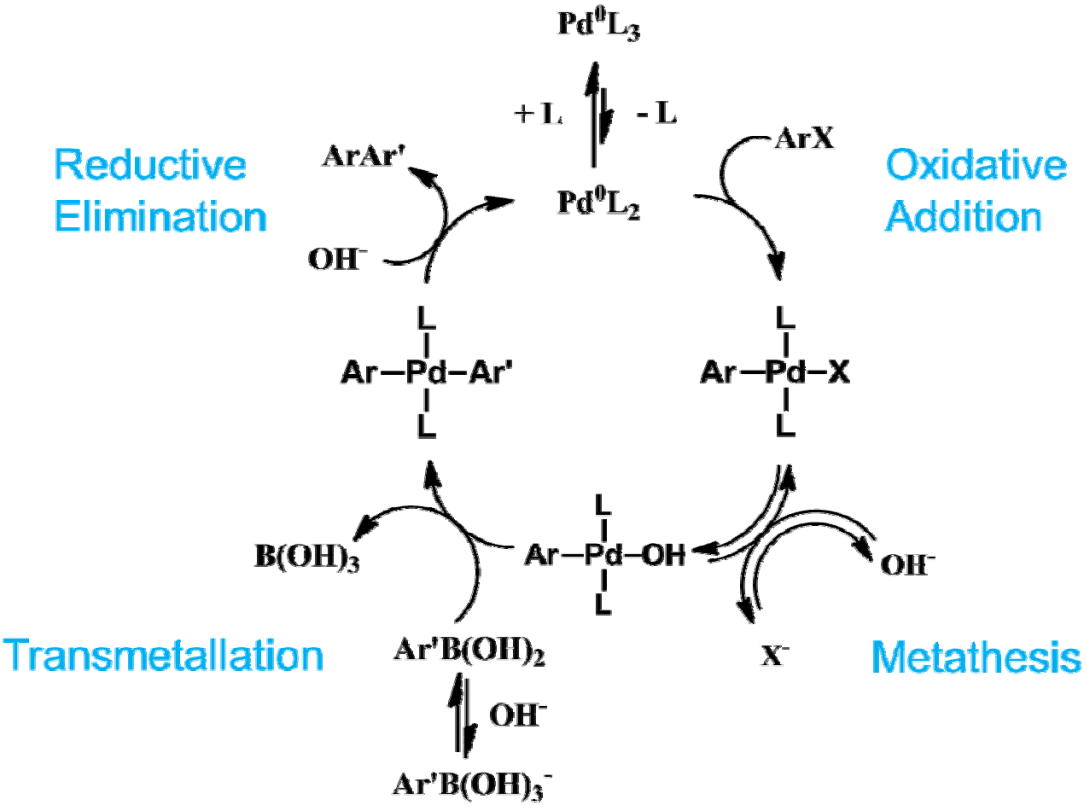

Figure 85 - Suzuki coupling mechanism.

4.1.3 Challenges of the Suzuki Reaction

The Suzuki reaction has many advantages but also presents a variety of challenges which keeps this field very much alive after over 30 years of intensive research. The exact mechanism remains elusive. Another challenge lies in the reactivity of the organohalides. It has been well established that the general order of reactivity for organohalides follows I > Br >> Cl.[4] Chlorinated substrates, however, are desirable from an industrial standpoint as they are cheaper than the corresponding bromo- and iodo- substrates. Additionally, they are readily available and the weight of the byproducts would be less than the bromo- and iodo- substrates. This is important to note for my work, though the specific goal of increasing the reactivity of chlorinated substrates has been pursued by other researchers.

Another challenge of the Suzuki coupling reaction is the efficient coupling of basic, nitrogen containing substrates. As briefly mentioned, heterocyclic biaryls are of special interest, particularly those containing nitrogen centers such as pyridines. However, application of the Suzuki reaction to basic, nitrogen containing substrates has proven challenging, resulting in low yielding or slow reactions (example: Figure 86).[18-19] Researchers in the Buchwald group have shown that aminopyridines can displace ligands to form bis(aminopyridine)palladium complexes (Figure 87) with low reactivity towards C-C bond forming cross coupling reactions.[20]

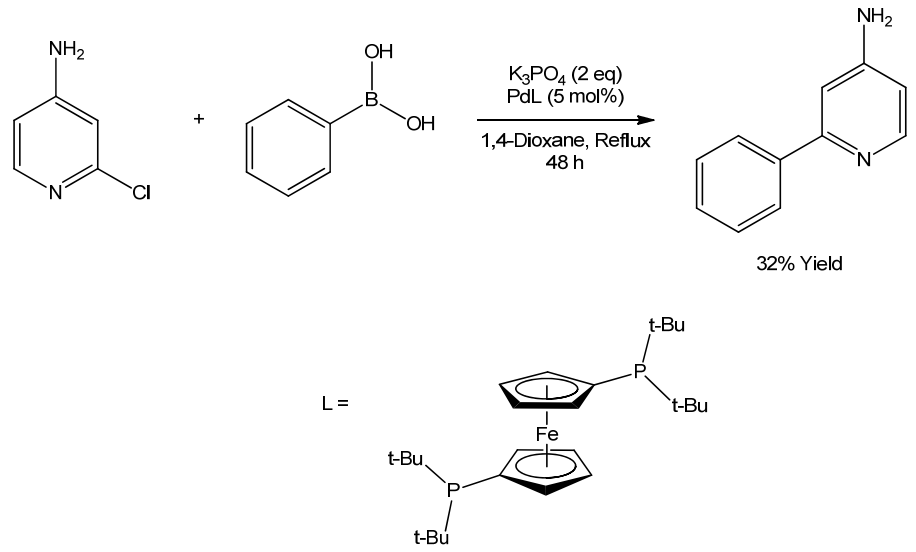

Figure 86 - Low yielding coupling of 4-amino-2-chloropyridine with phenylboronic acid.[21]

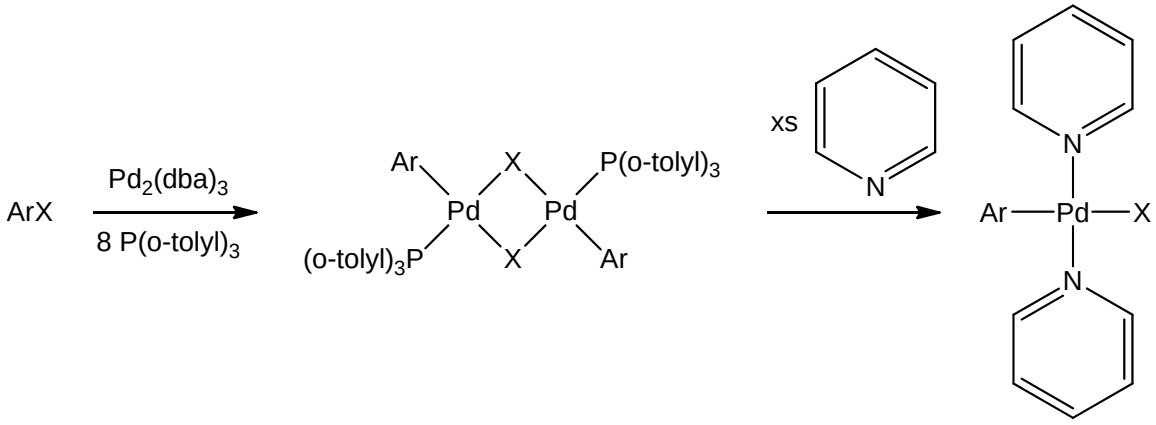

Figure 87 – Formation of bis(aminopyridine)palladium complexes which are less reactive towards cross-coupling reactions.

Itoh and Mase coupled a variety of aminochloropyridines with phenylboronic acid in the presence of $Pd(OAc)_2$, 1,10-bis(di-tert-butylphos phino)-ferrocene (D-t-BPF), potassium phosphate and 1,4-dioxane, at reflux (Figure 88). They observed moderate to good yields for all amines but the most basic, 4-amino-2-chloropyridine. They hypothesized that the highly basic amine was more likely to coordinate with the palladium, increasing the chance of forming the same inactive

bis(aminopyridine)palladium complex Buchwald described.[21] Both groups note that protection of the amine would likely reduce the basicity of the amino-pyridine and prevents coordination to the palladium, which would improve the efficiency of these substrates in palladium catalyzed cross couplings.

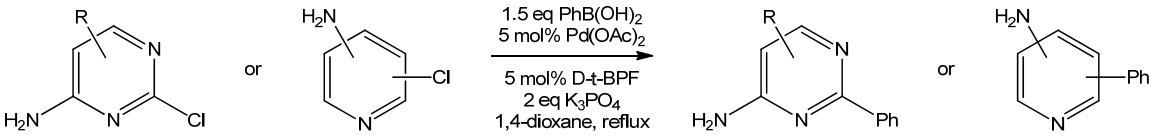

4a-i

Substrate	pK_a	Product	Number	Yield (%)
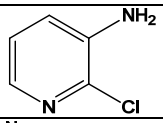	1.6	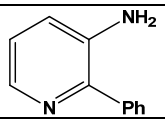	**4e**	93
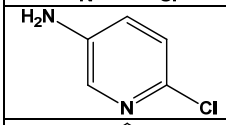	2.1	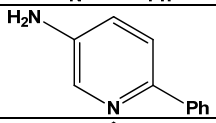	**4f**	82
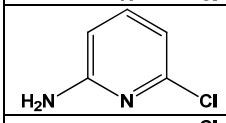	2.8	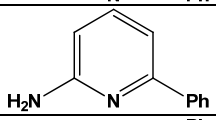	**4g**	68
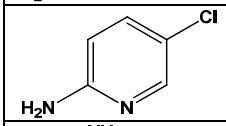	4.5	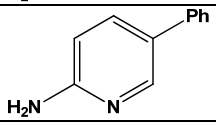	**4h**	72
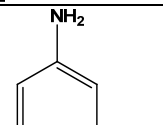	4.8	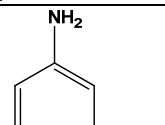	**4i**	30

Figure 88 - Yields and pK_a of the coupling of various aminochloropyridines with phenylboronic acid.

Protection/deprotection strategies are actually common methods of increasing the efficiency of aminopyridines in palladium cross coupling reactions. Caron et al. demonstrated that the reaction of 3-amino-2-chloropyridine with phenylboronic acid in the presence of palladium tetrakis(triphenylphosphine) and sodium carbonate yields no sign of the desired product.[18] However, protection of the amine with an acyl moiety and

then reaction under the same conditions proceeded in 86% yield of the desired biaryl, nitrogen containing product (Figure 89). The overall yield for the three steps, however, is only 48%. They demonstrated the protection of the same substrate with benzaldehyde to form the corresponding imine. Subsequent coupling with phenyl boronic acid under the same conditions as described above formed 90% of the desired product, after deprotection, which is a significantly higher yield than the acetyl protection. However, utilizing protection/deprotection strategies still increases the number of steps towards the desired product, increases the waste produced and, as demonstrated for the acetyl protection route, can result in lower overall yields of the product.

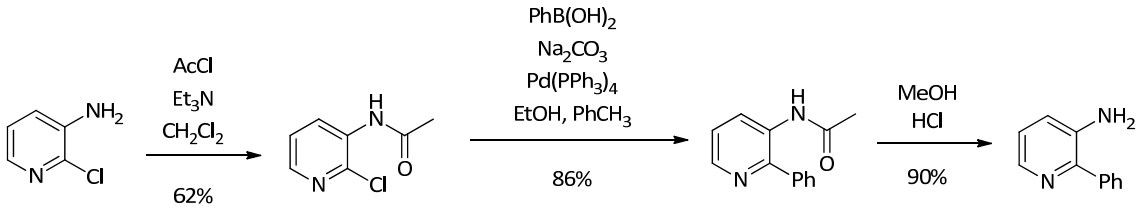

Figure 89 - Acetyl protection of 3-amino-2-chlorpyridine to promote reaction in Suzuki coupling.

Caron et al. also developed an *in situ* method for the protection route utilizing the benzylimine which increased the overall yield to 99% of the 3-amino-2-phenylpyridine (Figure 90). However, the final deprotection of the acetamide protected product was achieved through reflux with concentrated hydrochloric acid (HCl) which could be detrimental to other functional groups. Caron was able to utilize more dilute HCl solutions to deprotect the imine protected product, but even dilute acid can be detrimental to certain functional groups.[18]

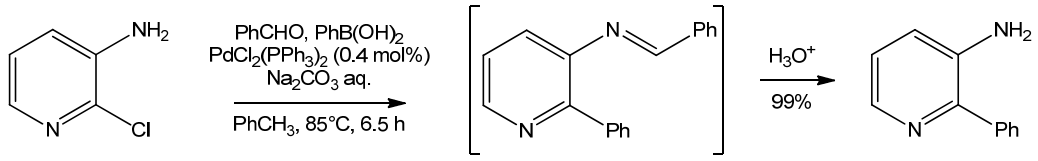

Figure 90 – *In situ* protection/deprotection strategy employed by Caron et al.

Another alternative to increase the reactivity of these amines is the use of designer ligands. The Buchwald group developed a series of novel, designer ligands to promote the couplings of chloro-containing substrates (Figure 91). These designer ligands utilize di-alkyl groups on the phosphorus to increase electron density on the phosphorus increasing the rate of oxidative addition while the size of the alkyl groups can increase rate of reductive elimination. Additionally, the biaryl attribute of these ligands contributes to the ligand's increased size and provides stabilizing Pd-aryl interactions to slow oxidative degradation of the catalyst, as well as promoting reductive elimination.

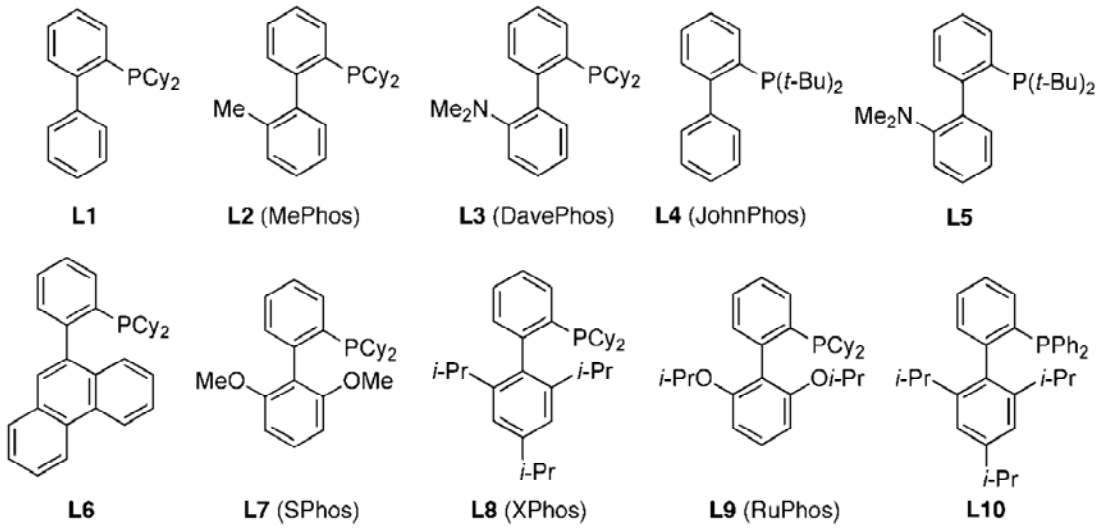

Figure 91 - Dialkylbiaryl ligands developed by Buchwald to promote reactions of chlorinated substrates.

The bulky ligands have also been shown to prevent coordination of amines to the palladium center.[3, 22] SPhos (L7, Figure 91), specifically, was shown to activate the cross-coupling of a variety of aminochloropyridines with phenyl boronic acids to provide the products in high yields (Figure 92). As shown above (Figure 88) Itoh utilized the bidentate ligand D-t-BPF (Figure 93) to successfully couple aminochloroypridines and pyrimidines with phenylboronic acids in high yields, as bidentate ligands had been shown to prevent formation of the bispyridine palladium complexes.[21] Though SPhos and other of Buchwald's designer ligands are now commercially available through Sigma-Aldrich and other sources, the additional cost can be prohibitive for certain applications.[23] Employing a cheaper catalyst system with no added ligand, such as $Pd(TPP)_2Cl_2$ would be desirable from an industrial and economic standpoint.[24]

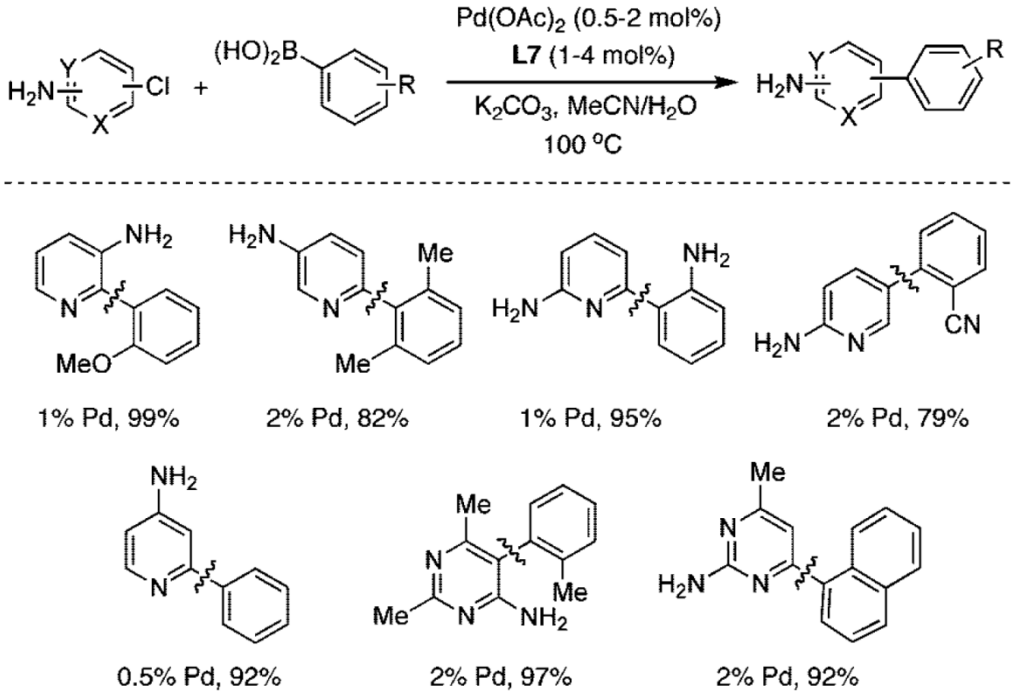

Figure 92 - Efficient coupling of aminochloropyridines utilizing designer ligand SPhos.

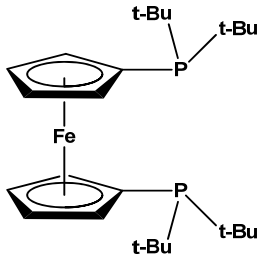

D-t-BPF

Figure 93 – Designer ligand: 1,10-bis(di-tert-butylphos phino)-ferrocene.

From an industrial point of view, it would be desirable to avoid both the added waste of additional protection/deprotection steps and the added cost of designer ligands. Direct or *in situ* strategies utilizing readily available and less expensive triphenylphosphine-based ligands would be preferred. As demonstrated in Chapter 3, CO_2 reacts with primary and secondary amines under certain conditions to form ammonium-carbamate species. Originally, these observations formed the basis for what was to be an *in situ* method of amine protection for the Suzuki coupling process. It was also recognized, however, that the application of CO_2 to protect basic nitrogen centers in the Suzuki reaction may be too simplistic. For those systems containing water this is especially relevant. The formation of ammonium bicarbonate species will supersede the formation of ammonium carbamate species. CO_2 is also known to react with water to form carbonic acid, which can then react with base to produce new phosphate and bicarbonate species (Figure 94). This change in aqueous phase composition can also result in a change in the effective pH at which reaction is occurring. Additionally, the application of CO_2 pressure is well known to affect the phase behavior of the solvent system and the accompanying rates of the individual steps in the reaction sequence.

Finally, the amount of water present in the solvent system will also affect the efficiency of the overall reaction by way of phase behavior and mass transfer. The complexity of the system requires careful consideration of all factors in order to determine the effect of CO_2 pressure on the Suzuki coupling of amine-containing substrates.

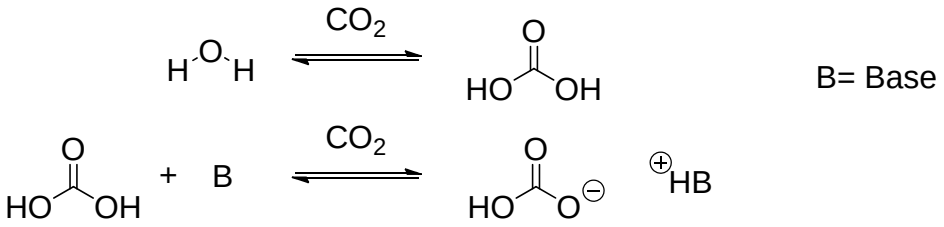

Figure 94 - Reaction of CO_2 with water and base to form new aqueous phase composition.

Herein, I describe the effect of CO_2 pressure, pH, and volume percent of water on the Pd-triphenylphosphine catalyzed Suzuki coupling of 4-amino-2-halopyridines and 2-halopyridines with phenylboronic acid employing potassium phosphate in acetonitrile-water at 70°C. The yields of the reactions under CO_2 and nitrogen (N_2) are compared, along with the relevant rate profiles for each reaction. Additionally, the yields of the coupled products as a function of pH are reported and discussed.

4.2 Results and Discussion

4.2.1 The Effect of CO_2 and Volume Percent of Water

The substrates, 4-amino-2-halopyridines and 2-halopyridines, were coupled with phenylboronic acid under the general conditions outlined in Figure 95. Reactions were conducted in a 300 mL Parr pressure reactor equipped with mechanical stirrer and temperature control under both CO_2 and N_2. The 4-amino-2-halopyridine substrates are solids at room temperature, while the 2-halopyridines are liquid. This called for slightly different protocols wherein the substrates were added at different points. The procedures

are briefly described in this section. Detailed protocols and analytical methods are located in the Experimental section.

In the typical reaction the palladium catalyst (0.08 mmol), phenylboronic acid (20.8 mmol) and potassium phosphate (48 mmol) were loaded into the Parr reactor. For the reactions with 4-amino-2-halopyridines, the substrates (16 mmol) were added at this point. The Parr reactor was then sealed and purged with CO_2 or N_2 for 15 minutes by flowing the appropriate gas through the reactor. For the reactions with 2-halopyridines, the substrates (16 mmol) were added via air tight syringe directly after purging. For both substrates, degassed acetonitrile (ACN) and water were then added via air tight syringe. Two solvent compositions were investigated: 75/25 v/v% ACN/H_2O (total volume: 40 mL) and 60/40 v/v% ACN/H_2O (total volume: 50 mL). For the reactions conducted under CO_2 pressure the reaction was pressurized to a pressure lower than the desired final pressure. In both cases the reactor was then heated to 70°C with stirring. Additional CO_2 pressure was added as needed to reach the final, target pressure for the reaction. The reactions proceeded for 24 hours unless otherwise stated. After cooling to room temperature and depressurization, methanol (~200 mL) was added to precipitate any inorganic salts. The yields were then determined via GC-FID. The reaction mixtures were also analyzed by ^1H NMR, and the yields obtained through GC-FID were supported by qualitative comparison to the yields obtained from product and starting material areas. Each reaction was repeated at least once so that all data points are the average of at least 2 trials.

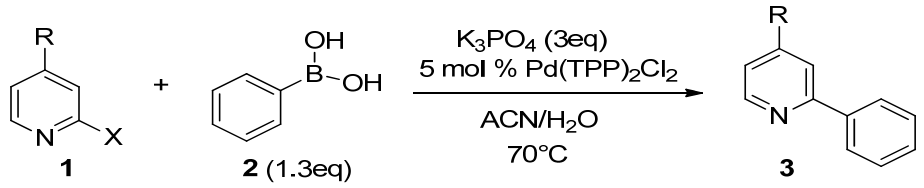

Figure 95 - Suzuki coupling scheme.

Table 29 summarizes the results for the Suzuki coupling of 4-amino-2-halopyridines and 2-halopyridines in a solvent system composed of 25/75 v/v% water and acetonitrile. The effects of various pressures of CO_2 were explored in comparison to an inert atmosphere (1 atm N_2). Both bromo- and chloro- 4-amino-2-halopyridine substrates couple poorly under nitrogen, yielding only 17% (Entry 1) and 21% (Entry 5) of the coupled product respectively. In contrast, 2-bromopyridine and 2-chloropyridine couple in high yields under nitrogen: 87% (Entry 7) and 100% (Entry 9) respectively. The addition of 30.6 atm CO_2 resulted in substantial increases in yield (30-50% increase) for the 4-amino-2-halopyridine substrates; 55% yield of the coupled product was observed for 4-amino-2-bromopyridine (Entry 3), and 71% yield for 4-amino-2-chlorpyridine (Entry 6). Varying the pressure of CO_2 on the Suzuki coupling reactions of 4-amino-2-bromopyridne from 6.8 to 44.2 atm resulted in a small increase in yield (Entries 2-4). Surprisingly, however, the application of CO_2 to the Suzuki coupling of 2-chloro- and 2-bromopyridines resulted in a significant decrease in yield. 2-Bromopyridine yielded only 7% of the coupled product under 30.6 atm of CO_2 (Entry 8); 2-chloropyridine yielded only 29% of the coupled product under the same conditions (Entry 10). It is important to note that the reactions under N_2 were conducted in 100 mL 3-neck Morton flasks. However, control reactions with 4-amino-2-bromopyridine under 1 atm nitrogen in the Parr and 100 mL 3-neck Morton flask yielded 39% and 35% of the coupled product respectively, confirming that the apparatus and reaction vessels had no effect on the reaction outcome.

Table 29 – Reactions run for 24 hours with 4-amino-2-halopyridines and 2-halopyiridines with 25% v/v of H_2O.

Entry	X=	R=	Atmosphere	Pressure (atm)	Yield (%)[a]
1[b]	Br	NH_2	N_2	1	17±4
2	Br	NH_2	CO_2	6.8	50±4
3	Br	NH_2	CO_2	30.6	55±6
4	Br	NH_2	CO_2	44.2	57±2
5[b]	Cl	NH_2	N_2	1	21±2
6	Cl	NH_2	CO_2	30.6	71±3
7[b]	Br	H	N_2	1	87±3
8	Br	H	CO_2	30.6	7±0.3
9	Cl	H	N_2	1	100±1
10	Cl	H	CO_2	30.6	29

(a). Yield calculated from GC-FID calibration curve.
(b). Reaction was run in a 100 mL 3-neck Morton flask.

As illustrated in Figure 96 the application of CO_2 has a significant effect on the phase behavior and pH of the reaction system. Under nitrogen, the reaction system is comprised of two liquid phases comprise: an organic phase and an aqueous phase. The pH of the system under nitrogen is around 13. Addition of CO_2 pressure, however, resulted in the following. 1) The aqueous phase reduced in volume. 2) An insoluble solid formed. Analysis of the solid phase showed that it was composed of potassium carbonate, bicarbonate and phosphate. And 3) the pH decreased to ~8. It is likely that CO_2 is reacting with the water layer to produce carbonic acid (Figure 97). This can in turn react with the phosphate base to produce a combination of phosphate and carbonate bases. The formation of a solid and reduction of the aqueous layer could be depriving the system of the base and water necessary to promote reaction. The effect of increased water was then investigated, to determine if solid formation and volume retention of the aqueous phase could be achieved, which could decrease mass transfer constraints and result in increased yields.

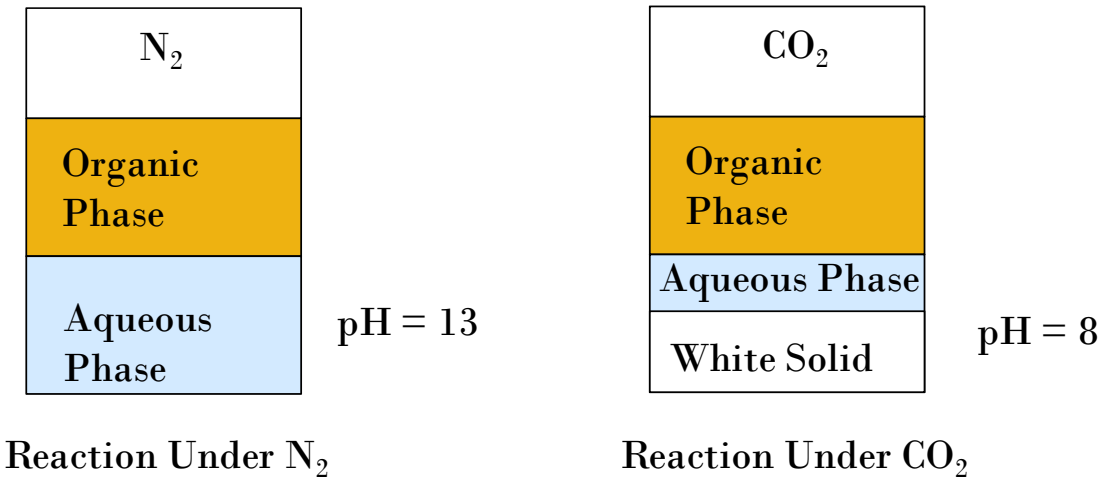

Figure 96 - Phase behavior of the Suzuki coupling system under nitrogen and carbon dioxide.

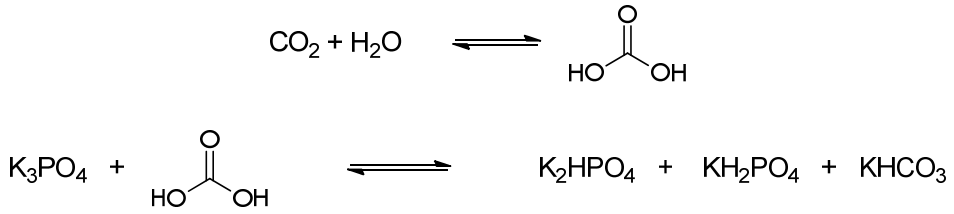

Figure 97 - Reaction of CO_2 with water and bases to form new inorganic phase composition.

The ratio of water to acetonitrile was therefore increased to 40/60 v/v%, while maintaining the original amounts of reactants (Table 30). Under nitrogen (23%, Entry 1) no significant change in yield was observed compared to the results with 25% water (17%). Physically, also, the system remained the same as observed with 25% water. The application of 30.6 atm of CO_2, however, did result in significant changes. No significant decrease was observed in the volume of the aqueous layer. Also, no significant formation of solid was observed. The yield, however, increased significantly to 99% (Entry 4), an increase of nearly double. Thus, additional water was necessary to prevent formation of the solid and promote the reaction under CO_2 pressure.

Calibration curves were utilized to determine the yields of all reactions. However, a control experiment was run in which 4-amino-2-bromopyridines was coupled with phenylboronic acid under 30.6 atm CO_2 pressure and 40% water. GC-FID analysis observed 99% of the coupled product. Isolation by column chromatography yielded 94% of the coupled product (details in Experimental section) providing confirmation for the method of analysis.

Ideally, in order to minimize safety risks and changes to the physical reaction system for an industrial company, the lowest pressures possible while maintaining high yields should be utilized. Application of 6.8 atm of CO_2 resulted in 91% yield of the coupled product for 4-amino-2-bromopyridine (Entry 3), similar to 30.6 atm CO_2. In fact, pressures as low as 2 atm CO_2 still achieved high yields of 83% (Entry 2).

Similar results were obtained for the 4-amino-2-chloropyridine substrate (Table 30). Though under nitrogen only 30% of the coupled product was obtained (Entry 5), the addition of only 6.8 atm of CO_2 increased the yield dramatically to 98% (Entry 7). This is also a significant increase from the corresponding system with 25% water and 30.6 atm CO_2 which yielded 71% of the coupled product. Again, even with pressures as low as 2 atm CO_2 we were able to obtain high yields (93%, Entry 6).

The 2-halopyridine substrates again demonstrated the opposite trend (Table 30). Under nitrogen, similar results were obtained for the system with 40% water as compared to the system with 25% water. The coupled product was produced in 92% yield for 2-bromopyridine (Entry 8) and 91% yield for 2-chloropyridine (Entry 10). The addition of 30.6 atm CO_2, however, yielded significantly decreased amounts of the coupled products: 15% for 2-bromopyridine (Entry 9) and 32% for 2-chloropyridine (Entry 11). Compared to the system under 25% water, however, these yields were slightly increased.

Table 30 - – Reactions run for 24 hours with 4-amino-2-halopyridines and 2-halopyiridines with 40% v/v of H_2O.

Entry	X=	R=	Atmosphere	Pressure (atm.)	Yield (%)[a]
1[b]	Br	NH_2	N_2	1	23±4
2	Br	NH_2	CO_2	2.0	83±0
3	Br	NH_2	CO_2	6.8	91±8
4	Br	NH_2	CO_2	30.6	99±2
5[b]	Cl	NH_2	N_2	1	30±2
6	Cl	NH_2	CO_2	2.0	93±3
7	Cl	NH_2	CO_2	6.8	98±3
8[b]	Br	H	N_2	1	92±5
9	Br	H	CO_2	30.6	15±0.3
10[b]	Cl	H	N_2	1	91±1
11	Cl	H	CO_2	30.6	32±6

(a). Yield calculated from GC-FID calibration curve.
(b). Reaction was run in a 100 mL 3-neck Morton flask.

It is important to note, at this point, that a protected version of 4-amino-2-bromopyridine was synthesized and reacted at pH 8 and pH 13 for comparison to the unprotected version. 4-(N-acyl)amino-2-bromopyridine was synthesized from 4-amino-2-bromopyridine in 50% yield following a literature procedure (Figure 98).[18]

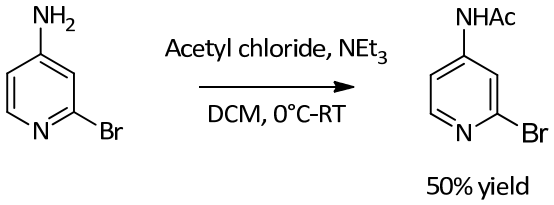

Figure 98 - Synthesis of 4-(N-acyl)amino-2-bromopyridine.

The protected amine was then coupled with phenylboronic acid in 60/40 v/v% ACN/H_2O with $Pd(TPP)_2Cl_2$ and base at 70°C (Figure 99). Buffers (K_3PO_4, K_2HPO_4) were utilized to obtain specific pH under nitrogen atmosphere. The yields are outlined in Table 31. Surprisingly, the protected amine couples in only 44% yield under a pH of

approximately 13. Decreasing the pH to approximately 8 resulted in a slight decrease in yield of 10%. The slight decrease in yield under lower pH is similar to the effect seen with the 2-halopyridines, but the overall poor reactivity of the protected amine in this system was unexpected.

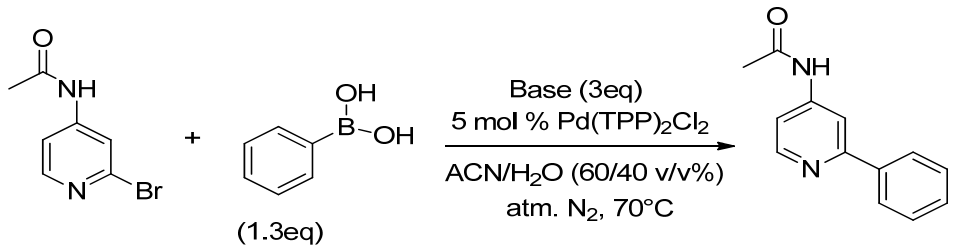

Figure 99 - Suzuki coupling of protected amine wtih phenylboronic acid.

Table 31 - Suzuki coupling of 4-(N-acyl)amino-2-bromopyridine with phenylboronic acid under pH = 8 and 12.

Base	pH	Yield (%)
K_3PO_4	12.07±0.14	44±6
K_2HPO_4	8.27±0.14	34±3

Utilizing increased water (40%), therefore, promoted the reaction of 4-amino-2-halopyridines under CO_2 pressure and prevented the formation of solids and reduction of the aqueous layer. Also, pressures as low as 2 atm CO_2 could be utilized to obtain high yields with 4-amino-2-halopyridines. However, the 2-halopyridine substrates exhibited the opposite trend: low yields under CO_2 pressure and nearly quantitative yields under nitrogen. Up to this point only the yields after 24 hours have been discussed. Observation of the reactions as a function of time and the effect of various conditions upon the kinetics can potentially assist in elucidating an explanation for the substrate differences.

Figure 100 illustrates the product yield vs. time for 4-amino-2-bromopyridine for both 25/75 and 40/60 v/v% water/CAN solvent systems, and under both 1 atm N_2 and

30.6 atm CO_2. In each case, the reactions are initially very fast. However, for the reactions under N_2 the reaction only proceeds minimally after the first hour. In fact, there is little difference between the results for 25% and 40% water systems under nitrogen. Both reach 15-25% yields within an hour and only reach yields of 20-30% after 24 hours. The reaction under 25% water and 30.6 atm CO_2 reaches a similar yield after the first hour (26%) as the nitrogen reactions, but proceeds at a higher rate thereafter producing 65% of the coupled product after 24 hours. The effect of added water is also clearly illustrated here, as the reaction with 40% water and 30.6 atm CO_2 proceeds at an even higher rate, reaching an initial yield of 57% after 1 hour and 100% after 24 hours.

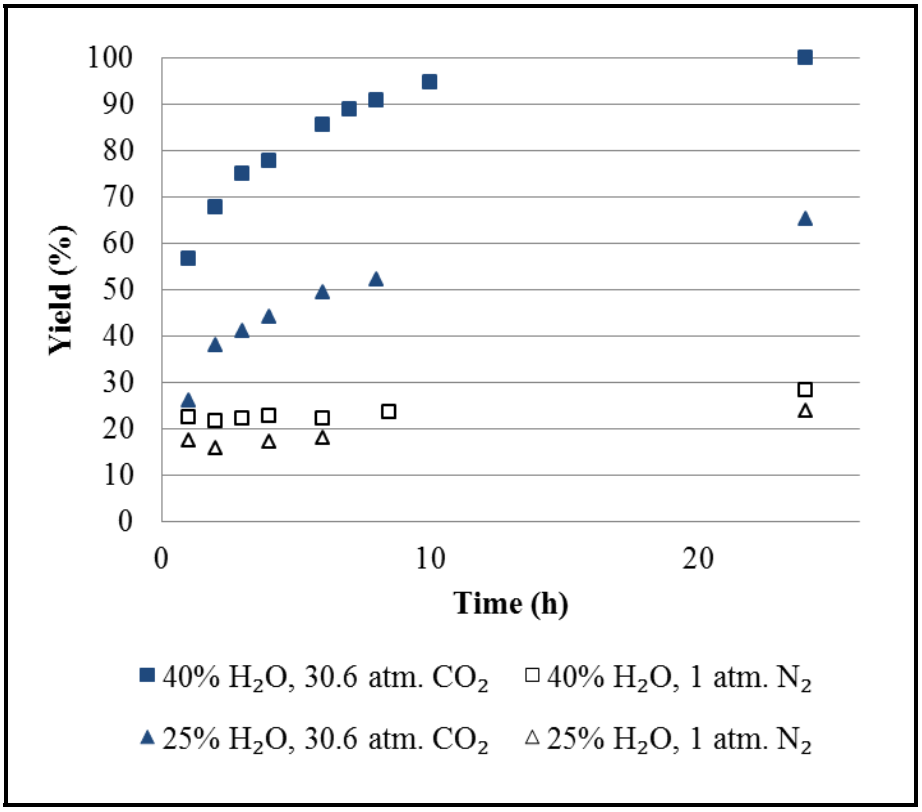

Figure 100 - 4-Amino-2-bromopyridine reaction progress as a function of time. % H_2O is measured as %v/v. Time = 0 corresponds to the reaction system reaching temperature.

Direct comparison of 4-amino-2-chloropyridine and 4-amino-2-bromopyridine susbtrates is displayed in Figure 101. Under nitrogen, the chloro- substrate approaches a 30% yield asymptotically over 24 hours. In contrast the bromo- substrate reaches 20% within the first hour, a significantly higher initial rate than the chloro- substrate, but then slows significantly only reaching around 30% after another 23 hours. More interestingly, under a low pressure of 2 atm CO_2 both chloro- and bromo- substrates display highly increased and similar rates. In fact, both substrates yield quantitative amounts of coupled product in around 24 hours. Under these conditions, therefore, the system is halogen independent.

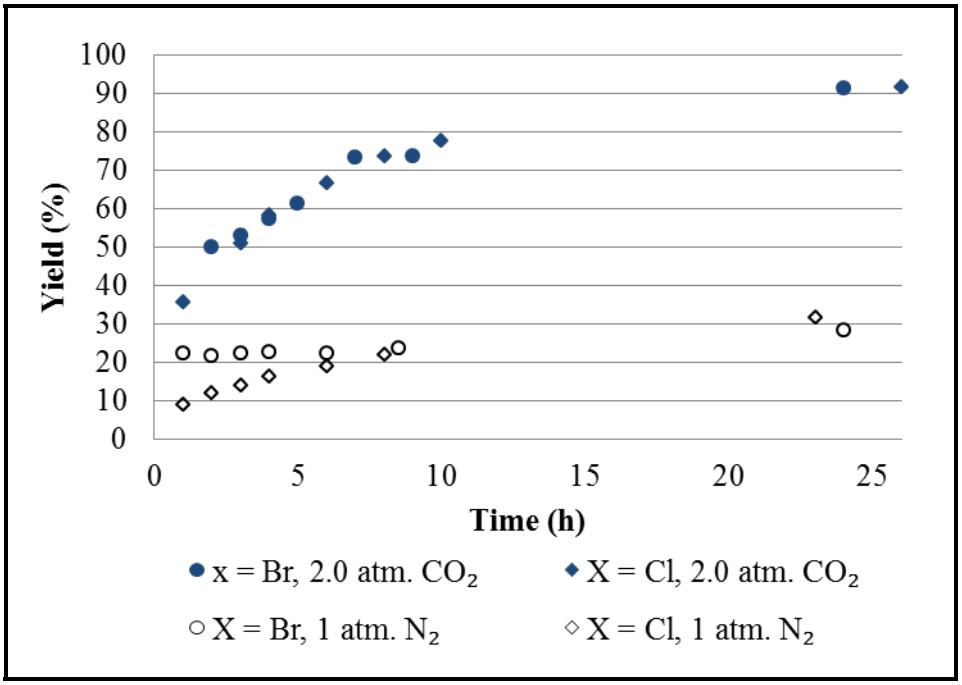

Figure 101 - Reaction progress as a function of time for 4-amino-2-halopyridines. Reactions run with 40% v/v water. Time = 0 corresponds to the reaction system reaching temperature.

As I mentioned previously, the reaction conditions necessary for optimum rates and yields are often substrate dependent. This is clearly illustrated in the differences we've observed between 4-amino-2-halopyridines and 2-halopyridines. The effects of

added water and CO_2 pressure on the rates of reaction for 2-halopyridines are displayed in Figure 102 and Figure 103. The rate of the reaction with 40% water is significantly increased from the rate with 25% water (Figure 102). For the system with 25% water, 31% of the coupled product is observed after 0.5 hours. In contrast, almost 50% of the coupled product is produced after 0.5 hours for the 40% water system. Also, the system with 40% water reaches completion in 13 hours, while the system under 25% water only displays 87% of the coupled product after 24 hours.

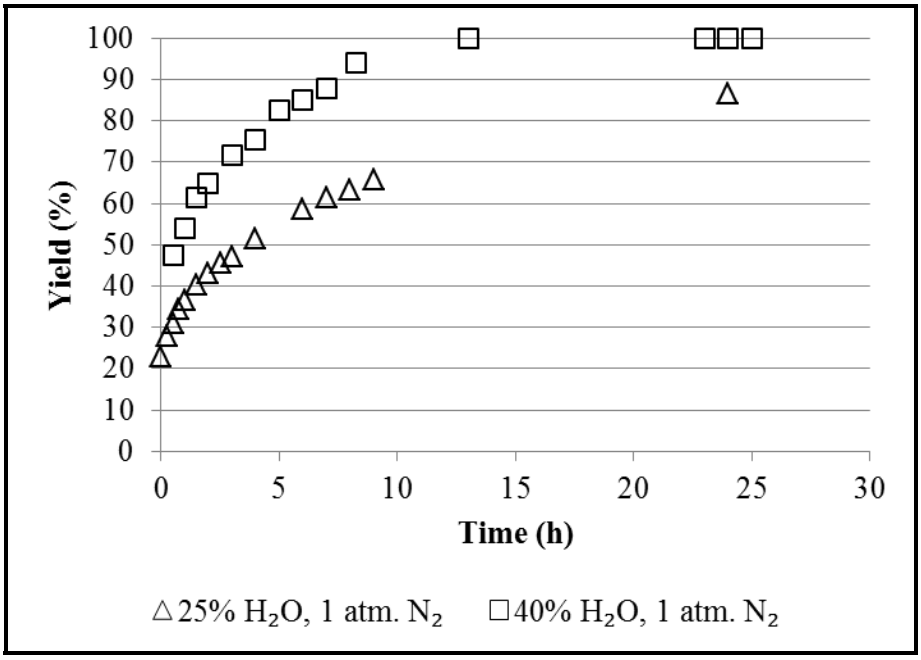

Figure 102 - 2-Bromopyridine reaction progress as a function of time under 1 atm. N_2. % H_2O is measured as %v/v. Time = 0 corresponds to the reaction system reaching temperature.

The effect of CO_2 pressure on the rates of reaction for 2-halopyridines is illustrated in Figure 103 for 2-chloropyridine. The reactions under nitrogen display a much higher initial rate, yielding 81% of the coupled product after 1 hour. In fact, the reaction reached completion in 2 hours. However, under 30.6 atm CO_2 the rate is

significantly decreased; only 6% product was observed after 1 hour and it only increased marginally to 32% after 24 hours.

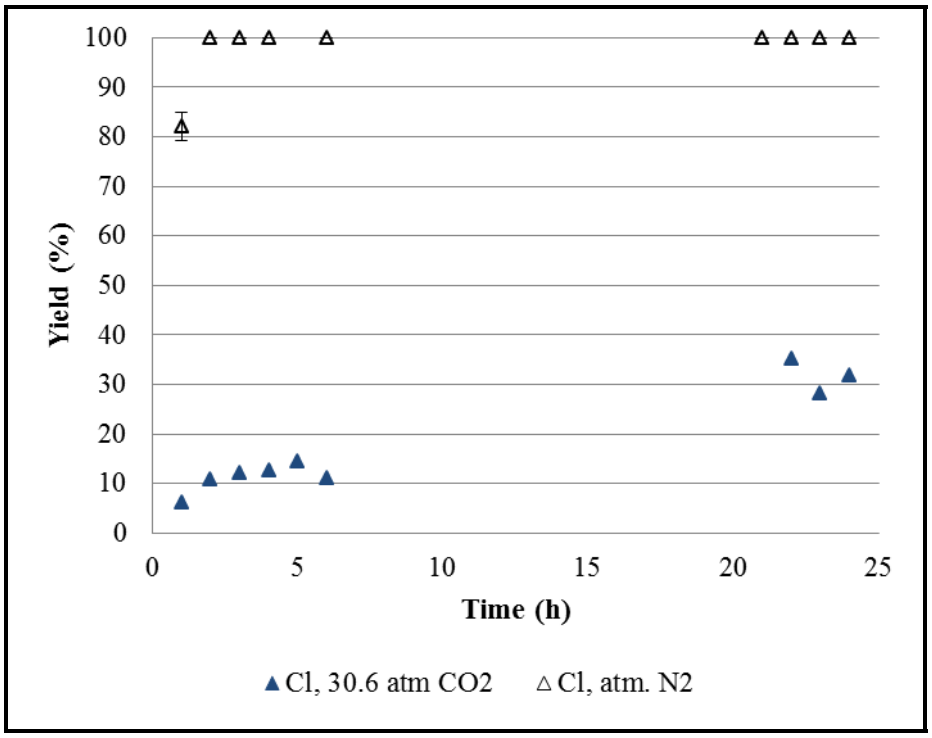

Figure 103 - Reaction progress as a function of time for 2-chloropyridines. Reactions run with 40% v/v water. Time = 0 corresponds to the reaction system reaching temperature.

4.2.2 Effect of pH Upon Yield of Coupled Products

Between the 4-amino-2-halopyridines and 2-halopyridines the only difference is the presence or absence of an amino moiety at the 4-position of the pyridine ring. However, each substrate performs very differently under the different conditions. The optimum conditions for each substrate differ mainly in pH. The 4-amino-2-halopyridine substrates couple well under a pH of approximately 8, produced by the reaction of CO_2 with water and the base. The 2-halopyridines couple best when CO_2 is not present and the pH of the system is approximately 12. Is pH the key to understanding the different

behavior of these substrates? We investigated the effect of pH upon yield for all four substrates by employing a variety of buffered systems (see Experimental for details) to control the pH during reaction. A clear trend was observed and is illustrated in Figure 104. The 4-amino-2-halopyridine substrates display increasing yields as pH decreases from ~12 to ~8 with the maximum yields observed at a pH of approximately 8. The 2-halopyridine substrates display the opposite trend, with yields increasing as pH increases from ~8 to ~12 with the maximum yields observed at a pH of approximately 12. Interestingly, a pH of 14 (not shown) resulted in a lower yield for 2-bromopyridine (69%). Unsurprisingly, pH's below 7 resulted in poor yields for both substrates (not shown). We also noted that potassium phosphate dibasic, under nitrogen, provides a similar pH (~8) as potassium phosphate tribasic under CO_2. The yield of the system was also approximately 100% which confirms that the main effect of CO_2 is to adjust the pH to the optimum level.

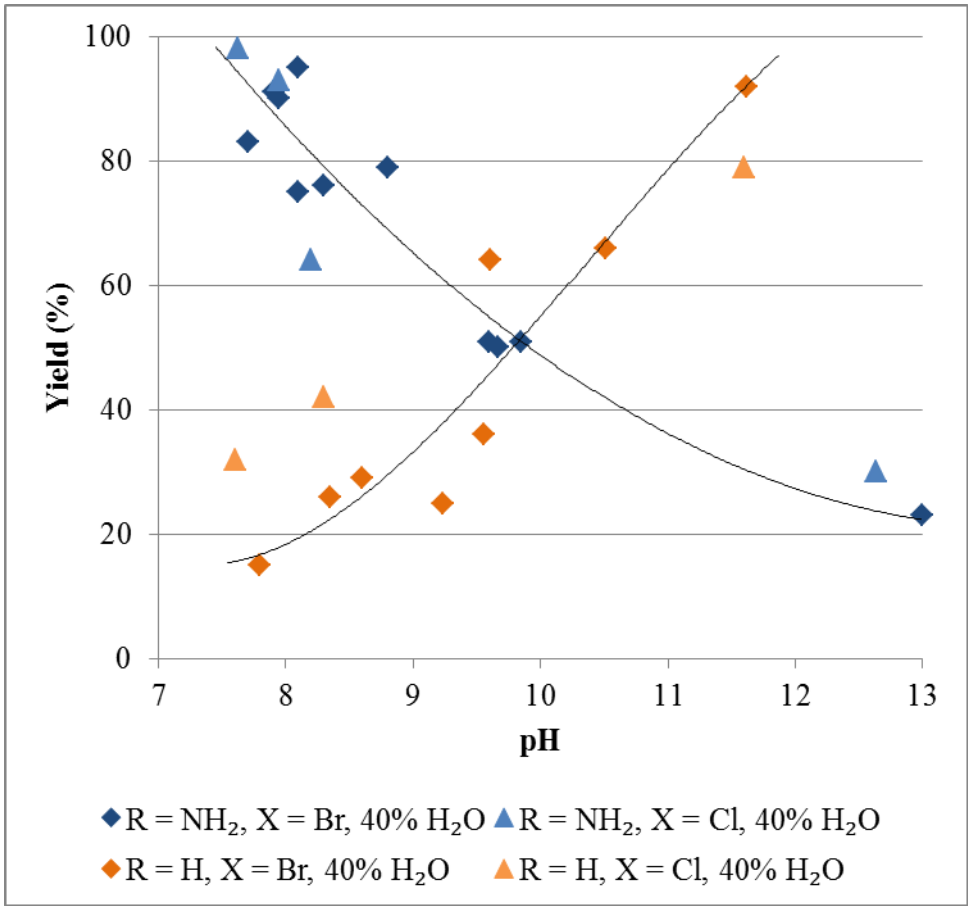

Figure 104 - Yield as a function of pH for 4-amino-2-halopyridines and 2-halopyridines.

The effect of pH on the system suggests that the acid-base properties of each substrate are one of the dominant factors that govern the efficiency of the reaction. In fact, the pK_a in water at room temperature for 4-amino-2-chloropyridine (4.8) differs greatly from that of 2-chloropyridine (0.7).[25-26] The pK_a values suggest that all four substrates are essentially in their unprotonated states. However, at a pH of 8, approximately 0.1% of the 4-amino-2-halopyridine is likely present in the protonated form. As discussed before, 4-amino-2-halopyridines perform poorly in Suzuki couplings under simple conditions without protection/deprotection strategies or designer ligands, an example of which was reported by Wagaw et al. (Figure 105) (conditions: $Pd(OAc)_2$, K_3PO_4, and bidentate ligand L in 1,4-dioxane at reflux; yield: 32% after 48 hours). One possible explanation for their poor performance is the effect of donation by the amine

into the pyridine ring, which could result in higher electron density on the carbon ipso to the halogen, which in turn could be detrimental to oxidative addition. The possibility then exists that the formation of protonated 4-amino-2-halopyridine can decrease electron density in the ring which, in turn, can increase the rate of oxidative addition for that substrate. Thus, at pH = 8 the formation of a small, steady state amount of the active form of the substrate promotes the reaction. If that were the case, then the rate of Suzuki coupling for the 4-amino-2-chloropyridine substrate would be much slower than the corresponding rate for the 2-chloropyridine. The data presented in Figure 101 and Figure 103 support this conclusion, as 2-chloropyridine reached quantitative yields in approximately 2 hours while 4-amino-2-chloropyridine requires 24 hours to reach completion.

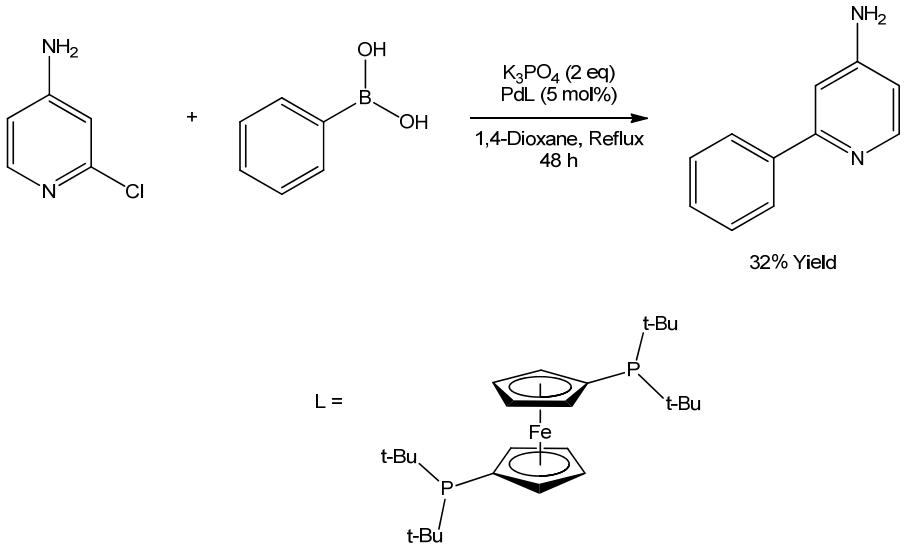

Figure 105 - Example low yielding Suzuki coupling of 4-amino-2-chloropyridine.

Additionally, the pH of the aqueous phase can affect the partitioning of reagents (substrate, product, catalyst) between the organic and aqueous phases. We investigated the partitioning of 4-amino-2-bromopyridine as a function of pH by buffering test systems with various phosphate buffers (K_3PO_4, K_2HPO_4, $K_4P_2O_7$) to obtain the desired pH. Our reaction systems are liquid-liquid biphasic and the ionic strength of the buffers were adjusted to ensure a phase split between the aqueous and organic phases of our test systems. Greater than 99% of the substrate was found in the organic phase over a range of pH's (7-14). The substrate partitioning, therefore, appears to be independent of pH, and, as such, the correlation between yield and pH is independent of partitioning.

4.2.3 Effect of Electronic Effects Upon Reaction Rate

In addition to the data I have just discussed, I investigated the effect of substitution upon the rate of reaction for a variety of different substituents. I report herein the effect of substituents on reaction rate for various 2-bromopyridines substituted with different electron withdrawing and donating effects and correspondingly different acid dissociation constants (pKa). Specifically, I utilized substituted 2-halopyridines with nitro ($-NO_2$), methoxy (-OMe), methyl ($-CH_3$), and amine ($-NH_2$) substituents in the 5 position (para to the bromine and meta to the pyridine nitrogen) as well as in the 4-position (para to the pyridine nitrogen and meta to the bromine). Each was coupled with phenylboronic acid as outlined in the following reaction scheme (Figure 106). The pH for all reactions was approximately 12.

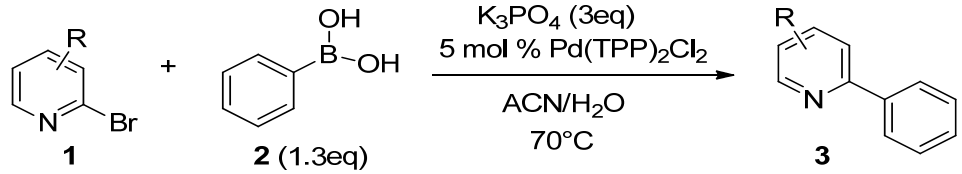

Figure 106 – Schematic for the coupling of substituted-2-bromopyridines with phenylboronic acid.

The general procedure was altered slightly from the previous examples. Two solutions - one containing catalyst, substrate, and acetonitrile, and a second one containing phenylboronic acid, base, and water - were heated to 70°C and then combined. In the typical reaction the palladium catalyst (0.08 mmol) was placed in a 3-neck, 100 mL Morton flask (Flask A). Solid substrates (16 mmol) were combined with the catalyst in Flask A. In a separate flask (Flask B) were loaded phenylboronic acid (20.8 mmol) and potassium phosphate (48 mmol). The flasks were then evacuated and backfilled with Argon. Liquid substrates (16 mmol) were added to Flask A after backfilling, via air tight syringe. Degassed acetonitrile (30 mL) was then added to Flask A and degassed water (20 mL) was added to Flask B. The flasks were then heated to 70°C with stirring. At 70°C Flask A displayed a solid-liquid biphasic system while Flask B displayed one homogenous liquid phase. The contents of Flask B were then transferred to Flask A at temperature via an air tight syringe. This point was denoted as time = 0. Samples (0.2 mL) were taken from the organic phase at periodic intervals (0, 2, 4, 6, 8, 10, 20, 40, 60, 120, 180 minutes) and diluted with methanol (0.8 mL) for GC-FID analysis. A sample GC-FID from the coupling of 4-amino-2-bromopyridine with phenylboronic acid is included in the Experimental. GC-MS was utilized to confirm the identity of each peak. Starting material, product, biphenyl, triphenylphosphine, triphenylphosphine oxide and boronic acid trimer were present in the GC of each reaction mixture. Otherwise the GC chromatograms were clean. Yields were determined from the area of the product over the sum of the areas of product and starting material. Half-lives were determined as the point at which 50% of the substrate was consumed. Each reaction was run twice and the yields versus time were plotted as an average of the two trials. An example of these graphs is shown in Figure 113. The graphs for each susbtrate can be found in Appendix C.

It is important at this point to note the phase-behavior of the system. Most reactions were liquid-liquid biphasic. However, 4- and 5-methoxy-2-bromopyrdine produced light tan solids after approximately 2 hours. Identification of the solid was not attempted at this time, as both reactions were significantly advanced (> 80% yield) at this point and I was mostly concerned with the initial kinetics and half-lives. Also, 4- and 5-nitro-2-bromopyridines produced black solid, most likely palladium black, after approximately 5 minutes. The coupling of 4-nitro-2-bromopyridine was complete in approximately 10 minutes. 5-Nitro-2-bromopyridine was complete in 4 minutes. As such the formation of palladium black should not have affected the initial kinetics.

4.2.2.1 Effect of substitution in the 5-position of 2-bromopyridine.

The half-lives ($t_{½}$) of the coupling reactions for each 5-substituted-2-bromopyridine substrate, the corresponding electronic parameters (σ_{meta}, σ_{para}), and the acid dissociation constants (pK_a) are displayed in Table 32.[26] The half-lives of each reaction increased in the order of $NO_2 < NH_2 < MeO < Me < H$. Direct correlations between the half-lives and electronic parameters are not obvious. Plots of the half-lives versus each electronic parameter (Figure 107-Figure 109) were developed.

Table 32 - Reactions run for 24 hours with 5-substituted 2-halopyridines and 40% v/v of H_2O, atm. N_2. Reactions run in 3-neck, 100 mL Morton flask.

Entry	5-R	$t_{½}$ (min)	σ_{meta}	σ_{para}	pK_a[27]
1	NH_2	2	-0.16	-0.66	1.87
2	MeO	4.6	0.12	-0.27	-2.22
3	Me	5.3	-0.07	-0.17	1.08
4	NO_2	1	0.71	0.78	-3.12

5	H	50	0	0	0.71[26]

In each case – half-life versus para electronic effects (Figure 107), meta electronic effects (Figure 108), or acid dissociation constants (Figure 109) - the same trend is seen: a maximum is observed. This could imply that a different mechanism or rate determining step is involved in electron donating vs. electron withdrawing substrates, however this would be more clearly seen through a Hammett plot, by comparing the initial rates to the electronic parameters.

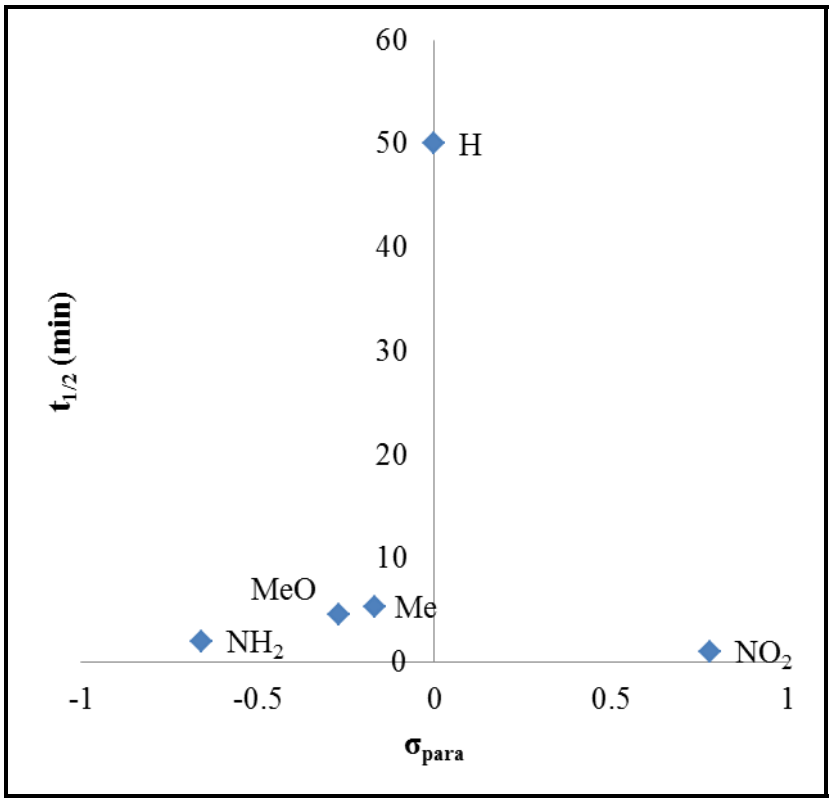

Figure 107 - Para effects versus half-lives for 5-substituted-2-bromopyridines.

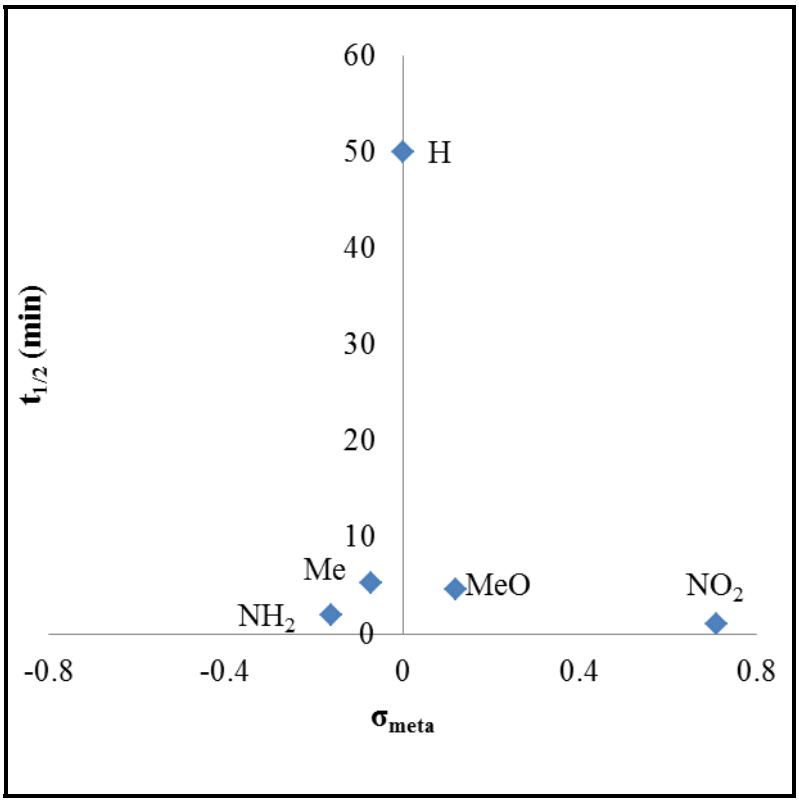

Figure 108 - Meta electronic effects versus half-lives for 5-substituted-2-bromopyridines.

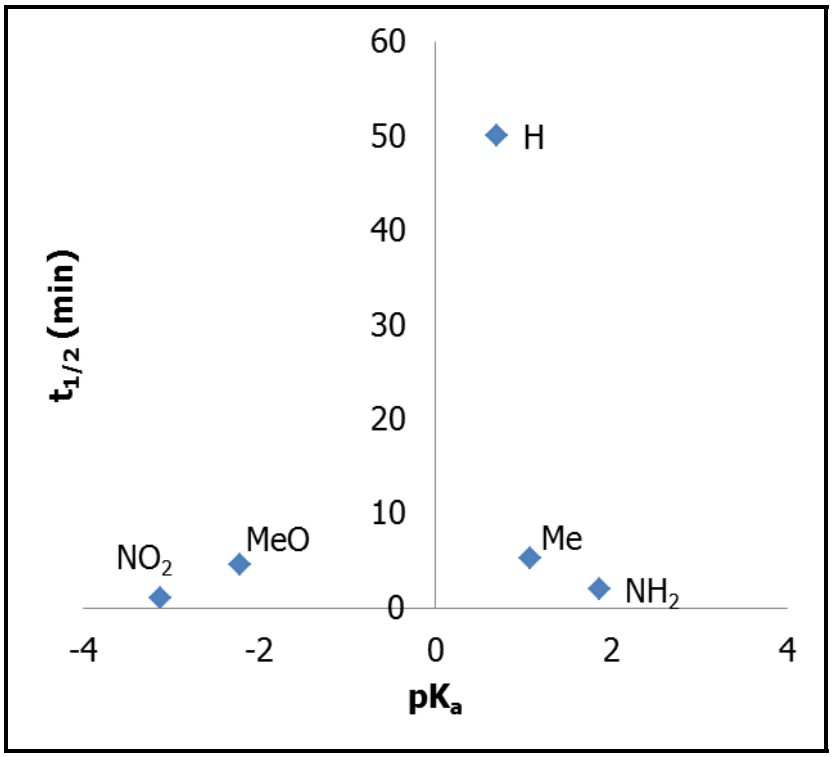

Figure 109 - Acid dissociation constants versus half-lives for 5-substituted-2-bromopyridines.

The Hammett equation, as it applies to kinetic phenomena, is a linear free energy relationship which can be used to relate rate constants to electronic effects for substituents according to

$$\log\left(\frac{k}{k_o}\right) = \sigma\rho$$

where k_o is the rate constant for the reaction of an unsubstituted compound, in our case 2-bromopyridine, and k is the rate constant for the corresponding 4- or 5-substituted-2-bromopyridine. A plot of $\log(k/k_o)$ versus σ, also known as a Hammett plot, can be used to infer information about the mechanism of a reaction. The electronic parameters (σ) are well known literature values that are pretty consistent over a variety of different aromatic systems.[28] These plots typically result in a straight line, from which the sign and magnitude of the slope (ρ) suggests whether: a negative charge is built up (or a postitive charge is lost) during the rate-determining step of the reaction (ρ>0); a positive charge is built up (or a negative charge is lost) during the rate-determining step (ρ<0); or no charge is built up or lost during the rate-determining step (ρ=0). This information can be utilized to help elucidate a mechanism for the reaction.

However, sometimes a non-linear plot is produced. It is also describes as not following a single Hammett plot. When a concave (upward) curve is observed it is correlated to a change in mechanism. Swain and Langsdorf observed upward curves for the substitution of benzyl chlorides with triethylamine in benzene at 100°C (Figure 110).[29] When a convex (downward) curve is observed it is correlated to substrates undergoing the same mechanism, but different rate determining steps. Hart and Sedor showcase an example of a downward curve produced from the cyclodehydration of 2-phenyltriarylcarbinols in 80% aqueous acetic acid containing 4% sulfuric acid at 25°C (Figure 111).[30] This information also assists in elucidation of the mechanisms involved.

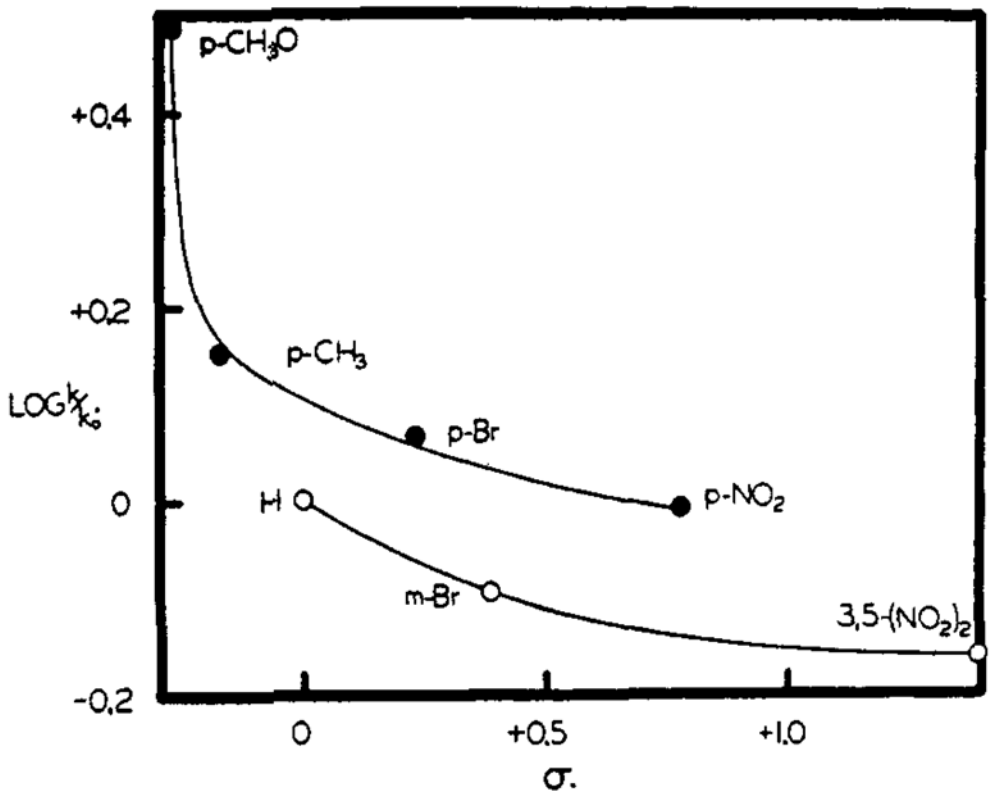

Figure 110 - Substitution of benzyl chlorides with triethylamine in benzene at 100°C

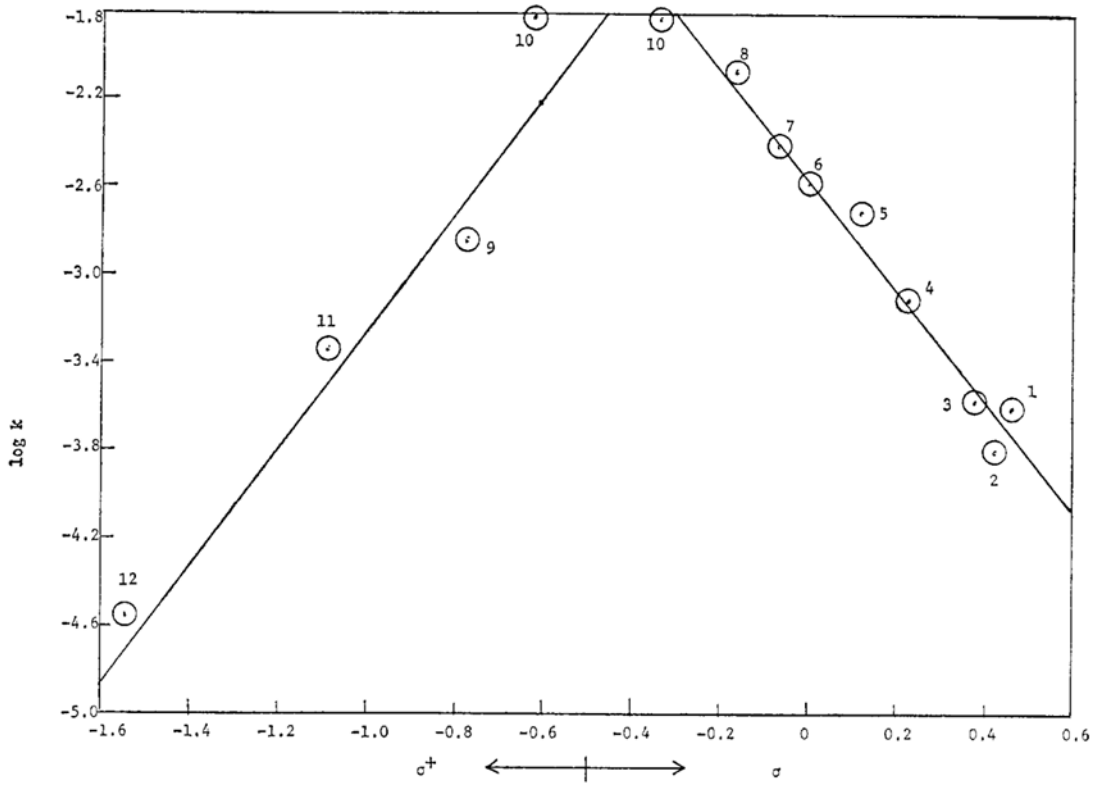

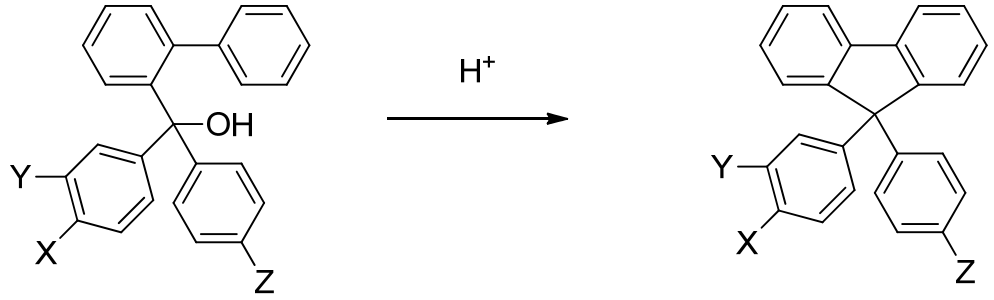

Compound	X	Y	Z
1	Cl	H	Cl
2	H	CF_3	H
3	H	Cl	H
4	Cl	H	H
5	H	OCH_3	H
6	H	H	H
7	H	CH_3	H
8	CH_3	H	H
9	OCH_3	H	H
10	CH_3	H	CH_3
11	CH_3	H	OCH_3
12	OCH_3	H	OCH_3

Figure 111 - Cyclodehydration of 2-phenyltriarylcarbinols in 80% aqueous acetic acid containing 4% sulfuric acid at 25°C.

The rates, and corresponding rate constants, of each reaction were approximated. Some assumptions were required. As is typical in catalytic kinetics (Michaelis-Menten kinetics, for example), the catalyst is assumed to remain constant to simplify the kinetic expression. The base is also assumed to be constant, another typical assumption.

The main substrates involved in the formation of the product through Suzuki coupling are the phenylboronic acid and arylhalide. However, the actual amount of phenylboronic acid in the reaction solution is 1.3 equivalents to 1 equivalent of arylhalide. The general reaction is a second order reaction, which can be described by the following equation where A and B are the substrates and P is the product.

$$A + B \rightarrow P$$

The rate of reaction is given by

$$\frac{d[A]}{dt} = -k[A][B]$$

where k is the rate constant. Integration of the rate expression gives

$$\frac{1}{[B]_o - [A]_o} \ln \frac{[B][A]_o}{[A][B]_o} = kt$$

where t is time, $[B]_o$ and $[A]_o$ are the initial concentrations of the substrates, and [B] and [A] are the concentrations at time t. As the initial concentrations of A and B approach equality, however, the first term of the equation approaches infinity.[28] In each reaction, biphenyl is rapidly formed, though the amount formed is never more than the excess phenylboronic acid added. However, it is possible that the initial concentration of phenylboronic acid actually involved in the coupling with the arylhalide is equal or nearly equal to the initial concentration of the arylhalide. If we assume $[B]_o = [A]_o$ then the rate expression can be simplified to

$$rate = k[A][B] \cong k_{pseudo}[A]^2$$

where k_{pseudo} is the approximated rate constant and the solution of the equation then becomes the following:

$$\frac{1}{[A]} = k_{pseudo}t + \frac{1}{[A]_o}$$

A plot of 1/[A] vs. t can therefore prepared from which the slope is equal to the pseudo rate constant ($k_{pseudo)}$.

For all substrates there appear to be at least two regions in the plots of yield versus time. An initial region of very fast reaction (0-2 minutes typically) and a second region of slower reactivity (2 minutes on). An example of this is displayed in Figure 113 for the Suzuki coupling of 4-methyl-2-bromopyridine with phenylboronic acid (Figure 112).

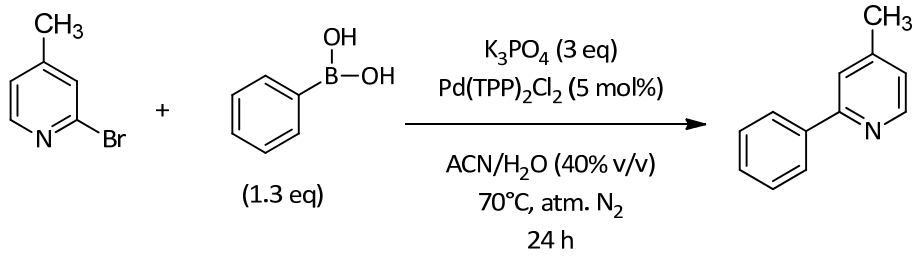

Figure 112 - Reaction scheme for the Suzuki coupling of 4-methyl-2-bromopyridine.

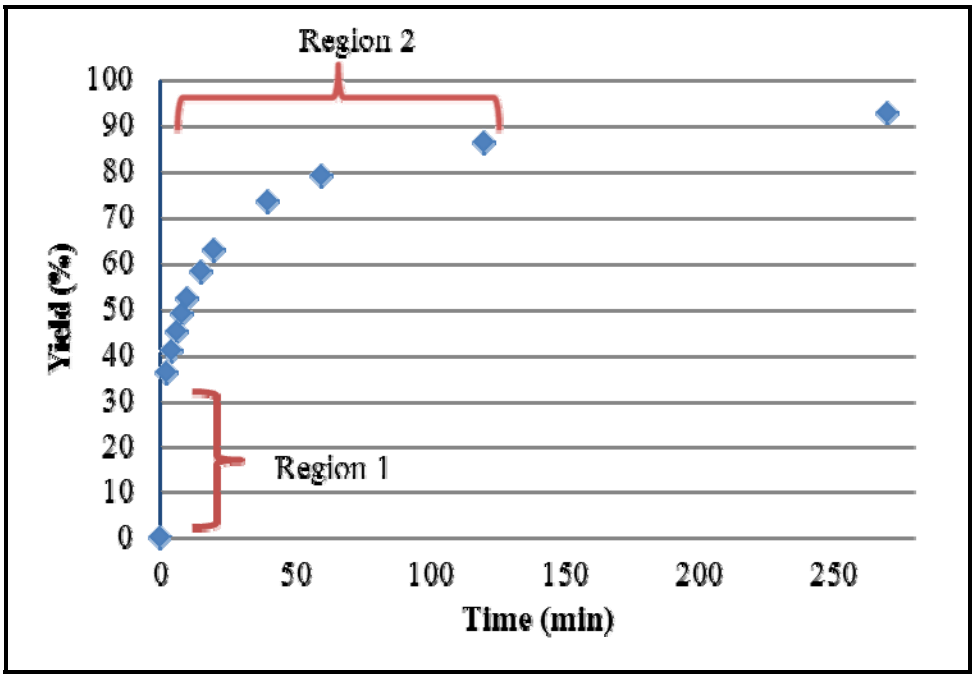

Figure 113 - Reaction progress as a function of time for 4-methyl-2-bromopyridine.

A plot of 1/[A] versus time for the substrate 4-methyl-2-bromopyridine is displayed in Figure 114. In this plot there are still two separate regions which are clearly discernible: a straight line denoted as Region 1, corresponding to the initial kinetic region; and another straight line, Region 2, which corresponds to the second kinetic region. These were plotted on separate graphs to obtain equations for each line (Figure 115 and Figure 116) and the data for each region was compared. Kinetically it is preferred to utilize initial rates, however there were only two points for these initial regions. As such, I compared the results for Regions 1, 2, and both regions together and found that the results are very similar, though the actual values might at first not appear to be. It is the overall trends that are the most interesting and will be discussed.

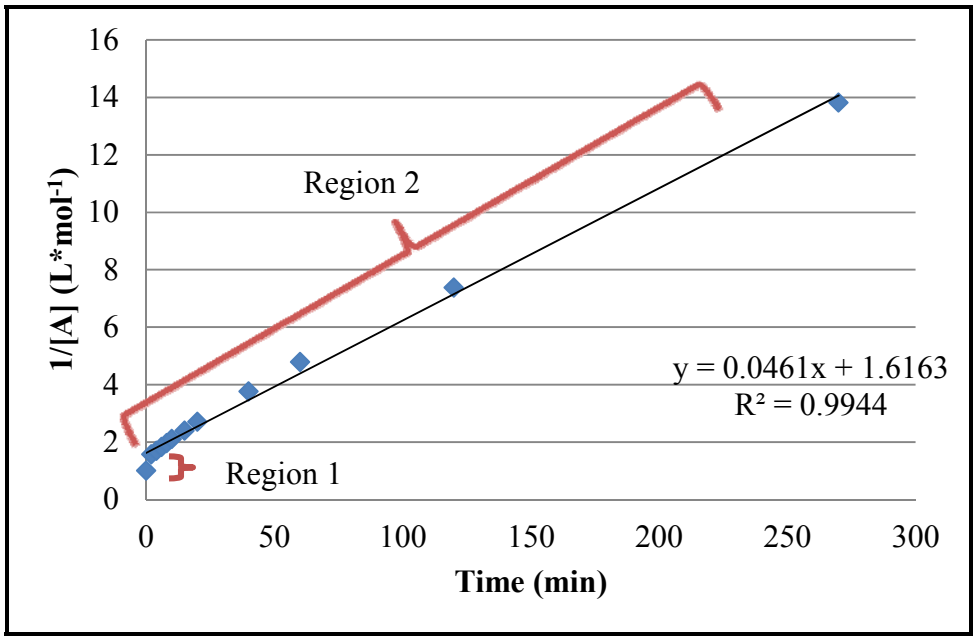

Figure 114 - Second order kinetic plot for 4-methyl-2-bromopyridine.

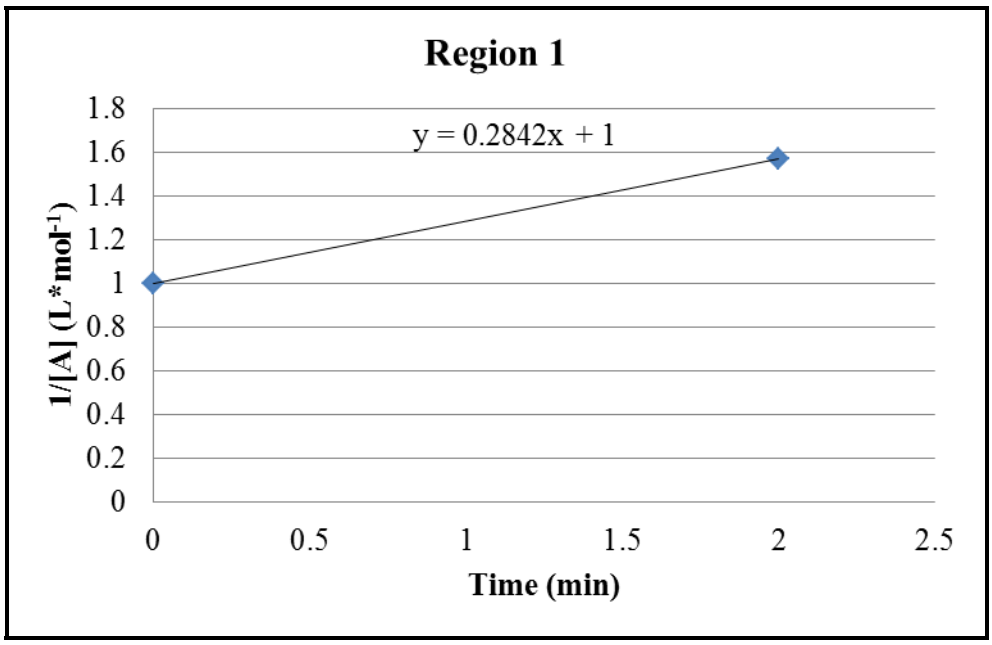

Figure 115 - Second order kinetic plot of initial region (Region 1) for 4-methyl-2-bromopyridine.

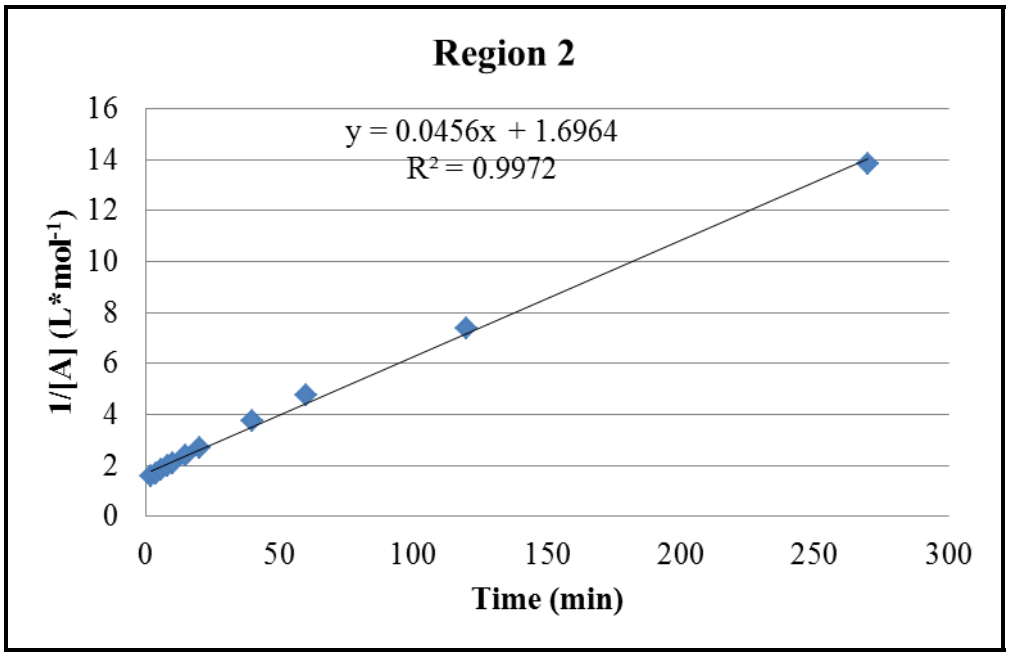

Figure 116 - Second order kinetic plot of later region (Region 2) for 4-methyl-2-bromopyridine.

The values obtained for k_{pseudo} for each region are displayed in Table 33 for the 5-substituted-2-bromopyridines. Unsurprisingly and immediately noticeable are that the values for Region 2 and Both Regions combined are similar. The values for Region 1 and Region 2 are not similar; however plots of k_{pseudo} versus σ_{para} for each region show the same general trend (Figure 117 and Figure 118). Both Region 1 and Region 2 show what is either a convex curve (an upward curve) or a linear plot with the data point for the nitro substituent as an outlier. This could possibly suggest that substrates with electron donating groups in the para position undergo a different mechanism than substrates with electron withdrawing groups in the para position, but this is not clear. An investigation of other para electron withdrawing groups would be necessary to confirm. However, the similar trends observed for both from Region 1 and Region 2 suggest that Region 1 is representative of the system as a whole. Additionally, though not shown here, the trends observed for meta electronic effects and pKa were similar for both regions. As the trends observed for Region 1 are clearer in general, I will focus on the kinetics of Region 1 in my discussion going forward.

Table 33 – Pseudo second order rate constants for Regions 1, 2, and both regions combined for 5-substituted-2-bromopyridines.

Entry	R	$t_{½}$ (min)	k_{pseudo}		
			Region 1	Region 2	Both Regions
1	NH_2	2	0.5404	0.0293	0.0312
2	MeO	4.6	0.4124	0.08	0.0384
3	Me	5.3	0.3284	0.0922	0.1131
4	NO_2	1	7.5905	4.19E+01	2.48E+01
5	H	50	0.1818	0.0136	0.00156

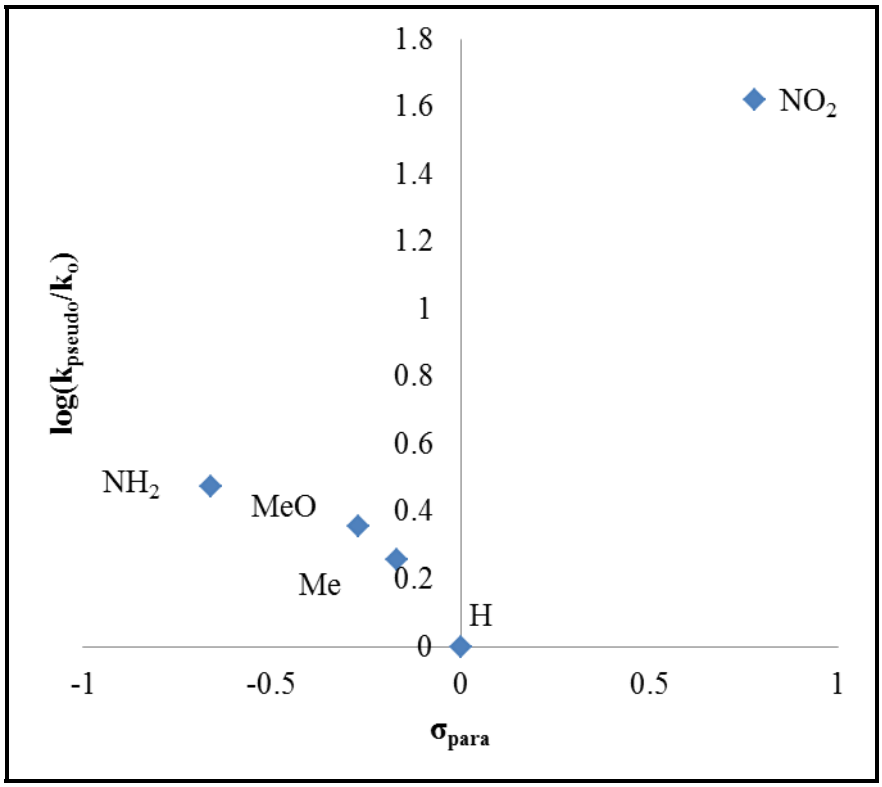

Figure 117 - Hammett plot of para electronic effects for 5-substituted-2-bromopyridines for Region 1.

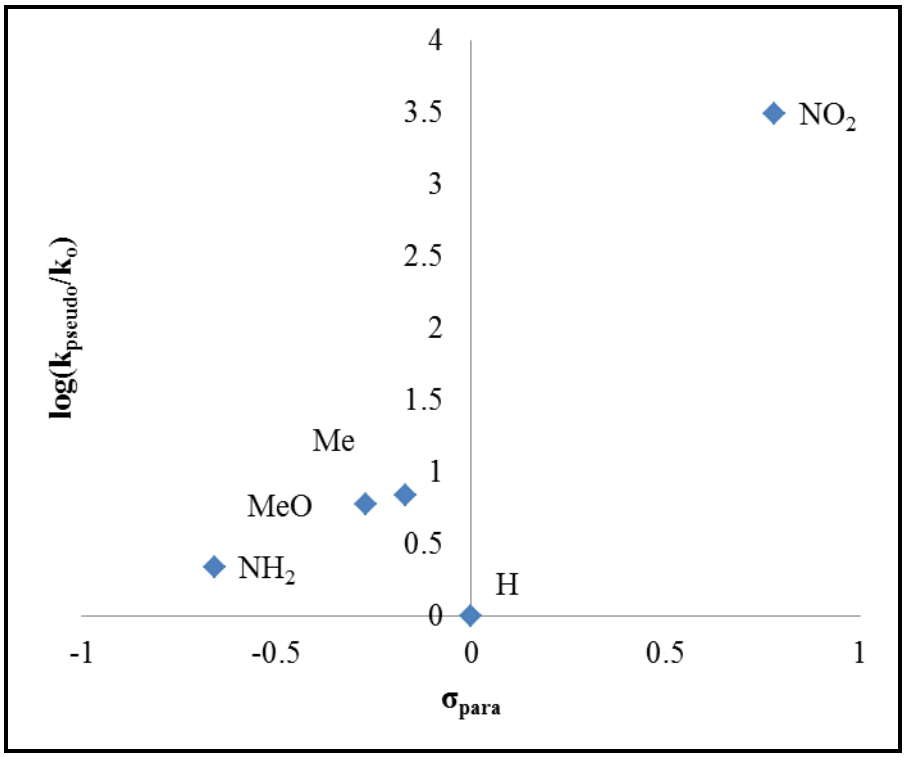

Figure 118 - Hammett plot of para electronic effects for 5-substituted-2-bromopyridines for Region 2.

The curve observed for the relationship between meta electronic effects and k_{pseudo} (Figure 119) clearly displayed an upward curve, as did the curve for the relationship between acid dissociation constants and the rate constants (Figure 120). This suggests the acidity and electronic effects appear to be effecting a change in mechanism for 5-substituted-2-bromopyridines. Additionally, the slopes of the Hammett plot of meta substituents are positive for electron withdrawing substituents, and negative for electron donating substitutents. This suggests that a buildup of negative charge, or loss of positive charge, is involved in the mechanism which is specific to these electron withdrawing susbtituents; and vice-versa for the electron donating substituents.

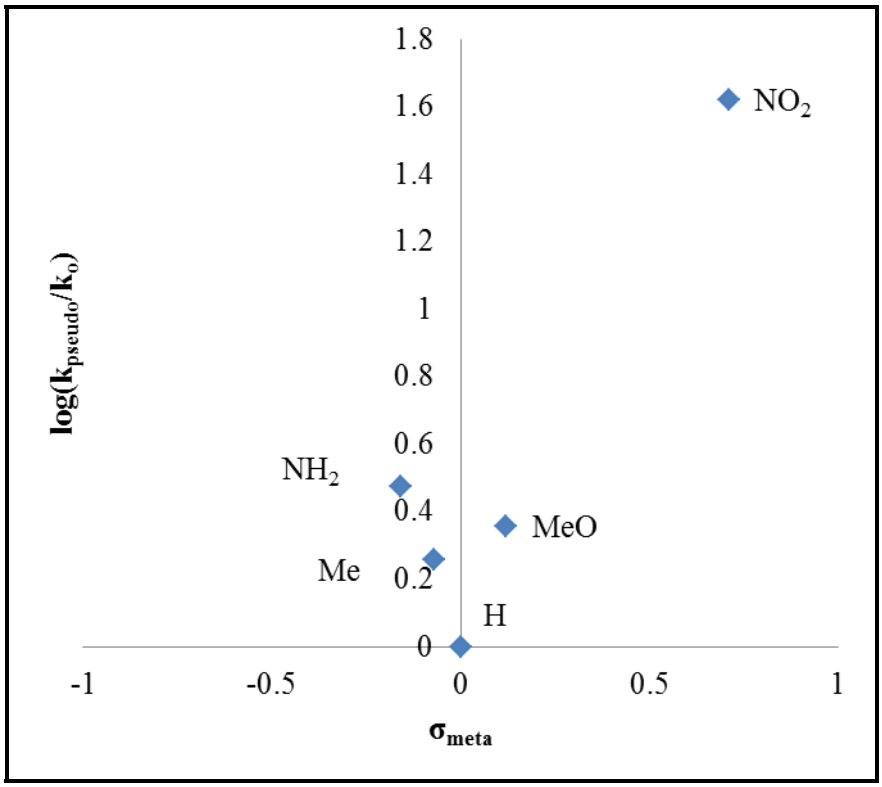

Figure 119 - Hammett plot of meta electronic effects for 5-substituted-2-bromopyridines.

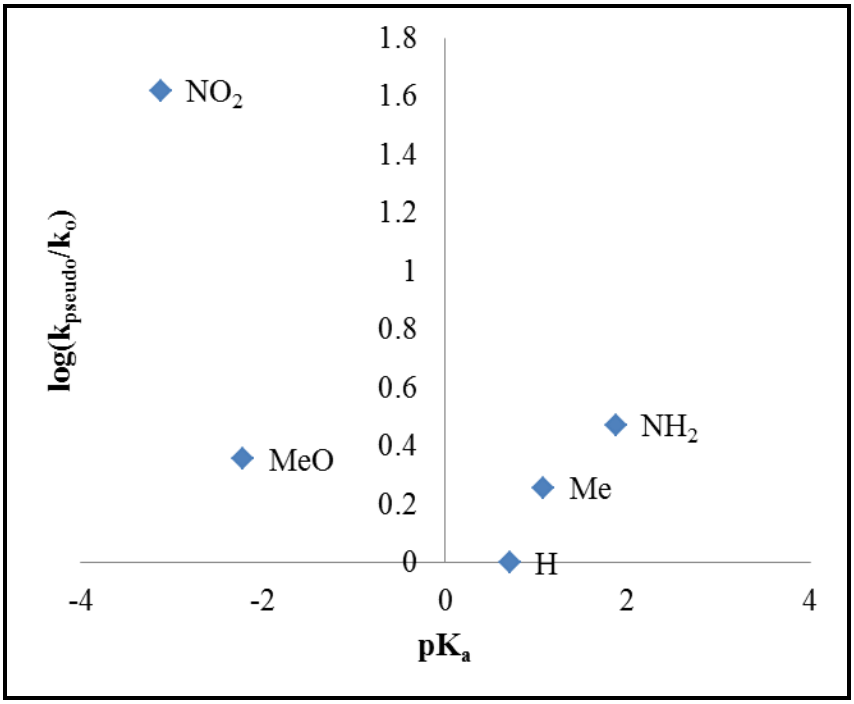

Figure 120 - Hammett plot of pKa for 5-substituted-2-bromopyridines.

4.2.2.1 Effect of substitution in the 4-position of 2-bromopyridine.

The same investigation was conducted for the 4-substituted-2-bromopyridines. The half-lives ($t_{½}$) of the coupling reactions, the corresponding electronic parameters (σ_{meta}, σ_{para}), and the acid dissociation constants (pK_a) are displayed in Table 34. The half-lives increased in the order of NO_2 < MeO < Me < H << NH_2. Except for the amine, whose half-life was greater than 24 hours under these conditions, this is very similar to the results obtained for the 5-substituted-2-bromopyridines.

Table 34 - Reactions run for 24 hours with 4-substituted 2-halopyridines and 40% v/v of H_2O, atm. N_2. Reactions run in 3-neck, 100 mL Morton flask.

Entry	4-R	$t_{½}$ (min)	σ_{meta}	σ_{para}	pK_a[1]
1	NH_2	1440	-0.16	-0.66	4.89
2	MeO	6	0.12	-0.27	2.1
3	Me	8.6	-0.07	-0.17	1.46
4	NO_2	1.4	0.71	0.78	-3.24
5	H	50	0	0	0.71[2]

[1]pKa's predicted by SciFinder: Calculated using Advanced Chemistry Development (ACD/Labs) Software V11.02 (© 1994-2014 ACD/Labs). [2]Literature source: Linnell, 1960.[26]

Again, in order to more clearly visualize possible trends, plots of half-life versus each electronic parameter (Figure 121-Figure 123) were developed. In each case – half-life versus para electronic effects (Figure 121), meta electronic effects (Figure 122), or acid dissociation constants (Figure 123) - the same trend is seen: an apparently linear plot for methoxy, methyl, nitro and hydrogen substituents, with the amine apparently as an outlier. The 4-amino-2-bromopyridine substrate is significantly outside the range of the other data. The rest of the 4-substituted amines follow a similar trend as the 5-substituted

amines. Again, Hammett plots of the rates and electronics were constructed to provide more insight.

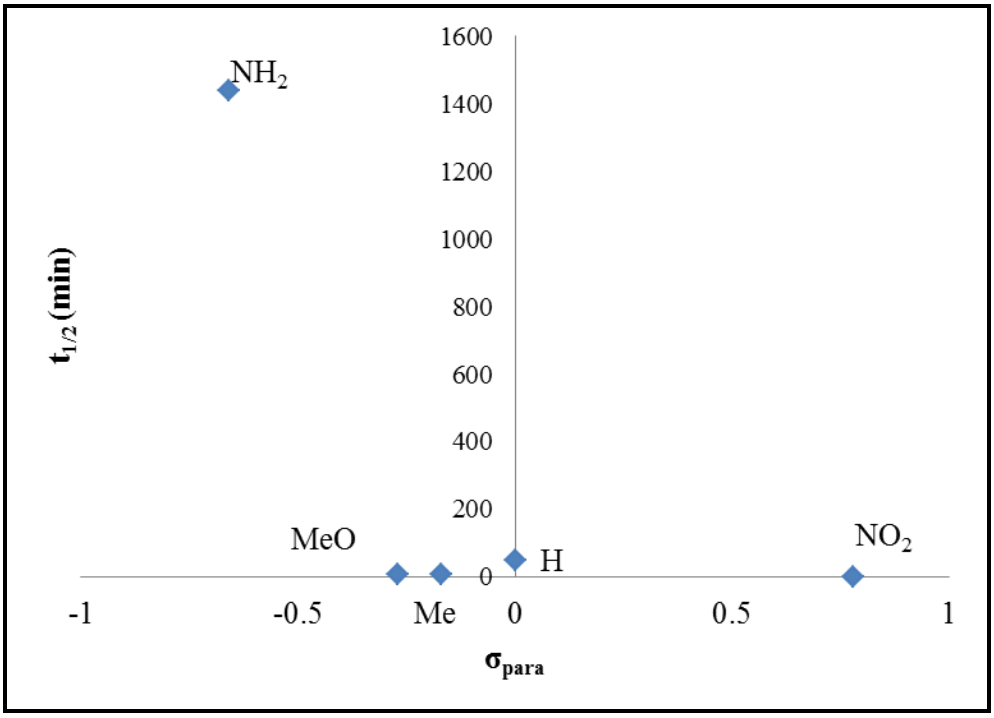

Figure 121 - Para effects versus half-lives for 4-substituted-2-bromopyridines.

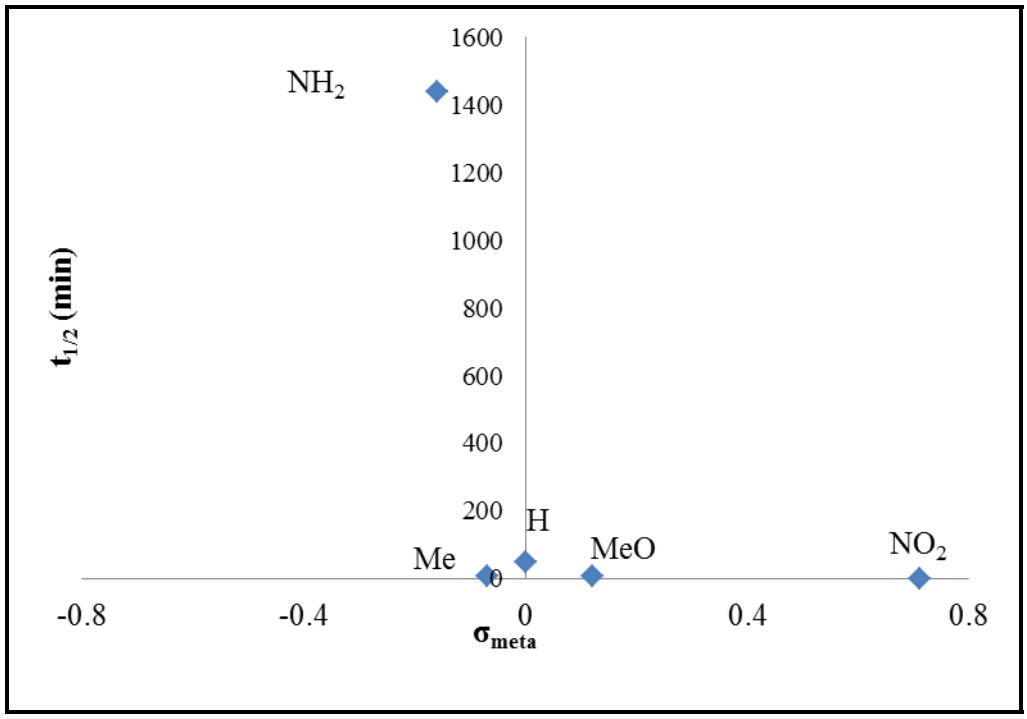

Figure 122 - Meta electronic effects versus half-lives for 4-substituted-2-bromopyridines.

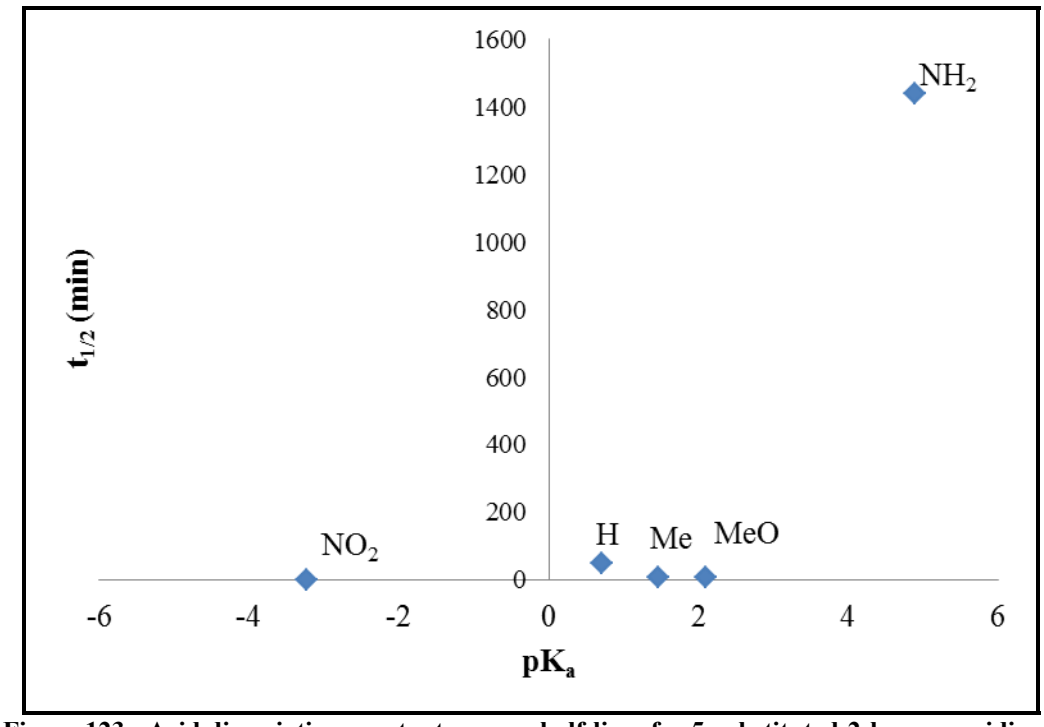

Figure 123 - Acid dissociation constants versus half-lives for 5-substituted-2-bromopyridines.

The approximated rate constants (k_{psuedo}) for the reactions of 4-substituted-2-bromopyridines are outlined in Table 35 for Regions 1, 2, and both combined. As in the previous section I will focus on the kinetics for Region 1. The Hammett plot of the para electronic effects (Figure 124) shows a shape similar to the curve observed for 5-substituted amines. However, 4-amino-2-bromopyridine lies significantly outside of the curve.

Table 35 - Second order rate constants for 4-substituted-2-bromopyridines.

Entry	R	$t_{½}$ (min)	k_{pseudo}		
			Region 1	**Region 2**	**Both Regions**
1	NH_2	1440	0.116	0.0004	0.0004
2	MeO	6	0.3381	0.0339	0.0352
3	Me	8.6	0.2842	0.0456	0.0461
4	NO_2	1.4	1.2988	2.3485	3.8778
5	H	50	0.1818	0.0136	0.00156

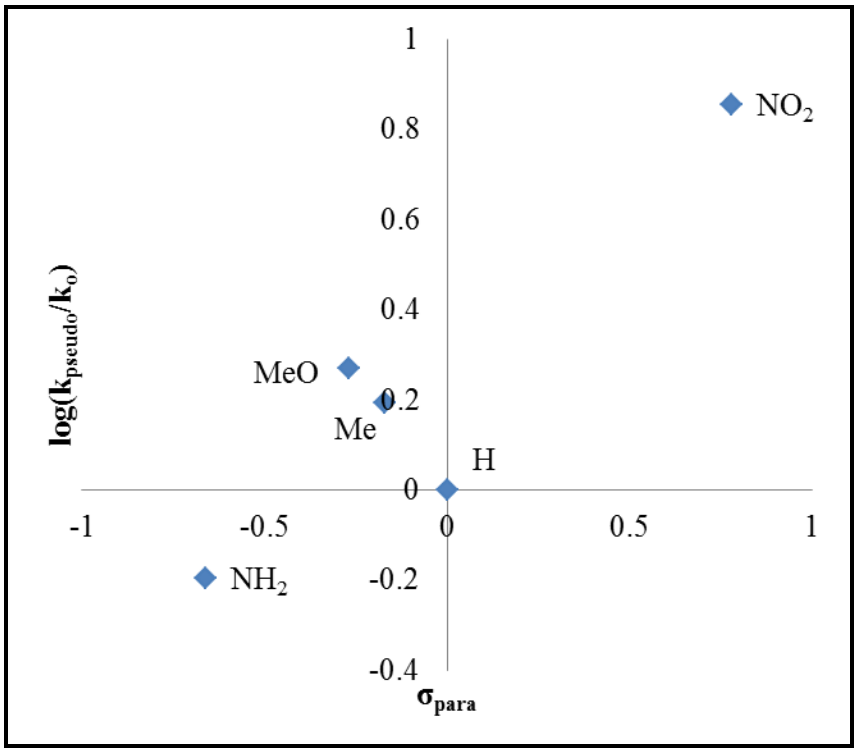

Figure 124 - Hammett plot of para electronic effects for 4-substituted-2-bromopyridines.

The same is seen for the Hammett plots of the meta electronic effects (Figure 125) and the pK_a's (Figure 126). An upward curve was clearly discernable for substituents in the 5-position, and a similar curve is seen here for substituents in the 4-position. However, again, the result for 4-amino-2-bromopyridine does not lie on the curve. The reason for this is as of yet unknown. Aside from the one outlier, these trends suggest that the electronics and acid-base properties of the substrates effect a change in mechanism.

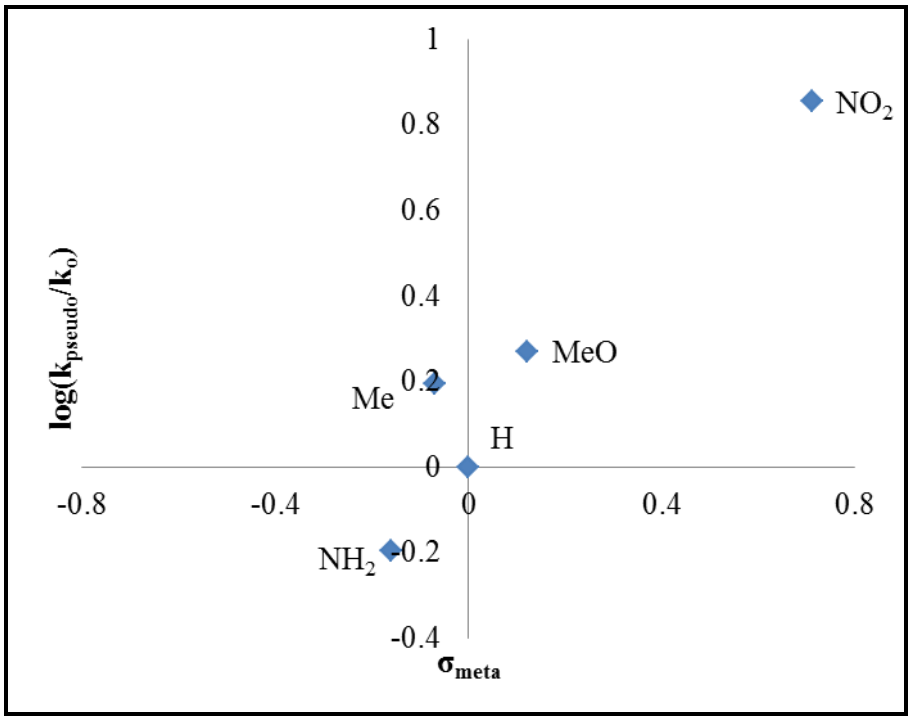

Figure 125 - Hammett plot of meta electronic effects for 4-substituted-2-bromopyridines.

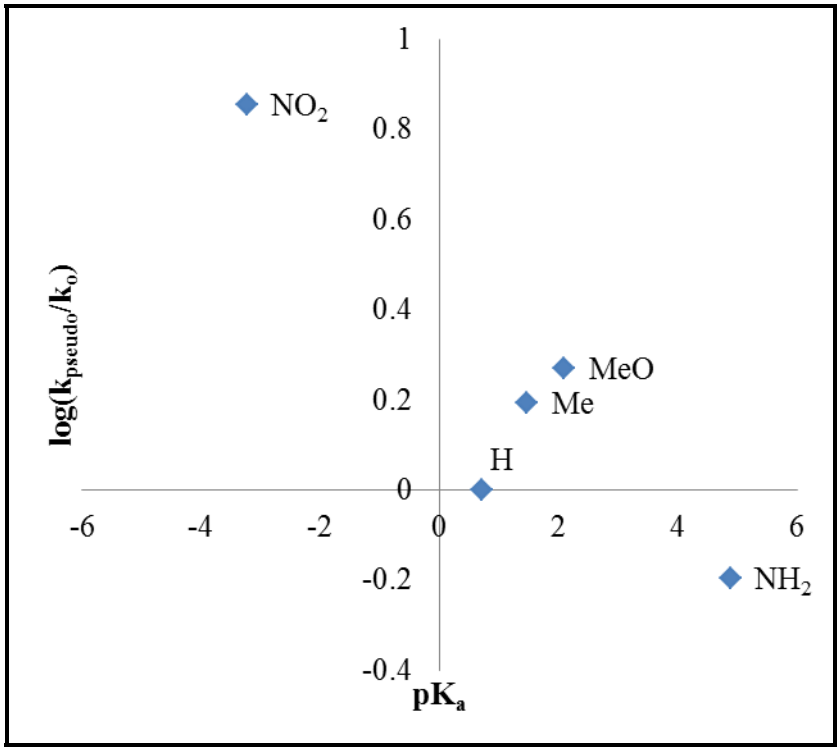

Figure 126 - Hammett plot of acid dissociation constants for 4-substituted-2-bromopyridines.

4.3 Conclusions

Utilizing increased water content (40%) and CO_2 pressure we were able to design an efficient and simple system for the Suzuki coupling of 4-amino-2-halopyridines in quantitative yields. Neither the addition of protection/deprotection steps nor expensive designer ligands were required to achieve this result, which is advantageous from an industrial and sustainable view-point by reducing waste and cost of the process. Additionally, CO_2 pressures as low as 2 atm could be utilized to produce high yields (>80%) of the coupled product.

Our investigations uncovered a substrate dependent optimum pH which we believe is due to the acid-base properties of the 4-amino-2-halopyridine and 2-halopyridine substrates. 2-Halopyridines couple in quantitative yields at a pH of ~12. 4-Amino-2-halopyridines couple in quantitative yields at a pH of ~8. It is proposed that a small (~0.01%), steady-state amount of the activated (protonated) 4-amino-2-halopyridine is produced at a pH of 8, promoting the coupling reaction. The rate profiles of the 4-amino-2-halopyridines and 2-halopyridines under the different conditions support this conclusion. Buffers such as potassium phosphate dibasic could be used instead of the combination of potassium phosphate tribasic and CO_2 pressure to produce similar pH (~8) and yield (~100%), which eliminates the risks of working with high pressure systems. Additionally, the halogen-independent nature demonstrated by these reactions allows for the use of the chloro-substrates in place of the more expensive bromo-substrates.

Additionally, Hammett plots were developed for the effect of electronics ($\sigma_{meta/para}$) and acid dissociation constants (pK_a) on the rates of various 4- and 5-substituted-2-bromopyridines. The 5-substituted-2-bromopyridines displayed upward

curved Hammett plots for each parameter (meta/para electronic effects and pK_a) which is typically linked to a change in mechanism. Interestingly, the 4-substituted-2-bromopyridines display the same trends except for 4-amino-2-bromopyridine. Further work would be required before conclusions could be drawn for this investigation; however, this information could be useful as a basis for further fundamental mechanistic studies into the Suzuki coupling reaction.

4.4 Experimental

4.4.1 Materials

All chemicals were purchased from Sigma-Aldrich, Matrix or VWR and used as received unless otherwise noted. All chemicals were stored under inert dry atmosphere. The CO_2 employed was SFC grade from Airgas, certified to contain less than < 250 ppb H_2O with a purity of 99.9999%.

4.4.2 Experimental Procedure

4.4.2.1 Procedures for 4-amino-2-halopyridine

Reaction of 2-halo-4-aminopyridine with phenylboronic acid under a nitrogen atmosphere.

4-Amino-2-chloropyridine (2.057 g, 16 mmol, 1 eq) or 4-amino-2-bromopyridine (2.768 g, 16 mmol, 1 eq), phenylboronic acid (2.536 g, 1.3 eq), K_3PO_4 (10.189 g, 3 eq), and $Pd(TPP)_2Cl_2$ (0.562 g, 5 mol%) were added to a 100 mL three-neck Morton flask. The flask was evacuated and backfilled with nitrogen. Degassed acetonitrile (30 mL) and degassed water (10 mL for 25% v/v reactions; 20 mL for 40% v/v reactions) were added by means of an air-tight syringe. The reaction vessel was insulated with glass wool and

heated to reflux at 70°C (monitored by internal thermometer) with magnetic stirring under an atmosphere of N_2 for 24 h. The initial reaction time (t = 0) was taken when the reaction mixture reached an internal temperature of 70°C; this took approximately 10-15 minutes. The reactions were biphasic with two liquid phases.

Reaction of 4-amino-2-halopyridine with phenylboronic acid under varying pressures of carbon dioxide.

4-Amino-2-chloropyridine (2.057 g, 16 mmol, 1 eq) or 4-amino-2-bromopyridine (2.768 g, 16 mmol, 1 eq), phenylboronic acid (2.536 g, 1.3 eq), K_3PO_4 (10.189 g, 3 eq), and $Pd(TPP)_2Cl_2$ (0.562 g, 5 mol%) were added to a 300 mL stainless steel bomb (Parr reactor). The Parr reactor was then purged with a flow of CO_2 for 15 minutes. Degassed acetonitrile (30 mL) and degassed water (10 mL for 25% v/v reactions; 20 mL for 40% v/v reactions) were then added by means of an air-tight syringe. The Parr reactor was then pressurized with CO_2 via a model 260D or 500D ISCO syringe pump to within ~6.8 atm of the desired pressure. The reaction mixture was mechanically stirred by means of a built-in impeller at a stirring rate of 415 rpm and heated to 70^{o}C as monitored by an internal thermocouple. The pressure of CO_2 was then increased to the desired pressure. The initial reaction time (t = 0) was taken when the reaction mixture reached an internal temperature of 70^{o}C and the final CO_2 pressure has been reached; this took approximately 10 minutes. Constant pressure was maintained throughout the reaction by the ISCO pump. The reaction mixture was heated for 24 h. The reactions are biphasic with two liquid phases.

Workup Procedure

After reacting for 24 h the reaction vessel was cooled to room temperature. Depressurization was necessary for the reactions conducted under an atmosphere of CO_2. Methanol was added (~100 mL) to the reaction mixture which resulted in the

precipitation of a solid. At this point the reaction mixture is characterized by two phases- a solid phase and a single liquid phase. The mixture was filtered and the filtrate analyzed by gas chromatography/flame ionization detector (GC-FID) using a Shimadzu GC-2010 gas chromatograph fitted with a Supelco PTA-5 (30m x 0.32 mm x 1.00 μm, length x inside diameter x film thickness) capillary column. Product yields were calculated using the calibration curves discussed below. The filtrate was then transferred to a round bottom flask and the solvent removed *in vacuo*. The crude product was analyzed by ^{1}H-NMR ($CDCl_3$) using a 300 MHz Varian NMR spectrometer and compared to standards to determine NMR yields (refer to section VI for example and calculation).

Reaction of 2-halo-4-aminopyridine with phenylboronic acid as a function of time.

To monitor reactions as a function of time, samples were taken from the organic layer for analysis by GC-FID.

Reactions Under Atmospheric Nitrogen

For reactions conducted under a nitrogen atmosphere the stirring was stopped briefly at specified times in order to allow the acetonitrile and water phases to separate. Air tight syringes were used to remove 0.2 mL samples from the organic phase; stirring was then resumed. The 0.2 mL sample was placed in a vial from which 0.1 mL was transferred to a GC vial by means of an Eppendorf calibrated pipette. Methanol (0.9 mL) was then added to the GC vial by an Eppendorf pipette and the sample analyzed by GC-FID.

Reactions Under CO_2 Pressure

For reactions conducted under CO_2 pressures, samples were removed through a stainless steel dip tube which extends into the organic phase. Stirring was stopped briefly to allow the acetonitrile and water phases to separate. The valve was opened so that the pressure differential slowly drove the sample out of the reactor into a vial in the form of

droplets. After ~0.2 mL was collected the valve was shut and stirring resumed. Then 0.1 mL of the sample was transferred from the vial to a GC vial by means of an Eppendorf pipette. Methanol (0.9 mL) was added to the GC vial by an Eppendorf pipette and the sample was analyzed by GC-FID.

4.4.2.2 Experimental procedures for 2-halopyridines.

Reaction of 2-halopyridine with phenylboronic acid under a nitrogen atmosphere.

Phenylboronic acid (2.536 g, 1.3 eq), K_3PO_4 (10.189 g, 3 eq), and $Pd(TPP)_2Cl_2$ (0.562 g, 5 mol%) were added to a 100 mL three-neck Morton flask. The flask was evacuated and backfilled with nitrogen. 2-Chloropyridine (1.817 g, 16 mmol, 1 eq) or 2-bromopyridine (2.528 g, 16 mmol, 1 eq), followed by degassed acetonitrile (30 mL) and then degassed water (10 mL for 25% v/v reactions; 20 mL for 40% v/v reactions) were added by means of an air-tight syringe. The reaction vessel was insulated with glass wool and heated to reflux at 70°C (monitored by internal thermometer) with magnetic stirring under an atmosphere of N_2 for 24 h. The initial reaction time (t = 0) was taken when the reaction mixture reached an internal temperature of 70°C; this took approximately 10-15 minutes. The reactions were biphasic with two liquid phases.

Reaction of 2-halopyridine with phenylboronic acid under varying pressures of carbon dioxide.

Phenylboronic acid (2.536 g, 1.3 eq), K_3PO_4 (10.189 g, 3 eq), and $Pd(TPP)_2Cl_2$ (0.562 g, 5 mol%) were added to a 300 mL stainless steel bomb (Parr reactor). The Parr reactor was then purged with a flow of CO_2 for 15 minutes. 2-Chloropyridine (1.817 g, 16 mmol, 1 eq) or 4-amino-2-bromopyridine (2.528 g, 16 mmol, 1 eq) followed by degassed acetonitrile (30 mL) and then degassed water (10 mL for 25% v/v reactions; 20 mL for 40% v/v reactions) were then added by means of an air-tight syringe. The Parr reactor was then pressurized with CO_2 via a model 260D or 500D ISCO syringe pump to within

~6.8 atm of the desired pressure. The reaction mixture was mechanically stirred by means of a built-in impeller at a stirring rate of 415 rpm and heated to 70^{o}C as monitored by an internal thermocouple. The pressure of CO_2 was then increased to the desired pressure. The initial reaction time (t = 0) was taken when the reaction mixture reached an internal temperature of 70^{o}C and the final CO_2 pressure has been reached; this took approximately 10 minutes. Constant pressure was maintained throughout the reaction by the ISCO pump. The reaction mixture was heated for 24 h. The reactions are biphasic with two liquid phases.

Workup Procedure

Workup was conducted in the same manner as described above for the 4-amino-2-halopyridines.

Reaction of 2-halopyridine with phenylboronic acid as a function of time.

Sampling was conducted in the same manner as described above for the 4-amino-2-halopyridines.

4.4.2.3 Reactions of 4-substituted- and 5-substituted-2-halopyridines (substituent effect).

Substrate (Table 36), and $Pd(TPP)_2Cl_2$ (0.562 g, 5 mol%) were added to a 100 mL three-neck Morton flask (Flask 1).

Phenylboronic acid (2.536 g, 1.3 eq) and K_3PO_4 (10.189 g, 3 eq) were added to a separate 100 mL three-neck Morton flask (Flask 2).

Both flasks were evacuated and backfilled with nitrogen. Degassed acetonitrile (30 mL) was added to Flask 1 and degassed water (20 mL) was added to Flask 2. Transfer of solvent was accomplished via an air-tight syringe. The reaction vessels were insulated with glass wool and heated to reflux at 70°C (monitored by internal thermometer) with magnetic stirring under an atmosphere of N_2. Upon reaching 70°C, the contents of Flask 2 were transferred by air-tight syringe to Flask 1 creating a biphasic,

liquid-liquid reaction mixture which was heated for the times described. Samples were obtained as outlined above and the reaction mixtures were worked up as outlined in the previous sections.

Table 36 - Amounts of reagent for substitution effect investigation.

Substrate (16 mmol, 1 eq)	Amount (g)
2-Bromo-(4 or 5)-methoxypyridine	3.008
2-Bromo-(4 or 5)-nitropyridine	3.248
2-Bromo-(4 or 5)-methylpyridine	2.752
(4 or 5)-Amino-2-bromopyridine	2.768
2-Bromopyridine	2.528

4.4.2.3 Isolation of 4-amino-2-phenylpyridine from the reaction of 4-amino-2-bromopyridine with phenylboronic acid under CO2 pressure.

4-Amino-2-bromopyridine (2.761 g, 15.96 mmol, 1 eq), phenylboronic acid (2.536 g, 1.3 eq), K_3PO_4 (10.189 g, 3 eq), and $Pd(TPP)_2Cl_2$ (0.562 g, 5 mol%) were added to a 300 mL stainless steel bomb (Parr reactor). The Parr was then purged with a flow of CO_2 for 15 minutes. Degassed acetonitrile (30 mL) and degassed water (20 mL) were then added by air-tight syringe. The Parr was then pressurized with CO_2 by means of a model 500D ISCO syringe pump to ~24 atm CO_2. The reaction mixture was mechanically stirred by means of a built-in impeller at a stirring rate of 415 rpm and heated to 70^{o}C as monitored by an internal thermocouple. The pressure was then increased to 30.6 atm CO_2. The initial reaction time (t = 0) was taken when the reaction mixture reached an internal temperature of 70^{o}C and the final CO_2 pressure has been

reached; this took approximately 10 minutes. Constant pressure was maintained throughout the reaction by the ISCO pump. The reaction mixture was heated for 24 h.

After 24 h the Parr reactor was cooled to room temperature and depressurized. Methanol was added (~100 mL) to the reaction mixture which resulted in the precipitation of a solid. At this point the reaction mixture is characterized by two phases- a solid phase and a single liquid phase. The mixture was filtered and the filtrate analyzed by GC-FID using a Shimadzu GC-2010 gas chromatograph fitted with a Supelco PTA-5 (30m x 0.32 mm x 1.00 μm, length x inside diameter x film thickness) capillary column. Using the above described calibration curves, the yield of 2-phenyl-4-aminopyridine was calculated to be 99%; the conversion was 100%. The filtrate was transferred to a round bottom flask and the solvent was removed *in vacuo* leaving a brown solid. The crude mixture was loaded onto neutral silica (~10 g) then added to a column packed with neutral silica (pH~7). A hexanes/ethyl acetate (EtOAc) gradient was used. Biphenyl was removed first under 100% hexanes. The EtOAc concentration was gradually increased to 50% and then held at 50% until the product had completely eluted from the column as indicated by TLC. The product fractions were combined and the solvent removed *in vacuo* to yield 94% 4-amino-2-phenylpyridine as yellow crystalline solid (2.54 g, 14.992 mmol). ^{1}H and ^{13}C NMR of the pure product are shown below (Figure 127 and Figure 128).

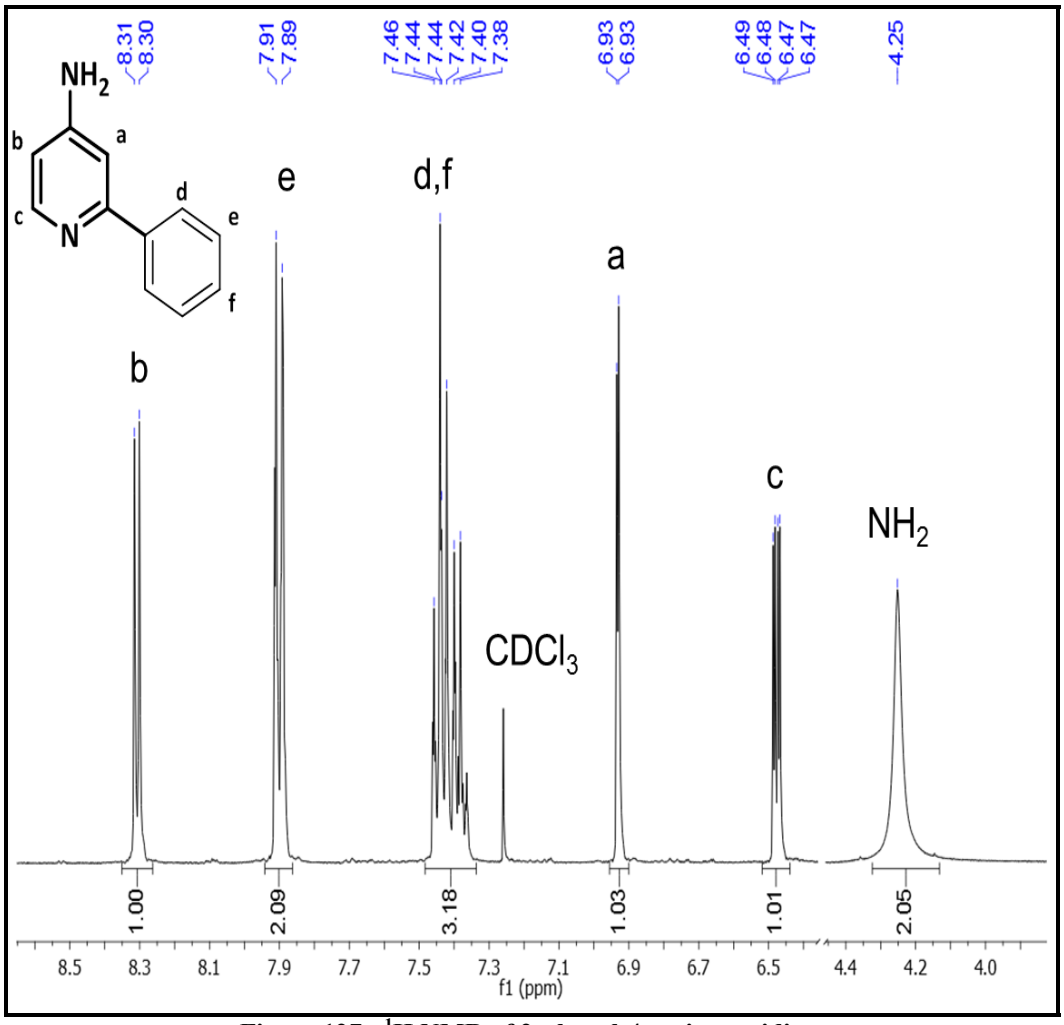

Figure 127 - ^{1}H NMR of 2-phenyl-4-aminopyridine.

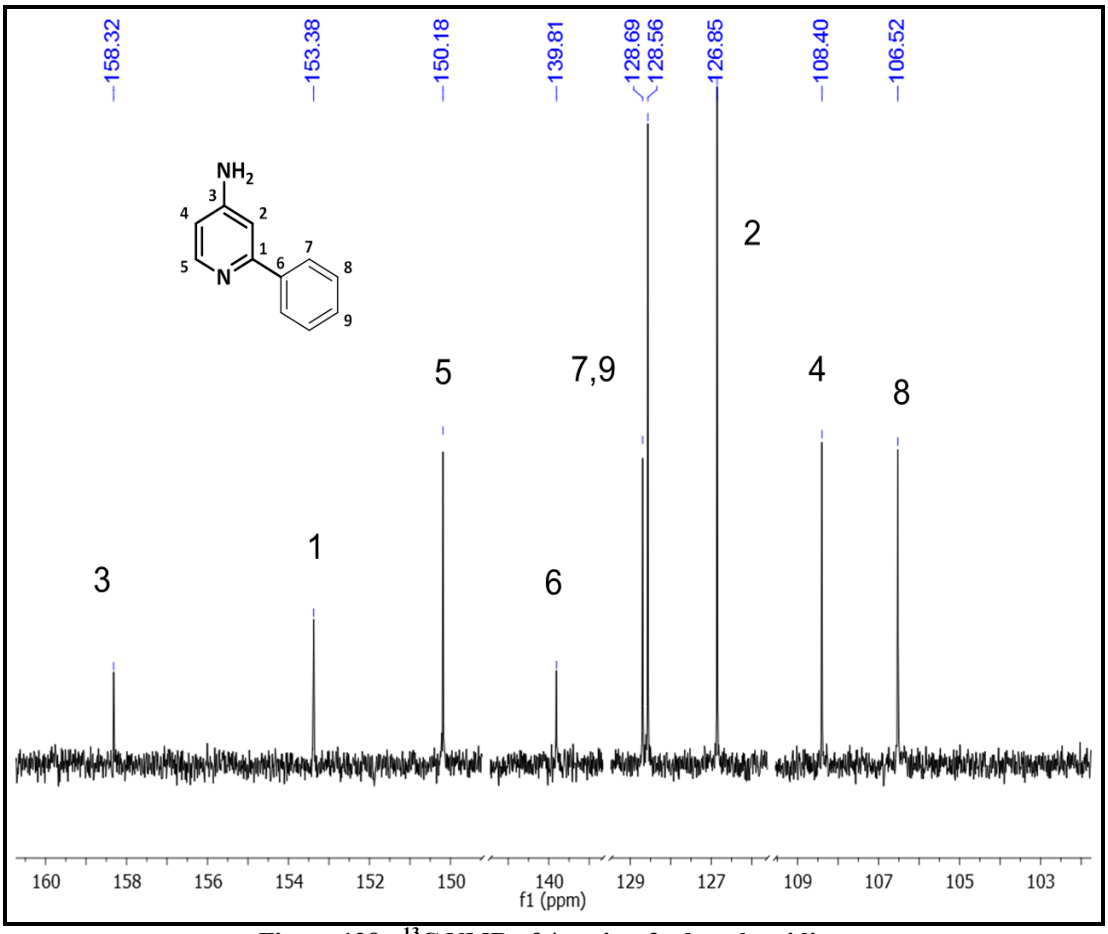

Figure 128 - ^{13}C NMR of 4-amino-2-phenylpyridine.

4.4.2.4 Composition of Buffered Phases for pH vs. Yield

The following tables detail which base(s), the equivalents of the base (relative to the substrate), the pH before and after reaction, and the yields for each reaction used for the study of pH's effect on yield (Table 37-Table 41).

Table 37 – Buffer compositions for 4-amino-2-bromopyridine at 40% water.

4-NH_2-2-BrPyr, 40% H_2O			
Base (equiv.)	**Yield (%)**	**pH before**	**pH after**
K_3PO_4 (3)	23±4	13	13
$K_4P_2O_7$ (3)	50±1	10.58	9.67
K_2HPO_4/$KHCO_3$ (1/2)	79±3	9.2	8.8
K_2HPO_4/$KHCO_3$ (3/3)	51±3	9.64	9.6
K_2HPO_4 (3)	90±2	9.5	7.95
K_3PO_4, 30 psi CO_2 (3)	83±0	N/A	7.7
K_3PO_4, 100 psi CO_2 (3)	91±8	N/A	7.9
K_2HPO_4/$KHCO_3$/KH_2PO_4 (2.4/3.5/0.6)	51±4	8.4	9.85
precond. K_3PO_4* (3)	76±6	8	8.3
pre-cond. SM. and K_3PO_4* (3)	75±2	7.9	8.1
CsF (3)	95±4	8.97	8.1

***Reagents and solvents were preconditioned with CO_2 then purged and run under N_2.**

Table 38 –Buffer compositions for 4-amino-2-bromopyridine at 25% water.

4-NH_2-2-BrPyr, 25% H_2O		
Base (equiv.)	**Yield (%)**	**pH after**
KH_2PO_4 (3)	3	5.9
K_3PO_4 (3)	17±3	13
K_2HPO_4/K_2CO_3 (3/3)	23	11.3
$K_4P_2O_7$ (3)	26±4	10.6
K_2HPO_4/$KHCO_3$ (1/2)	35±1	9.2
K_2HPO_4/$KHCO_3$ (3/3)	41±3	10.3
K_2HPO_4 (3)	41±8	9.8

Table 39 - Buffer compositions for 2-bromopyridine at 40% water

2-BrPyr, 40% H_2O			
Base (equiv.)	**Yield**	**pH before**	**pH after**
K_3PO_4 (3)	92±5	12.8±0.3	11.6±0.5
K_3PO_4, 450 psi CO_2 (3)	15±0.3	12.8±0.3	7.8±0.5
K_2HPO_4 (3)	26±2	9.4±0.1	8.4±0.3
K_2HPO_4/$KHCO_3$ (1/2)	36±8	9.2±0.1	9.6±0.3
KH_2PO_4 (3)	23±4	5.2±0.0	3.4±0.1
K_2CO_3 (3)	66±1	11.9±0.1	10.5±0.2
$KHCO_3$ (3)	64±5	8.9±0.1	9.6±0.3
K_2HPO_4/$KHCO_3$/KH_2PO_4 (2.4/3.5/0.6)	25±2	8.5±0.1	9.2±0.1
CsF (3)	29±7	N/A	8.6±0.2
KOH (3)	69±6	14.75±0.07	11.7±0.0

Table 40 - Buffer compositions for 4-amino-2-chloropyridine at 40% water

4-NH_2-2-ClPyr, 40% H_2O			
Base (equiv.)	**yield**	**pH before**	**pH after**
K_3PO_4 (3)	30±2	N/A	12.635
K_2HPO_4 (3)	64±2	9.533333	8.2
K_3PO_4, 30 psi CO_2 (3)	93±3	N/A	7.95
K_3PO_4, 100 psi CO_2 (3)	98±3	N/A	7.625

Table 41 - Buffer compositions for 2-chloropyridine at 40% water

2-ClPyr, 40% H_2O			
Base (equiv.)	**Yield**	**pH before**	**pH after**
K_3PO_4 (3)	79±1	13.2±0.1	11.6±0.1
K_3PO_4, 450 psi CO_2 (3)	32±6	13.2±0.1	7.6±0.1
K_2HPO_4 (3)	42±9	9.3±0.1	8.3±0.1
K_2CO_3 (3)	94±2	11.7±0.1	10.5±0.0

4.4.3 Analyses

4.4.3.1 GC-FID Chromatograms and Calibration Curves

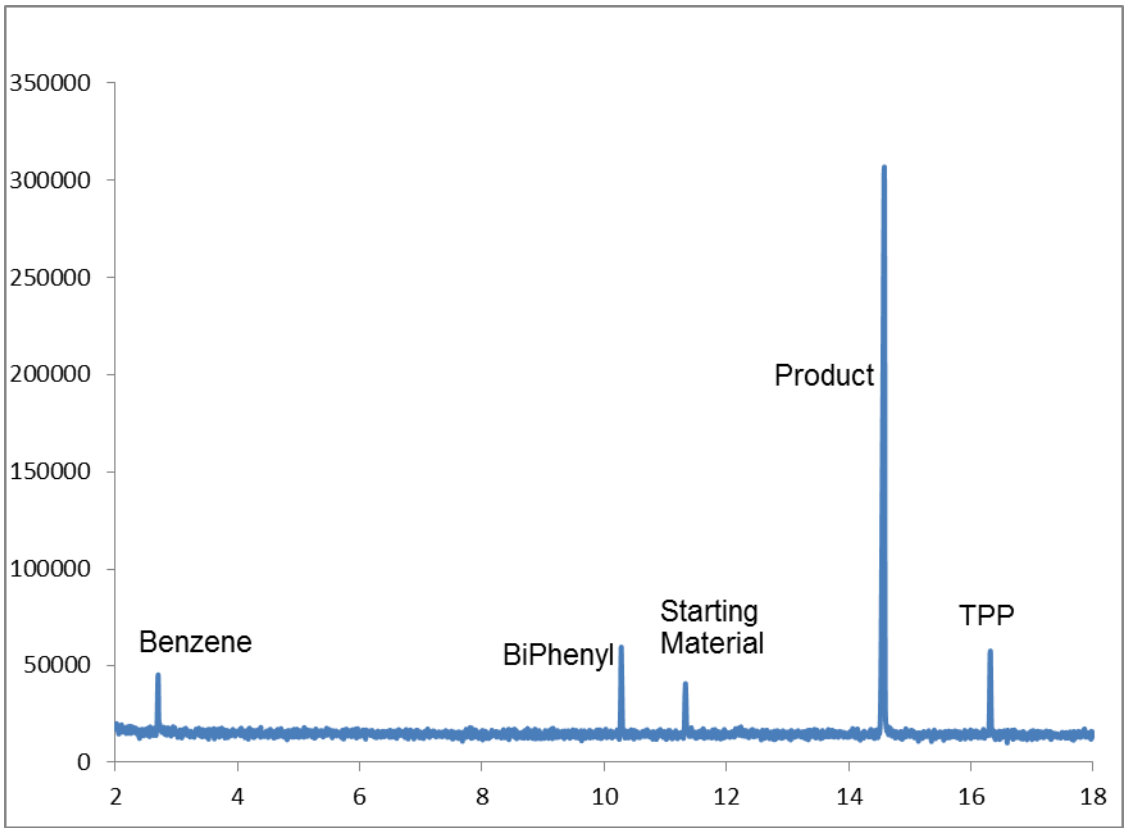

Figure 129 - Example GC-FID spectra: reaction of 4-amino-2-bromopyridine with phenylboronic acid under 2 atm CO2 and 40% water after 24 h after workup. Calibration curves are used to relate the area of each peak to a concentration, which is then used to calculate yield and conversion.

Calibration curves were created from pure substrate and product standards. Stock solutions (1 M) were made using a 75/15/10 mixture of methanol/acetonitrile/water to mimic the solvent system of the reaction systems after workup. Multiple samples of concentrations between 0.01 M and 0.5 M were then made from dilution of the stock solution with the same solvent mixture and analyzed by GC-FID. Plots of concentration versus area were created for each compound using Microsoft Excel and a trendline analysis used to provide the calibration curve and confirm the plot followed a straight line. Calibration curves for 4-amino-2-chloropyridine, 4-amino-2-bromopyridine, and 2-

bromopyridin-4-ylamine are displayed in Figures 2-4. Calibration curves for 2-chloropyridine, 2-bromopyridine and 2-phenylpyridine are displayed in Figure 130-Figure 135.

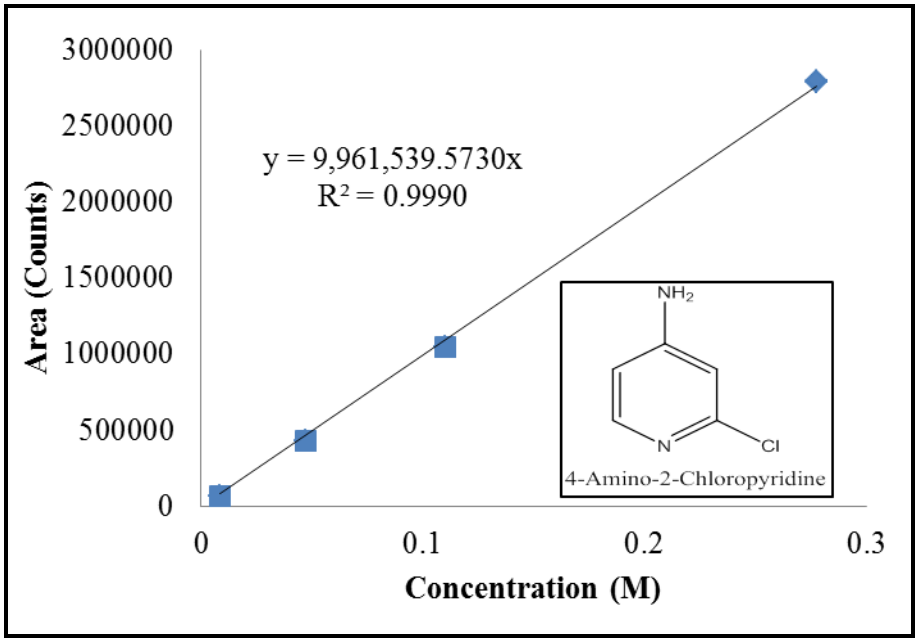

Figure 130 - GC-FID calibration curve of 4-amino-2-chloropyridine.

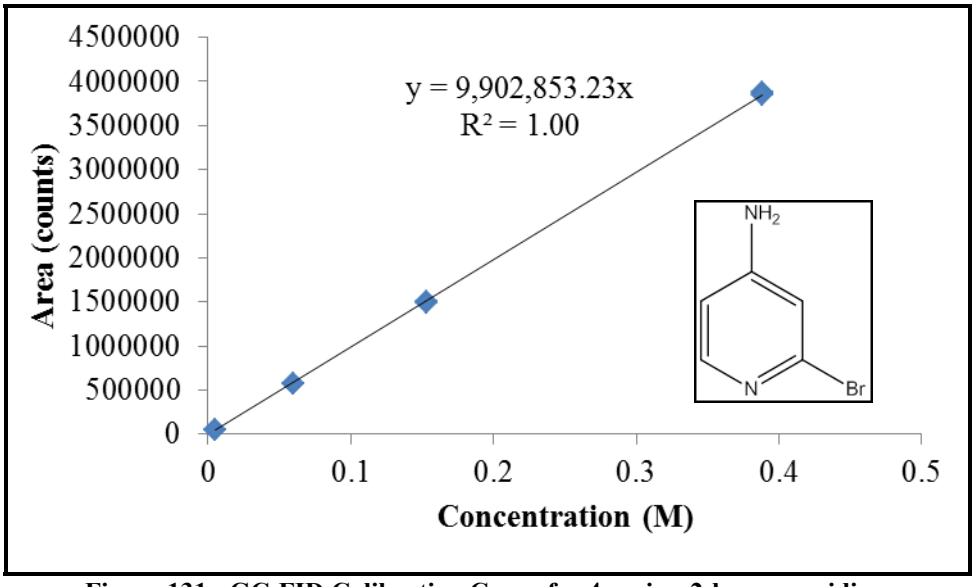

Figure 131 - GC-FID Calibration Curve for 4-amino-2-bromopyridine.

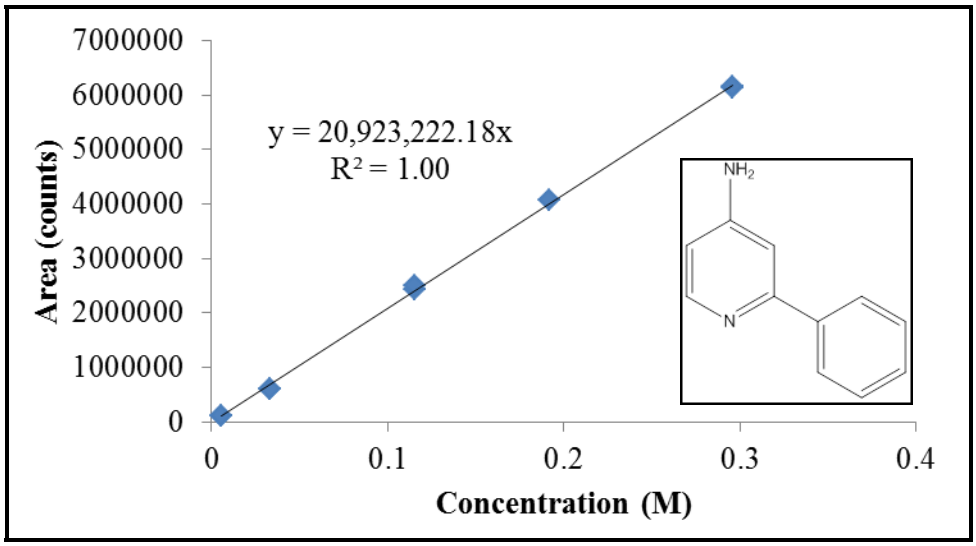

Figure 132 - GC-FID Calibration Curve for 2-phenylpyridine-4-ylamine

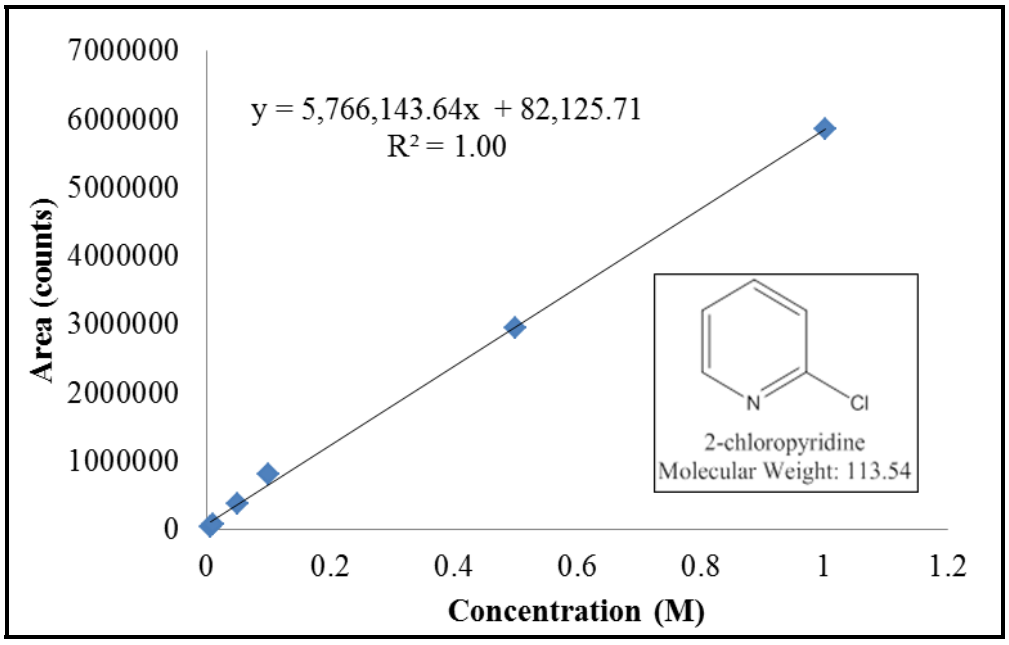

Figure 133 - GC-FID Calibration Curve for 2-chloropyridine.

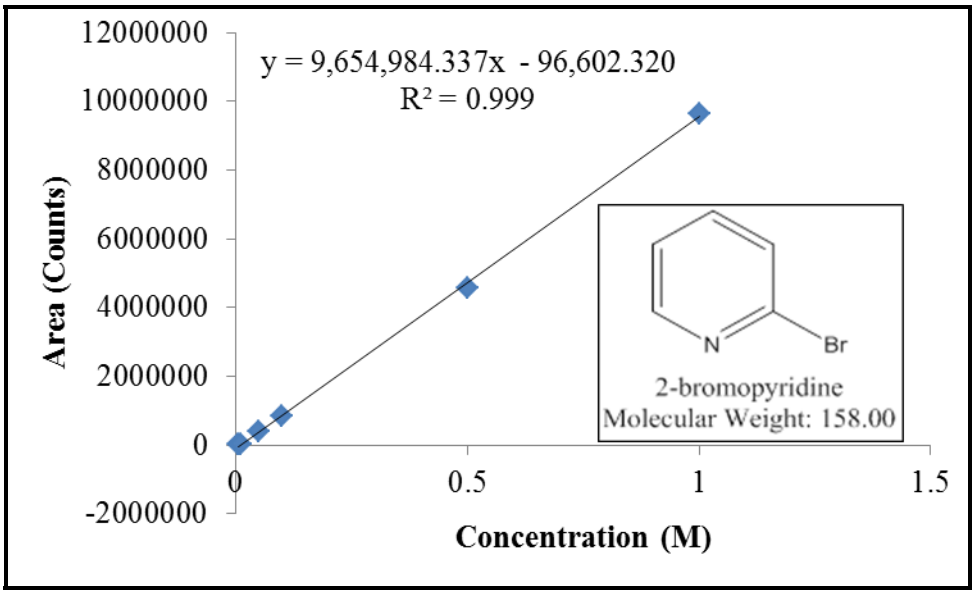

Figure 134 - GC-FID Calibration Curve for 2-bromopyridine.

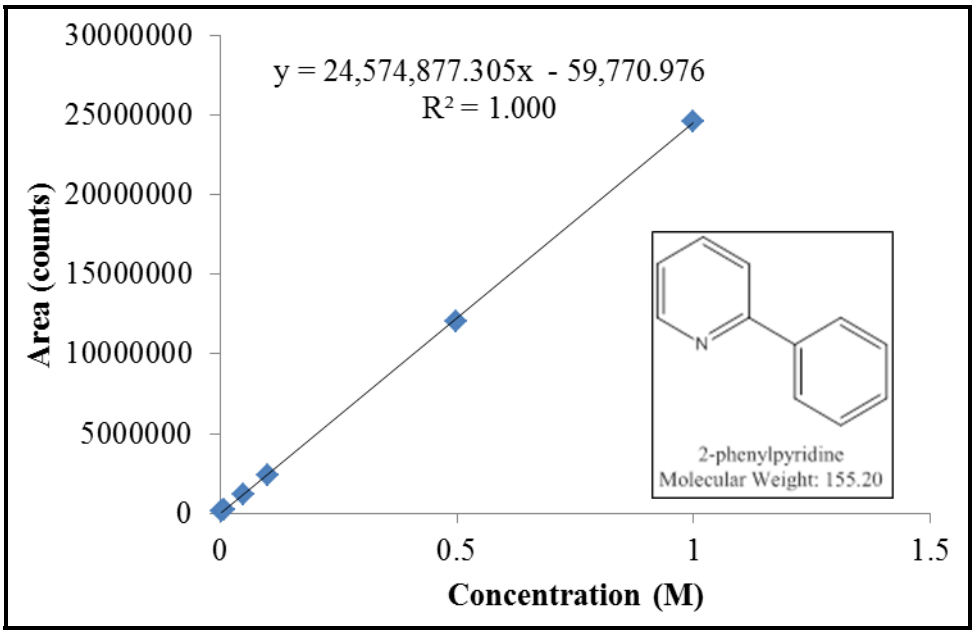

Figure 135 - GC-FID Calibration Curve for 2-phenylpyridine.

4.4.3.2 NMR

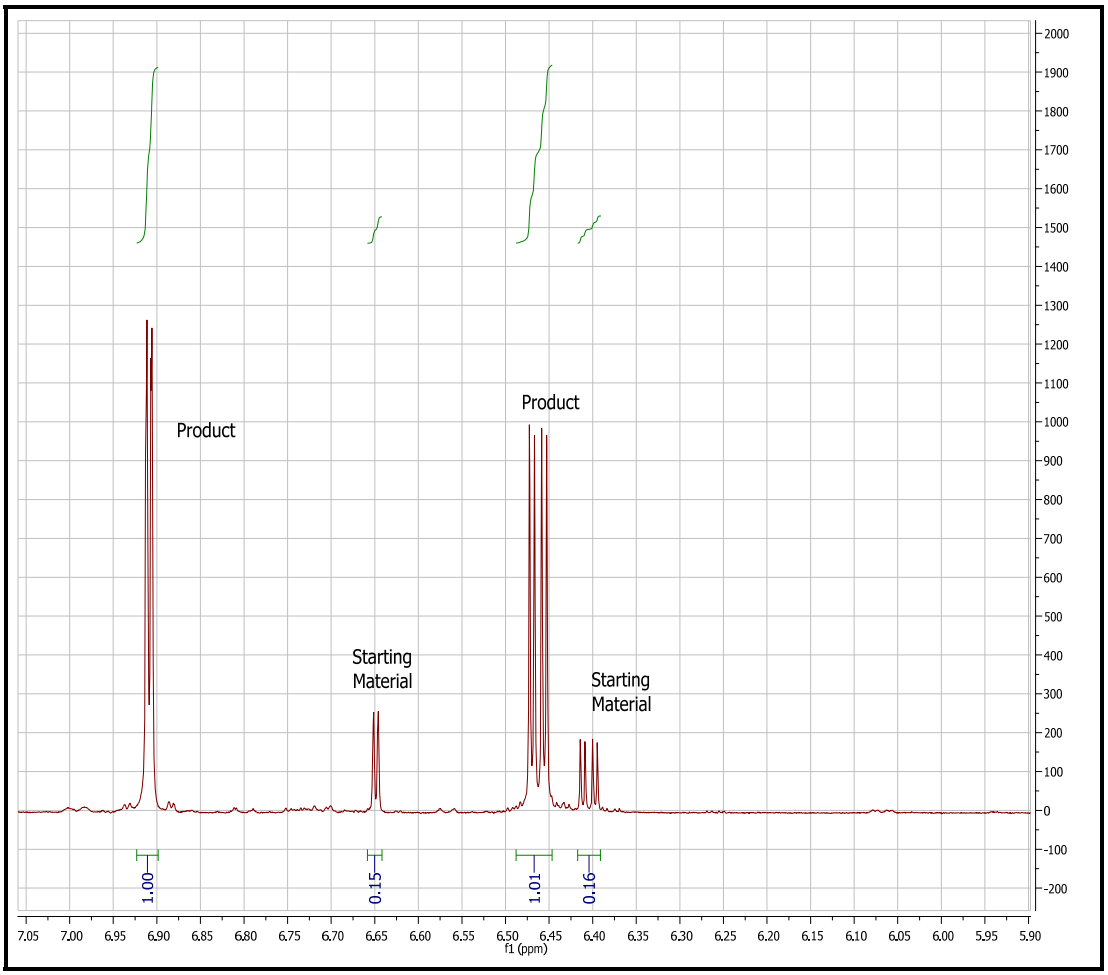

Figure 136 - Example NMR spectra: reaction of 4-amino-2-bromopyridine with phenylboronic acid under 2 atm CO_2 with 40% water, 24 h, after workup.

NMR spectra were used to determine amount of starting material and product in reaction mixtures after workup by comparison to standards of each compound. NMR Yields were calculated according to the following:

$$NMR\ Yield = \frac{I_{Prod.}}{I_{SM}+I_{Prod.}}$$

where $I_{prod.}$ and I_{SM} denote the area integrals of the product and substrate respectively.

4.5 References

1. Torborg, C.; Beller, M., Recent Applications of Palladium-Catalyzed Coupling Reactions in the Pharmaceutical, Agrochemical, and Fine Chemical Industries. *Advanced Synthesis & Catalysis* **2009,** *351* (18), 3027-3043.

2. Lusis; al., e. WO2013120852 A1, 2013.

3. Billingsley, K. L.; Anderson, K. W.; Buchwald, S. L., A highly active catalyst for Suzuki-Miyaura cross-coupling reactions of heteroaryl compounds. *Angew Chem Int Ed Engl* **2006,** *45* (21), 3484-8.

4. Miyaura, N.; Suzuki, A., Stereoselective Synthesis of Arylated (E) -Alkenes by the Reaction of Alk-1 -enylboranes with Aryl Halides in the Presence of Palladium Catalyst. *J Chem Soc Chem Commun* **1979**, 866.

5. Littke, A. F.; Fu, G. C., A Convenient and General Method for Pd-Catalyzed Suzuki Cross-Couplings of Aryl Chlorides and Arylboronic Acids. *Angew Chem Int Ed Engl* **1998,** *37* (24), 3387.

6. Miyaura, N.; Suzuki, A., Palladium-Catalyzed Cross-Coupling Reactions of Organoboron Compounds. *Chem Rev* **1995,** *95*, 2457-2483.

7. Fan, G. Z.; Duan, Z. X.; Wang, M., Suzuki Reaction Catalyzed by Pd(II) Anchored on Polymer in Supercritical Carbon Dioxide. *Advanced Materials Research* **2012,** *466-467*, 216-219.

8. Liu, C.; Ni, Q.; Bao, F.; Qiu, J., *Green Chemistry* **2011,** *13*, 1260.

9. Miyaura, N.; Yamada, K.; Suzuki, A., A NEW STEREOSPECIFIC CROSS-COUPLING BY THE PALLADIUM-CATALYZED REACTION OF 1-ALKENYLBORANES WITH 1-ALKENYL OR l-ALKYNYL HALIDES. *Tetrahedron Lett* **1979,** *36*, 3437-3440.

10. Kaga, H.; Ahmed, Z.; Gotoh, K.; Orito, K., New Access to Conjugated Dien- and Enamides. Synthesis of Dehydropipernonaline, Pipernonaline and Related Biologically Active Amides. *Synlett* **1994**, 607.

11. MARTIN, R.; BUCHWALD, S. L., Palladium-Catalyzed Suzuki-Miyaura Cross-Coupling Reactions Employing Dialkylbiaryl Phosphine Ligands. *Accounts Chem Res* **2008,** *41* (11), 1461-1473.

12. Amatore, C.; Jutand, A.; Duc, G. L., *Chem. Eur. J.* **2011,** *17*, 2492.

13. Miyaura, N.; Suzuki, A., Palladium-Catalyzed Cross-Coupling Reactions of Organoboron Compounds. *Chem Rev* **1995,** *95* (7), 2457-2483.

14. Barder, T. E.; Walker, S. D.; Martinelli, J. R.; Buchwald, S. L., Catalysts for Suzuki-Miyaura coupling processes: scope and studies of the effect of ligand structure. *J Am Chem Soc* **2005,** *127* (13), 4685-96.

15. Brown, J.; Cooley, N. A., <Brown JChemSOCChemComm 1988 1345.pdf>. *J. Chem. SOC., Chem. Commun.* **1988**, 1345-1347.

16. Gillie, A.; Stille, J. K., *J. Am. Chem. SOC.* **1980,** *102*, 4933.

17. Ozawa, F.; Hidaka, T.; Yamamoto, T.; Yamamoto, A., <Ozawa J Organomet Chem 1987 330 253.pdf>. *J. Organomet. Chem.* **1987,** *330*, 253-263.

18. Caron, S.; Massett, S.; Bogle, D.; Castaldi, M.; Braish, T., An Efficient and Cost-Effective Synthesis of 2-Phenyl-3-aminopyridine. *Org Proc R&D* **2001,** *5*, 254-256.

19. Miller, J. A.; Farrell, R. P., Preparation of Unsymmetrical Biaryls via Ni- or Pd-Catalyzed Coupling of Aryl Chlorides With Arylzincs. *Tetrahedron Lett* **1998,** *39*, 6441-6444.

20. Wagaw, S.; Buchwald, S. L., The Synthesis of Aminopyridines: A Method Employing Palladium-Catalyzed Carbon-Nitrogen Bond Formation. *J Org Chem* **1996,** *61*, 7240-7241.

21. Itoh, T.; Mase, T., Direct synthesis of hetero-biaryl compounds containing an unprotected NH2 group via Suzuki–Miyaura reaction. *Tetrahedron Lett* **2005,** *46* (20), 3573-3577.

22. Kudo, N.; Perseghini, M.; Fu, G. C., A versatile method for Suzuki cross-coupling reactions of nitrogen heterocycles. *Angew Chem Int Ed Engl* **2006,** *45* (8), 1282-4.

23. Walker, S. D.; Barder, T. E.; Martinelli, J. R.; Buchwald, S. L., A rationally designed universal catalyst for Suzuki-Miyaura coupling processes. *Angew Chem Int Ed Engl* **2004,** *43* (14), 1871-6.

24. Sigma-Aldrich http://www.sigmaaldrich.com/united-states.html.

25. Itoh, T.; Mase, T., Direct synthesis of hetero-biaryl compounds containing an unprotected NH2 group via Suzuki-Miyaura reaction. *Tetrahedron Lett* **2005,** *46* (20), 3573-3577.

26. Linnell, R. H., *J Org Chem* **1960,** *25*, 290.

27. SciFinder. Calculated using Advanced Chemistry Development (ACD/Labs) Software V11.02 (© 1994-2014 ACD/Labs). .

28. Wiberg, K. B., *Physical Organic Chemistry*. John Wily & Sons, Inc.: New York, 1966.

29. Swain, C. G.; William P. Langsdorf, J., Concerted Displacement Reactions. VI. rn- and p-Substituent Effects as Evidence for a Unity of Mechanism in Organic Halide Reactions1. *J Am Chem Soc* **1951,** *73*, 2813.

30. Hart, H.; Sedor, E. A., Mechanism of Cyclodehydration of 2-Phenyltriarylcarbinols. *J Am Chem Soc* **1967,** *89*, 2342.

CHAPTER 5

Conclusions and Recommendations

5.1 General Conclusions

The twelve green chemistry principles introduced in Chapter 1 have served as a guideline for the three industrially relevant projects presented herein. Each project was approached with the goal of designing a sustainable solution that is both economically and environmentally sound. My conclusions and recommendations for each project are presented here.

5.2 Degradation and Stabilization of Polyvinylchloride: Integrating Model and Bulk Polymer Studies

5.2.1 Conclusions

We have developed a library of 6 model compounds which incorporate various regio- and stereochemical chlorine arrangements to represent micro-structures present in bulk PVC polymer. The models were utilized neat, as both solvent and reactant to mimic the industrial conditions. The kinetics of each model was determined for the reaction with sodium acetate and PTC to analyze the effects of the "naked" acetate ion on our system. With the small, strongly nucleophilic "naked" acetate ion substitution of the chlorine was the dominant pathway observed with the model compounds.

Isotactic PVC models demonstrated increased reactivity (k_{pseudo}: $9.99 \cdot 10^{-4}$ min^{-1}) compared to syndiotactic models (k_{pseudo}: $3.56 \cdot 10^{-4}$ min^{-1}) of PVC, due to sterics. While

vicinal defects were determined to have minimal participation in the stabilization or degradation of PVC due to low reactivity (meso k_{pseudo}: $2.25 \cdot 10^{-4}$ min^{-1}; enantiomeric k_{pseudo}: $0.40 \cdot 10^{-4}$ min^{-1}), allylic (k_{pseudo}: $27.8 \cdot 10^{-4}$ min^{-1}) and tertiary (S_N1 elimination, k_{pseudo}: $3.91 \cdot 10^{-4}$ min^{-1}) defects are "labile" chlorines where degradation is likely to begin.

Product distribution from the reaction of model acetates and PTC with the model comopunds suggests that sterics strongly effect which pathway dominates: substitution versus elimination. The "defect-free" model, 2,4-dichloropentane displayed mainly substitution products (4-chloropentan-2-yl acetate and pentan-2,4-diyl acetate), as did the models for vicinal (4-chlorohexan-3-yl acetate and hexan-3,4-diyl acetate) and allylic defects (but-3-en-2-yl acetate). However, as the sterics of the model were increased, as for the longer allylic model ((*E*)-6-Chloronon-4-ene) and the tertiary model (3-chloro-3-ethylpentane) mainly elimination products were observed. As the models approach the steric hindrance seen in PVC due to length (the allylic model) or due to branching (tertiary model) we observe that sterics begin to promote the elimination of chlorines over substitution. Similar observations were made for $ZnSt_2$ and $CaSt_2$ with 2,4-dichloropentane, where substitution products were not observed. GC-MS analysis of the headspace of the reaction provided evidence for the formation of elimination products. Many peaks corresponding to cationic forms of 2,4-pentadiene were observed.

This is supported by the observed degradation of both 2,4-dichloropentane with $ZnSt_2$ and DIDP-plasticized PVC blended with $ZnSt_2$. The thermograph of $ZnSt_2$ and plasticized PVC demonstrates a period of good stabilization (<0.1% weight loss) of about 10 minutes, after which a catastrophic weight loss occurs which is similar to the thermograph resultant from the blend of $ZnCl_2$ and plasticized PVC. Similar color stability was witnessed for $ZnSt_2$ and $ZnCl_2$ in 2,4-dichloropentane. However, both color stability and thermal stability are increased in blends which include both $CaSt_2$ and $ZnSt_2$.

The information obtained from model kinetic and color change studies combined with that obtained from color change and weight-loss studies with the bulk PVC polymer

led to a proposed mechanism of PVC degradation and subsequent stabilization by $ZnSt_2$. We suggest that $ZnSt_2$ acts as an HCl sink to prevent auto-catalyzed degradation of PVC and $CaSt_2$ is necessary to prevent build-up of $ZnCl_2$, a much stronger Lewis acid which promotes degradation of PVC. The dominance of the elimination pathway in the more sterically hindered systems supports this hypothesis.

5.2.2 Recommendations

There are some areas which would benefit from further study. As mentioned in Chapter 2, the model compounds we investigated displayed a shift in mechanism from substitution to elimination as the model compounds and/or model stearates increased in size and/or sterics. It would therefore be interesting to observe the reactions of the zinc and calcium stearates with model compounds which are increasingly similar to PVC polymer. I suggest synthesizing and investigating the following model compounds (Table 42) which would have the potential to confirm our hypothesis. Analysis of the kinetics of substitution or elimination of these model compounds with 1) model stearates and PTC, and 2) metal stearates could provide further insight into the effect of sterics on the mechanisms of stabilization and degradation in the bulk PVC system. The models I propose will still be small enough that conventional analyses such as GC-FID could be utilized to observe the reaction kinetics with model acetates, and NMR could potentially still be utilized to observe the reaction kinetics with zinc and calcium acetates. Additionally, I have not found evidence in literature of the use of the latter two models for PVC models. They would therefore represent the potential for to increase the impact of this investigation in the field of PVC kinetics as well as potentially adding further support to the proposed mechanism. However, all three will need to be synthesized on a large scale (~100 g) for use in the kinetics studies.

Table 42- Proposed PVC model compounds for further study.

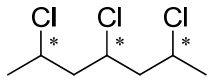 2,4,6-trichloroheptane
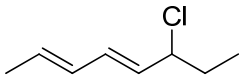 (2*E*,4*E*)-6-chloroocta-2,4-diene
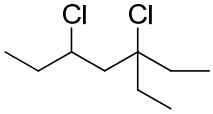 3,5-dichloro-3-ethylheptane

Generally, the main added feature offered by these three models is increased sterics which more closely mimics the bulk PVC system. 2,4,6-Trichloroheptane displays increased sterics compared to 2,4-dichloropentane due to the increased length of the model compounds. Also, the addition of a third chlorine to the backbone would provide the opportunity to study the relative rates of substitution or elimination for isotactic, syndiotactic, and atactic regions, which we have not had the opportunity to observe in previous model compounds. The allylic model (2E,4E)-6-chloroocta-2,4-diene could provide information as to the effect of increased conjugation on the rate of substitution or elimination, as well which interaction is preferred under increased sterics. Finally, 3,5-dichloro-2-ethylheptane displays increased sterics as compared to 3-chloro-3-ethylpentane, as well as the opportunity to observe the relative rates of substitution or elimination of secondary and tertiary chlorines.

I have proposed a synthesis for 3,5-dichloro-3-ethylheptane (Figure 137), though I did not pursue it due to time constraints and the discovery of the simpler synthesis of 3-chloro-3-ethylpentane. Esterification of 3-hexenedioic acid to produce dimethyl trans-3-

hexenedioate and subsequent ozonolysis is predicted to give two equivalents of methyl 3-oxopropanoate based on analogous reactions.[1-2] The intermediate 3-oxo ester would prove difficult to isolate. Similar 3-oxo esters have proven unstable, as such methyl 3-oxopropanoate should be reacted with ethylmagnesium bromide directly to yield 3-ethyl-heptane-3,5-diol.[3] Reaction of the diol with $SOCl_2$, similar to the formation of 2,4-dichloropentane from 2,4-pentanediol, is predicted to yield the desired 3,5-dichloro-3-ethylheptane.

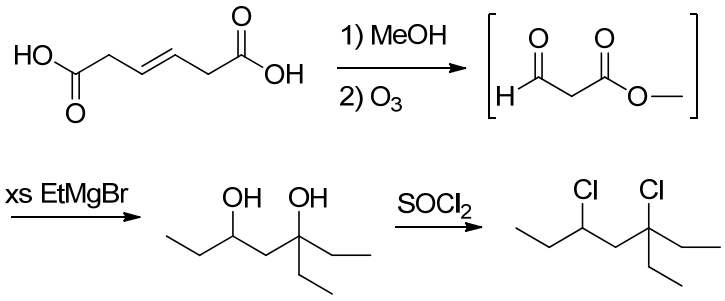

Figure 137 - Proposed synthesis of 3,5-dichloro-3-ethylheptane.

There are literature precedents for the synthesis of 2,4,6-trichloroheptane (Figure 138).[4] The example below utilizes addition of HCl across the double bonds of hepta-1,6-dien-4-ol to yield 45% of 2,6-dichloroheptan-4-ol, followed by chlorination utilizing thionyl chloride in DMF to yield 2,4,6-trichloroheptane in 47% yield.

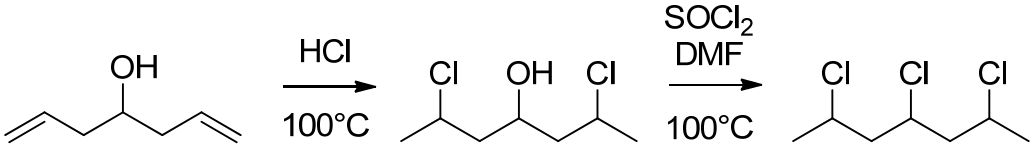

Figure 138 - Literature synthesis of 2,4,6-trichloroheptane.

Synthesis of (2E,4E)-6-chloronona-2,4-diene can be achieved in a similar manner as (*E*)-6-Chloronon-4-ene through the Grignard reaction of nPrMgBr with commercially available (2E,4E)-hexa-2,4-dienal followed by chlorination with phosphorous trichloride.

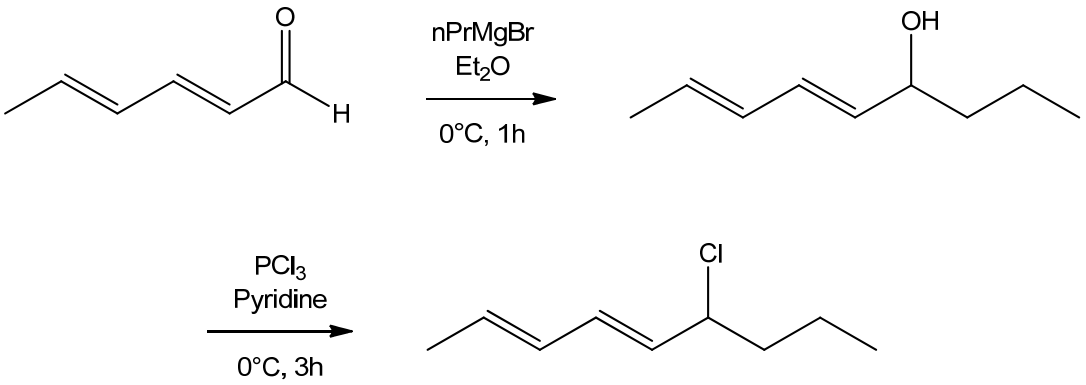

Figure 139 - Proposed synthesis of (2E,4E)-6-chloronona-2,4-diene.

Should the synthesis of the model compounds prove facile, the knowledge gained could prove pivotal for confirming the mechanism of degradation and stabilization that we propose. However, these syntheses are complex, and the literature synthesis of 2,4,6-trichloroheptane are low yielding. If time and money are not available, the effort involved would be prohibitive.

5.3 Design, Synthesis and Evaluation of Nonaqueous Silylamines for Efficient CO_2 Capture

5.3.1 Conclusions

Iterative structural modifications of 3-(aminopropyl)triethylsilane (TEtSA) were utilized to establish structure-property relationships through which CO_2 capture solvents can be designed to meet industrial specifications. Thirteen silylamines were designed and synthesized to determine the effects of Si-NH_2 proximity, branching, unsaturation, and

amine order upon industrially relevant properties (CO_2 uptake capacity, viscosity, enthalpy of regeneration and reversal temperature). We have demonstrated that we can design CO_2 capture solvents that achieve a competitive CO_2 uptake of, on average, 0.59 moles CO_2 per mole of amine while minimizing viscosity and energy of reversal. In fact, the amines demonstrate an enhanced maximum capacity of 0.67 moles CO_2 per mole amine. This is due to the formation of stabilized carbamate-carbamic acid species.

Several important conclusions were derived from our work as to the effect of structure on the relevant properties. Reversal temperature and enthalpy of regeneration may be reduced by varying the order of the amine or introducing branching alpha to the amine to increase steric hindrance. Viscosity of the RevIL is heavily influenced by silylamine structure. Additionally, the viscosity can be controlled by limiting conversion (CO_2) uptake, which is unique to switchable solvent systems such as ours, unlike traditional or functionalize ionic liquids. In combination with the effect of temperature some amines demonstrate RevIL viscosities which are industrially viable (<100 cP). Two silylamines, TEtSMA and *trans*-TEtSA, have been recommended for further studies based on the properties they displayed, as outlined in Table 43. Both demonstrate high CO_2 uptake capacities, viable reversal temperatures, and reasonable enthalpies of regeneration. Their viscosities are lower than the other amines studied and can be further reduced by controlling CO_2 uptake to meet industry-operating specifications.

Table 43 – Summary of the properties of TEtSMA and *trans*-TEtSA

Property	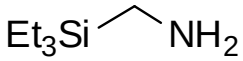 **TEtSMA**	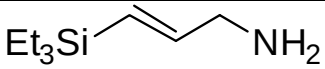 ***trans*-TEtSA**
CO_2 Uptake (mol CO_2/mol amine, 25°C)	0.59 ± 0.01	0.61 ± 0.03
CO_2 Uptake (mol CO_2/kg amine, 25°C)	4.09 ± 0.08	3.56 ± 0.20
Reversal Temperature (°C)	78 ± 5	48 ± 2
Enthalpy of Regeneration ($kJ \cdot molCO_2^{-1}$)	76 ± 7	85 ± 7
RevIL Viscosity at 25°C (cP)	2373 ± 206	3889 ± 252
RevIL Viscosity at 40°C (cP)	625 ± 58	362 ± 19

5.3.2 Recommendations

However, again, some areas would benefit from further study. For one, the synthesis of the two amines recommended for further study (Table 43) would need to be optimized before industrial implementation could be considered. Also, the reversal temperature of *trans*-TEtSA (48°C) would not be industrially viable, as CO_2 capture would likely be conducted at ~40°C. To increase the reversal temperature slightly, a dimethyl-ethyl substitution as was observed with DMESA about the silicon could be utilized. Though DMESA did form a solid upon reaction with CO_2, in combination with unsaturation on the backbone, which demonstrated significantly low viscosities in certain amines, solid formation could potentially be prevented. Formation of *trans*-3-

(dimethylethylsilyl)prop-2-en-1-amine could be achieved via hydrosilylation of dimethylethylsilane and propargylamine (Figure 140).

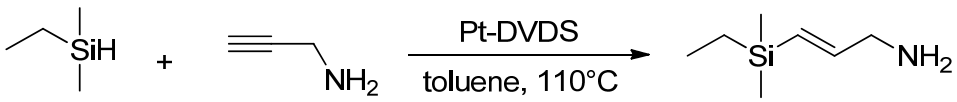

Figure 140 - Proposed synthesis of *trans*-3-(dimethylethylsilyl)prop-2-en-1-amine.

Additionally, flue gas contains a small percentage of water and the effect of this water on the non-aqueous design of the RevIL system should be investigated. A good starting point would be the article Brennecke et al. recently published on the interaction of ionic liquids with water.[5] Though ionic liquids are salts, and intuitively should be soluble with water, this is not true in practice. The self-aggregation of the ionic species limits dissolution of the ionic liquid in water. Thus, water solubility in ionic liquids would not be a straight forward determination. However, the inclusion of water would likely result in the formation of ammonium-bicarbonates over ammonium-carbamates, an entirely different system. This could prove beneficial in increasing CO_2 capacities and reducing viscosities, even at low percentages of water. However, the addition of even a small amount could result in additional energy penalties in the reversal process.

Finally, the reversible ionic liquid system developed has the potential for many alternate applications. Thesis by my coworkers Emily Nixon and Amy Ethier discuss their application in nanoparticle synthesis.[6-7] My thesis discusses only low pressure CO_2 applications, however Amy Ethier utilized a sapphire cell to observe the effects of increased CO_2 pressure by ATR-FTIR at pressures up to 70 bar. Physical absorption begins to play a larger part in capacity at higher pressures.[6] These studies in conjunction with the structure-property relationships described in Chapter 3 could prove a good

starting point for developing solvents for CO_2 separation from methane. Other high-pressure applications may also exist for these RevILs.

5.4 Effect of CO_2 Pressure and pH on the Suzuki Coupling of Basic, Nitrogen Containing Substrates

5.4.1 Conclusions

Utilizing increased water content (40%) and CO_2 pressure we were able to design an efficient and simple system for the Suzuki coupling of 4-amino-2-halopyridines in quantitative yields, without the use of added ligand or protection/deprotection strategies. Our investigations uncovered a substrate dependent optimum pH which is likely due to the acid-base properties of the 4-amino-2-halopyridine and 2-halopyridine substrates. 2-Halopyridines couple in quantitative yields at a pH of ~12. 4-Amino-2-halopyridines couple in quantitative yields at a pH of ~8. A small (~0.01%), steady-state amount of the activated (protonated) 4-amino-2-halopyridine is produced at a pH of 8, promoting the coupling reaction. The rate profiles of the 4-amino-2-halopyridines and 2-halopyridines under the different conditions support this conclusion.

Additionally, a Hammett plot study was conducted of various 4- and 5-substituted-2-bromopyridines. The 5-substituted-2-bromopyridines displayed convex (upward curved) Hammett plots for each parameter (meta/para electronic effects and pK_a) which is typically linked to a change in mechanism. The apex of the curve is at the reference 2-bromopyridine for each electronic parameter, suggesting that the different electronics of the amines (donating vs. withdrawing) are the parameters effecting this change in mechanism. Interestingly, the 4-substituted-2-bromopyridines display the same trends except for 4-amino-2-bromopyridine. This amine appears to either be an outlier or to require a different rate-determining step from the other amines substituted with a

donating group. At this point the exact mechanisms remain unknown and further work would be required to complete this mechanistic study.

5.4.2 Recommendations

The original goal of developing an efficient and sustainable method of coupling basic, nitrogen substrates has been met. However, the substrate dependent optimum pH for efficient coupling is not yet fully understood. I propose the following experiments to provide further insight into this phenomenon.

Though I have briefly discussed our initial investigation of the Suzuki coupling of acetyl protected 4-amino-2-bromopyridine, our results were puzzling. An alternative method would be to synthesize 2-bromo-N,N,N-trimethylpyridin-4-aminium - from 4-(N,N-dimethylamino)-2-bromopyridine with methyliodide (Figure 141), based on an analogous literature procedure[8] – and couple it with phenylboronic acid under the same conditions as decribed for the acetyl protected aminopyridine (Figure 142). The trimethylammonium structure more closely mimics our proposed "activated" amine that is formed from 4-amino-2-bromopyridine at a pH of 8. The information obtained through the Suzuki coupling of this amine could provide support for our hypothesis.

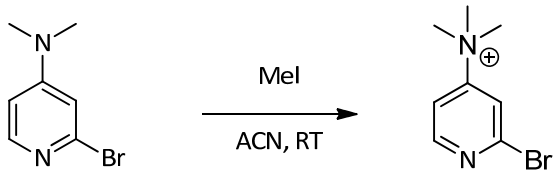

Figure 141 – Proposed synthesis of 2-bromo-N,N,N-trimethylpyridin-4-aminium.

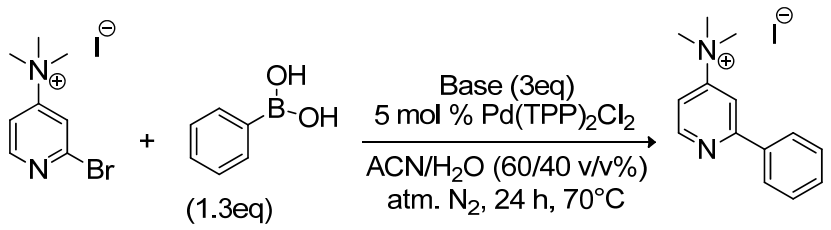

Figure 142 - Proposed couplding of trimethylammonium version of 4-amino-2-bromopyridine.

Determining the reason for the decrease in rates of reaction over time could prove pivotal in understanding the mechanism involved. As demonstrated, the rates of reaction for all four substrates (under the optimum pH) display initial high rates of reaction which quickly level off. This could be due to a number of factors including catalyst degradation or the consumption of a vital, limited reactant such as trace amounts of oxygen.

The use of Phosphorous NMR to track the state of the catalyst during reactions is well documented. Utilization of this analysis in the couplings of 4-amino-2-halopyridines and 2-halopyridines with phenylboronic acids under different pH could provide insight into the state of the catalyst for our specific reactions. Initial attempts were made in our group to do this but the results were not promising. However, this is possibly due to the lack of a set procedure, which would need to be defined in order to ensure accurate results. Ideally, the state of catalyst at pH of 8 and 13 should be compared for all 4 substrates.

Though oxygen is sometimes considered detrimental to the reaction, and our system utilized degassed solvents to great effect (yields of ~100% for all 4 substrates at optimum pH), there are examples of reactions which proceed well under oxygen rich atmospheres (>98% yield of a variety of para-substituted bromobenzenes in water, $PdCl_2$ or $Pd(OAc)_2$, K_2CO_3 and additives).[9-10] Conducting reactions under an oxygen atmosphere could provide insight into the possible role of trace amounts of oxygen.

Investigating the applicability of this system in alternative organic/aqueous systems could also prove interesting. Would we still observe the same substrate

dependent optimum pH? Or is this phenomenon system dependent? I would propose investigating organic/aqueous solvent systems incorporating THF, toluene, or ethyl acetate to begin. These systems will display different solvent properties, including dielectric constants which will modify partitioning of the substrates, while maintaining a biphasic organic/aqueous system.

Additionally, the yields presented in the Hammett plot studies are based on the areas of the product and starting material from the GC-FID chromatograms. Calibration curves should be created for each product and starting material to cement the validity of the observations I have reported. Also, investigating additional substrates should be investigated to fill in gaps in the Hammett Plots. I have provided a few options for substrates which would fill in the gaps in Table 44 and Table 45. Depending on the price and availability of these substrates, a few could be strategically chosen to finish this investigation.

Table 44 - Proposed substrates to complete Hammett Plot of 5-susbtituted-2-bromopyridines.

5-position			
R	**σ_{meta}**	**σ_{para}**	**pK_a**
CN	0.56	0.66	-2.66
CHO	0.35	0.42	-1.01
$COCH_3$	0.38	0.5	-1.01

Table 45 - Proposed substrates to complete Hammett Plot of 4-susbtituted-2-bromopyridines.

4-position			
R	**σ_{meta}**	**σ_{para}**	**pK_a**
CN	0.56	0.66	-2.56
CHO	0.35	0.42	-1.18
$COCH_3$	0.38	0.5	-0.91
$N(CH_3)_2$	-0.15	-0.83	5.03
OH	-0.37	0.12	7.94

Additionally, further investigation into the mechanism of the Suzuki reaction could be valuable in cementing a firm understanding of the cause behind the substrate dependent optimum pH. Indeed, the mechanisms of many transition-metal catalyzed carbon-carbon couplings are still not fully understood. Unlocking the secret to the mechanism of the Suzuki reaction could pave the way towards understanding all of them. This is a lofty goal, however if the time and funding were readily available the results could provide invaluable insight into the field of transition metal catalyzed cross-coupling reactions. The work I present on the effect of substituents and the resultant Hammett plots could be a good starting point towards further mechanistic studies.

5.5 References

1. Chio, F. K.; Warne, J.; Gough, D.; Penny, M.; Green, S.; Coles, S. J.; Hursthouse, M. B.; Jones, P.; Hassall, L.; McGuire, T. M.; Dobbs, A. P., On the choice of Lewis acids for the Prins reaction; two total syntheses of (±)-Civet. *Tetrahedron* **2011,** *67* (27-28), 5107-5124.

2. Dinh, M.-T.; Bouzbouz, S.; Péglion, J.-L.; Cossy, J., Synthetic efforts toward the synthesis of octalactins. *Tetrahedron* **2008,** *64* (24), 5703-5710.

3. Trincone, A.; Pagnotta, E.; Sodano, G., CHEMOENZYMATIC SYNTHESIS AND STEREOCHEMISTRY OF ALEPPOTRIOLOSIDE, A NATURALLY OCCURRING GLUCOSIDE. *Tet. Letters* **1994,** *35* (9), 1415-1416.

4. Schilling, F. C.; Schilling, M. L., Convenient Synthesis of 2,4,6-Trichloroheptane, the Trimer Model of Poly(vinyl chloride). *Macromolecules* **1988,** *21*, 1530-1532.

5. Ficke, L. E.; Brennecke, J. F., *Journal of Physical Chemistry B* **2010,** *114*, 10496.

6. Ethier, A. APPLICATIONS OF REVERSIBLE AND SUSTAINABLE AMINE-BASED CHEMISTRIES: CARBON DIOXIDE CAPTURE, *IN SITU* AMINE PROTECTION AND NANOPARTICLE SYNTHESIS. Georgia Institute of Technology, Atlanta, GA, 2013.

7. Nixon, E. SILANES IN SUSTAINABLE PROCESSES: APPLICATIONS IN POLYMER GRAFTING, CARBON DIOXIDE CAPTURE, AND GOLD NANOPARTICLE SYNTHESIS. Georgia Institute of Technology, Atlanta, GA, 2012.

8. Ortega, *Organic & Biomolecular Chemistry* **2008,** *6* (18), 3264.

9. Mondal, M.; Bora, U., An efficient protocol for palladium-catalyzed ligand-free Suzuki-Miyaura coupling in water. *Green Chemistry* **Accepted For Publication**.

10. Liu, C.; Ni, Q.; Bao, F.; Qiu, J., *Green Chemistry* **2011,** *13*, 1260.

APPENDIX A

Epoxidized Linolenic Acid Salts for Color and Thermal Stability of ESO-Plasticized PVC

A.1 Introduction

As discussed in Chapter 2, plasticizers are utilized in PVC formulations to modulate properties of the bulk polymer, specifically the flexibility, workability and distensibility. Formulations contain up to 30-45 parts per hundred resin (phr) of plasticizers such as phthalates, which are common due to their compatibility with the polar functionality of PVC. Bio-based alternatives such as epoxidized soybean oil (ESO) have been applied to recent commercial formulations. The epoxide rings of ESO assist in the solubility of ESO in PVC, however they are prone to attack from HCl released during thermal degradation of the polymer.[1-2] This can be advantageous, in that it has been shown to stabilize PVC formulations, including in combinations with metal stearates.[1, 3-6] It can also be disadvantageous; as the epoxides are converted to chlorohydrins, the compatibility of ESO with PVC changes. This can decrease ESO's ability to plasticize the polymer. [1-2] At lower temperatures polymer migration is actually far more dominant than dehydrochlorination and effects PVC performance on a larger scale, so plasticizer maintenance is crucial.

While previous studies have examined ESO's synergistic effect with metal stearates for thermal stabilization they have not addressed its role as plasticizer. Herein, we have developed sacrificial epoxidized linolenic acid metal salts as alternatives to traditional metal stearate stabilizers. The sacrificial stabilizers include both epoxide

functionalities to react with liberated HCl in the place of ESO, and metal carboxylates to absorb HCl in a fashion similar to $ZnSt_2$/$CaSt_2$. This provides a potentially significant advantage over traditional metal stearates. The zinc and calcium salts of epoxidized linolenic acid were synthesized and analyzed for their ability to stabilize blends of DIDP- and ESO-plasticized PVC. The ring-opening kinetics of cyclic and linear epoxides were also investigated to obtain additional information for the design of future thermal additives for PVC stabilization.

A.2 Results and Discussion

Novel stabilizers were designed containing the carboxylate of zinc and calcium stearates and the epoxide functionality of ESO to act as sacrificial stabilizers to protect ESO. Epoxide salts ZnEp and CaEp were synthesized in two steps from linolenic acid (Figure 143). The thermal and color stability of blends featuring the novel additives were then explored. Mixtures of PVC, 30 phr plasticizer (DIDP or ESO) and 5 phr stabilizer(s) ($CaSt_2$, $ZnSt_2$, ZnEp, and CaEp) were blended and analyzed via thermographic analysis (TGA) at 170°C for 2 hours to determine the thermal stability. Similar to the studies reported in Chapter 2, the temperature, 170°C, was chosen to simulate degradation occurring over months and years in an experimentally viable time period. Qualitatively, color stability was observed as function of additives from the color change of the blends after heating. The rate of epoxide ring opening was also observed for model epoxides with hydrochloric acid (HCl) by ^{1}H NMR.

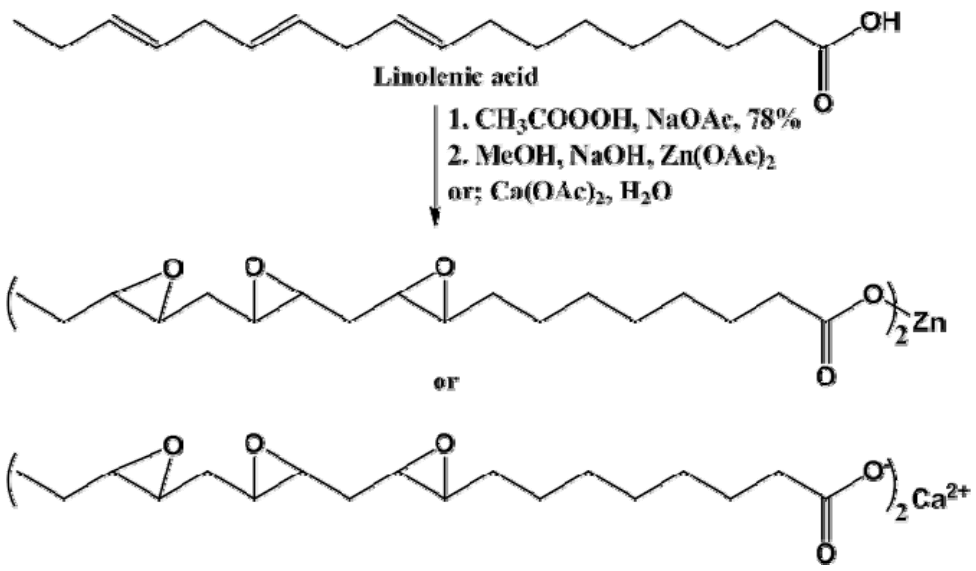

Figure 143 - Synthesis of ZnEp and CaEp from linolenic acid.

A.2.1 Thermal Stability of Plasticized PVC

To establish a baseline, the thermal stability of neat PVC, PVC blended with diisodecylphthalate (DIDP), and PVC blended with epoxidized soybean oil (ESO) were analyzed by TGA (Figure 144). Neat PVC shows minimal weight loss of less than 1% over 2 hours. DIDP-plasticized PVC displays less thermal stability than neat PVC, losing almost 6% over 2 hours. DIDP was analyzed by TGA in a control experiment and accounted for only 0.027% of the loss observed, which does not account for the difference between DIDP-plasticized PVC and neat PVC. We hypothesize that the increased movement of PVC chains due to plasticization facilitated the escape of HCl.

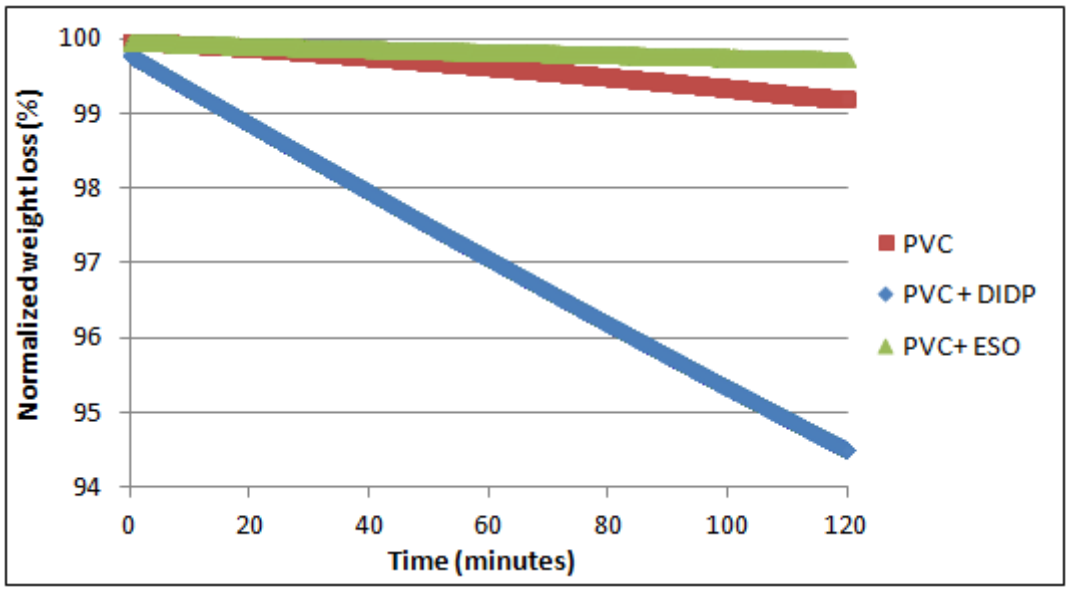

Figure 144 - Weight loss at 170°C over 2 hours for PVC of PVC and plasticizer blends; weight normalized against the mass of PVC in each blend.

Interestingly, blends of ESO and PVC showed less weight loss after 2 hours than neat PVC. This is due to the reaction of HCl with the epoxides of ESO to form chlorohydrins (Figure 145). The oxirane rings are able to scavenge HCl at a rate faster than the liberation of HCl from the PVC backbone. As ESO is only present in 30 phr there would be a point at which all oxirane rings have reacted, though this is not represented in Figure 145. This reaction, however, is what leads to the reduced plasticization performance of ESO. The sacrificial epoxide stabilizers were developed to prevent this from occurring.

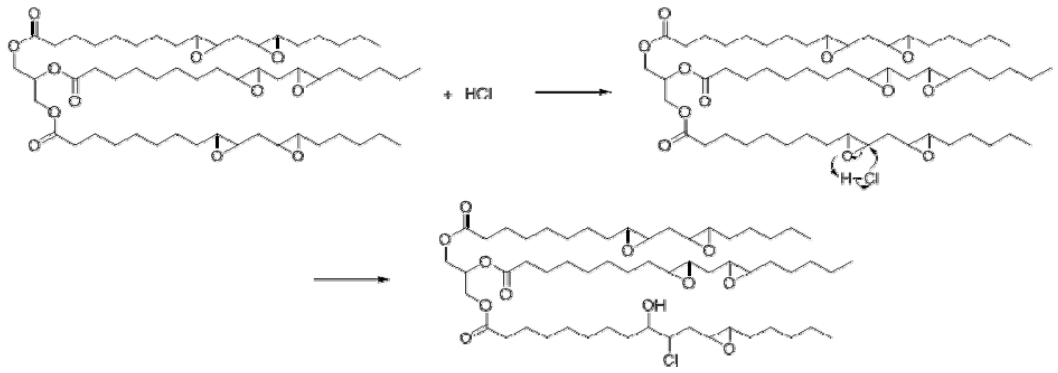

Figure 145 - Chlorohydrin formation by ESO scavenging of HCl.

The color stability of the blends was also observed and examples are displayed in Figure 146Neat PVC is originally a white powder, and plasticized blends maintain the light coloring initially. Though difficult to see due to image quality, ESO- plasticized PVC displayed the best color stability, maintaining areas of lighter color. Both PVC and DIDP-plasticized PVC, however, displayed poor color stability forming dark brown/black powders after reaction. This information is used as a baseline for the reactions with stabilizers.

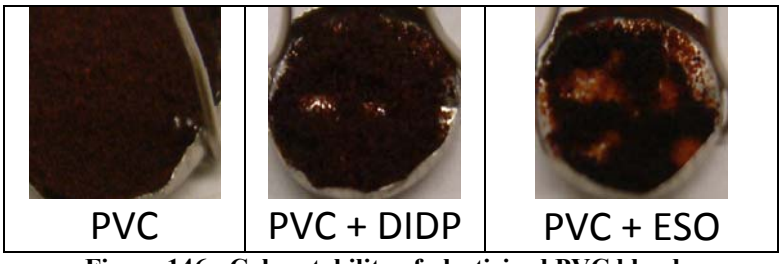

Figure 146 - Color stability of plasticized PVC blends.

A.2.2 Thermal and Color Stabilities of DIDP-Plasticized PVC Blends with ZnEp and CaEp

Thermal and color stabilities were compared for blends of DIDP-plasticized PVC and stabilizers: $ZnSt_2$ and/or $CaSt_2$ versus ZnEp and/or CaEp (Figure 147). Almost all blends with novel stabilizer exhibited improved weight loss as compared to its metal stearate analog. As discussed in Chapter 2, $ZnSt_2$ showed initial stability followed by drastic weight loss, resulting in 30% mass lost after 2 hours. ZnEp maintained a moderate stability, and displayed no sign of drastic weight loss, losing only 15% after 2 hours. The $CaSt_2$ blends resulted in a loss of approximately 7% after 2 hours, and CaEp resulted in a similar loss. The combination of $CaSt_2$ and $ZnSt_2$ in 1:1 ratio resulted in a 10% loss over 2 hours. The combination of ZnEp and CaEp (1:1) lost only 7% after 2 hours, an increased stability compared to both the combination of $CaSt_2$ and $ZnSt_2$ as well as ZnEp on its own. This shows that a) ZnEp is likely acting similarly to $ZnSt_2$ in absorbing HCl to form $ZnCl_2$; b) the combination of CaEp and ZnEp successfully prevents the buildiup of $ZnCl_2$ and displays the best thermal stability; and c) the increased performance of ZnEp and the blend of ZnEp/CaEp confirmed the beneficial effects of the epoxides in absorbing HCl.

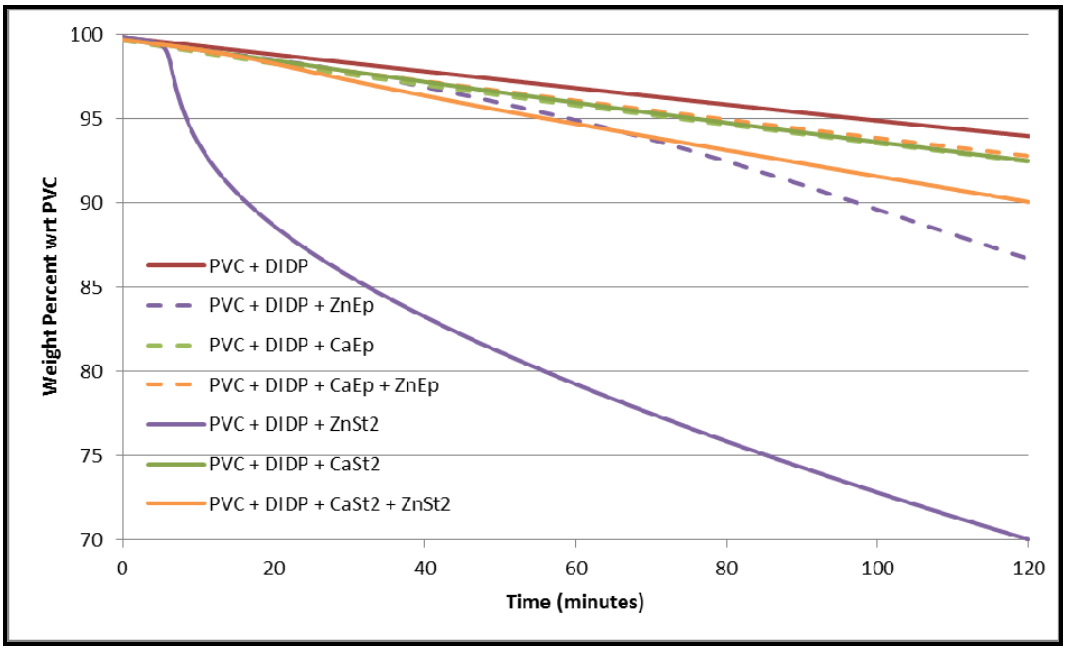

Figure 147 - Weight loss of DIDP-plasticized PVC blends incorporating novel epoxide stabilizers during the heat treatment and degradation process at 170°C; weight normalized against the mass of PVC in each blend.

Examples of the color stability displayed by synergistic blends of zinc and calcium stabilizers are displayed in Figure 148. As detailed in Chapter 2, blends of zinc or calcium stearates displayed poor color stability on their own, similar to DIDP-plasticized PVC. The blend including both $ZnSt_2$ and $CaSt_2$ showed better color stability compared to DIDP-plasticized PVC. However, the difference between the metal stearates and the blend with both ZnEp and CaEp is drastic. The ZnEp/CaEp blend showed significantly increased color stability, with only specks of black powder visible in an otherwise orange/red powder. Though the weight loss and color stability are not ideal for industry, they are vastly improved for the ZnEp and CaEp stabilizers.

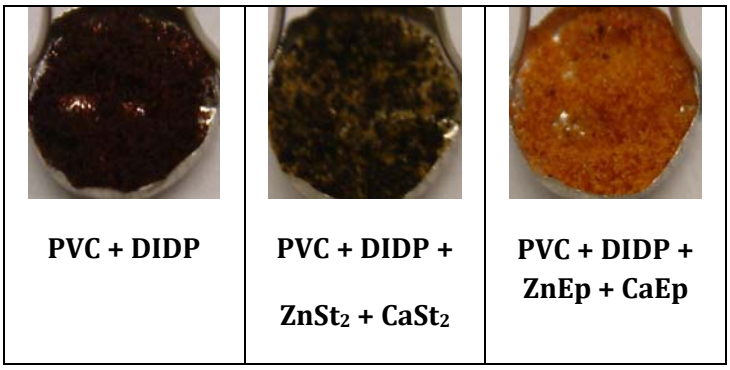

Figure 148 - Color comparison of DIDP-plasticized PVC blends incorporating novel epoxide stabilizers after thermal treatment (2 hours, 170°C).

A.2.3 Thermal and Color Stabilities of ESO-Plasticized PVC with ZnEp and CaEp

Though the thermal stability of ESO-plasticized PVC (Figure 149) was greater than neat PVC, the color stability (Figure 150) was poor and leaves plenty of room for improvement. As in the blend of DIDP-plasticized PVC with $ZnSt_2$, ESO-plasticized PVC blended with $ZnSt_2$ displayed an initial period of stability followed by drastic weight loss. However, this drastic change occurs almost two hours later than in the first case. Also, after two hours, the overall weight loss of this blend was only 1% instead of 30%. It appears the rate of dehydrochlorination and subsequent reaction of HCl with ESO is faster than chloride abstraction by $ZnSt_2$, which delayed the formation of $ZnCl_2$. ESO-plasticized PVC blended with ZnEp did not display any drastic weight loss, maintaining stability over the two hours and losing less than 0.5% of the initial weight of PVC. Interestingly, the blend of ESO-plasticized PVC and ZnEp showed the best weight loss for all blends incorporating a stabilizer. CaEp blends actually displayed the worst stability with around 0.8% mass lost, slightly less than the blends with $CaSt_2$. The blends of both calcium and zinc salts display similar weight losses of approximately 0.5% for

both stearates and epoxidized salts. These results were unexpected but were mirrored by the color stability results.

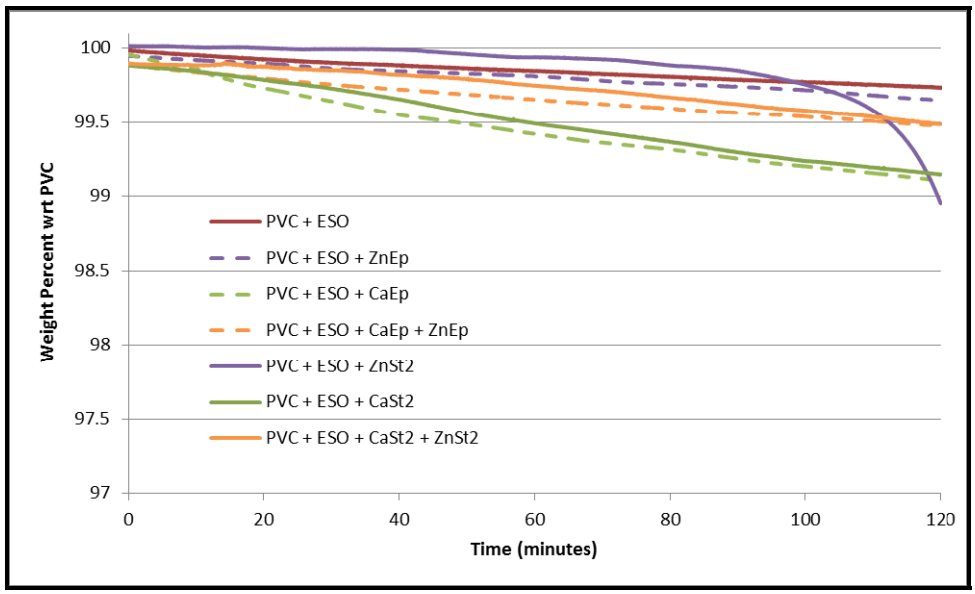

Figure 149 - Weight loss of ESO-plasticized PVC blends incorporating novel epoxide stabilizers during the heat treatment and degradation process at 170°C; weight normalized against the mass of PVC in each blend.

ESO-plasticized PVC (Figure 150), PVC, and ESO-plasticized PVC plus $CaSt_2$ show similar color stability. Blends of plasticized PVC with $ZnSt_2$ or a combination of $ZnSt_2$ and $CaSt_2$ displayed similarly excellent color stability. The $ZnSt_2$ blend, however, still resulted in a drastic weight loss after 2 hours, which is undesirable. The blend of ZnEp and CaEp showed slightly poorer color stability, while the blend with ZnEp displayed the best color stability. It is unknown at this point why ZnEp on its own displays the best color and thermal stability.

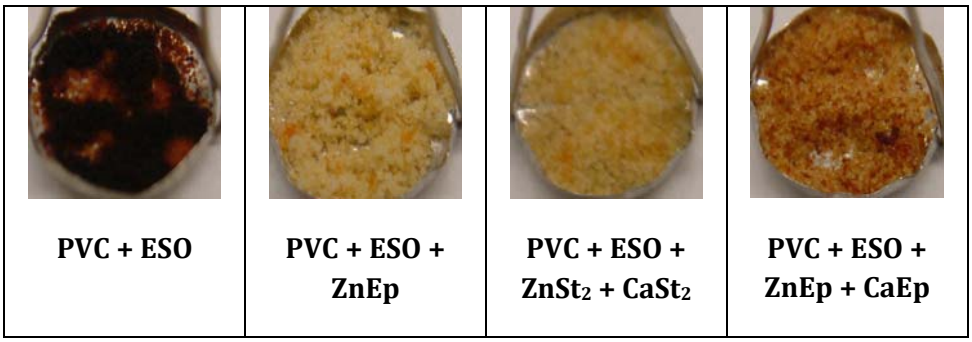

Figure 150 - Color comparison of ESO-plasticized PVC blends incorporating novel epoxide stabilizers after thermal treatment (2 hours, 170°C).

A.2.4 Epoxide Ring Opening Studies

In order to develop an improved form of our sacrificial epoxidized stabilizer which will react with HCl faster than the epoxides of ESO, we investigated the rates of chlorohydrin formation for cyclic and linear epoxides. A solution of HCl in *ortho*-dichlorobenzene (o-DCB) was formed by bubbling o-DCB with HCl for approximately three minutes. The final concentration of HCl in solution was determined gravimetrically. Epoxide was then added to the solution in ratios of 1:1 or 20:1 (epoxide:HCl). The solutions were stirred at room temperature and aliquots of the reaction mixture were analyzed by ^{1}H NMR. Utilizing specific non-overlapping peaks in the NMR spectra, yields were determined by the ratio of the product area to the total area of product and starting epoxide.

Linear epoxide, 1,2-epoxyhexane (EH) was obtained commercially and analyzed by ^{1}H NMR (Figure 151). The area of the two protons of C_1 at 2.4 ppm were used in subsequent NMR spectra to determine product yields. EH was reacted in a 1:1 ratio with

HCl for 90 minutes (Figure 152). Two chlorohydrin products were formed: 2-hydroxy-1-chlorohexane (major) and 1-hydroxy-2-chlorohexane (minor).

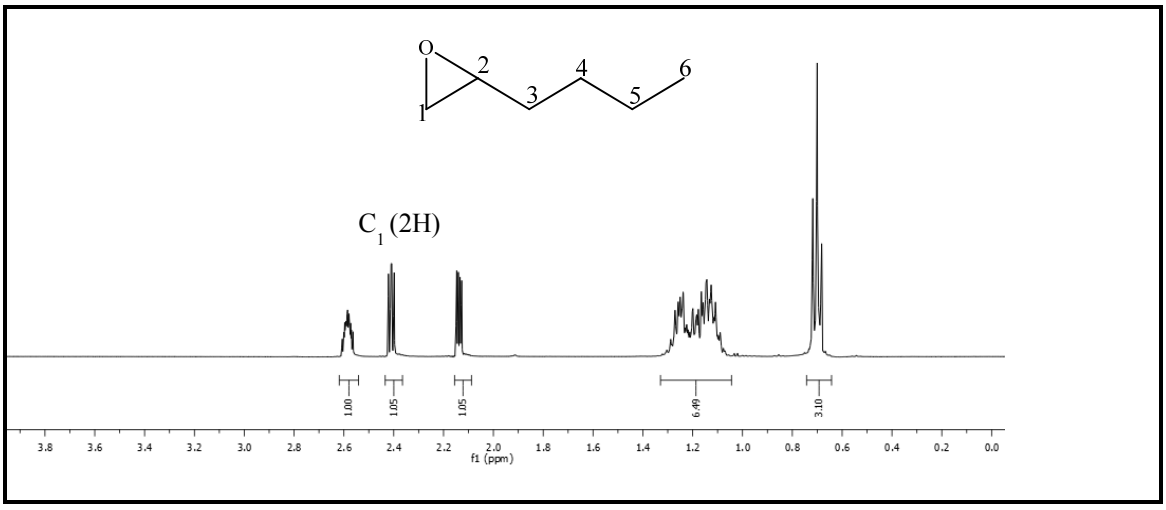

Figure 151 - ^{1}H NMR of neat 1,2-epoxyhexane.

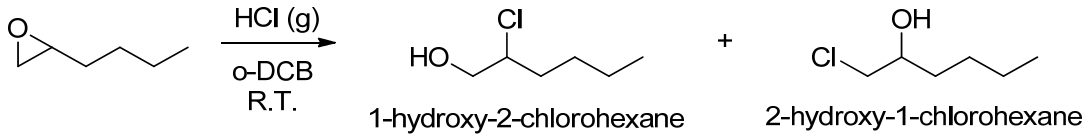

Figure 152 - Epoxide ring opening reaction of 1,2-epoxyhexane with HCl (g).

The ^{1}H NMR of the reaction of 1:1 EH with HCl after 90 minutes at room temperature is shown in Figure 153. The peak areas of the protons used to determine yields of each product are labeled A (EH), B (major product) and C (minor product). The estimated yield of the major product was determined to be 35.9%; the minor product was formed in 16.3% yield. Total conversion of the product is estimated to be 52.2%.

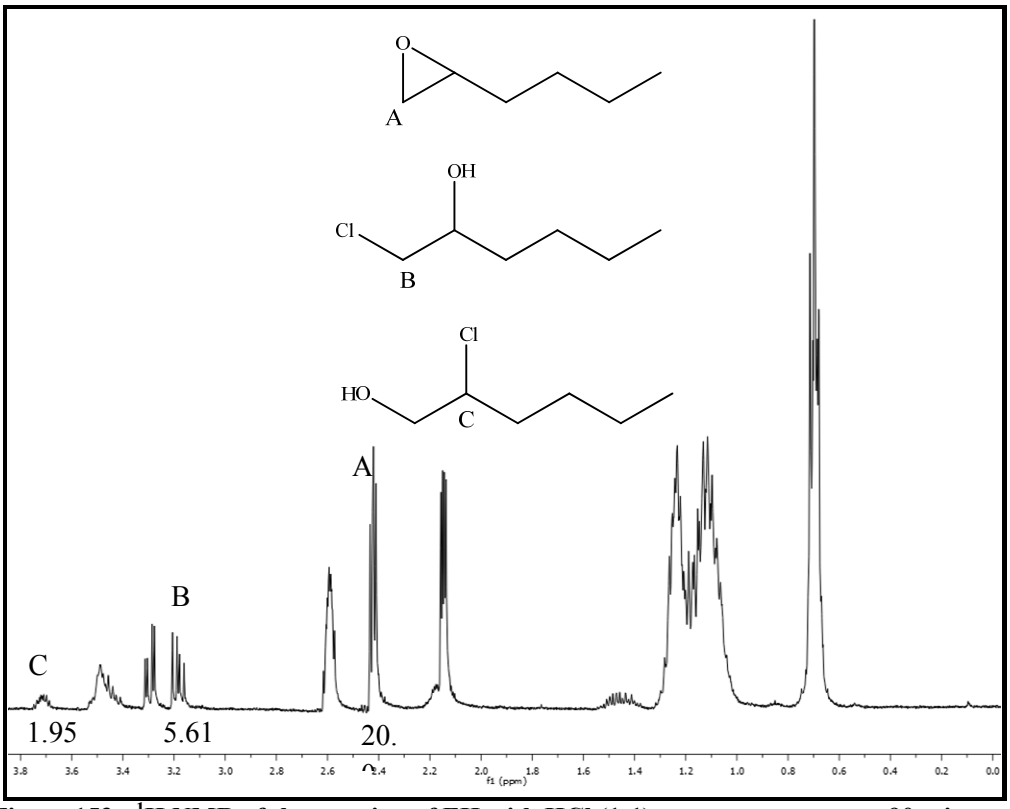

Figure 153 - ^{1}H NMR of the reaction of EH with HCl (1:1), room temperature, 90 minutes.

Cyclic epoxide, cyclohexene oxide (CHO) was also obtained commercially and analyzed by ^{1}H NMR (Figure 154). The reaction of CHO with 1:1 HCl at room temperature for 90 minutes yielded 2-chlorohexanol (Figure 155).

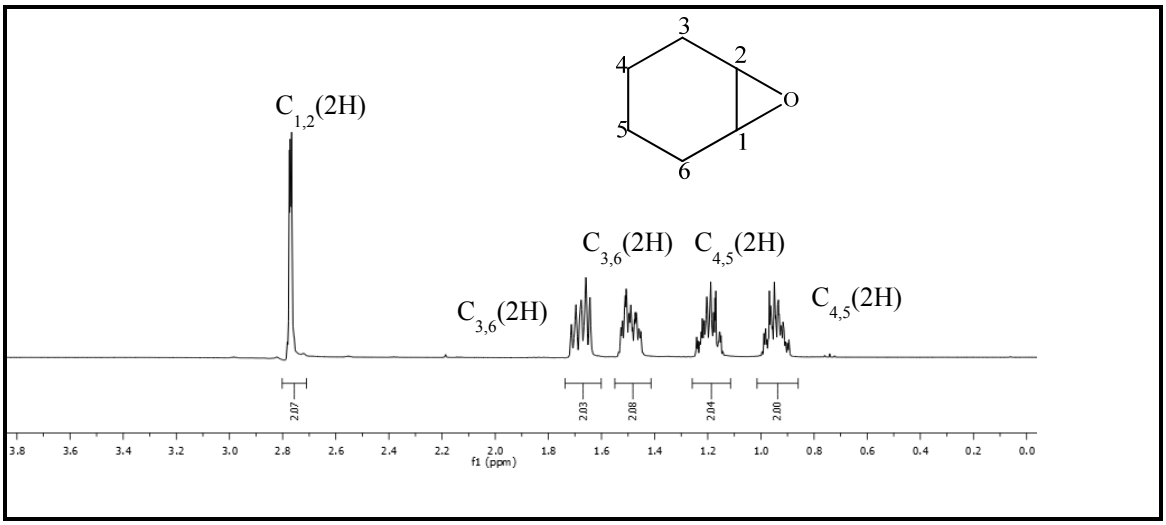

Figure 154 - ^{1}H NMR of pure cyclohexene oxide.

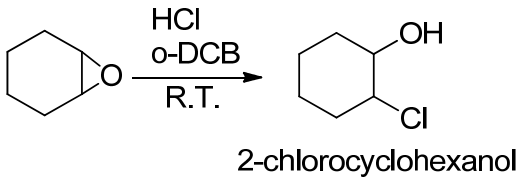

Figure 155 - Epoxide ring opening reaction of cyclohexene oxide with HCl.

Analysis of the ^{1}H NMR of the reaction mixture (Figure 156) afforded a yield of approximately 45% 2-chlorocyclohexanol. Yield was determined from the peaks labeled B (product) and A (starting material). The conversions of cyclic and linear epoxides in separate reactions were similar, 45% after 90 minutes (cyclic) versus 52% after 90 minutes (linear).

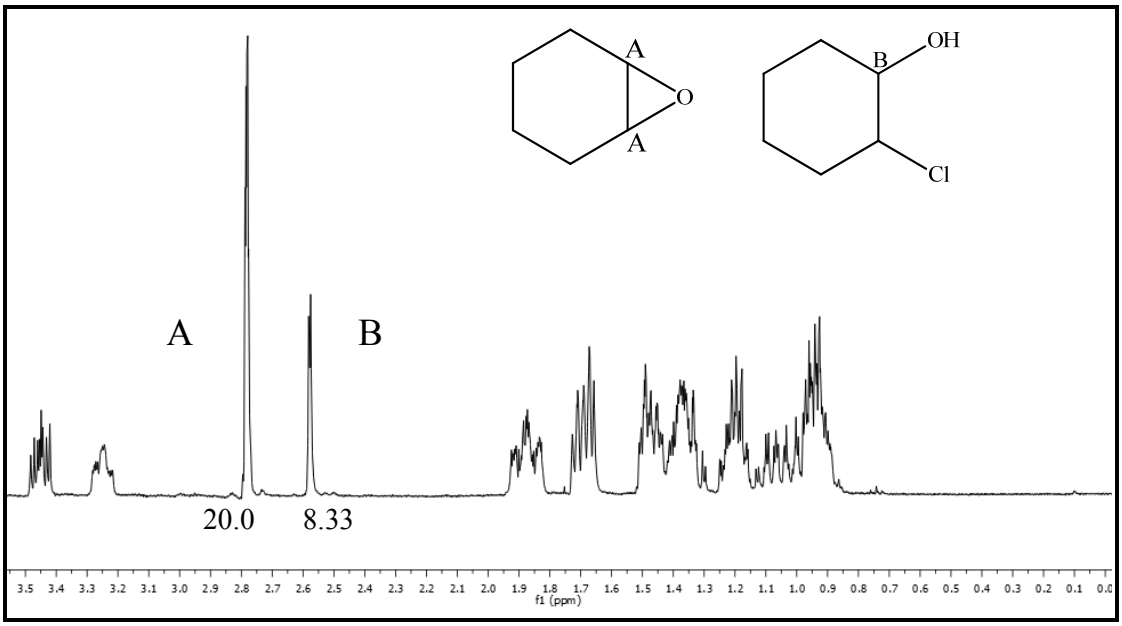

Figure 156 - ^{1}H NMR of the reaction of cyclohexene oxide with HCl (1:1), room temperature, 90 minutes.

A competitive study of the two was then performed with 0.5 equivalents each of CHO and EH to 1 total equivalent of HCl (Figure 157). Analysis of the reaction mixture after 90 minutes at room temperature by ^{1}H NMR showed a 58.5% conversion of EH (52.8% yield of major product, 5.7% yield of the minor product) as compared to a 78.4% conversion of CHO. In the competitive reaction, the cyclic epoxide clearly reacts at a faster rate than the linear epoxide.

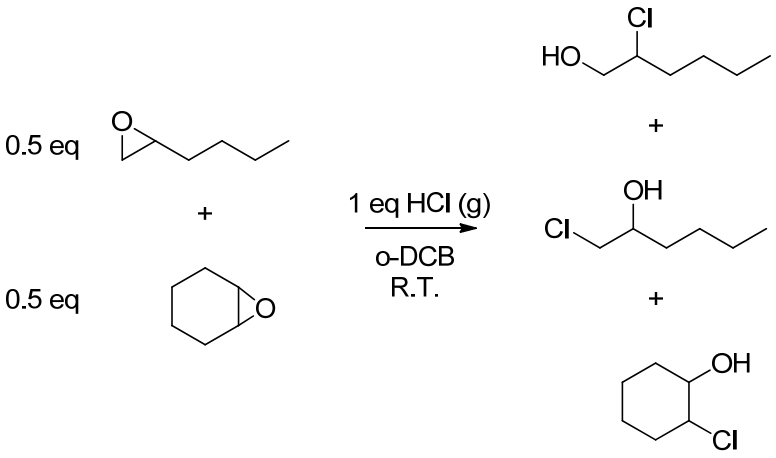

Figure 157 - Competitive reaction of CHO and EH with HCl, room temperature for 90 minutes.

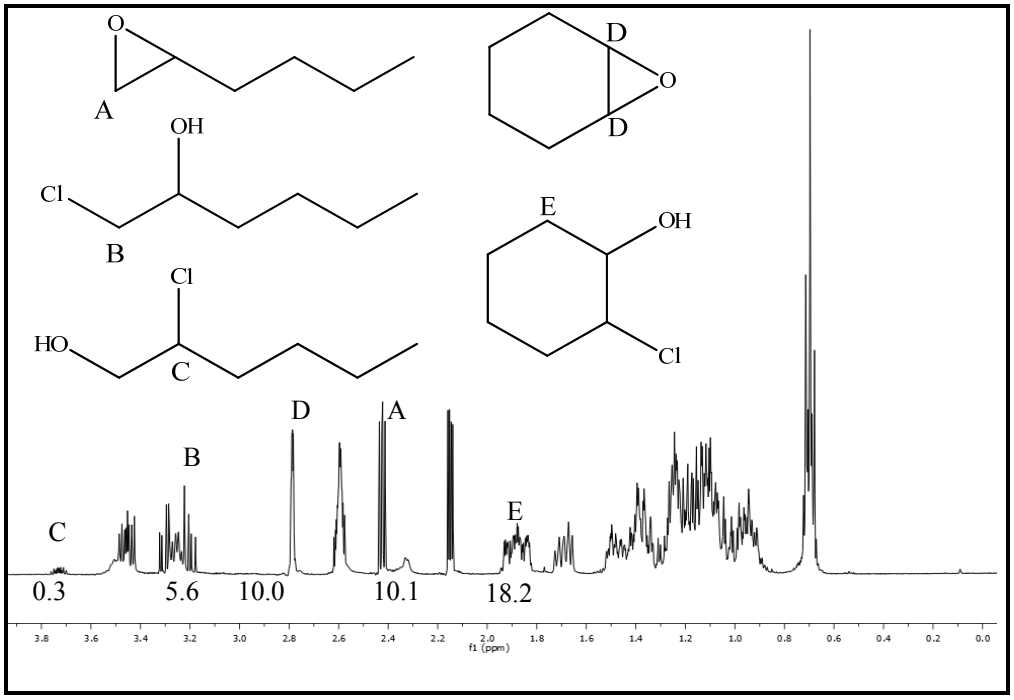

ESO was also reacted with HCl at various concentrations and the reaction was monitored by ^{1}H NMR. By monitoring the total area of the epoxide protons compared to the area of the tertiary proton adjacent to the ester moiety, conversion of epoxide to chlorohydrin was estimated. Reaction of ESO with 1 eq of HCl yielded complete conversion after 5 minutes. Reaction of ESO and HCl in 20:1 ratio yielded only semi-quantitative evidence of conversion.

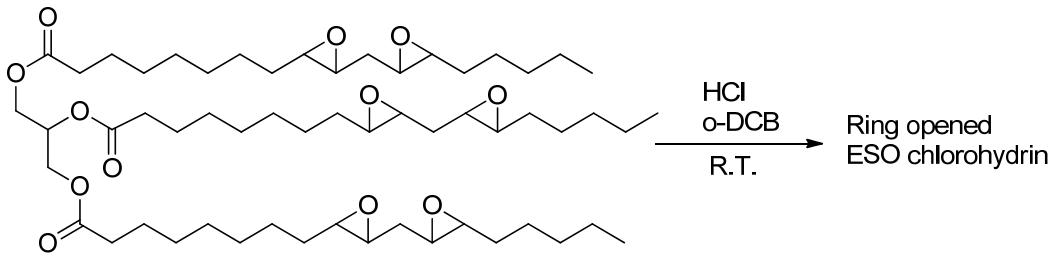

Figure 158 - Epoxidized soybean oil reaction with HCl.

It is possible, based on the information in this section, that incorporation of a cyclic epoxide into the structure of a sacrificial stabilizer like ZnEp and CaEp may prevent reaction of ESO and improve both color and thermal stabilities.

A.3 Conclusion

The thermal stability and color stability of plasticized PVC blended with stabilizers ($ZnSt_2$, $CaSt_2$, ZnEp and CaEp) was studied to determine the utility of novel, sacrificial stabilizers developed to protect ESO while providing improved performance.

DIDP-plasticized PVC blends displayed improved performance for the epoxide salts as compared to their stearate analogs. The best performance was observed for the blend with both ZnEp and CaEp, most likely due to the prevention of $ZnCl_2$ buildup and the trapping of HCl by the oxirane moieties. Blends of ESO-plasticized PVC with ZnEp surprisingly showed the best color and thermal stabilities compared to other mixtures, including the combination of ZnEp and CaEp. Little difference was seen between epoxide salts and metal stearates for ESO-plasticized PVC blends. This could be due to the faster reaction of HCl with epoxides, as we have not yet determined which epoxides are reacting first, the epoxide salts' or ESO's oxiranes. However, the improved thermal and color stability displayed by ZnEp and ESO-plasticized PVC presents a great starting point for the development of future additives to protect ESO. To that end, the epoxide ring opening studies suggest that cyclic epoxides would be potential candidates, due to their increased rate of reaction compared to linear epoxides.

A.4 Experimental

A.4.1 Materials

Diisodecyl phthalate (DIDP), calcium acetate ($Ca(OAc)_2$), sodium acetate (NaOAc, anhydrous) and zinc stearate ($ZnSt_2$, purum, 10-12% zinc metal basis) were obtained from Sigma-Aldrich. Calcium stearate ($CaSt_2$) was obtained from Alfa Aesar. PVC powder (Oxyvinyls 240F) and Epoxidized Soybean Oil (ESO) was provided by Dow Chemical Company. Helium and nitrogen were obtained from Airgas. All materials were >97% purity or ultra-high purity unless otherwise stated and used as received from the manufacturer

A.4.2 Synthesis of ZnEp and CaEp

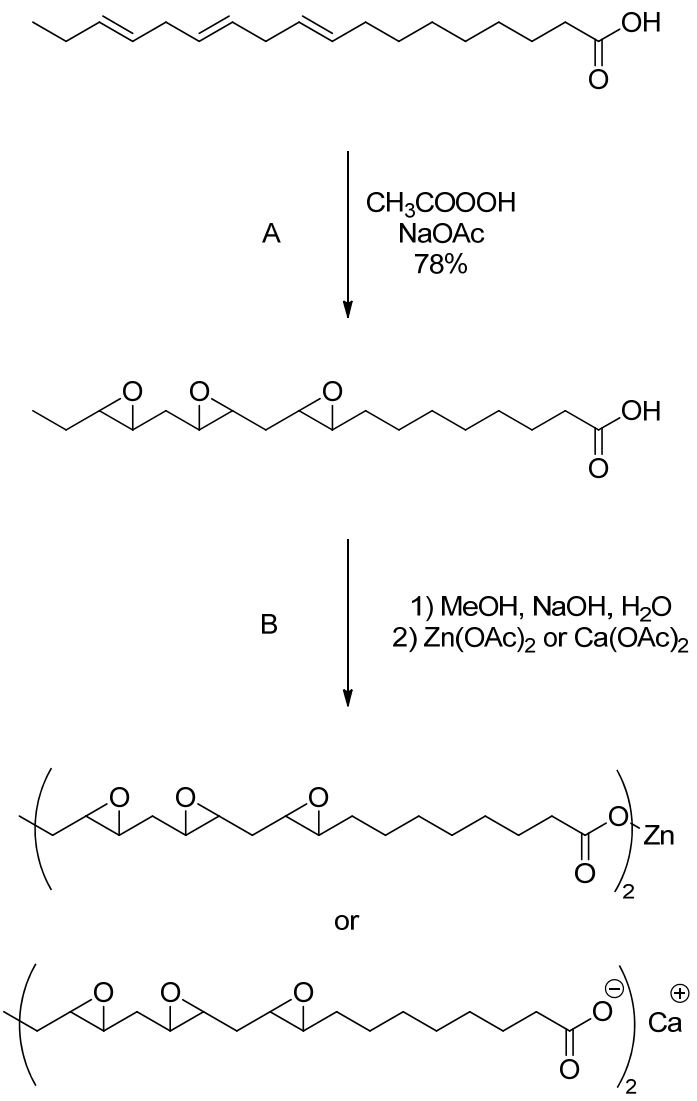

Figure 159 - Synthesis of ZnEp and CaEp

Synthesis of 9,12,15-triepoxylinolenic acid (A)

Neat linolenic acid (5.4 mL, 0.049 mol) was added to a round bottom flask and cooled in an ice bath to 0 ^{o}C. A solution of sodium acetate (1.1 g, 0.069 mol) in peracetic acid (18 mL, 0.069 mol) was then added dropwise over 1 h at 0°C. The reaction was stirred for 1 h at the same temperature. The organics were then extracted with diethylether (2 x 10 mL). The combined organic layers were washed with water (5 x 50 mL), dried over MgSO4 and concentrated *in vacuo* to yield 4.6 g (78%) of colorless semisolid product.

Synthesis of Zn or Ca salt of 9,12,15-triepoxylinolenic acid (ZnEp or CaEp) (B)

NaOH (0.5 g, 0.132 mol) in water (15 mL) was added to triepoxylinolenic acid (4.3 g, 0.0132 mol) dissolved in methanol (10 mL) at room temperature. The homogenous reaction was stirred for 15 min. $Zn(OAc)_2$ (1.2g, 0.007mol) (use $Ca(OAc)_2$ for preparation of Ca salt) in water (15 mL) was then added to the above homogeneous reaction mixture. The appearance of a white precipitate was noted. The mixture was then cooled to 0°C to precipitate the product. The solid was filtered and washed with water (3 x 20 mL), acetone (2 x 10 mL) and dried under vacuum to yield 3.5 g (76%) of Zn-triepoxylinoleniate (Ca-triepoxylinoleniate: 51%) as a white solid. Elemental analysis for Zn – Calc. 9.13; found 9.33; Ca – calc. 5.80; found 6.17.

A.4.3 Method for Blending of the PVC, Plasticizer and Stabilizers

Dry-blended samples consisted of 3 g of PVC powder, 30 phr (0.9 g) plasticizer (DIDP or ESO), and 5 phr (0.15 g) additional additives ($ZnSt_2$ and/or $CaSt_2$ or novel additives ZnEp and/or CaEp). The PVC powder and one-half of the plasticizer (0.45 g) were physically combined, heated to 95°C in an oil bath, and thoroughly mixed. In a separate vessel, the remaining plasticizer (0.45g) and all other additives were combined

and heated to 95°C. The two mixtures were then combined, heated to 95°C and thoroughly mixed. This temperature is above the glass transition temperature of PVC (approximately 80°C) which facilitated the efficient absorption of the additive by the PVC. This two pot blending technique of the plasticizer with the PVC afforded the complete uptake and uniform distribution of the additives. It should be noted that these additives are not incorporated into the PVC matrix by themselves.

A.4.4 Thermal Analysis of PVC Blends

Thermogravimetric analysis (TGA) was performed using a TA Instruments TGA Q50. Isothermal weight loss studies were conducted between 150°C and 180°C for up to three hours under a flow of nitrogen (100 mL/min). Constant ramp rate studies were conducted at 1, 5, and 10°C per minute from 20°C to 500°C. In all cases, approximately 20 mg of a dry blended sample was used in duplicate runs to confirm repeatability. Weight loss is reported with respect to only the PVC, excluding the additives.

A.4.5 Epoxide Ring Opening Studies

HCl (gas) was bubbled through o-dichlorobenzene (o-DCB, 35 mL) at room temperature for 3 minutes. The amount of HCl complexed with the o-DCB was determined by weighing the reaction vessel before and after HCl addition. The epoxide (cyclohexene oxide, 1,2-epoxyhexane or ESO) in a 1:1 or 20:1 (epoxide:HCl) molar ratio dissolved in o-DCB (2mL) was then added to the HCl solution. The reaction was stirred at room temperature and an aliquot of the mixture was taken and analyzed for the epoxide conversion and corresponding product formation by ^{1}H NMR spectroscopy.

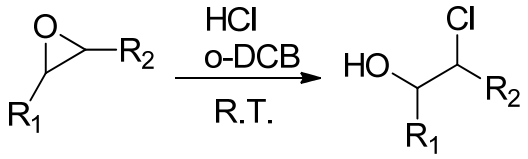

Figure 160 - Example epoxide ring opening reaction

A.4.6 Color Stability Analysis of PVC Blends

Photographs of the each PVC blend was taken post thermal treatment. These photographs were used to qualitatively compare the discoloration of the PVC polymer.

A.5 References

1. Bouchareb, B.; Benaniba, M. T., Effects of epoxidized sunflower oil on the mechanical and dynamical analysis of the plasticized poly(vinyl chloride). *Journal of Applied Polymer Science* **2008,** *107* (6), 3442-3450.

2. Wang, Q.; Nagy, S., Improving gamma-radiation stability of PVC--a review. *Journal of Vinyl & Additive Technology* **1999,** *5* (1), 4.

3. Iida, T.; Kawato, J.; Tanie, S.; Goto, K., Stabilization of Polyvinyl-Chloride -10. *Journal of Applied Polymer Science* **1989,** *37* (6), 1685-1698.

4. Iida, T.; Nakanishi, M.; Goto, K., Stabilization of Polyvinyl-Chloride -2. *Journal of Applied Polymer Science* **1975,** *19* (1), 243-250.

5. Odilora, C. A., On the thermal degradation of polyvinyl-chloride - synergistic effect of mixtures of lead and zinc carboxylates. *Acta Polymerica* **1989,** *40* (8), 541-545.

6. Okieimen, F. E., Studies in the utilisation of epoxidised vegetable oils as thermal stabiliser for polyvinyl chloride. *Industrial Crops and Products* **2002,** *15* (1), 71-75.

APPENDIX B

Polyamines for CO_2 Capture

B.1 Introduction

The silylamines presented in Chapter 3 demonstrated high capacities approaching the theoretical 0.67 moles CO_2 per mole amine. Modification of the structures to include multiple amine sites was hypothesized to provide increased capacity. The following polyamines were proposed to examine the effect of multiple reactive sites on capacity and the other relevant industrial properties (Table 46). CP10 is commercially available and was included in our investigation because of the reduced viscosity demonstrated by polyols in amine blends for CO_2 capture.[1-2] DEDPSA, CP11 and CP12 were not commercially available. The syntheses are discussed herein. DEDPSA was investigated as an analog of TEtSA which contains a silicon atom and two amines. DETA (commercially available), CP11 and CP12 were proposed as examples with more than two amine sites for CO_2 capture. Additionally, DETA and CP10-12 contain oxygen or nitrogen moieties along the backbone which were proposed to assist in stabilization of the ammonium through hydrogen bonding (Figure 161). This could result in changes in properties such as viscosity, reversal temperature and capacity.

Table 46 - Polyamines propsed for CO_2 capture with enhanced capacity.

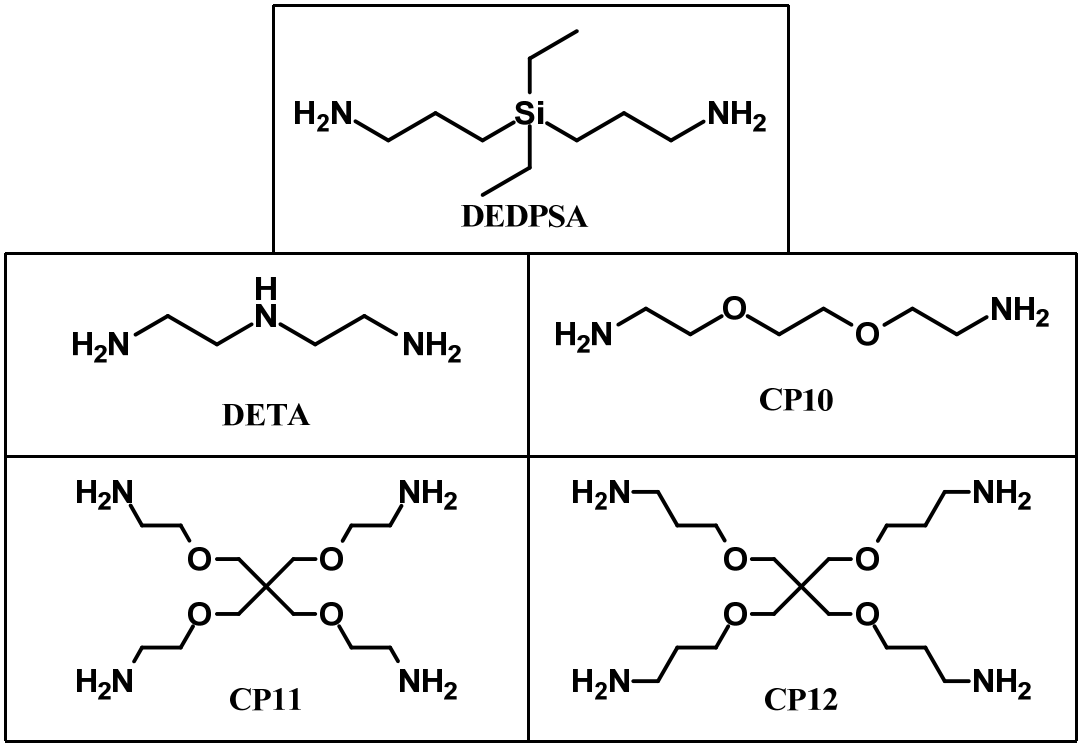

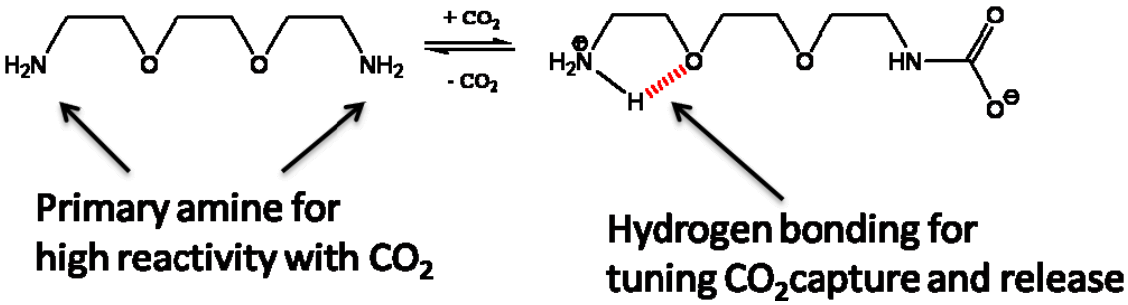

Figure 161 - Proposed stabiliztion due to oxygen moiety in CP10.

Furthermore, we reported in Chapter 3 the dramatic reduction in viscosity for secondary amines as compared to their primary analogs. DEDPSA and CP10 RevILs demonstrated very high viscosities. Thus, the secondary versions of these amines were synthesized and analyzed in an attempt to demonstrate decreased viscosity while

maintaining higher capacity (Table 47). The syntheses of each and the results gathered are discussed herein.

Table 47 - Proposed secondary versions of polyamines for CO_2 capture with reduced viscosity.

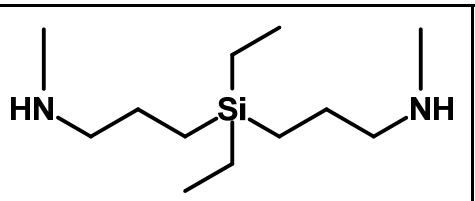 S-DEDPSA	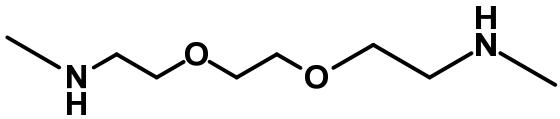 S-CP10

B.2 Synthesis

The synthetic pathways and purification of the amines which were not commercially available will be discussed briefly in this section. Detailed experimental and characterization of each compound is discussed in the Experimental section. Optimization of the syntheses was not pursued at this juncture as our primary goal was to evaluate the candidates for the desired properties and pursue optimization of the best candidates.

B.2.1 Polyamines

B.2.1.1 Synthesis of DEDPSA

3,3'-(Diethylsilanediyl)bis(propan-1-amine) (DEDPSA) was synthesized in a similar manner to TEtSA by the hydrosilylation of diethylsilane and two equivalents of allylamine with PtDVDS (Figure 162). Distillation yielded DEDPSA as a colorless liquid in 41%.

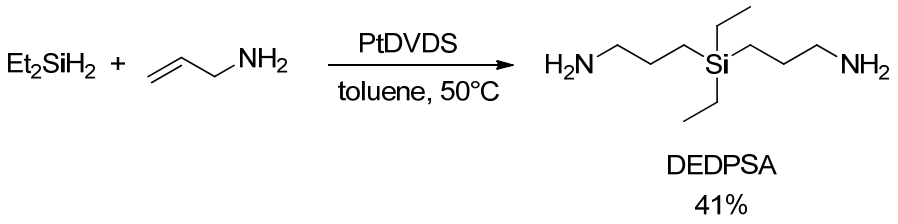

Figure 162 - Synthesis of DEDPSA by hydrosilylation.

B.2.1.2 Attempted Synthesis of CP11

The proposed route for the synthesis of CP11 is outlined in Figure 163. The Michael addition of pentaerythritol and acrylonitrile in the presence of KOH in toluene proceeded well to yield the tetranitrile intermediate (**2**) in 81% yield. Conversion of **2** to the tetra-acid (**3**) also proceeded well. **3** was isolated by continuous liquid-liquid extraction and concentrated *in vacuo* to yield 40% of the pure tetra-acid **3**. However, the Curtius rearrangement with triethylamine and diphenylphosphoryl azide (DPPA), followed by addition of *tert*-butanol to trap the boc-protected amine, did not proceed as desired. NMR analysis of the crude product showed formation of a urea and no sign of the expected product tetrakis[([N-Boc]-aminoethoxy)methyl]methane (**4**). At this point, literature sources were located which describe CP12, commonly used in dendrimer synthesis, as a viscous oil[3]. It is likely that reaction with CO_2 would form a solid or oil with a viscosity higher than 100 cP. Thus, the synthesis of both CP11 and CP12 were then discontinued.

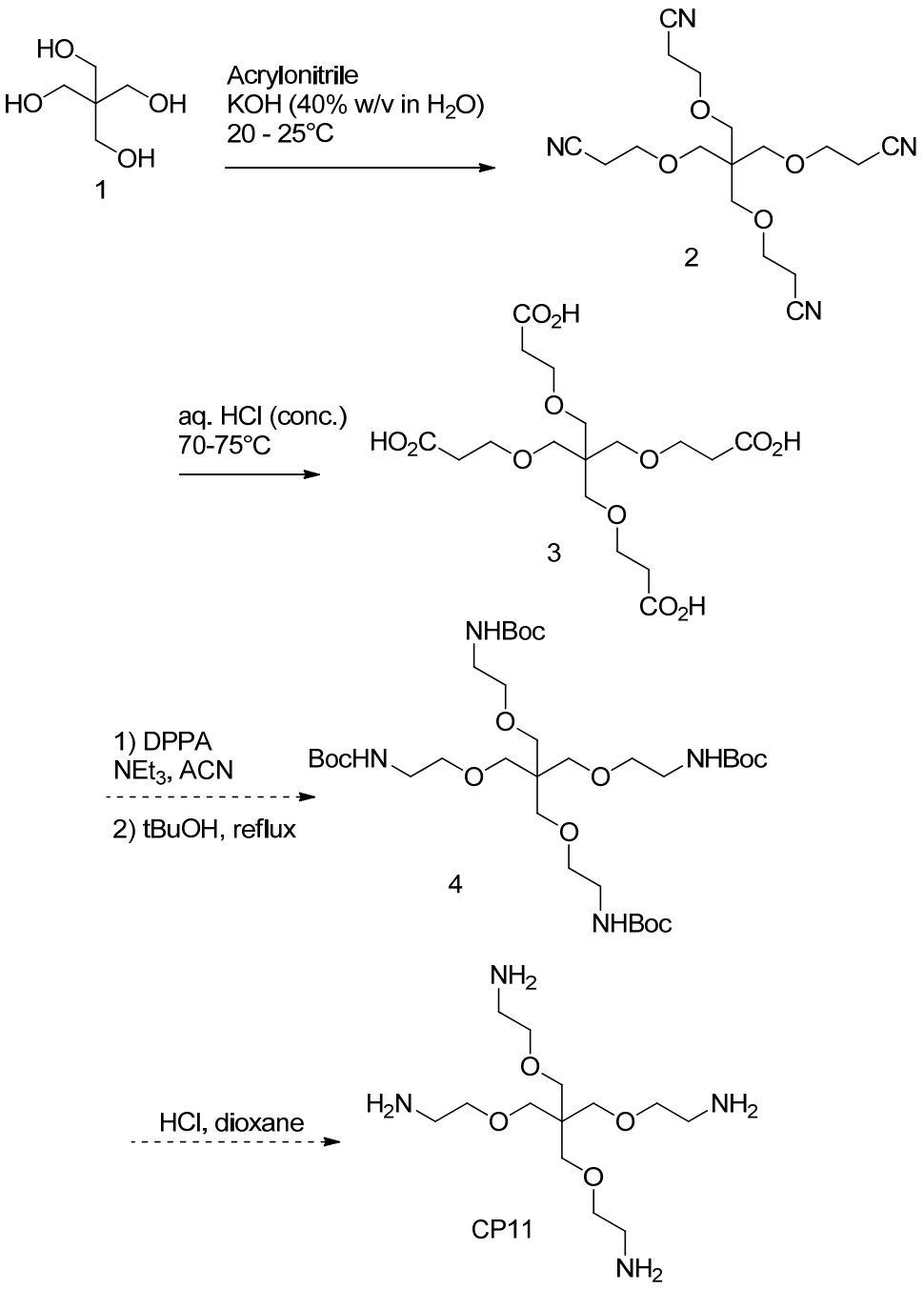

Figure 163 – Proposed synthetic route to CP11

B.2.1.3 Attempted Synthesis of CP12

The synthesis of CP12 was attempted in parallel with CP11 diverging from the procedure for CP11 after intermediate **2**. The tetranitrile intermediate **2** was prepared as

described above. However, reduction of the nitrile groups to amines did not proceed as expected. Two methods were attempted (Figure 164). The first attempt utilized $LiAlH_4$ in THF to reduce the nitrile groups. After 30 days of reaction, workup yielded no sign of CP12. MS analysis did show the presence of partially reduced **2**, however, this method had not been demonstrated for a species containing four nitrile groups, only on simpler nitrile starting materials. A second attempt utilized hydrogenation via PtO_2 with 125 psi of H_2 in EtOH. ^1H NMR analysis of the reaction mixture showed no sign of **2** after reaction and the formation of other species. However, upon neutralization and workup, no tetra-amine was recovered. Previous reports showed that CP12, commonly used in dendrimer synthesis, is a viscous oil[3]. It is likely that reaction with CO_2 would form a solid or oil with a viscosity higher than 100 cP and as such this synthesis was discontinued.

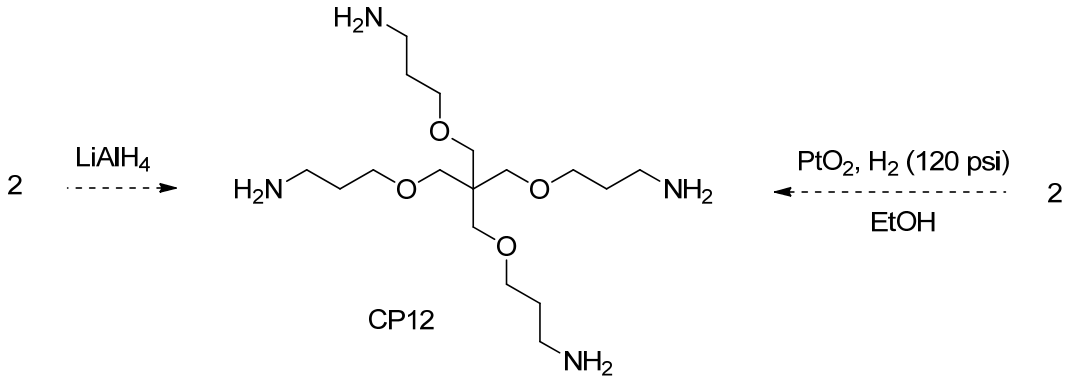

Figure 164 – Attempted synthesis of CP12 by reduction of tetranitrile 2 from Figure 163.

B.2.1 Secondary Polyamines

B.2.1.1 Synthesis of S-CP10

S-CP10 was synthesized in a similar manner to the secondary amines from Chapter 3. 2,2'-[1,2-Ethanediylbis(oxy)]bis-ethanamine (CP10) and 2.2 equivalents of ethyl formate were combined under inert atmosphere and heated to 60°C overnight (Figure 165). The reaction mixture was concentrated *in vacuo* to remove ethanol and excess reactants yielding the crude product as a light yellow liquid (99% yield). Without further purification, the crude product was reduced by slow addition of lithium aluminum hydride (LAH) in anhydrous THF at 60°C followed by stirring overnight at 60°C. Distillation after workup yielded 2,2'-(ethane-1,2-diylbis(oxy))bis(N-methylethanamine) as a colorless liquid (65% yield).

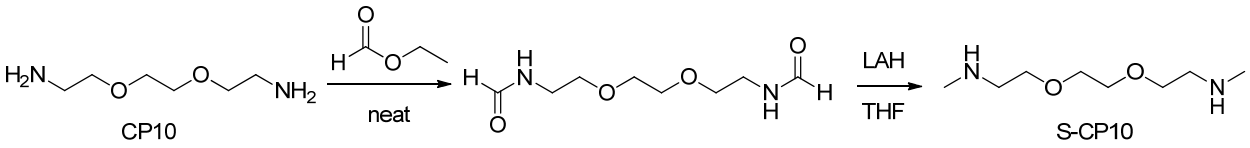

Figure 165 - Synthesis of S-CP10

B.2.1.2 Attempted Synthesis of S-DEDPSA

The synthesis of S-DEDPSA was attempted in the same manner as described above. DEDPSA (1 eq) and ethylformate (2.2 eq), neat, were combined under inert atmosphere and heated to 60°C overnight. The reaction mixture was concentrated *in vacuo* and analyzed by NMR. The starting material was completely consumed, however, a mixture of both mono-formylated and di-formylated DEDPSA products were observed at a ratio of approximately 0.1:1 by integration (Figure 166). Reduction of the mixture to both mono-S-DEDPSA and S-DEDPSA (Figure 167) was not attempted. Instead, the

possibility of an asymmetric N-methylated amine was pursued, as the asymmetry of the amine was hypothesized to result in reduced viscosity as compared to the symmetric version.

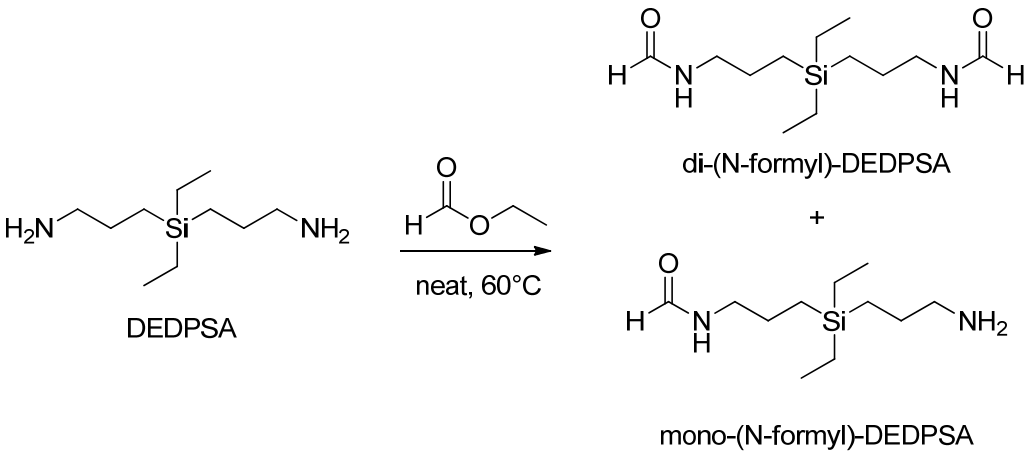

Figure 166 - Formylation of DEDPSA

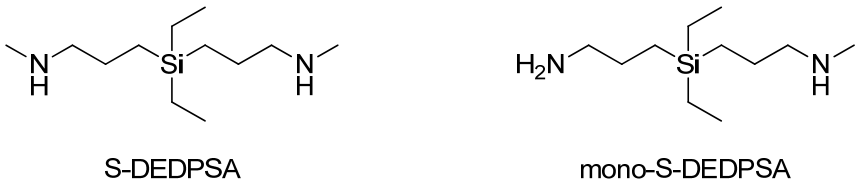

Figure 167 - S-DEDPSA and mono-S-DEDPSA structures.

In an attempt to preferentially form mono-(N-formyl)-DEDPSA, a reduced amount of ethylformate (1.1 eq) was added dropwise to DEDPSA (A, Table 48). This did not affect the product distribution of mono- to di-(N-formyl)-DEDPSA. Diluting ethylformate in EtOH (0.1 M, Entry B) increased the product distribution to 0.5:1 mono- to di-(N-formyl)-DEDPSA. Diluting DEDPSA in EtOH (0.1 M) and addition of 0.1 M ethylformate (Entry C) had no further affect. Decreasing the reaction temperature of the solution to room temperature, however, slowed the reaction considerably (Entry D). After

26 hours ^{1}H NMR showed mainly starting material with traces of what appear to be a mixture of mono- and di-(N-formyl)-DEDPSA. At this point an alternative route to achieve mono-S-DEDPSA has been proposed and is outlined in the proposal for future work (Section B.5).

Table 48 - Conditions attempted for formation of mono-N-methyl-DEDPSA by reaction of DEDPSA and 1.1 eq Ethylformate

Entry	DEDPSA conc. in EtOH	Ethylformate conc. in EtOH	Temperature (°C)	Product ratio (Mono:Di)
A	neat	neat	60	0.1:1
B	neat	0.1 M	60	0.5:1
C	0.1 M	0.1 M	60	0.45:1
D	0.1 M	0.1 M	Room Temp.	SM*

B.3 Results and Discussion

B.3.1 Polyamines

The CO_2 capture properties of capacity, viscosity and reversal temperature were investigated for CP10, DETA and DEDPSA. The RevILs were formed in the same manner as described in Chapter 3. Though a complete investigation of all relevant CO_2 catpure parameters was not undertaken for these amines, valuable information was obtained for the viscosities. High viscosities were observed for all polyamines studied, which would limit their application in CO_2 capture. As such, it was not considered necessary to complete these investigations.

B.3.1.1 CO_2 Uptake Capacity

The CO_2 uptake capacity measured for each polyamine is similar to TETSA (0.63 mol CO_2/mol amine) on a mole/mole basis (Table 49). However, on a mole CO_2 per kilogram amine basis the polyamines do reach capacities that are somewhat higher (0.5 – 1.8 moles CO_2 per kilogram amine greater) than TEtSA (3.5 mol CO_2/kg amine).

However, they do not reach the theoretical capacity predicted for each molecular liquid, possibly due to the viscosity displayed by the RevILs. The purpose of the polyamine system was to take advantage of increased capacity by having increased reaction sites, without significantly increasing the weight of the amine. The capacities reached are not measuring up to the full potential for these systems.

Table 49 – Polyamine gravimetric CO_2 uptake capacities after reaction with 1 bar CO_2 at 25°C.

Abbreviation	CO_2 Uptake (mol CO_2/mol amine)	CO_2 Uptake (mol CO_2/kg amine)	Theoretical CO_2 Uptake (mol CO_2/kg amine)
CP10	0.602 ± 0.006	4.06 ± 0.02	6.75
DETA	0.55 ± 0.05	5.3 ± 0.5	14.54
DEDPSA	0.79*	4.25	5.38

B.3.1.2 RevIL Viscosity

The viscosities of CP10-RevIL and DETA-RevIL were much higher at 25°C than TEtSA-RevIL (6088 cP) (Table 50). The RevIL of DEDPSA was a highly viscous gel, with a viscosity at 25°C that was too high to be measured by our equipment. These viscosities are not applicable in CO_2 capture systems. Decreased capacities were observed for both CP10-RevIL and DETA-RevIL at 35°C, however, even the significantly decreased viscosity of DETA-RevIL (5,500 cP) was not low enough to make it viable for implementation as a CO_2 capture solvent.

Table 50 - Effect of Proximity Upon RevILViscosity at 25°C and 40°C.

Abbreviation	Viscosity at 25°C (cP)	Viscosity at 35°C (cP)
CP10	16,000 ± 5,000	15,500 ± 1,000
DETA	16,000 ± 2,500	5,500 ± 1,000
DEDPSA	TV	N/M

N/M – not measured. TV – Too Viscous: Viscosity was higher than upper limit of our instrument.

We hypothesized that the amines could be forming extensive networks of inter and intramolecular bonding upon reaction with CO_2 which could result in the high viscosities observed. An example of these interactions for DETA is displayed in Figure 168. Since the CO_2 uptake capacity of the amines was not much increased from TEtSA, the option of controlling viscosity by controlling conversion would not be an ideal route. Lower conversions would decrease any advantage to utilizing the polyamines, providing further evidence that these polyamines are not ideal for CO_2 capture.

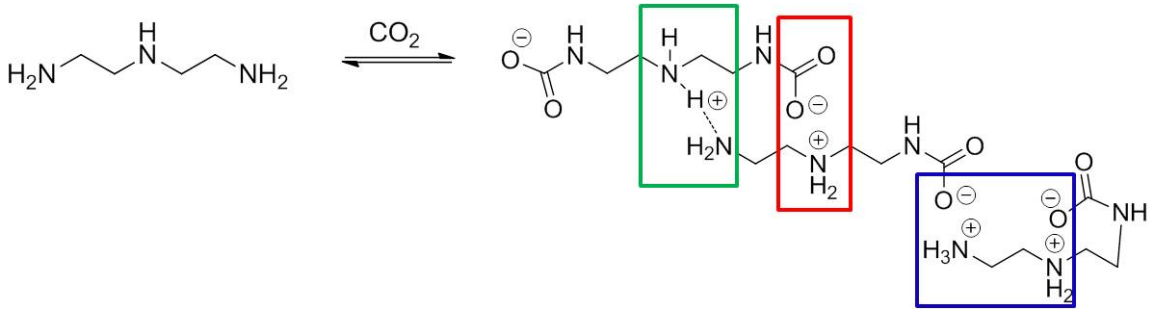

Figure 168 - Inter and intramolecular interactions leading to high viscosities in polyamines.

B.3.1.3 Reversal Temperatures

The reversal temperatures of CP10-RevIL and DETA-RevIL were obtained from the corresponding DSC. Both amines displayed reversal temperatures higher than TEtSA (71°C). DETA is in fact almost double the reversal temperature. Though CP10-RevIL

displays a reversal temperature below 100°C, the viscosity and capacity of the system limit the applicability of this system in CO_2 capture.

Table 51 - Reversal temperatures of CP10-RevIL and DETA-RevIL.

Abbreviation	Reversal Temperature (°C)[a]
CP10	91.25
DETA	131.69

[a]**For these amines DSC was only run once.**

B.3.2 Secondary Polyamines

When bubbled with a 200 mL/min stream of CO_2, *via* a diffuser tube, S-CP10-RevIL was found to have a capacity of 1.037 ± 0.002 moles CO_2 per mole amine (5.892 ± 0.011 mol CO_2/kg amine), which is higher than both CP10 and TEtSA. The viscosity, however, was 59,000 ± 5,000 cP at 25°C which is significantly higher than CP10 and, in fact, much higher than expected. We do not understand why the viscosity is so much higher for the secondary analog as of yet. However, the primary analog has not reached full conversion so it is possible the increased conversion of the secondary analog could be what led to such a higher viscosity. Overall, the viscosity of these systems is too severely limiting to pursue this further.

B.4 Conclusions

Although polyamines display somewhat increased capacities, the capacities observed do not approach the theoretical capacities predicted, without which these systems have no advantage. Secondary polyamines do reach a significantly higher capacity. However, the gel-like materials formed upon reaction with CO_2 result in high viscosities and high reversal temperatures for both polyamines and secondary

polyamines. These results limit the application of these systems in anhydrous conditions for CO_2 capture. The possibility of utilizing the polyamines as additives to other amines, to increase capacity while maintaining lower viscosity, remains a possible route for investigation.

B.5 Proposal for Future Work

B.5.1 Polyamines

Though the polyamines studied did not show promise as CO_2 capture solvents, I still believe it would be of interest to explore geminal diamines. These could potentially form a six-membered, cyclic, intramolecular ammonium carbamate pair (Figure 169). The intramolecular, six-membered, cyclic RevIL could then prevent the intermolecular bonding we believe to be the cause of the higher viscosities in the previous polyamines. It would then be possible to achieve higher capacities while maintaining reduced viscosities. Commercially available model compounds such as 2-piperidinamine (top) and 2-pyrrolidinamine (bottom) would be an ideal place to start to confirm formation of a six-membered cyclic carbamate pair.

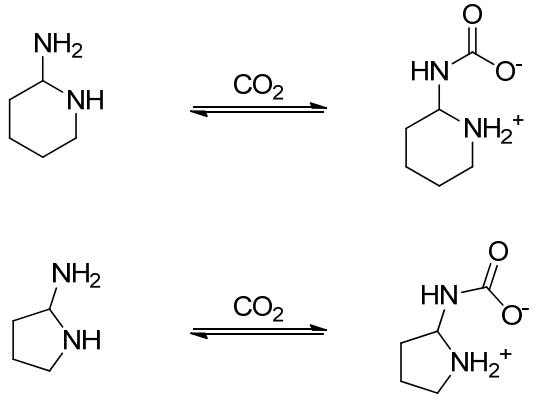

Figure 169 - Formation of Diamine Carbamate Pairs

From there the development of the silicon containing versions - silyl-geminal-diamines - could be pursued, should the previous study prove favorable. As mentioned before, silicon-containing analogs of sugars are liquids while the sugars themselves are solid. The proposed syntheses for two possible silyl-geminal-diamines are shown below (Figure 170) based on analogous work by Piest et al. and Gupta et al.[4-5] The preparation of chloromethyltriethylsilane from chloromethyltrichlorosilane by reaction with ethylmagnesium bromide is known (Figure 171).[6] (2-Chloromethyl)triethylsilane is prepared from triethylvinylsilane and HCl (Figure 172).[7]

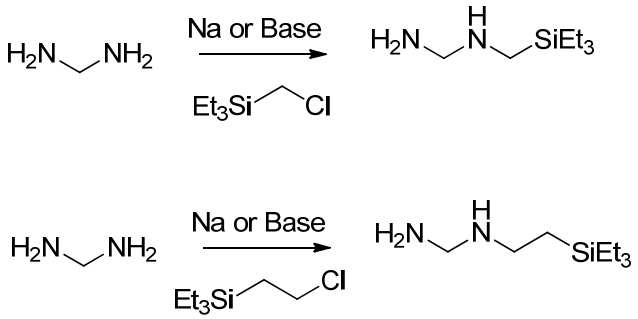

Figure 170 - Proposed Synthesis of Silyl-Geminal-Diamines

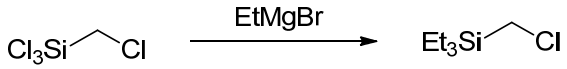

Figure 171 - Preparation of Chloromethyltriethylsilane

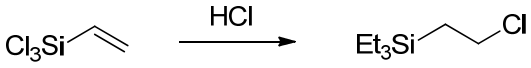

Figure 172– Preparation of (2-Chloroethyl)triethylsilane

B.4.2 Secondary Polyamines

My unsuccessful attempts to preferentially form mono-S-DEDPSA *via* the formylation of DEDPSA led to the proposal of an alternative route from diethylchlorosilane (Figure 173). Hydrosilylation of the commercially available mono-chloro-diethylsilane with allylamine and subsequent substitution of the chlorine with a Grignard reagent could potentially yield the desired mono-S-DEDPSA.

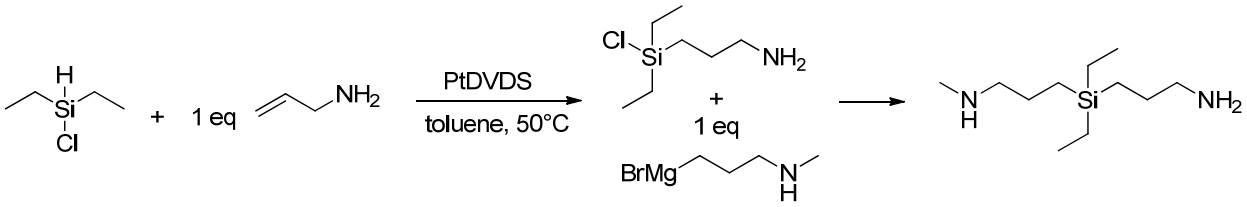

Figure 173 - Proposed Synthesis of mono-S-DEDPSA

The Grignard reagent can be obtained from 3-bromopropylamine hydrobromide, a commercial material already available in our labs (Figure 174). Should formation of the desired amine (mono-S-DEDPSA) prove fruitful, it can then be analyzed for the relevant CO_2 capture properties.

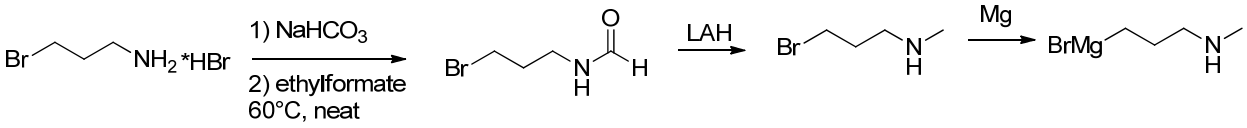

Figure 174 - Formation of Grignard Reagent

B.6 Experimental

B.5.1 CO_2 reactions

Reactions of molecular liquids were performed by syringing a sample of the desired molecular liquid from the glove box into a dram vial. The vial was capped with a septum and a diffuser tube attached to a CO_2 line was used to introduce CO_2. CO_2 was flowed through the samples at a flow rate of 200 mL/min for 75 minutes. The diffuser tube was stirred in the solution as the reaction progressed to ensure mixing. The formed RevIL was then subjected to analytical experiments to understand the role of structure on RevIL properties.

B.5.2 DSC/TGA

DSC measurements were performed in triplicate with a Q20 TA DSC Instrument. Sample weight was recorded in an aluminum hermetic pan crimped with an aluminum lid and measured against an empty pan. The DSC was calibrated with an Indium standard. Samples were held at -40^{o}C and ramped to 400°C at a ramp rate of 5°C/min. Reversal temperature was determined from the intersection of two tangents drawn at the beginning and bottom of the reversal endotherm. A similar treatment was used to determine the temperature of evaporation. Heat of regeneration was calculated by integrating the reversion endotherm with respect to time.

B.5.3 Viscometry

The viscosity of each ionic liquid was measured using a Rheosys Merlin II cone and plate viscometer. Samples were applied to the plate and were allowed to reach thermal stability prior to data collection. Shear rates varied between 10 and 2000 s^{-1}. The average viscosity over the shear range was recorded.

B.5.4 Synthesis of Amines

B.5.4.1 Synthesis of DEDPSA

Diethyldipropylsilylamine (DEDPSA) was synthesized *via* the hydrosilylation of diethylsilane and 2 equivalents of allylamine with PtDVDS in the same manner as TEtSA (See Chapter 3).

B.5.4.2 Synthesis of CP11 and CP12

Tetrakis[(cyanoethoxy)methyl]methane:

Pentaerythritol (5.1 g) was added to a mixture of toluene (30 mL) and 4.1 mL of a 40% KOH solution in water. The mixture was stirred vigorously. Acrylonitrile (35 mL) was added dropwise keeping the temperature below 25^{o}C. The reaction was stirred at RT for 3 hrs and then 2M HCl was added slowly. The toluene layer was washed with brine, dried over $MgSO_4$, and the solution concentrated via rotovap. The crude oil was distilled to remove the bis-cyanoethylether (110°C at 0.5 mmHg) and the remaining oil was pure tetranitrile (11.6 g, 81% yield). ^{1}HNMR (400 Hz, CDCl3) 3.65 (t, 8H), 3.48 (s, 8H), 2.60 (t, 8H) ^{13}CNMR (400 Hz, CDCl3) 118.17, 68.66, 65.57, 45.55, 18.75

tetrakis[(carboxyethoxy)methyl]methane:

Tetrakis[(cyanoethoxy)methyl]methane (15 mmol) was added to concentrated aqueous HCl (25 mL) and heated at 75°C for two hours. The reaction mixture was diluted with water and continuously extracted with ethyl ether for four days. The ether layer was separated, dried with $MgSO_4$ and concentrated *in vacuo* to yield 40% of solid tetrakis[(carboxyethoxy)methyl]methane (2.5 g). mp: 95-98°C ^{1}HNMR (400 Hz, d6-DMSO) 3.50 (t, 8H), 3.21 (s, 8H), 2.38 (t, 8H) this was consistent with literature reports.[8]

Attmpted Synthesis of Tetrakis-[3-(aminopropoxy)methyl]methane:

Tetrakis[(cyanoethoxy)methyl]methane (0.599 g, 1.4 mmol) was added to 15 mL of anhydrous THF under argon. $LiAlH_4$ (1M in THF) (8.6 mL, 8.6 mmol) was added and the reaction was stirred at 50°C. After 19 days, a 2 mL aliquot was removed and water and NaOH were added. ^{1}HNMR did not show desired reaction. The reaction was let stir for 30 days total. The reaction was quenched with 20 mL H_2O, 30 mL 20% NaOH, and 20 mL H_2O. 30 mL of brine were added. There were no bubbles indicative of $LiAlH_4$ quenching and the reaction was found to have only the singly and doubly reduced nitriles by LC-MS.

Attempted Synthesis of Tetrakis-[3-(aminopropoxy)methyl]methane:

Tetrakis[(cyanoethoxy)methyl]methane (0.702 g, 2 mmol) was added to a solution of EtOH (25 mL) and 1M HCl (1 mL). To a 250 mL parr reactor was added PtO_2 (100 mg) and the Parr was flushed with nitrogen and vacuum was pulled. The starting material solution in EtOH was then syringed in. Hydrogen gas was pressurized to 125 psi in the Parr reactor and the mixture was stirred vigorously with mechanical stirring. The temperature was brought to 50°C and the reaction was carried out for 3 days under hydrogen. The reaction was then cooled and depressurized. A 1 mL aliquot was taken and the solvents rotovapped. EtOAc was used to dissolve the crude and the solution was washed with saturated $NaHCO_3$ solution and rinsed with water and brine and dried over $MgSO_4$. The solvent was removed and a ^{1}HNMR did not show indicative peaks of the desired product.[5]

B.5.4.3 Synthesis of S-CP10

2,2'-[1,2-Ethanediylbis(oxy)]bis-ethanamine (68.2 mmol) and ethyl formate (150.04 mmol, 2.2 eq) were combined under inert atmosphere and heated to 60°C overnight (Scheme 9). The reaction mixture was concentrated *in vacuo* to remove ethanol and excess reactants yielding the crude product as a light yellow liquid (13.82g, 99%

yield). Without further purification, the crude product was diluted in anhydrous THF (135 mL) under inert atmosphere. A solution of LAH (148.94 mmol) in anhydrous THF (150 mL) was then added slowly at 60°C then allowed to stir overnight at 60°C. The mixture was cooled to 0°C and excess water was slowly added. The mixture was then concentrated *in vacuo* and the residue was extracted with dichloromethane (2 x 50 mL). The combined organic layers were dried over $MgSO_4$, filtered and concentrated *in vacuo*. The crude product was distilled at 55-59°C at 0.9 mmHg to yield the pure product as a clear liquid (43.9 mmol, 65% yield). Characterization by ^{1}H and ^{13}C NMR was performed, elemental analysis are pending.

B.5.4.4 Attempted Synthesis of S-DEDPSA

DEDPSA (1 eq) and ethylformate (2.2 eq), neat, were combined under inert atmosphere and heated to 60°C overnight. The reaction mixture was concentrated *in vacuo* and analyzed by NMR. The starting material was completely consumed however a mixture of what appear to be mono-formylated and di-formylated DEDPSA products were apparent at a ratio of approximately 0.1:1 by integration (Scheme 12).

In an attempt to preferentially form mono-(N-formyl)-DEDPSA the equivalents of ethylformate were reduced to 1.1 eq and this was added dropwise to DEDPSA at the dilutions and temperatures listed below (Table 52). Decreasing the equivalents of ethylformate to 1.1 eq did not change the product distribution of mono- to di-(N-formyl)-DEDPSA (Entry A) but diluting the ethylformate to 0.1 M concentration in EtOH did increase the ratio to 0.5:1 mono- to di-(N-formyl)-DEDPSA (Entry B). Subsequent dilution of DEDPSA and ethylformate to 0.1 M in EtOH did not affect the ratio (Entry C). Decreasing the temperature of the 0.1 M DEDPSA and 0.1 M ethylformate to room temperature slowed the reaction considerably. After 26 hours NMR of an aliquot showed mainly starting material with traces of what appear to be a mixture of mono- and di-(N-formyl)-DEDPSA (Entry D). Due to the difficulty in synthesizing mono-S-DEDPSA

through formylation of DEDPSA an alternative route to achieve mono-S-DEDPSA has been proposed and is outlined in Future Work.

Table 52 – Ratios of amine to ethylformate utilized to attempt to form mono-S-DEDPSA.

Entry	DEDPSA conc. in EtOH	Ethylformate conc. in EtOH	Temperature (°C)	Product ratio (Mono:Di)
A	neat	neat	60	0.1:1
B	neat	0.1 M	60	0.5:1
C	0.1 M	0.1 M	60	0.45:1
D	0.1 M	0.1 M	Room Temp.	SM*

B.7 References

1. Seo, J. B.; Jeon, S. B.; Lee, S. S.; Kim, J. Y.; Oh, K. J., *Korean Journal of Chemical Engineering* 2011, *28*, 1698.

2. Tan, J.; Shao, H. W.; Shao, J. H.; Xu, J. H.; Du, L.; Luo, G. S., *Industrial & Engineering Chemistry Research* 2011, *50*, 3966.

3. Hukkamaki, J.; Pakkanen, T. T., Study on catalytic hydrogenation in synthesis of four-directional amine-terminated dendritic molecules. *Journal of Molecular Catalysis a-Chemical* 2001, *174* (1-2), 205-211.

4. Gupta, V. K.; Al Khayat, M.; Singh, A. K.; Pal, M. K., Nano level detection of Cd(II) using poly(vinyl chloride) based membranes of Schiff bases. *Analytica Chimica Acta* 2009, *634* (1), 36-43.

5. Piest, M.; Lin, C.; Mateos-Timoneda, M. A.; Lok, M. C.; Hennink, W. E.; Feijen, J.; Engbersen, J. F. J., Novel poly(amido amine)s with bioreducible disulfide linkages in their diamino-units: Structure effects and in vitro gene transfer properties. *Journal of Controlled Release* 2008, *130* (1), 38-45.

6. Kabachnik, M. I.; Zakharov, L. S.; Molchanova, G. N.; Drozdova, T. D.; Petrovskii, P. V., Synthesis and study of thermal stability of silicon-containing phosphorus esters. 3. Thermal rearrangement of (triorganosilyl)methyl diphenyl phosphates. *Izvestiya Akademii Nauk SSSR, Seriya Khimicheskaya* 1989, (7), 1664-70.

7. Fleming, I.; Dunogues, J.; Smithers, R., The electrophilic substitution of allylsilanes and vinylsilanes. *Organic Reactions (Hoboken, NJ, United States)* 1989, *37*, No pp given.

8. Newkome, G. R.; Weis, C. D., *Organic Preparations and Procedures International* 1996, *28*, 242.

APPENDIX C

Data for Suzuki Electronic Effects

C.1 5-Substituted-2-Bromopyridines

The half-lives outlined in Table 53 were obtained from Figure 175-Figure 179. Note: each graph is produced from the average of two trials.

Table 53 - Reactions run for 24 hours with 5-substituted 2-halopyridines and 40% v/v of H_2O, atm. N_2. Reactions run in 3-neck, 100 mL Morton flask.

Entry	5-R	$t_{½}$ (min)	σ_{meta}	σ_{para}	pK_a[1]
1	NH_2	2	-0.16	-0.66	1.87
2	MeO	4.6	0.12	-0.27	-2.22
3	Me	5.3	-0.07	-0.17	1.08
4	NO_2	1	0.71	0.78	-3.12
5	H	50	0	0	0.71[2]

[1]pKa's predicted by SciFinder: Calculated using Advanced Chemistry Development (ACD/Labs) Software V11.02 (© 1994-2014 ACD/Labs). [2]Literature source: Linnell, 1960.[2]

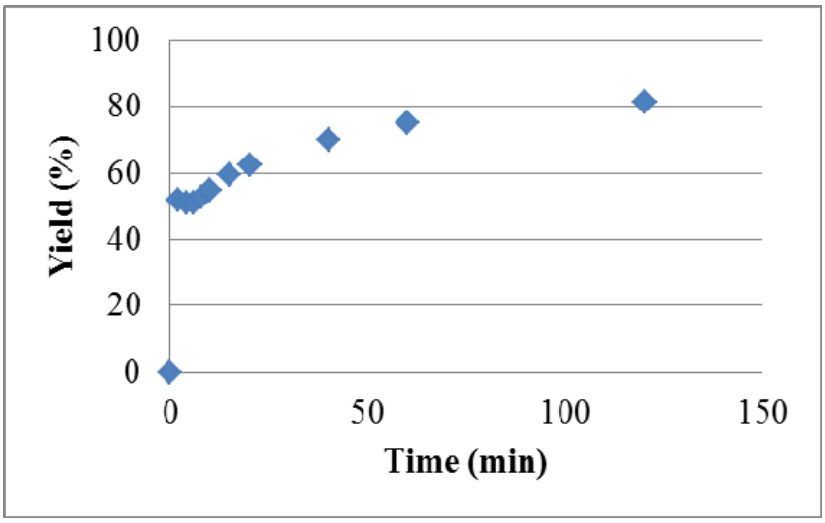

Figure 175 - Yield over time for 5-amino-2-bromopyridine.

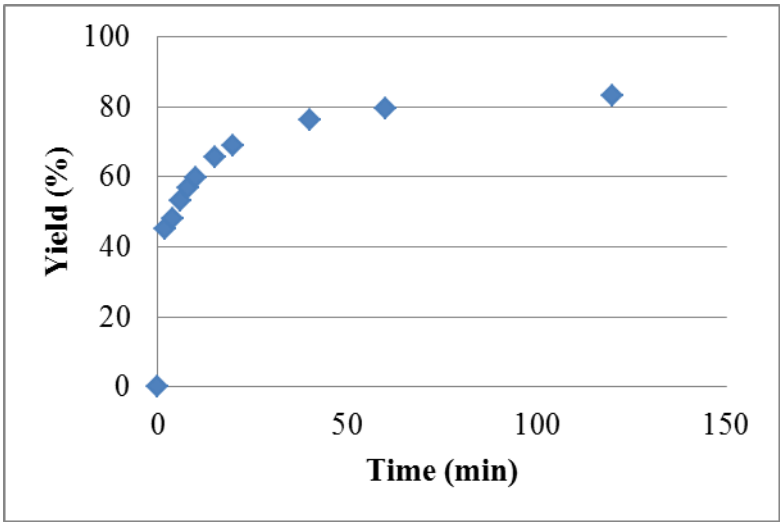

Figure 176 - Yield over time for 5-methoxy-2-bromopyridine.

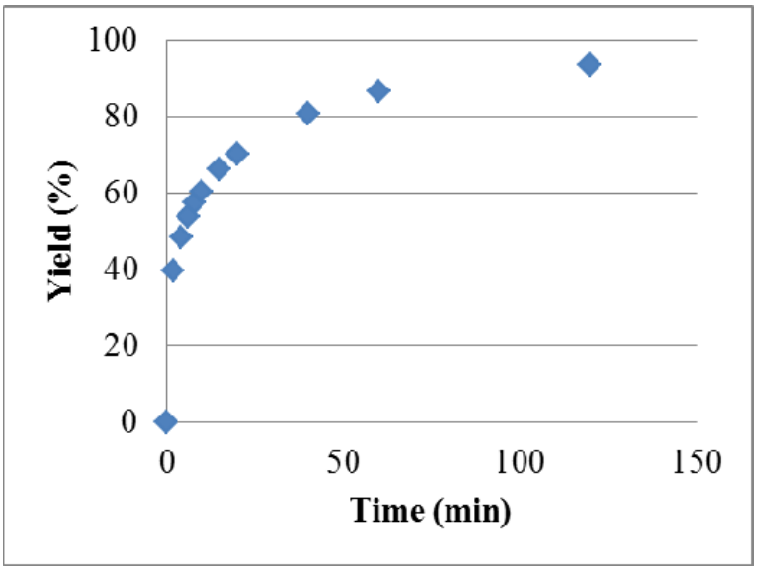

Figure 177 - Yield over time for 5-methyl-2-bromopyridine.

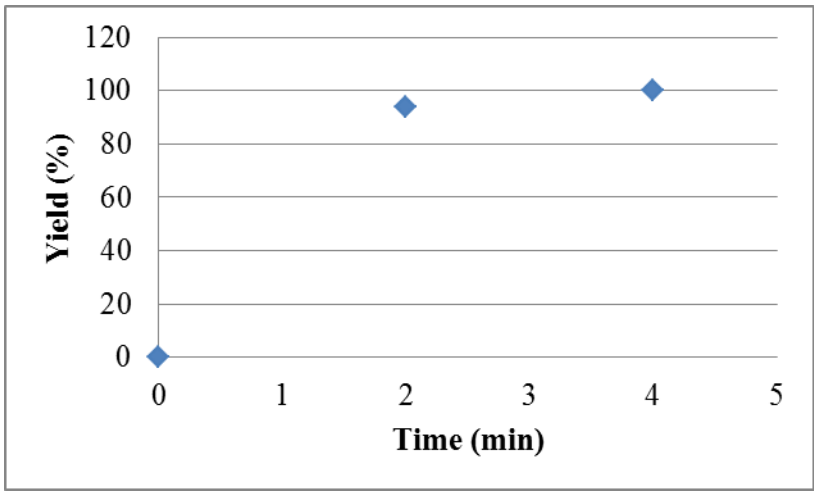

Figure 178 - Yield over time for 5-nitro-2-bromopyridine.

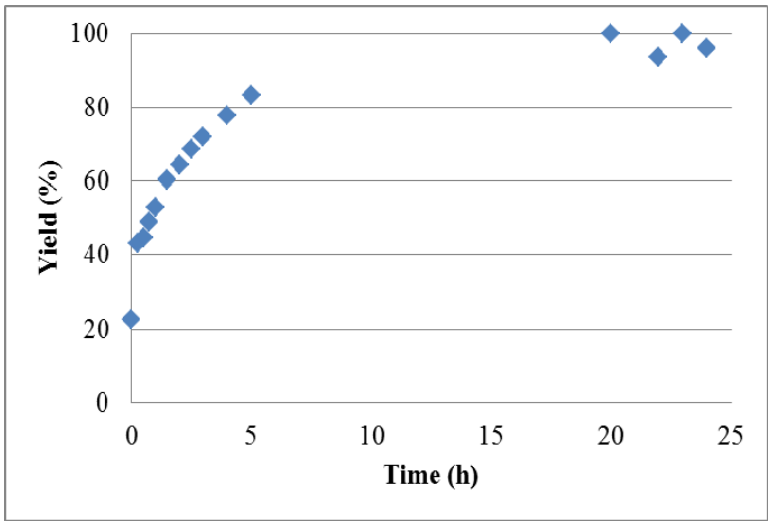

Figure 179 - Yield over time for 2-bromopyridine.

C.2 4-Substituted-2-Bromopyridines

The half-lives outlined in Table 54 were obtained from Figure 180-Figure 183. Note: each graph is produced from the average of two trials. The graph for 2-bromopyridine is located in the previous section (Figure 179).

Table 54 - Reactions run for 24 hours with 4-substituted 2-halopyridines and 40% v/v of H_2O, atm. N_2. Reactions run in 3-neck, 100 mL Morton flask.

Entry	4-R	$t_{½}$ (min)	σ_{meta}	σ_{para}	pK_a[1]
1	NH_2	1440	-0.16	-0.66	4.89
2	MeO	6	0.12	-0.27	2.1
3	Me	8.6	-0.07	-0.17	1.46
4	NO_2	1.4	0.71	0.78	-3.24
5	H	50	0	0	0.71[2]

[1]pKa's predicted by SciFinder: Calculated using Advanced Chemistry Development (ACD/Labs) Software V11.02 (© 1994-2014 ACD/Labs). [2]Literature source: Linnell, 1960.[2]

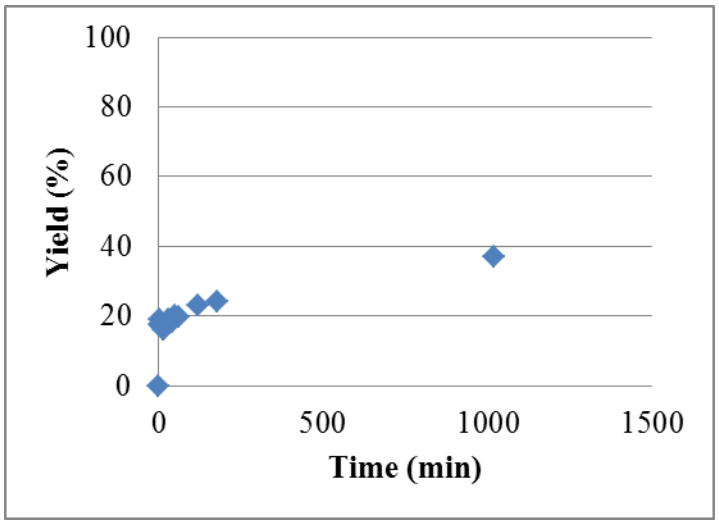

Figure 180 - Yield over time for 4-amino-2-bromopyridine.

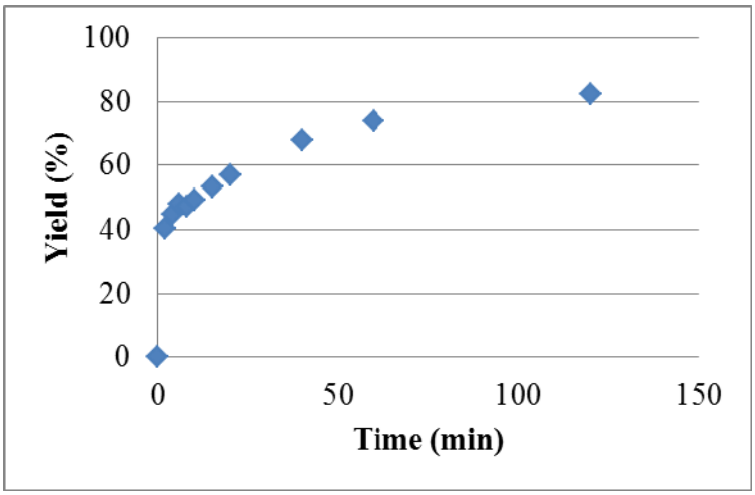

Figure 181 - Yield over time for 4-methoxy-2-bromopyridine.

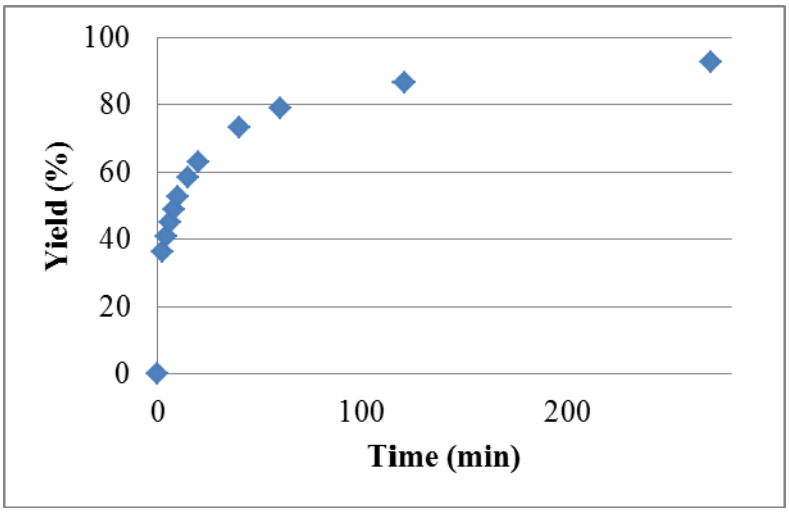

Figure 182 - Yield over time for 4-methyl-2-bromopyridine.

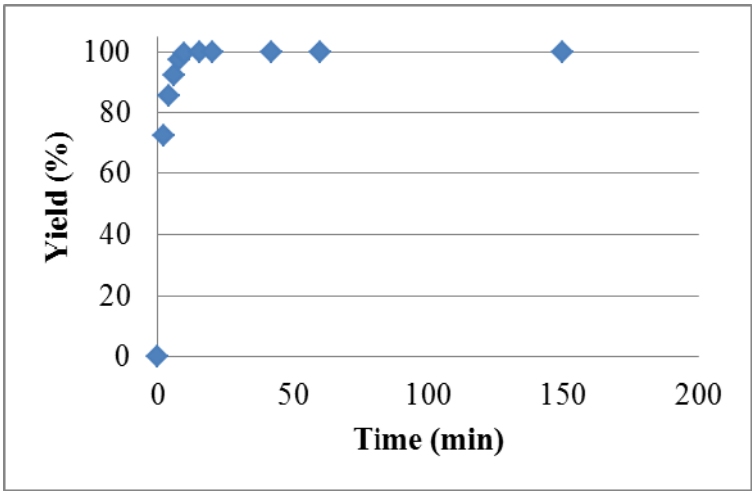

Figure 183 - Yield over time for 4-nitro-2-bromopyridine.

C.3 References

1. SciFinder. Calculated using Advanced Chemistry Development (ACD/Labs) Software V11.02 (© 1994-2014 ACD/Labs). .

2. Linnell, R. H., *J Org Chem* 1960, *25*, 290.

VITA

Amber C. Rumple

Amber Rumple was born on October 29, 1985 in Dayton, OH to Paul and JoAnne Rumple. She was actively involved in living life and exploring her surroundings. Amber participated in concert band, marching band, and was a founding member of the Anime Club at Beavercreek High School. She attended Wright State University in Dayton, Ohio where she was involved in concert band and was a founding member, president and vice-president of the Association for Consciousness Exploration of WSU. She was awarded the Green and Gold Scholarship for three consecutive years (2004-2007). She received a B.Sc. in Chemistry from Wright State University in 2008 and a M.Sc. in Organic Chemistry from Wright State University in 2010. She worked for the Air Force Research Labs, RZPS for two years during her schooling, where she was awarded an internal award for excellent work in 2008. She was also awarded the Outstanding Teaching Assistant award from Wright State University in 2010. She continued her chemistry career by enrolling in the graduate program at Georgia Tech in 2010 to pursue a doctorate in Organic Chemistry. She received the Cherry Emerson Fellowship for three consecutive years (2010-2013). She joined the Eckert-Liotta Research group where she was awarded the Conoco-Phillips fellowship for three consecutive years (2011-2014). When she is not working, Amber enjoys swing dancing, social dancing, yoga, running, exploring Atlanta, and spending time with friends.